TIME-SPACE VARIABILITY OF PARALIC DEPOSITIONAL ENVIRONMENTS: EMPHASIS ON BARRIER ISLAND PRESERVATION AND PALEOMORPHODYNAMICS

by

Julia Storer Mulhern

A dissertation submitted to the faculty of
The University of Utah
in partial fulfillment of the requirements for the degree of

Doctor of Philosophy

in

Geology

Department of Geology and Geophysics

The University of Utah

December 2016

The University of Utah Graduate School

STATEMENT OF THESIS APPROVAL

The dissertation of **Julia Storer Mulhern**

has been approved by the following supervisory committee members:

Cari Johnson	, Chair	**09/08/16** Date Approved
Lauren Birgenheier	, Member	**09/08/16** Date Approved
Peter Lippert	, Member	**09/08/16** Date Approved
Lisa Stright	, Member	**09/08/16** Date Approved
Anton Wroblewski	, Member	Date Approved

and by **Thure Cerling**, Chair of

the Department of **Geology and Geophysics**

and by David B. Kieda, Dean of The Graduate School.

ABSTRACT

Paralic depositional environments link terrestrial and marine settings and include a variety of environments such as deltas, lagoons, estuaries, barrier islands, tidal deltas, and strand plain shorelines. Influenced by both terrestrial and marine processes, these settings are complex and variable, which both limits and favors their preservation over various timescales through an interplay of deposition, motion, reworking, and ravinement. This dissertation addresses paralic depositional environments with analysis of both modern and ancient examples. An unusually thick succession of marine, paralic, and nonmarine strata from the Cretaceous of southern Utah (John Henry Member, Straight Cliffs Formation) is documented, with a focus on regressive-transgressive cycles and evolution of this part of the Western Interior Seaway, including controls on accommodation and sediment supply. This outcrop analysis leads to a detailed inquiry into barrier island systems, which is addressed by facies models and recognition criteria for three types of barrier island expressions. Databases of modern barrier islands (mapped in Google Earth) and ancient examples from the literature were assembled to further investigate links and disconnects between modern and ancient systems. This analysis is a first step toward developing paleomorphodynamic relationships to predict barrier island dimensions. It also highlights the uncertainty surrounding comparisons between modern and ancient barrier islands, which stems from the complexity of controls on modern barrier island motion and morphology. Additional analysis of the modern database

challenges a long-held assumption in coastal geomorphology, which suggests that barrier island shape is a function of tidal range and wave height. Based on shape parameters applied to 702 mapped barrier islands and spits, I determine that tidal range and wave height control <10% of barrier island morphology. Substantial complexity exists in the other 90% of controlling factors, justifying the need for future studies that test the relationship between modern and ancient barrier island systems.

TABLE OF CONTENTS

ACKNOWLEDGEMENTS

I am very grateful for all who have helped me over the last four years. A special thanks to Dr. Cari L. Johnson, whose support and encouragement made this research possible. I've truly enjoyed working with Cari over the last four years and I'm so grateful to have such a wonderful advisor. She is an exceptional mentor and role model and is responsible for my progress and growth as a scientist. In Cari we trust, always. I would like to thank my committee members: Lauren Birgenheier, Lisa Stright, Pete Lippert, and Anton Wroblewski for their thoughtful comments, reviews, and support in the completion of this dissertation. I am indebted to the help of many colleagues, particularly John Martin, who took the time to teach me Matlab and whose curiosity elevated the quality and depth of my research. I am also grateful to Brenton Chentnik, Ryan Purcell, Jon Primm, Tyler Szwarc and the other members of the Rocks to Models research group, whose collaborations were invaluable. I am grateful to everyone who took the time to help me in the field. Without all of your help and hard work, this would not have been possible. My deepest thanks goes out to my family and friends who have supported me throughout this entire process. A special thanks goes to my parents, Chris and Ann, for their patience with me through this process. Thank you mom and dad for instilling in me a quest for knowledge and a love for the outdoors, which have been fundamental to my career as a geologist.

This research was supported by the Rocks2Models research consortium, Cari Johnson and Lisa Stright, PI's, with funding from Chevron, ConocoPhillips, Hess I Corporation, Shell, and Statoil. I am very grateful to David Pocknall of Hess Corporation for providing biostratigraphic analyses, and Laura Webb and Daniel Jones at the University of Vermont for performing $^{40}Ar/^{39}Ar$ geochronological analysis cited in this study. I am also grateful to have received the University of Utah Graduate Research Fellowship, the ConocoPhillips Graduate Research Fellowship, the Rocky Mountain Association of Geologists Foundation Babcock Scholarship, and the SEPM Rocky Mountain Section Donald Smith Research Grant.

INTRODUCTION

Siliciclastic shallow marine coastlines are incredibly dynamic, composed of constantly moving barrier islands, tidal inlets, estuaries, lagoons, deltas, and other environments. These environments lie within the paralic zone, which links the terrestrial and marine realms. Paralic environments are highly complex and variable, yet critically important because they commonly record sea level rise during transgression. Understanding how barrier islands respond to sea level rise will be critical to coastal communities and infrastructure as climate driven sea level rise continues. Transgressive deposits are central to sequence stratigraphy (Arnott, 1995), documenting changes in base level and the motion of the shoreline through time. These strata can also form volumetrically important hydrocarbon reservoirs (Reynolds, 1999; Ahlbrandt et al., 2005). Because transgressive intervals tend to be highly complex and stratigraphically variable, they are relatively understudied compared to regressive equivalents.

Transgressive strata are broadly perceived to have poor preservation potential (Nichols and Biggs, 1985; Davis et al., 1987; Demarest and Kraft, 1987) and therefore lack robust facies models to guide their recognition and interpretation in outcrop and subsurface examples. Early models emphasize flooding surfaces and were based on asymmetric glacio-eustatic cycles with slow glacial growth followed by fast melting and flooding. Models for these settings do not fully encompass the variability present in both the modern and ancient. The facies, architecture, and preservation of transgressive strata

have been the subject of renewed interest (Cattaneo and Steel, 2003). Progress toward understanding transgressive systems (e.g., Roehler, 1988; Devine, 1991; Olsen et al., 1999; Sixsmith et al., 2008; Allen and Johnson, 2011; Kieft et al., 2011) raises additional questions about their dynamics and preservation.

Many of these questions surround barrier islands, which are controversial and debated in both modern and ancient literature. Barrier islands are elongate sand bodies, separated from the mainland by a back-barrier (Oertel, 1985; Davis Jr., 1994) and can be preserved as thick (>6 m), cliff-forming sandstones (Mulhern and Johnson, 2016). These deposits do not fit well in existing sequence stratigraphic models, which predict ravinement during transgression, resulting in lag or condensed interval deposition (Vail et al., 1977; Van Wagoner et al., 1988). The preservation of barrier islands is poorly understood, and therefore interpretations are primarily based on modern analog comparisons. However, it is unclear how modern barrier islands scale and relate to the dimensions of ancient barrier island deposits. The paleomorphodynamics, or quantitative dimensional scaling, of barrier islands has not been investigated in detail; therefore predictions of barrier island dimensions are largely unconstrained.

This dissertation contains four chapters, each prepared as an independent, peer-reviewed publication. The first chapter is published (Mulhern and Johnson, 2016), whereas the remaining three are in progress. Together, these papers use outcrop examples and database analysis to address these outstanding questions surrounding barrier islands and transgressive strata:

1) What can the temporal-spatial variability of transgressive facies tell us about the paleogeography, sequence stratigraphy, and depositional history of foreland

basins?

2) How are barrier islands recognized and preserved in the stratigraphic record?
3) What controls barrier island morphology, and are there predictive paleomorphodynamic scaling relationships between modern and ancient systems?

Chapter 1 is a detailed sedimentological analysis of previously unstudied strata which document the lateral and vertical facies variability in a high-accommodation, high-sediment supply setting. The John Henry Member (JHM) of the Upper Cretaceous Straight Cliffs Formation (SCF) of southern Utah provides an opportunity to study fluvial to shallow marine interaction within a foreland basin system. The John Henry Member succession at Buck Hollow preserves stacked paralic facies deposited in deltaic, estuarine, barrier island, strand plain, and shelfal environments. It is also unusually thick, 2-3 times expanded relative to correlative successions 15-40 km away. This paper explores autogenic and allogenic controls on accommodation and finds that the expansion at Buck Hollow likely results from local tectonics.

Recognition and interpretation of barrier island facies at Buck Hollow raised questions about the outcrop expression of barrier islands. Chapter 2 presents detailed barrier island facies and recognition criteria based on outcrop examples from the John Henry Member at Buck Hollow as well as Alvey Wash, both in the Kaiparowits Plateau. This paper describes four facies associations that stack to create three types of barrier island successions with distinct lateral and vertical outcrop expressions. These facies and recognition criteria are based on outcrop observations and, therefore, incorporate post-depositional processes (erosion, ravinement, reworking, and stacking). These successions depart from existing facies models (e.g., Reinson, 1992), which are based primarily on

modern analogs. The new barrier island successions, presented here, consider and account for barrier island motion and preservation at both modern and geologic timescales.

Chapter 3 compares the dimensions of modern and ancient barrier islands to investigate potential scaling relationships. Modern barrier islands were mapped from Google Earth and compared to the dimensions of ancient examples gathered from published literature. Qualitative and statistical analysis shows that modern and ancient barrier islands have distinctly different dimensions. A small portion of the difference results from the measurement methods, whereas the remaining difference indicates that ancient barrier islands record lateral, shore-perpendicular, and vertical motion through time. This comparative analysis is the first step in developing paleomorphodynamic relationships for barrier island systems.

Chapter 4 expands the modern database developed in Chapter 3 to investigate controls on modern barrier island morphology. A long-standing paradigm suggests that tidal range and wave height control barrier island morphology (Hayes, 1979). To test the validity and predictive utility of this hypothesis, the shapes of 702 modern barrier islands and spits were quantified using shape parameters and combined with tidal range and wave height data. Statistical and qualitative analysis shows that tidal range and wave height account for <10% of barrier island morphology. The variability of the data show that tidal range and wave height do not predict barrier island morphology and vice versa. Further analysis is needed to determine the controls on the remaining >90% of variability in barrier island morphology.

While the study addresses key knowledge gaps in the understanding of barrier

island dynamics and transgressive sedimentology, the results of these studies are accompanied by several unanswered questions, enabling more-targeted future studies. The revised recognition criteria presented here may facilitate future barrier island interpretation and provide additional examples of preserved barrier islands. Additional examples and analysis will also strengthen ties between modern and ancient barrier islands systems. The paleomorphodynamic foundation initiated here could be expanded with additional data or through direct, one-to-one, subenvironment comparisons. The modern and ancient barrier island dimensions could be transposed to develop an equation to quantitatively predict island dimensions. Accurate predictions also depend on improved understanding of controls on modern barrier islands. In addition to providing an opportunity to further assess barrier island shape, the modern barrier island database could be leveraged to investigate how the distribution and variability of sub-environments vary laterally along coastlines. This would allow mesoscale comparisons of the distribution of depositional environments and could lend insight into understanding the facies distribution within transgressive intervals. As the field of quantitative sedimentology continues to grow and expand, the ideas here are only a few of the possible ways to continue the investigation of modern and ancient paralic environments.

References

Ahlbrandt, T.S., Charpentier, R.R., Klett, J.W., Schmoker, C.J., Schenk, G.F., and Ulmishek, T.S., 2005, Global resource estimates from total petroleum systems: American Association of Petroleum Geologists Memoir, v. 86, p. 1–334.

Allen, J.L., and Johnson, C.L., 2011, Architecture and formation of transgressive-regressive cycles in marginal marine strata of the John Henry Member, Straight Cliffs Formation, Upper Cretaceous of Southern Utah, USA: Sedimentology, v. 58, no. 6, p. 1486–1513, doi: 10.1111/j.1365-3091.2010.01223.x.

Arnott, R.W.C., 1995, The parasequence definition--are transgressive deposits inadequately addressed? Journal of Sedimentary Research, v. Vol. 65B, no. 1, p. 1–6, doi: 10.1306/D42681D0-2B26-11D7-8648000102C1865D.

Cattaneo, A., and Steel, R.J., 2003, Transgressive deposits: a review of their variability: Earth-Science Reviews, v. 62, no. 3-4, p. 187–228, doi: 10.1016/s0012-8252(02)00134-4.

Davis, R.A., Davis Jr., R.A., and Clifton, H.E., 1987, Sea-level change and the preservation potential of wave-dominated and tide-dominated coastal sequences, *in* Nummedal, D., Pilkey, O.H., and Howard, J.D. eds., Sea-level Fluctuation and Coastal Evolution, SEPM Special Publication, 41, p. 167–178.

Davis Jr., R.A., 1994, Barrier island systems- a geologic overview, *in* Davis Jr., R.A. ed., Geology of Holocene Barrier Island Systems, Springer-Verlag, Berlin, p. 1–46.

Demarest, J., and Kraft, J.C., 1987, Stratigraphic record of Quaternary sea levels: implications for more ancient strata, *in* Nummedal, D., Pilkey, O.H., and Howard, J.D. eds., Sea-Level Fluctuation and Coastal Evolution, SEPM Special Publication, 41, p. 223–239.

Devine, P.E., 1991, Transgressive origin of channeled estuarine deposits in the Point Lookout Sandstone, northwestern New Mexico: a model for Upper Cretaceous, cyclic regressive parasequences of the US Western Interior: American Association of Petroleum Geologists Bulletin, v. 75, no. 6, p. 1039–1063, doi: 10.1306/0C9B28C1-1710-11D7-8645000102C1865D.

Hayes, M.O., 1979, Barrier island morphology as a function of tidal and wave regime, *in* Leatherman, S.P. ed., Barrier Islands from the Gulf of Mexico to the Gulf of St. Lawrence, Academic Press, New York, p. 1–28.

Kieft, R.L., Hampson, G.J., Jackson, C.A.L., and Larsen, E., 2011, Stratigraphic architecture of a net-transgressive marginal- to shallow-marine succession: Upper Almond Formation, Rock Springs Uplift, Wyoming, U.S.A.: Journal of Sedimentary Research, v. 81, no. 7, p. 513–533, doi: 10.2110/jsr.2011.44.

Mulhern, J.S., and Johnson, C.L., 2016, Time-space variability of paralic strata deposited in a high accommodation, high sediment supply setting: example from the Cretaceous of Utah, *in* Hampson, G.J., Reynolds, A.D., Kostic, B., and Wells, M.R. eds., Sedimentology of Paralic Reservoirs: Recent Advances and their Applications, Geological Society, London, Special Publications.

Nichols, M.M., and Biggs, R.B., 1985, Estuaries, *in* Davis, R.A. ed., Coastal Sedimentary Environments, Springer-Verlag, Berlin, p. 77–186.

Oertel, G.F., 1985, The barrier island system: Marine Geology, v. 63, no. 1, p. 1–18, doi: 10.1016/0025-3227(85)90077-5.

Olsen, T.R., Mellere, D., and Olsen, T., 1999, Facies architecture and geometry of landward-stepping shoreface tongues: the Upper Cretaceous Cliff House Sandstone (Mancos Canyon, south-west Colorado): Sedimentology, v. 46, no. 4, p. 603–625,

doi: 10.1046/j.1365-3091.1999.00234.x.

Reinson, G.E., 1992, Transgressive barrier island and estuarine systems, *in* Walker, R.G. and James, N.P. eds., Facies Models: Response to Sea-Level Changes, Geological Association of Canada, St. John's, Newfoundland, p. 179–194.

Reynolds, A.D., 1999, Dimensions of paralic sandstone bodies: American Association of Petroleum Geologists Bulletin, v. 83, no. 2, p. 211–229, doi: 10.1306/00AA9A48-1730-11D7-8645000102C1865D.

Roehler, H.W., 1988, The Pintail coal bed and barrier bar G - a model for coal of barrier bar - lagoon origin, Upper Cretaceous Almond Formation, Rock Springs Coal Field, Wyoming: U.S. Geological Survey Professional Paper, v. 1398.

Sixsmith, P.J., Hampson, G.J., Gupta, S., Johnson, H.D., and Fofana, J.F., 2008, Facies architecture of a net transgressive sandstone reservoir analog: The Cretaceous Hosta Tongue, New Mexico: American Association of Petroleum Geologists Bulletin, v. 92, p. 513–547, doi: 10.1306/01020807017.

Vail, P.R., Mitchum Jr., R.M., and Thompson III, S., 1977, Seismic stratigraphy and global changes of sea level, Part 3: Relative changes of sea level from coastal onlap, *in* Payton, C.E. ed., Seismic Stratigraphy: Applications to Hydrocarbon Exploration, American Association of Petroleum Geologists, p. 63–81.

Van Wagoner, J.C., Posamentier, H.W., Mitchum, R.M., Vail, P.R., Sarg, J.F., Loutit, T.S., and Hardenbol, J., 1988, An overview of the fundamentals of sequence stratigraphy and key definitions, *in* Wilgus, C.K., Posamentier, H.W., Ross, C.K., and Kendall, C.G. eds., Sea-level Changes: An Integrated Approach, SEPM Special Publication, 42, Tulsa, p. 39–45.

1. TIME-SPACE VARIABILITY OF PARALIC STRATA DEPOSITED IN A HIGH ACCOMMODATION, HIGH SEDIMENT SUPPLY SETTING: EXAMPLE FROM THE CRETACEOUS OF UTAH[1]

Abstract

A previously unstudied section of the John Henry Member (Upper Cretaceous, Straight Cliffs Formation) preserves four stacked regressive-transgressive cycles of paralic strata from the Kaiparowits Plateau in south-central Utah. Mesoscale (10-100s m thick) shoreface, wave-dominated delta, and estuary depositional environments stack vertically and show the complexity of paralic facies in a single location through time. Correlations to nearby exposures show the palaeogeographic variability up-dip and along-strike over ~6.5 My. Such variability highlights the importance of high accommodation settings in preserving transgressive deposits including landward-stepping barrier island and lagoon systems. The Buck Hollow section is 2-3x expanded compared to correlative successions only 15-40 km away. Tectonics, eustasy, and climate contributed to relative base level shifts, but these regional controls do not explain the dramatic, local thickening observed. Local controls on accommodation were quantified

[1] Julia S. Mulhern and Cari L. Johnson. Accepted 2/16/16 *In:* Hampson, G.S. and Reynolds, T. (eds) *Sedimentology of Paralic Reservoirs: Recent Advances*, Geological Society of London Special Publication

through decompaction analysis. Results show that the expanded John Henry Member thickness in Buck Hollow can be explained by decompaction differences (~9%), local erosion by fluvial incision (~5%), early compaction (~30%), and local structures such as faults (~100-150%). This outcrop-based study illustrates facies variability within a thick paralic succession, and investigates accommodation controls on preservation of these strata, with the goal of improving predictive models for analogous deposits.

Introduction

Paralic deposits are generally underrepresented in the geological literature, due partly to their locations along complex coastal margins with distinct but dynamic energy-type controls (wave, tide, rivers; e.g., Davies 1964; Galloway 1975; Hayes 1979; Davis Jr. & Hayes 1984; Gani & Bhattacharya 2007; Ainsworth *et al.* 2011; Vakarelov & Ainsworth 2013). Paralic strata, particularly as they are linked to transgressive depositional settings, are also broadly perceived to have poor preservation potential (Nichols & Biggs 1985; Davis Jr. & Clifton 1987; Demarest & Kraft 1987), and thus there is a lack of robust facies models to guide recognition and interpretation of these systems. Nevertheless, paralic strata form volumetrically important, but heterogeneous and complex, hydrocarbon reservoirs (Reynolds 1999; Ahlbrandt *et al.* 2005).

In addition to their economic significance, transgressive paralic intervals form an important component of the rock record and are central to sequence stratigraphic interpretations (Arnott 1995). While progress has been made towards documenting transgressive deposits (Roehler 1988; Devine 1991; Olsen *et al.* 1999; Hubbard *et al.* 2002; Davies *et al.* 2006; Ambrose & Ayers 2007; Plink-Björklund 2008; Sixsmith *et al.*

2008; Allen & Johnson 2011; Kieft *et al.* 2011; Painter *et al.* 2013), models for these settings do not fully encompass the variability present in both modern and ancient examples, or the interactions of wave, tide, storm, and fluvial energy that define coastal settings (Zaitlin & Shultz 1990; Cooper 1993). These models also usually reflect a single "snapshot" in time, and do not consider interactions between the transgressive and regressive components of paralic shorelines through time (Davis Jr. & Clifton 1987; Yoshida *et al.* 2004). Sequence stratigraphic interpretations are limited by our understanding of how transgressive deposits stack at the mesoscale (10s-100s m; e.g. Yoshida *et al.* 2004; Plink-Björklund 2008; Kieft *et al.* 2011). Similarly, the preservation of transgressive deposits is closely tied to both autogenic and allogenic controls on accommodation (Curray 1964; Schlager 1993; Muto & Steel 1997). In addition to incision and ravinement, tectonics, eustasy, pre-existing topography, and compaction can all play a role in determining the space available for deposition and the likelihood of preservation (Posamentier & Allen 1993), though relatively few studies investigate the latter two factors (e.g., Reynolds *et al.* 1991).

This study assesses the time-space variability of paralic strata within the Cretaceous Straight Cliffs Formation of southern Utah, U.S.A. (Fig. 1.1). These deposits have received less attention than other Western Interior Seaway successions, yet their interpretation is central to some prominent sequence stratigraphic models (Shanley & McCabe 1991, 1994, 1995). Shoreface, delta, and estuary strata of the John Henry Member from a previously unstudied location (Buck Hollow) in the northern Kaiparowits Plateau are documented in detail. Quantitative delineation of facies relationships at the depositional environment scale (10s-100s of m vertically) shows the variability possible

in a single locality that spans ~7 km along strike. Temporal variability and evolution are also documented through the 456 m-thick succession, spanning ~6.5 My in duration. Correlations to other locations of John Henry Member deposition in the Kaiparowits Plateau reveal unusual thickening patterns. Possible causes of this local thickening are considered, highlighting some of the unusual characteristics of the Kaiparowits Plateau, with implications for other paralic deposits and foreland basin settings.

Geological Background

The late Turonian to early Campanian aged Straight Cliffs Formation records fluvial to marginal marine deposition in the Kaiparowits Plateau, along the western edge of the Cretaceous Western Interior Seaway (Fig. 1.1; Peterson 1969*a, b*; Eaton & Nations 1991). Subduction of the Farallon plate beneath the North American plate created a broad, asymmetric foreland basin (Kauffman 1977; DeCelles 2004; DeCelles & Coogan 2006) through flexural loading (Jordan 1981; Pang & Nummedal 1995; Currie 2002; Painter & Carrapa 2013) and dynamic subsidence (Mitrovica *et al.* 1989; Liu *et al.* 2011; Liu *et al.* 2014). This depression was flooded during the Cretaceous global eustatic highstand (Haq *et al.* 1987; Miller *et al.* 2005) to create an epicratonic seaway (Kauffman 1977; Hancock & Kauffman 1979). The Kaiparowits region was located along the Utah Bight (McGookey *et al.* 1972), a large embayment of the palaeoshoreline in south-central Utah (Fig. 1.1).

In simple foreland basin models, fold-thrust belts are generally the primary control on both accommodation (through loading) and sediment supply (through erosional exhumation of the orogeny and deposition in the basin; DeCelles & Giles 1996;

DeCelles 2012). The preserved geology of the Kaiparowits Plateau shows interactions and conditions more complex than the simplified model. Provenance and sediment-dispersal studies indicate that the basin mainly received sediment via distributive fluvial systems fed from the Mogollon Highlands and the Cordilleran Magmatic Arc (Fig. 1.1A; Lawton *et al.* 2003, 2014; Szwarc *et al.* 2014), with comparatively less input directly from the Sevier fold-thrust belt. These river systems were generally oriented subparallel to the Sevier fold-thrust belt, which generated much of the proximal foredeep accommodation through load-driven subsidence (Jordan 1981; Pang & Nummedal 1995; Currie 2002; Painter & Carrapa 2013). There is also evidence for longshore drift from the north (Allen & Johnson 2010*a*; Szwarc *et al.* 2014). Therefore, sediment supply and accommodation were at least partly decoupled during Straight Cliffs Formation deposition. As a result, the basin dynamics and relative sea level changes within the Kaiparowits region were nuanced and complicated, controlled by processes occurring locally in the basin, in the adjacent Sevier fold-thrust belt, and multiple regional source areas.

Coal resource assessment motivated early investigations of the Straight Cliffs Formation (Peterson 1969*a, b*; Vaninetti 1979; Hettinger 2000). Peterson (1969*b*) divided the formation into four members: the Tibbet Canyon Member, the Smoky Hollow Member, the John Henry Member, and the Drip Tank Member (Fig. 1.2). The lowermost, Tibbet Canyon Member consists of shallow marine facies and overlies the Tropic Shale, recording the transition from offshore marine mudstone deposition to more proximal shoreface and nonmarine sedimentation. The Smoky Hollow Member is predominantly terrestrial and is comprised of carbonaceous floodplain mudstones and thin coals

interbedded with isolated fluvial channels. The top of the Smoky Hollow Member is marked by the Calico Bed, an interval of amalgamated, coarse-grained fluvial channels (Bobb 1991). The John Henry Member forms the bulk of the Straight Cliffs Formation and is the focus of this study. The Drip Tank is the uppermost member and is composed of amalgamated fluvial sandstones deposited in distributive fluvial systems (Lawton *et al.* 2014; Gooley *et al.* in press).

The John Henry Member (JHM) is the thickest and most laterally variable of the four members of the Straight Cliffs Formation. In the southern and western Kaiparowits Plateau, the John Henry Member preserves coastal plain and fluvial systems flowing northeast (Gallin *et al.* 2010; Gooley *et al.* in press). To the east, the strata transition to offshore, shoreface, and tidal facies, which are grouped into seven intervals labeled "A" to "G" in stratigraphic order of the main shoreface deposits (Fig. 1.2; Peterson 1969*a*, *b*; Allen & Johnson 2010*a, b*, 2011; Dooling 2013). Initial sequence stratigraphic interpretations divided the Straight Cliffs into four unconformity-bound depositional sequences based on a west to east transect through the middle of the Kaiparowits Plateau (Fig. 1.2; Shanley & McCabe 1991, 1993, 1994, 1995; McCabe & Shanley 1992). Recent stratigraphic assessments from various locations around the plateau have refined this initial model, including recognition of basin-axial fluvial drainage networks and modification of the sequence boundary interpretations (Allen & Johnson 2011; Szwarc *et al.* 2014; Chentnik *et al.* 2015; Gooley *et al.* in press).

Notably, the Straight Cliffs succession north of Highway 12 was not included in the early studies (cf. Hettinger *et al.* 1993; Shanley & McCabe 1995). Moving ~14 km to the northeast of Main Canyon, this study documents strata in an unstudied portion of the

north Kaiparowits Plateau, with the main goals of documenting the time-space variability of a thick, mainly transgressive paralic succession, as well as investigating first-order controls on sedimentation and preservation.

Field Analysis

Buck Hollow is located along Posey Lake Road, 15 km north of Escalante, Utah (Fig. 1.1B). The study area consists of a ~7 km long along-strike outcrop exposure (Figs. 1.1B & 1.3) which preserves all four members of the Straight Cliffs Formation (Figs. 1.1B, 1.2 & 1.3). The cliff face has ~1,700 m relief and displays the most distal facies of the John Henry Member preserved in the Kaiparowits Plateau. These outcrops are immediately adjacent to the prominent Escalante Monocline, a presumed Laramide-style, basement-involved feature (Sargent & Hansen 1982; Davis 1999). Structural (N=128) measurements record a local structural dip of 15° west consistently through the Straight Cliffs Formation (Fig. 1.1B) at Buck Hollow.

Measured section analysis (17 sections, totaling 2,008 m) collectively spans from the top of the Tropic Shale, through all four members of the Straight Cliffs Formation, into the basal portion of the overlying Wahweap Formation (Figs. 1.1B, 1.3 & 1.4). All sections record vertical changes in grain size, texture, sorting, sedimentary structures, bedding, trace and body fossils, and palaeocurrent indicators. Correlations between measured sections were extended by walking along bedding contacts and analyzing aerial photography. Palaeocurrent directions (N=1,472) were collected from trough-cross stratification (axes), tabular accretion sets, and ripple laminations (Fig. 1.4; Allen 1966; Miall 1974). Data from Buck Hollow were combined with recent work from White

Mountain, Main Canyon (Chentnik *et al.* 2015), and Left Hand Collet (Dooling 2013), and aerial photography for regional correlation and analysis. Provenance data, specifically sandstone modal compositions and U/Pb detrital zircon geochronology, of Buck Hollow samples (Szwarc *et al.* 2014) were also considered. Mudstone samples were collected throughout the Straight Cliffs Formation for biostratigraphy (Fig. 1.5) and examined for palynomorphs (48 samples), nannofossils (18), and foraminifera (18). These data are used here to support depositional environment and general age interpretations; a full assessment of the biostratigraphy data is in progress and will be published at a later date (D. Pocknall pers. comm. 2015). Finally, biotite grains from a bentonite layer in the lower John Henry Member were analyzed for $^{40}Ar/^{39}Ar$ geochronology, with methods and results described in the Supplementary Material.

Stratigraphy

The paralic strata of Buck Hollow are described using 15 lithofacies (LF) identified based on lithology, primary bedding structures, and trace and body fossils (Table 1.1). The lithofacies are combined to describe 15 facies associations (Table 1.2). Facies associations are grouped to define three depositional environments, interpreted below. Dinoflagellates and nannofossils help constrain the timing of deposition, and suggest the John Henry Member at Buck Hollow is late Coniacian to early Campanian in age, generally consistent with other studies (Fig. 1.5; Eaton 1991; Dyman & Cobban, 2002; Szwarc *et al*. 2014).

Facies Association One

Description

Facies associations 1.1-1.5 (Table 1.2; Fig. 1.6A) include sandstone and mudstone units which make laterally continuous, coarsening upwards, stacked cliff faces (17-51 m thick). Facies association 1.1 is composed of planar to wavy laminated, fissile, gray mudstones (LF1, Fig. 1.6J) and interbedded sandstones (LF2) containing occasional Inoceramid and oyster shell fragments. Mudstone intervals contain diverse dinoflagellate assemblages and common nannofossils (Fig. 1.5). Facies association 1.2 is composed of mm-scale laminated mudstones and sandstones (1-10 cm thick; LF2; Fig. 1.6B) grading vertically into hummocky and swaley cross-stratified sandstone beds (2-50 cm thick; LF3). The sandstone beds (LF3) of FA1.2 contain *Arenicolites* (Fig. 1.6E) and have *Thalassinoides* on the uppermost bedding surfaces. Facies association 1.3 contains hummocky and swaley cross-stratified sandstone beds 0.1-1 m thick (LF3; Fig. 1.6H,I) grading into planar laminated and trough cross-stratified sandstone beds (LF4; Fig. 1.6C). These sandstone beds are separated by mm-cm scale, planar laminated mudstone layers (LF1; Fig. 1.6B). Facies association 1.4 is composed of blocky bedded (0.5-2 m thick), fine- to medium-grained, trough cross-stratified and planar-laminated, sandstones containing *Skolithos* (Fig. 1.6F), *Ophiomorpha* (LF4; Fig. 1.6D), and *Cylindrichnus concentricus* (Fig. 1.6G). Beds are laterally continuous and separated by thin (<1 cm thick) interbeds of fissile, laminated, gray mudstones (LF1; Fig. 1.6K). Facies association 1.5 is a single bed (1-2 m thick) of planar laminated medium-grained sandstone (LF5) with occasional shell fragments and 0.5 cm-diameter mudstone clasts.

Interpretation

Facies association one is composed of vertically stacked offshore (FA1.1), distal lower shoreface (FA1.2), proximal lower shoreface (FA1.3), upper shoreface (FA1.4), and foreshore (FA1.5) deposits. Facies association one is interpreted as a wave-dominated shoreface environment (Table 1.2; Fig. 1.6). These sequences were deposited on a wave- and storm- dominated shelf (Plint 2010; Li *et al.* 2011). The packages thicken and shoal vertically, suggesting the shoreline prograded during deposition (Van Wagoner *et al.* 1988). The preserved trace fossils, nannofossils, and the diverse dinoflagellate assemblages are commonly found in marine settings (Figs. 1.5 & 1.6D,E,F,G; MacEachern *et al.* 2010; Ekdale & Harding 2015), suggesting marine deposition for these facies. Large intervals of mudstone (FA1.1; Fig. 1.3B) represent stacked offshore deposits, the distal expression of a marine shoreface.

Facies Association Two

Description

Facies association 2.1 is composed of sharp-based, gently inclined (<5 degrees; Fig. 1.7J), hummocky and swaley cross-stratified sandstones (LF3) and trough cross-bedded and planar fine- to medium-grained sandstones (LF4). These sandstone units contain *Ophiomorpha,* shell fragments (Fig. 1.7), and leaf impressions (Fig. 1.7H). Sandstone beds are tabular and increase in size from 10 cm to ~2 m thick towards the top of the interval (Fig. 1.7B,F); these are separated by laterally discontinuous mudstone layers of variable thickness (0.1-1 cm; Fig. 1.7G). The facies association is stacked into two coarsening-upwards cliff faces (~21-27 m) to the northeast (<5 degrees; Fig. 1.7J).

Although tabular, the individual beds pinch out into intervening mudstone intervals over 10s of metres laterally. However, the cliffs are continuous laterally across the entire study area (~7 km). The thickness of individual sandstone beds increases vertically (Fig. 1.7B), showing increased amalgamation towards the top of the cliff faces as the internal sedimentary structures change from swaley cross-stratification to trough and planar cross-stratification (Fig. 1.7J).

Interpretation

Facies association two is composed of vertically stacked offshore (FA1.1), distal lower shoreface (FA1.2), and wave-dominated delta front facies (FA2.1; Table 1.2; Fig. 1.7) and is interpreted as wave-dominated delta deposits. The same facies associations are used to interpret the basal portions of the wave-dominated shoreface deposits and the wave-dominated delta deposits, because the distal expression of the two environments is indistinguishable in outcrop (Bhattacharya & Walker 1991; MacEachern & Pemberton 1992; Reading & Collinson 1996).

Moving vertically into the upper delta front, the facies show distinct deltaic characteristics. Blocky, gently inclined, trough and planar cross-stratified sandstone beds in the upper portion of the delta front facies are interpreted as storm-reworked, shore-parallel, mouth bar deposits (Fig. 1.7J; Gingras *et al.* 1998). This sand was output from a fluvial source as mouth bars, and then reworked onto the shoreface through wave and storm action (Bhattacharya & Giosan 2003). Individual pulses of sand to the delta front result in obliquely-exposed clinoforms (0.1-2 m thick and 25-100 m wide; Gani & Bhattacharya 2007; Graham *et al.* 2015). The clinoforms are dipping (<5°) to the

northeast revealing progradation of the delta shoreface (21-27 m thick). Abundant plant material (Fig. 1.7I), shell fragments (Fig. 1.7E,H), and wavy bedding (Fig. 1.7C) within the delta front suggest the proximity of these deposits to the shoreline, and rapid deposition. These characteristics indicate proximity to sediment source, river influence, and rapid sedimentation, distinguishing the delta front from proximal lower and upper shoreface strata. The thinning and pinch out of tabular beds over 10s of metres suggests rapid, pulsated deposition, with dewatering contributing to the discontinuous nature of the beds.

Trace fossils are commonly used to distinguish between wave-dominated deltas and wave-dominated shoreface coastlines (MacEachern & Pemberton 1992; Li *et al.* 2011); however, burrowing within both the upper shoreface and delta front at Buck Hollow is not distinct, with preservation of *Ophiomorpha* and *Skolithos* burrows of similar distribution and intensity in both settings. Pellet-lined *Ophiomorpha nodosa* burrows (Fig. 1.6D) suggest a high-energy environment (Droser & Bottjer 1989) with water conditions suitable for suspension feeding (MacEachern *et al.* 2010). A low diversity of trace fossils suggests a stressed environment, consistent with rapid deposition (Gingras *et al.* 1998), fitting for both a wave-dominated delta and/or shoreface experiencing high sedimentation rates.

Facies Association Three

Description

Facies association 3 is highly variable (Figs. 1.8 & 1.9), containing eight sub-environments. Facies association 3.1 is comprised of carbonaceous shales and coals (Fig.

1.8E). Commonly capped by 10-100 cm thick coal beds (Fig. 1.8E), these carbonaceous mudstones and siltstones have significant sulphur residue, abundant plant material (Fig. 1.8J), and can contain sporadic shell fragments. These fine-grained facies are slope forming and cut into by isolated bodies of facies associations 3.2, 3.3, and 3.4. Facies association 3.2 is comprised of lens-shaped, medium-grained sandstone deposits (Fig. 1.8C) with internal trough cross-stratification (LF9) and pockets of convolute bedding and soft sediment deformation. Throughout the lenses, there are prevalent, large (>15 cm) oyster shell fragments (Fig. 1.8C), which are grouped into lags and lenses (LF8). There is heavy bioturbation including *Palaeophycus* (Fig. 1.8D), *Ophiomorpha nodosa*, and a few large (>20 cm) *Teredolites* assemblages.

Facies association 3.3 is composed of sandstone-dominated outcrops (~3.5 m thick; Fig. 1.8I) subdivided into 1-50 cm thick beds composed of inclined heterolithic strata (LF14), homogenous sandstone beds (LF16), heavily bioturbated beds (LF15), convolute beds (Fig. 1.8G), and laminated mudstone intervals (LF7). Bioturbation is prevalent throughout the facies association, with burrows both concentrated on bedding planes (*Thalassinoides*; Fig. 1.8B), cross-cutting strata (*Skolithos;* Fig. 1.8F), and within beds (*Cylindrichnus concentricus*; Fig. 1.8L). Minor shell fragments (including gastropods), sharks' teeth (Fig. 1.8K), and ammonite impressions (Fig. 1.8H) occur throughout this interval.

Facies association 3.4 is made up of large (30 m thick), amalgamated, lenticular, coarse-medium grained, erosional sandstone deposits (LF10; Fig. 1.8O), which cut into underlying carbonaceous mudstones and coals (LF6). The amalgamated, lenticular sandstones contain wood material (Fig. 1.8P), leaf fossils, *Teredolites* (Fig. 1.8R), and

shell fragments (Fig. 1.8M). Between the individual channels, large (>10 cm) mudstone clasts (Fig. 1.8Q) are present in a coarse-grained matrix.

Facies association 3.5 is generally a slope-forming succession, consisting of blocky to wavy interbedded mudstones with mm-scale laminations of alternating light and dark gray mudstone (LF7). These deposits include occasional (~1 cm) coarse-grained sandstone layers and round burrows, ~3-8 mm in diameter, filled with coarse-grained sandstone. Facies association 3.5 is cut into by facies associations 3.6, 3.7, and 3.8. Facies association 3.6 is composed of medium-grained, lens-shaped sandstone bodies (LF11; Fig. 1.9B) that contain trough cross-stratification, bidirectional cross-stratification, and double mud drapes. These sandstones commonly erode into underlying deposits with 0.5 to 5 m of relief. Facies association 3.7 is composed of medium-grained sandstones divided into beds by master surfaces with distinct, variably inclined (~1-20°), lateral accretion generally to the south (Fig. 1.9D). The beds exhibit trough cross-stratification and bidirectional cross-stratification (LF12, LF13) and form 3-15 m thick sheets. These beds occasionally contain rhizoliths (Fig. 1.9H) and trace fossils (*Diplocraterion* and *Palaeophycus*; Fig. 1.9E,G,I). In some locations, facies association 3.7 overlies coal deposits (FA3.1), with distinct *Thalassinoides* at the base (Fig. 1.9F). Facies association 3.8 displays stacked, tabular, westward-inclined fine- to medium-grained sandstone beds (LF16), which vary in thickness laterally from .2 to 2 m. Some beds have well-indurated shell fragment lags along the basal incision surface, whereas others have abundant mudstone clasts. Fissile gray mudstone interbeds (LF7) separate the sandstones.

Interpretation

Facies association 3 records the juxtaposition of high and low energy facies. Areas of fine-grained carbonaceous mudstones and coals (FA3.1; Fig. 1.8E; Table 1.2) are interpreted as estuary fill, indicating deposition in a protected back-barrier setting with flanking swamps (Holz *et al.* 2002). These low energy deposits are cut into by higher energy deposits interpreted as washover fans (FA3.2), bayhead delta deposits (FA3.3), and distributary channels (FA3.4). Overall, facies association 3 is interpreted as a wave-dominated estuary (Table 1.2). Dinoflagellates from within the estuarine deposits indicate a brackish water setting (Fig. 1.5).

Washover fans (FA3.2; Fig. 1.8A,C) record sand entering the estuary during storms (Schwartz 1982; Sedgwick & Davis Jr. 2003; Hudock *et al.* 2014), and with marine shells (Fig. 1.9C,M) they suggest deposition in a coastal transgressive setting (Roehler 1988; Wadsworth *et al.* 2010). The stacked, inclined, heterolithic, upward-coarsening sandstone units of FA3.3 (Fig. 1.8I) are interpreted as the distal portion of a bayhead delta (Joeckel & Korus 2012). These deposits contain thin (1-25 cm) wavy and inclined strata (Fig. 1.8I) interbedded with finer-grained facies, similar to the facies patterns seen in cores from the modern Trinity River bayhead delta in Texas (McEwen 1969). Convolute bedding (Fig. 1.8G) suggests loading (Dzuynski & Smith 1963) and rapid deposition, known to occur in modern bayhead deltas, such as the Atchafalaya delta in Louisiana (van Heerden & Roberts 1988). Sharks' teeth (Fig. 1.8K), bioturbation (Fig. 1.8B,F,L), and ammonite impressions (Fig. 1.8H) indicate marine influence (Becker *et al.* 2010; Cumbaa *et al.* 2010; Kirkland *et al.* 2013). Combined, these characteristics help to differentiate bayhead delta deposits from other estuarine sandstone bodies.

Distributary channels (FA3.4; Fig. 1.8O) are recognized by coarse-grained sandstone lenses containing terrigenous material (Fig. 1.8P) and fluid mud layers (Ichaso & Dalrymple 2009). These distributary channels pinch laterally into finer-grained, central-estuary bay fill (FA3.5). Erosional features at the base of the interval are interpreted as tidal channels (FA3.6; Fig. 1.9B; Hughes 2012). Laterally, tidal channels (FA3.6) pinch out into fine-grained laminated strata (FA3.5) interpreted as tidally influenced central estuary bay deposits (Kvale 2012). Flood tidal delta (FA3.8) deposits reflect the interaction of both wave and tide processes near a tidal inlet (Fitzgerald *et al.* 2012).

Estuary intervals are capped with a tidal bar complex (FA3.7; Fig. 1.9D) and back stepping barrier island strata (FA1.3, FA1.4; Fig. 1.9A,J). Tidal bar deposits (FA3.7; Fig. 1.9D) are identified based on lateral accretion master surfaces (Dalrymple & Choi 2007; Olariu *et al.* 2012), creating longitudinal tidal bars (Dalrymple & Rhodes 1995). Shoreface sandstones (FA1.3, FA1.4; Fig. 1.9J) sharply juxtaposed above estuary fill (Fig. 1.9C) are interpreted as barrier island deposits. These shoreface deposits are distinguished by a planar erosional surface at the base (Olsen *et al.* 1999) followed by a mix of planar and trough cross-bedded sandstones with abundant *Ophiomorpha* burrows, similar to modern and recent examples (e.g., Carter 1978; Reinson 1992; Willis & Moslow 1994; Tye *et al.* 1999).

Decompaction Analysis

One-dimensional basin modeling was performed to extract decompacted thicknesses for representative stratigraphic sections from Buck Hollow and Main Canyon

(Fig. 1.10). Lithologies for the facies at Buck Hollow and Main Canyon were selected to best match measured section descriptions and field observations. Thicknesses and lithologies of the overburden were compiled and estimated from the literature (Table 1.3 and references therein). Auto-calculated seawater interface temperature (SWIT) estimates for 37° west latitude, North America were used (Kauerrauf & Hantschel 2009). Heat flow was held at a constant 60.00 mW/m^2. Decompacted thicknesses were extracted from the thickness overlay feature of the basin history output.

The decompacted thickness of Buck Hollow is 802 m, 1.76x expanded from its present-day measured thickness (456 m). The decompacted thickness of Main Canyon is 321 m, 2.03x expanded from its present-day measured thickness (158 m). After decompaction the John Henry Member at Buck Hollow is 481 m (2.5x) thicker than Main Canyon (Table 1.3). Sensitivity analysis was performed to assess the compaction variability of different coal lithologies (Table 1.4), and shows that the various coal lithologies tested all expanded 3-4x during decompaction.

Discussion

Depositional Model

Four regressive-transgressive (R-T) cycles define a depositional model for the John Henry Member at Buck Hollow. The letter-assigned shoreline intervals ("A-G" of Peterson 1969*a*; Fig. 1.5) of the John Henry Member are grouped into R-T cycles to describe the sequence stratigraphic architecture. R-T cycles are used (Cattaneo & Steel 2003; Zecchin 2007; Allen & Johnson 2011) rather than parasequence models (Kamola & Van Wagoner 1995; Posamentier & Allen 1999; Hampson & Storms 2003; Catuneanu *et*

al. 2009), because R-T cycles are more applicable to successions with significant transgressive deposits (Helland-Hansen & Gjelberg 1994; Arnott 1995; Zecchin, 2010). In this study, cycles begin with regressive surfaces (cf. T-R cycles of Embry & Johannessen 1993), because major tidal ravinement occurs at the base of transgressive units, creating irregular and variable boundaries (e.g., Swift 1968; Cattaneo & Steel 2003; Sixsmith *et al.* 2008; Chentnik *et al.* 2015). Conversely, combined wave-ravinement/flooding surfaces (Arnott 1995), which mark the base of regressive intervals, are relatively flat across the study area, creating consistent boundaries and datums. The John Henry Member R-T cycles at Buck Hollow (summarized below, in stratigraphic order) are likely third or fourth order, based on their thickness, expression, and averaged individual time duration of ~1.5 My (Vail *et al.* 1977; Vail & Mitchum 1979; Emery & Myers 1996). Within them, numerous higher-frequency cycles are present, the expression of which varies by depositional environment (e.g., coarsening-upwards parasequences in shoreface intervals and estuary-infilling coals).

R-T Cycle 1 ("A-B" Interval)

R-T cycle 1 is composed of a ~150 m-thick offshore mudstone interval (FA1.1). The base is a wave-ravinement/flooding surface (Fig. 1.4), characterised by a quartzite pebble conglomerate layer that can be traced regionally into Main Canyon (Chentnik *et al.* 2015) and Left Hand Collet Canyon (Fig. 1.1; Dooling 2013). This surface is flat and marks the base of the John Henry Member. The conglomerate layer is directly overlain by a thick (~150-163 m) succession of offshore mudstone comprising the "A" and "B" intervals of Peterson (1969*a, b*), henceforth "A-B". The transgressive portion of the cycle

cannot be distinguished from the regressive portion based on the outcrop exposure or from the biostratigraphic data. Therefore the two are not specifically differentiated. This interval is laterally continuous across the entire field area (~7 km along strike; Fig. 1.4).

The upper limit of R-T cycle 1 is a correlative conformity that can be traced up dip to the Lower John Henry Member Sequence Boundary (LJHMSB) in Main Canyon (Fig. 1.11). This surface exhibits significant (up to 22 m) incision along N-S trending erosional valleys in Main Canyon (Chentnik *et al.* 2015). However, there is no indication of subaerial exposure in Buck Hollow, only uninterrupted offshore sedimentation, suggesting a correlative conformity (Fig. 1.4). The position of the correlative conformity surface is estimated to be a few metres below the base of the first well-exposed cliff band of the "C" interval in R-T cycle 2 (Fig. 1.3B). This is supported by the biostratigraphic data that imply a relative shallowing (Fig. 1.5). Within the offshore "A-B" interval there are several bentonite beds. $^{40}Ar/^{39}Ar$ dating of biotite grains from the upper-most bentonite bed yielded an age of 88.6 ± 0.79 Ma (Fig. 1.5; Appendix).

R-T Cycle 2 ("C" and "D" Intervals)

R-T cycle 2 is ~140 m thick and records forced regression, resulting in basinward-stepping delta deposition followed by estuarine deposition during accretionary transgression (Figs. 1.4 & 1.12). R-T cycle 2 begins above the correlative conformity marking the upper limit of R-T cycle 1. Across that conformable surface, the offshore mudstone deposits of the "A-B" interval grade into more proximal siltstone and mudstone units of the basal "C" interval, with biostratigraphic indicators shifting to more proximal marine environments (Fig. 1.5). The regressive portion of R-T cycle 2 is composed of a

prograding wave-dominated delta (Figs. 1.3B & 1.12A). The delta interval comprises two ~21-27 m thick, coarsening-upwards, progradationally-stacked sequences of shore-parallel mouth bars, composed of delta front facies (FA2.1; Fig. 1.12A,B,J). These two smaller cycles are separated by a ~8 m-thick interbedded mudstone and sandstone interval, representing a minor basinward shift in facies which juxtaposes offshore deposits on top of deltaic upper shoreface deposits. The upper deltaic sequence contains more proximal facies relative to the lower deltaic sequence, suggesting basinward (northeast) progradation.

Strong longshore, storm-driven shelf currents are expected for the Western Interior Seaway (Slingerland & Keen 1999; Hampson 2010), and this is supported by palaeocurrent measurements from trough cross-beds within the delta front (Fig. 1.5). It is possible that these longshore currents made the delta asymmetrical (Bhattacharya & Giosan 2003). However, the subaerial morphology cannot be determined from the available along-strike outcrop exposures. The mouth bars preserved at Buck Hollow show wave influence and contain abundant terrigenous material (Fig. 1.7I), suggesting wave-dominated deposition in an area close to a sediment source (Fielding *et al.* 2005; Charvin *et al.* 2010). The delta is classified as wave-dominated because it contains combined-flow features within the delta front, but lacks the channelized and graded beds indicative of a river-dominated delta front (Li *et al.* 2011).

Above the regressive-transgressive turn around, a tidal ravinement surface juxtaposes tidal channel facies (FA3.6; Fig. 1.9B) directly on top of upper delta front facies (FA2.1; Fig. 1.7A,B), marking the base of the transgressive phase of R-T cycle 2. Laterally variable incision of 1-3 m occurs along this undulatory tidal ravinement surface,

which formed the estuary (Fig. 1.4). The back-barrier was infilled by coals (FA3.1; Fig. 1.8E) and distributary channels (FA3.4; Fig. 1.8O) during at least two different fill events. These coals grade from carbonaceous shale to coal vertically in a wetting-upward patterns (Fig. 1.8E; Wadsworth *et al.* 2010; Allen & Johnson 2011), suggesting partial infilling and buildup of terrigenous material within the estuary before continued transgression (Allen & Johnson 2011).

Estuary facies of the "D" interval vary laterally from north to south, reflecting a complex interplay of depositional subenvironments existing contemporaneously (Fig. 1.12B). Higher energy, channelized facies are concentrated in the northern part of the field area (North Mountain; Fig. 1.1B), whereas the lower energy, finer-grained facies are preserved in the southern portion of the field area (Skull Mountain; Figs. 1.1B & 1.3B). The facies distribution suggests the estuary did not have a classic funnel shape (Dalrymple *et al.* 1992). Instead, the estuary was likely broad and terraced, similar to modern Galveston Bay, Texas (Anderson *et al.* 2008). Galveston Bay shows shallow, protected deposition occurring away from channels and inlets, juxtaposing high and low energy deposits in pattern similar to those preserved in Buck Hollow. Abundant laminated mudstone intervals (FA3.5) and carbonaceous shales and coals (FA3.1; Fig. 1.8E) suggest that the finer-grained portion of terrestrially-derived estuarine sediment was trapped within the estuary.

Washover fans (FA3.2; Fig. 1.8A,C), tidal channels (FA3.6; Fig. 1.9B), and tidal bars (FA3.7; Fig. 1.9D) record the influx of marine sediment into the estuary. Longshore drift delivered clean, winnowed sand to the Buck Hollow shoreline, creating a barrier island and unusually sandy tidal deposits (Fig. 1.9A,J). The tidal deposits are not as

heterolithic as commonly implied by tidal facies models (Longhitano *et al.* 2012). The bimodal grainsize of correlative mudstone and medium- to coarse-grained sandstone facies within the estuary suggests rapid deposition and limited reworking. A similar distribution is present in Winyah Bay, South Carolina, USA, where >50% of the river-derived sediment is trapped within the main body of the estuary (Patchineelam *et al.* 1999). This creates both sandy and muddy bodies within the estuary, while longshore currents deliver sand to the barrier island and tidal deltas.

R-T cycle 2 is capped with a barrier island (FA1.3, FA1.4; Figs. 1.9J & 1.12C), which records the final stepped transgression during the "D" interval. The barrier island is bound both above and below by wave-ravinement surfaces. The basal wave-ravinement surface juxtaposes barrier island shoreface facies above estuary fill (e.g., Demarest & Kraft 1987). This surface is planar and laterally continuous across the Buck Hollow area; however, it is not obvious regionally. Therefore, we interpret the wave-ravinement surface at the base of the barrier island as a local feature, representing small-scale cyclicity, and the upper surface as the more significant wave-ravinement/flooding surface that bounds R-T cycle 2. This upper surface juxtaposes offshore deposits on top of upper shoreface strata as it truncates the barrier island deposits and caps the "D" interval. Erosion from wave ravinement removed the subaerial and foreshore components of the barrier island and was likely <10 m, roughly corresponding to fair weather wave base (Saito 1994; Cattaneo & Steel 2003). These barrier island deposits are similar to other examples of prograding shoreface successions overlying back-barrier facies (e.g., Mellere *et al*. 2005). However, because only back-barrier deposits are present 14 km up-dip in Main Canyon (rather than time-equivalent shoreface deposits), the "D" interval

shoreface succession section at Buck Hollow is interpreted as barrier islands detached from the mainland. We hypothesize that pulsated transgression (e.g., Rampino & Sanders 1980; Salzmann *et al.* 2013) caused the island to back step into the accommodation of the correlative estuary and briefly prograde before wave ravinement truncated the island, marking the top of R-T cycle 2.

The thickness of the transgressive portion of R-T cycle 2 (~65 m) suggests deposition on a shoreline with an accretionary trajectory. Advances in the understanding of shoreline trajectories (Cattaneo & Steel 2003; Bullimore *et al.* 2008; Henriksen *et al.* 2009) and study of outcrop examples, such as this one, suggest significant transgressive successions can be preserved in the right circumstances. Specifically, accumulation and preservation should occur on an accretionary shoreline, where the angle of the shoreline trajectory determines the thickness of transgressive deposits (Thorne & Swift 1991; Helland-Hansen & Hampson 2009; Allen & Johnson 2011), allowing for aggradation during transgression. Significant transgressive intervals are not accounted for in most sequence stratigraphic models (Arnott 1995), which predict sediment starvation and condensed deposition, or winnowing and lag deposition, during transgression (Van Wagoner *et al.* 1990; Posamentier *et al.* 1988; Galloway 1989).

Evidence for shoreline progradation in the middle of the transgressive estuary interval (repeated estuary sequences, distributary channel deposits, and development of multiple coals) questions the commonly used end-member distinction between estuaries (Dalrymple *et al.* 1992) and deltas (Bhattacharya 2003, 2010). Based on recent definitions (Dalrymple 2006; Dalrymple *et al.* 2012), an estuary becomes a delta when it is a “net exporter” of sediment. However, an estuary with ebb-dominance can be a “net-

exporter" if distributary channels infill with fluvially-derived sediment, causing it to act like a delta. Pulsated infilling can occur within a longer-duration, overall transgressive period (Roehler 1988; Souza-Filho *et al.* 2009; Hassan *et al.* 2012), defined as an estuary based on current depositional models. The transition from estuary to delta or vice versa is not unusual for the Western Interior Seaway (Roehler 1988; Plink-Björklund 2008; Kieft *et al.* 2011) and is also seen in the Quaternary and modern (Lessa *et al.* 1998; Gonzalez *et al.* 2001; Milli *et al.* 2013). These observations of pulsated progradation during estuary filling suggests estuaries are capable of "net-exporting" sediment, and that a more flexible definition including deltas and other facies may be appropriate for interpreting many ancient successions.

"D" interval strata are interpreted as estuarine rather than lagoonal, because of the visible river input and evidence for fluvial input to the shoreline in the Buck Hollow area. Both early (Pritchard 1967; Reddering 1980) and recent (Dalrymple *et al.* 1992; Boyd *et al.* 2006; Dalrymple *et al.* 2012) definitions of estuaries require proximity to a fluvial source. In contrast, early descriptions and definitions of lagoons do not reference fluvial input (Barnes 1980; Kjerfve 1986; Kjerfve & Magill 1989). More recent distinctions state that lagoons have little to no freshwater influx (Davis Jr. 1994). However, the term lagoon has been applied to the low energy areas of back-barrier systems with significant river input (Nichols 1989). The distinction between the two has been the subject of some discussion (Day 1980, 1981; Reddering 1980) because the morphology and characteristics of lagoons and estuaries are determined by a variety of processes, once again reflecting the complexity of paralic settings. Occasionally, the distinction is avoided by using the term "embayment" to described brackish conditions

(MacEachern *et al.* 1998). Improved nomenclature is required, particularly because a variety of classification schemes are currently being used (Dalrymple *et al.* 1992; Hume & Herdendorf 1988; Elliott & McLusky 2002; Potter *et al.* 2010), and some recent facies models (James & Dalrymple 2010) do not distinguish between estuaries and lagoons (Boyd 2010).

R-T Cycle 3 ("E" and "F" Intervals)

R-T cycle 3 is ~130 m thick and composed of regressive, prograding shoreface deposits ("E" interval; Fig. 1.12D) overlain by transgressive estuary deposits ("F" interval; Fig. 1.12E). The base of the R-T cycle 3 is marked by a combined wave-ravinement/flooding surface which juxtaposes offshore facies (FA1.1) on the truncated barrier island strata of the "D" estuary (FA1.3, FA1.4; Figs. 1.3 & 1.9J), marking the transgressive-regressive turn around. The regressive "E" interval contains three progradationally to aggradationally stacked, upward-coarsening wave-dominated shoreface successions (Fig. 1.6A,K), deposited as the shoreline built basinward. A tidal ravinement surface marks the regressive-transgressive turn around within R-T cycle 3, separating the tidal channels of the overlying transgressive "F" interval from the underlying regressive "E" upper shoreface deposits. The surface shows highly variable incision (~0-12 m; Fig. 1.4). The transgressive "F" estuary interval preserves tidal channels (FA3.6; Fig. 1.9B) at the base, deposited during estuary formation. Moving vertically up-section, it contains carbonaceous estuary fill (FA3.1; Fig. 1.8E) and bayhead delta deposits (FA3.5; Fig. 1.8I). The bayhead delta deposits in the "F" interval are laterally discontinuous over ~30-50 m indicating that a more proximal portion of the

estuary is preserved compared to the more distal portion preserved in the "D" interval. This suggests either more landward deposition, or an estuary that was narrower in the shore-perpendicular direction. Transgressive barrier island strata (FA1.3, FA1.4; Fig. 1.9J) overlie the bayhead delta succession. A wave-ravinement surface truncates the barrier island and a combined wave-ravinement and flooding surface separates R-T cycle 3 from overlying offshore facies (FA1.1) of R-T cycle 4.

R-T Cycle 4 ("G" Interval)

R-T cycle 4 is ~60 m thick and is the uppermost cycle of the John Henry Member. It is composed of the regressive "G" shoreface interval. The "G" interval consists of a single prograding wave-dominated shoreface succession (Fig. 1.12D), which exhibits a normal shoaling shoreface progression (FA1.1- 1.5; Fig. 1.6A; Plint 2010), grading vertically from offshore through foreshore deposits. A process change from marine to fluvial marks the top of the "G" interval. The facies grade conformably from foreshore into fluvial deposits. The first clearly trough cross-bedded, medium-grained, channelised sandstones are interpreted as the basal Drip Tank Member based on lithostratigraphic definitions (Peterson 1969*a*). The boundary is somewhat gradational, lacking clear evidence for prolonged subaerial exposure. Analysis by Lawton *et al*. (2014) in other parts of the Kaiparowits Plateau moved the location of the sequence boundary associated with the Drip Tank Member to near the top of the interval based on architectural, provenance, and palaeocurrent shifts just below the overlying Wahweap Formation (cf. Shanley & McCabe 1991). Accordingly, the top of R-T cycle 4 at Buck Hollow is interpreted as a process change from marine shoreface deposition to fluvial

sedimentation, probably below the main sequence boundary.

Energy Regime

Energy regime, a classification scheme based on the relative proportion of tide versus wave energy, is used to characterise and compare both modern and ancient coastlines (Hayes 1979; Davis Jr. & Hayes 1984; Vakarelov *et al.* 2011; Vakarelov & Ainsworth 2013; Ainsworth *et al.* 2015). The delta, shoreface, and estuary facies interpreted for Buck Hollow are consistent with deposition along a wave-dominated coastline (Davis Jr. & Hayes 1984; Davis Jr. 2013). This is fitting because the Western Interior Seaway was generally microtidal (Slater 1985; Ericksen & Slingerland 1990; Slingerland *et al.* 1996; Slingerland & Keen 1999), allowing wave energy to dominate relative to tidal energy. Energy and process indicators in the strata also support this hypothesis: both the deltaic and shoreface deposits contain abundant hummocky and swaley cross-stratification, grading into trough cross-bedding and planar to wavy laminations (Li *et al.* 2011; Vakarelov *et al.* 2011). The upper shoreface and upper delta front both lack tidal indicators expected for tidally influenced shoreface deposits, such as ebb-oriented current ripples and oscillation ripples (Dashtgard *et al.* 2009, 2012).

Transgressive estuarine deposits of the John Henry Member display increased tidal influence (FA2; Figs. 1.8 & 1.9) relative to the shoreface (FA1; Fig. 1.6) and deltaic strata (FA2; Fig. 1.7). This is the result of deposition in a protected back barrier, sheltered from the wave action of the open coast, with tidal magnification due to estuary funneling (Dalrymple 2010). The Kaiparowits region was located along the Utah Bight during John Henry Member deposition (Fig. 1.1; McGookey *et al.* 1972; Hampson 2010). The curved

embayment of the Utah Bight likely magnified the tides by dampening wave energy, similar to the modern Georgia Bight on the U.S. Atlantic coast. The Georgia Bight (~1,000 km long, ~400 km wide) increases from micro- (0-2 m) to meso-tidal (2-4 m) toward its apex (Davies 1964; Hayes 1994) and is roughly twice as a large as the ancient Utah Bight (~500 km long, ~200 km wide; McGookey *et al.* 1972). The tides heightened by the Utah Bight curvature probably contributed to the distinct tidal facies visible within the transgressive intervals of the John Henry Member. Despite this increased tidal influence, the John Henry Member estuaries are interpreted as wave-dominated. The presence of a barrier island system bounding the estuary aligns the Buck Hollow deposits most closely with the wave-dominated estuary end-member facies model (Dalrymple *et al.* 1992). Process regime changes are known to occur on short (4^{th} or 5^{th} order) timescales (Yoshida *et al.* 2007), and previous work suggests that Western Interior Seaway strata can record shifts from wave- to tide-dominated deposition (Seidler & Steel 2001; Plink-Björklund 2008). However, this variation in energy regime is not required for the John Henry Member at Buck Hollow. Instead, the coastline remained wave-dominated throughout deposition, leading to wave-influenced shoreline deposits and visible tidal indicators within protected back-barrier settings.

Regional Correlation

Regional correlations across the northern Kaiparowits Plateau show the time-space palaeogeographic variability of the foreland basin. The depositional model and relative sea level curve (Fig. 1.13) for Buck Hollow are similar but not identical to patterns interpreted across the northern Kaiparowits Plateau at Main Canyon (Fig. 1.11)

and Left Hand Collet (Fig. 1.14). Analysis of the north Kaiparowits Plateau reveals that a regional regression occurred during the "A-B-C" intervals. The shoreline shifted at least 14 km basinward between the "B" and "C" intervals as the coast prograded toward Buck Hollow (Fig. 1.13). The shoreface deposits that are preserved at Main Canyon (up dip; 14 km southwest) and Left Hand Collet (along strike, 40 km south southeast; Fig. 1.1) during the "A" and "B" intervals pinch out into offshore facies in Buck Hollow.

Throughout John Henry Member deposition, raised coal mires in the centre of the plateau (McCabe 1987; McCabe & Shanley 1992; Hettinger 2000) diverted low gradient, basin-axial fluvial systems northeast toward Main Canyon and Buck Hollow (Szwarc *et al.* 2014). The north- and northeast-flowing rivers resulted in valley incision at Main Canyon and delta deposition at Buck Hollow during the "C" interval (Fig. 1.11). The regression is described as forced because incision occurs at Main Canyon, implying potential down-stepping of the shoreline (Chentnik *et al.* 2015), and corresponding to a significant progradation of the shoreline at Buck Hollow marked by the progradation of delta-front facies over offshore deposits. This forced regression led Chentnik *et al.* (2015) to move the most significant hiatus within the lower John Henry Member from the "A" sequence boundary (as suggested by Shanley & McCabe 1992, 1993; Fig. 1.2) to the Lower John Henry Member Sequence Boundary (LJHMSB; Figs. 1.4 & 1.11) between the "B" and "C" shoreface intervals in the northern Kaiparowits Plateau. This suggestion is supported by the relatively old age for the lower John Henry Member (88.6 ± 0.79 Ma) documented in Buck Hollow (Fig. 1.5; Appendix), which implies that the "A-B" interval is older than previously thought and that a hiatus occurred higher in the section, i.e., during the LJHMSB and the "C" interval.

The forced regression ("C" interval) is capped by a tidal-ravinement surface marking the regressive-transgressive turn around in the basin, visible in all three areas (Figs. 1.11 & 1.14). Stepped, accretionary transgression ("D" interval) was then preserved across the northern Kaiparowits Plateau. The pulsated rise in relative sea level resulted in proximal estuarine facies at Main Canyon (Fig. 1.11), more distal estuarine and barrier island facies at Buck Hollow, and lower energy lagoon and barrier island facies at Left Hand Collet (Fig. 1.14). Abundant accommodation and sediment supply allowed Buck Hollow to have an accretionary shoreline trajectory (Helland-Hansen & Gjelberg 1994; Helland-Hansen & Martinsen 1996), leading to the deposition and preservation of thick transgressive packages.

The wave-ravinement/flooding surface at the base of the "E" interval is chosen as the datum for regional correlations (Figs. 1.11 & 1.14) due to its consistent expression at the base of easily-mappable, extensive exposures of similar facies. The "E" interval is comprised of prograding shoreface deposits in all three areas. Shoreface successions at Main Canyon and Left Hand Collet pinch out into offshore deposits at Buck Hollow. Continued progradation led to deposition of additional shoreface parasequences within the "E" interval at Buck Hollow (Fig. 1.4). A tidal-ravinement surface truncates the "E" interval, as "F" interval tidal channels cut into underlying upper shoreface strata (Figs. 1.11 & 1.14). Correlations between Main Canyon and Buck Hollow are less clear for the upper portion of the John Henry Member because coal fires have altered the strata at Main Canyon, creating clinker beds and masking the stratigraphy. Along strike in Left Hand Collet, a lagoon and barrier island interval (Dooling 2013) correlates to the estuary and barrier island interval at Buck Hollow. The "F" transgression was followed by a final

shoreface progradation (>10 km) during the "G" interval.

The R-T cycles of the north Kaiparowits Plateau reflect relative sea level shifts of ~10-50 m over ~1.5 My duration, interpreted as third or fourth order eustatic, tectonic, and/ or climatic signatures (Vail *et al.* 1977; Vail & Mitchum 1979; Emery & Myers 1996), similar to others interpreted for the John Henry Member (Fig. 1.1; Allen & Johnson 2010*b*, 2011). The R-T cycles at Buck Hollow do not seem to correspond to the "third order" eustatic fluctuations of the most recent global sea level curves (Fig. 1.13; Haq *et al.* 1987; Miller *et al.* 2005; Cloetingh & Haq 2015). Along with additional observations outlined below, this suggests that in addition to eustasy, other controls influenced relative sea level and deposition in the Kaiparowits Plateau.

Depositional Controls

Regional correlations show that the John Henry Member at Buck Hollow is highly expanded (2-3x) relative to other areas of deposition across the Kaiparowits Plateau. The JHM at Buck Hollow (456 m, compacted) is 289% of the Main Canyon section (158 m thick compacted; Fig. 1.11), and 179% of the Left Hand Collet section (255 m thick compacted; Fig. 1.14). These thickness variations imply local-scale (<15 km) variations in both sediment supply and accommodation, both considered here.

Sediment supply was unusually high at Buck Hollow because the area received sediment from multiple sources. Palaeocurrent data from the southern Kaiparowits region (Fig. 1.1; Gallin *et al.* 2010; Gooley *et al.* in press) show sediment was delivered to the shoreline mainly from the south in large distributive fluvial systems running transverse to the Mogollon Highlands and axial to the Sevier fold-thrust belt (Lawton *et al.* 2014;

Szwarc *et al.* 2014). Fluvial sediment supply was further heightened during the "C" interval through local incision at Main Canyon (Fig. 1.11). The monsoonal climate of the Western Interior Seaway increased summer runoff (Leier *et al.* 2005; Fricke *et al.* 2010). Monsoons are thought to be responsible for the high volumes of sediment delivered to the Kaiparowits region during Drip Tank Member deposition (Lawton *et al.* 2014), and the John Henry Member likely experienced similar effects. Buck Hollow also received sediment from south-directed coastal currents (Slingerland & Keen 1999) via longshore drift and storm reworking. Combined, these three processes supplied copious amounts of sediment to the Buck Hollow shoreline.

Sedimentation rate calculations allow comparisons between localities in the northern Kaiparowits Plateau (Table 1.5). A lack of precise age control prevents high-resolution calculations of sedimentation rates for each interval within the John Henry Member. Here, estimates were made for the entire John Henry Member (~4.1-8.5 My total duration) using youngest maximum depositional age ranges from detrital zircon U/Pb geochronology (Table 1.5; Szwarc *et al.* 2014). These ages are supported by the new $^{40}Ar/^{39}Ar$ bentonite date and biostratigraphy presented here, which indicates a late Coniacian to early Campanian age range for the John Henry Member (cf. Eaton 1991). Both the biostratigraphic and the zircon data suggest that John Henry Member deposition extended into the early Campanian, younger than previously acknowledged (Eaton 1991; Dyman & Cobban 2002). The John Henry Member at Buck Hollow was deposited at a compacted rate of 72.3 m/My and a decompacted rate of 127.3 m/My (Table 1.5). These rates are higher than compacted rates calculated for other areas of the plateau (25.1 m/My for Main Canyon, 53.5 m/My for Rogers Canyon, 56.2 m/My for Left Hand Collet; Table

1.5; locations shown in Fig. 1.1; Allen & Johnson 2010*b*; Dooling 2013). These rates are also twice the previous subsidence estimates of 25.6 m/My for the John Henry Member (Shanley & McCabe 1995, Fig. 21), which was based on subsidence curve showing 575 m of deposition (compacted) in the Kaiparowits Plateau over 22.5 My.

Calculated sedimentation rates for all three John Henry Member localities (Table 1.5) fall within the range of global sedimentation rates calculated at million year time scales (Sadler 1981, 1999; Sommerfield 2006). However, the values are high relative to estimates for other localities around the Western Interior Basin (Table 1.6). In comparing the strata of Buck Hollow to other formations within the Western Interior Seaway, we also note that some isopach maps, mainly derived from well data (Weimer 1960; Roberts & Kirschbaum 1995; Painter & Carrapa 2013) do not fully account for preserved outcrop thicknesses in the region (Doelling *et al.* 2000; Hettinger *et al.* 2009).

In addition to high sediment supply, high rates of accommodation are required to preserve these thick accumulations of strata. Multiple autogenic and allogenic controls could have contributed to the overall regional thickness patterns, as well as the observed 2-3x expanded thickness increase over 14 km along depositional dip in the northern Kaiparowits Plateau. Below possible explanations are explored including: regional tectonics, eustasy, local structures/tectonics, pre-existing topography, and differential and early compaction (Fig. 1.15). Decompaction analysis and calculated sedimentation rates help to tease apart the complex and interrelated controls.

High accommodation across the Kaiparowits Plateau was likely the result of eustasy and/or regional tectonics, whereas more local controls are required to explain the dramatic thickness differences between Buck Hollow and other nearby locations. Global

sea level curves indicate possible short-term ~5-100 m amplitude shifts possible during the Late Cretaceous (Fig. 1.13), interpreted as third order cycles (Miller *et al.* 2005; Cloetingh & Haq 2015). Eustasy could have contributed to the regional sedimentation patterns. However, we note that new age data and refined sea level curves indicate a disconnect between regional and global signals versus local expressions in the Kaiparowits region (Fig. 1.13).

Flexural loading by the Sevier fold-thrust belt created tectonic subsidence in the Kaiparowits region (Jordan 1981; Currie 2002; Painter & Carrapa 2013) which was enhanced by dynamic processes (Mitrovica *et al.* 1989; Liu *et al.* 2011, 2014). Detrital zircons from the Sevier fold-thrust belt are more prevalent in the upper portion of the John Henry Member (Szwarc *et al.* 2014), suggesting syn-depositional tectonism and increased sediment supply from uplift-driven, and possibly climate-enhanced, erosion. Duplex development occurred on the Paxton thrust sheet (DeCelles *et al.* 1995; Ismat & Mitra 2001; DeCelles & Coogan 2006; Szwarc *et al.* 2014) while the Wah Wah and Blue Mountain thrust sheets were also active (Goldstrand 1994). This Sevier tectonism occurred ~200 km west of the Kaiparowits Plateau (DeCelles 2004; DeCelles & Coogan 2006; Tindall *et al.* 2010), and the inferred forebulge was located perhaps as far east as central Colorado (White *et al.* 2002; DeCelles 2004). This placed the Kaiparowits Plateau within the 'medial' part of the foredeep. Given the evidence for Mogollon-derived sediment being delivered into the basin (Szwarc *et al.* 2014), the Mogollon Highlands might also be considered a flexural control on subsidence in this part of the foredeep, although only local evidence for Cretaceous-aged thrusting has been clearly documented (Salem 2009).

Regional tectonics, eustasy, climate, and associated sediment supply variations can explain regionally high deposition and preservation rates, but they do not easily account for the local differences between Main Canyon and Buck Hollow. Some of the local thickness differences can be attributed to incision and sediment bypassing. During the "C" interval, up to 22 m of strata are removed from Main Canyon during incised valley formation (Fig. 1.15; Chentnik *et al.* 2015). Additional sediment removal could have occurred during other intervals, perhaps up to ~50 m. The erosion and bypassing occurring in Main Canyon relate to delta deposition in Buck Hollow, suggesting an inherent accommodation difference between the two areas at that time. Similarly, pre-existing topography such as a local shelf-edge break could accentuate even relatively small variations in relative sea level (Dolson *et al.* 1991).

Perhaps the most plausible explanation for the thickness differences between Main Canyon and Buck Hollow is local structural activity (Fig. 1.15). Structural deformation in the northern Kaiparowits is generally thought to have occurred after John Henry Member deposition, specifically during early-stage Laramide tectonism, the beginning of which has been extended into the Campanian in this region (Davis and Bump 2009; Tindall *et al*. 2010). A nearby example of syn-tectonic oblique reverse faulting caused 2.8x thickening locally within the Wahweap Formation (80-76 Ma) on the western edge of the Kaiparowits Plateau (Tindall & Davis 1999; Tindall *et al.* 2010). Applying similar fault-driven thickening (~2.8x) to the compacted thicknesses of Main Canyon and Left Hand Collet yields a range of possible local tectonic accommodation (~450-700 m) for Buck Hollow (Fig. 1.15). Located further east, Buck Hollow is in the proximity of local structural features such as the Dutton Monocline (Hettinger 2000), as

well as numerous small-scale folds, specifically, a slight fold in Main Canyon that appears to be syn-depositional (Chentnik 2014). To date there is no reported evidence of Sevier-related blind thrusts propagating this far into the foredeep. Thus, although most of the John Henry Member is Santonian in age, we suggest there could be some overlap with very early, Laramide-style structures, perhaps related to the adjacent Circle Cliffs Uplift (Sargent & Hansen 1982; Davis 1999; Davis & Bump 2009).

Finally, differential compaction is considered as an additional, simple explanation for the observed John Henry Member thickness variation in the northern Kaiparowits Plateau. However, both locations have similar lithologies and overburden histories, and thus preliminary calculations indicate similar expansion for both Buck Hollow (1.76 x measured thickness) and Main Canyon (2.03 x measured thickness; Fig. 1.10). Because the decompaction rates of the two areas are fairly similar, the geometries of the regional correlation (Fig. 1.11) hold, suggesting that the interpreted relationships and surfaces are valid. If 1.76x expansion is applied to the original thickness of Main Canyon (158 m), the decompacted thickness is 278 m. The difference between this and the calculated decompacted thickness (321 m) is 43 m, representing the accommodation accounted for by postdeposition compaction (Fig. 1.15). This accounts for ~9% of the total (481 m) accommodation difference between the areas. Thickness differences may also be attributed to the presence of coal. Peat to coal compaction rates are not well constrained, with estimates varying from 1.4:1 to 30:1 (Ryer & Langer 1980; Collinson & Scott 1987; McCabe 1987). Sensitivity analysis was carried out to assess whether variable compaction of coal could be responsible for the thickness differences in the study areas. Common coal and carbonaceous silt lithologies assessed in PetroMod® showed 3-4x

postdepositional decompaction (Table 1.4). Therefore, the variation in coal thickness (<5 m) between Buck Hollow and Main Canyon is accounted for in the overall calculations, and is probably not responsible for the 481 m thickness difference between the two areas.

Early differential compaction, which creates space from loading and dewatering during deposition, is not often considered as a control on accommodation. Compaction has been studied in detail by soil engineers to understand small scale compaction (10^0 m) at geologically instantaneous time scales (10^1 years) in the modern (Terzaghi 1943; British Geotechnical Society 1975), and it is has been considered at broader time scales for some geological basins (>10^5 years; Athy 1930; Weller 1959). The effects of compaction at meso-scale (10^1-10^3 years) are poorly understood, yet can play a key role in deposition and preservation (Guber & Slingerland 1981; Kooi & de Vries 1998; Meckel *et al.* 2006, Meckel *et al.* 2007; Rosati 2009). These meso-scale processes are absent from the mechanical compaction models used in standard basin modeling software.

Early differential compaction could have occurred in both the offshore and estuary facies at Buck Hollow. The ~160 m thick "A-B" interval may have undergone early compaction and dewatering. Because compaction was taking place, sediment could accumulate without altering the available accommodation. This would have stabilized relative sea level locally and allowed prolonged deposition. Recent advances in mudstone depositional processes suggest that hyperpycnal flows deliver abundant sediment to basins (Schieber *et al.* 2007; Schieber & Southard 2009), making accommodation the limiting control on deposition. Compaction is dependent on the overlying load and the duration of deposition. Therefore, it is difficult to integrate estimates for ancient

examples. Mud compaction is estimated to occur at 0.1 mm/yr with >40% compaction possible (Kooi & de Vries 1998). If similar rates are applied to the decompacted thickness of the "A-B" interval mudstones, a maximum of 145 m of accommodation could have been created over 1.45 million years. If the deposits did not reach their maximum early compaction during deposition, further compaction could have occurred during deposition of the "C" interval when 50 m of delta sandstones were rapidly deposited on top of the underlying "A-B" mudstones.

It is probable that syn-depositional differential compaction also took place during the "D" and "F" intervals as barrier island shorefaces stepped landward, compressing the underlying fine-grained, carbonaceous bay fill and peat (Olsen *et al.* 1999; Rosati *et al.* 2010), which is known to compact during deposition (Nadon 1998). Modern silt and peat compaction rates are highly variable, ranging over three orders of magnitude (Table 1.7), however, they can be used to estimate possible early compaction in the ancient. If the ~9 m of coaly facies at Buck Hollow compacted by 40% (Bloom 1964; van Asselen 2011) it could have created a maximum of 3.6 m of space in 144 years using the rate of 0.025 m/yr (Rosati *et al.* 2010). This accounts for some, but not all of the accommodation required to preserve the 10-31 m thick barrier island deposits in the "D" and "F" intervals. Early compaction of both the "A-B" interval mudstones and the coals of the "D" interval account for a maximum of 148 m of accommodation (Fig. 1.15), which is 31% of the thickness difference between Main Canyon and Buck Hollow (Figs. 1.10 & 1.11).

In summary, while the primary and more regional-scale controls on accommodation and sediment supply are relatively well known, differentiating the local-

scale controls is challenging (Fig. 1.15). Tectonic and eustatic controls on both accommodation and sediment supply are acknowledged and were likely primary signals in the Cretaceous Kaiparowits region, in addition to climate as a moderating factor on sediment supply. Even at this broad scale, however, questions remain regarding the importance of the Mogollon Highlands both on sediment input into the basin as well as possible additional flexural load, not currently accounted for in most models for the Sevier foredeep. The possible role of dynamic subsidence also has not been fully explored, but probably impacted an area much larger than the one being considered here (Liu *et al.* 2011, 2014). Similarly, at the more local scale, while tectonic or structural controls are the most likely explanation for dramatic thickening in the northern Kaiparowits Plateau, there is not yet a discrete structure or other feature than can be linked directly to tectonic activity. Initiation of what would become basement-involved Laramide structures seems the best working hypothesis, but this suggests much earlier development of the "broken foreland" than previously interpreted (Dickinson *et al.* 1988; McQueen & Beaumont 1989). Finally, palaeotopography and differential compaction, particularly early compaction of mudstone and peat, could be a significant factor on the same order as predicted eustatic excursions for the same time scales (Fig. 1.15), though these are not typically considered in many subsidence history analyses.

Conclusions

The John Henry Member at Buck Hollow provides a new example of the time-space variability possible for paralic facies in a single location, providing new data to improve facies, depositional, and predictive models. The high accommodation, high

sediment supply setting allowed for preservation of multiple thick, stacked, regressive-transgressive cycles, including delta and shoreface successions interbedded with more heterogeneous estuary deposits. Sedimentary structures preserved within the strata suggest that the coastline was wave-dominated throughout John Henry Member deposition. The transgressive estuarine deposits display clear tidal influence, likely the result of protection from wave reworking provided by barrier islands, as well as tidal magnification due to funneling and the Utah Bight embayment.

The John Henry Member at Buck Hollow varies from up-dip equivalent strata at Main Canyon and along-strike strata at Left Hand Collet. Within the forced regression of the "A-B-C" intervals, delta deposition occurred at Buck Hollow, down-dip of incised valleys at Main Canyon. Buck Hollow shows more river influence relative to Left Hand Collet, displaying fluvial input in the form of distributary channels and bayhead delta deposits within the estuary intervals, which were deposited during stepped, accretionary transgressions. Despite these differences, shoreline trends were consistent regionally, and major surfaces extend across the basin. Correlations from Buck Hollow both up-dip and along-strike show the variability possible in a basin with partially disconnected accommodation and sediment supply controls.

The John Henry Member at Buck Hollow is 2-3x expanded relative to other localities across the Kaiparowits Plateau. While tectonics, eustasy, and climate moderated relative sea level for the basin as a whole, these regional processes cannot explain the local (<14 km) thickness differences and unusual geometries preserved in the northern Kaiparowits Plateau. Decompaction calculations show that the unusual geometries are not purely the result of postdepositional differential compaction. Differential compaction

does account for ~43 m of accommodation while erosion from incision contributes up to 22 m. However, these two processes only explain ~13.5% of the accommodation differential between Main Canyon and Buck Hollow. Tectonic activity on local structures is the most plausible explanation for the accommodation difference between the areas and could account for up to ~450-700 m additional deposition at Buck Hollow. Not often considered in foreland basin studies, early compaction could have contributed up to ~145 m of accommodation. Quantification of local controls highlights the myriad of processes contributing to the preservation of paralic strata in the Kaiparowits Plateau.

Acknowledgements

This research is supported by the Rocks2Models research consortium, Cari Johnson and Lisa Stright, PI's, with funding from Chevron, ConocoPhillips, Hess Corporation, Shell, and Statoil. We are very grateful to David Pocknall of Hess Corporation for providing biostratigraphic analyses, and Laura Webb and Daniel Jones at the University of Vermont for performing $^{40}Ar/^{39}Ar$ geochronological analysis cited in this study. Julia Mulhern also received funding from a University of Utah Graduate Research Fellowship, Rocky Mountain Association of Geologists Foundation Babcock Scholarship, and SEPM Rocky Mountain Section Donald Smith Research Grant. We acknowledge Schlumberger for academic licenses for PetroMod® basin modelling software and other software. We also thank the Grand Staircase Escalante National Monument and the Dixie National Forest for their support of field based research in the Kaiparowits Plateau. We are grateful for the many colleagues and students who assisted in the field and contributed to discussions, particularly B. Chentnik. Finally, we thank

Gary Hampson, Massimo Zecchin, and an anonymous reviewer for their constructive comments, which improved the original manuscript.

References

AHLBRANDT, T.S., CHARPENTIER, R.R., KLETT, J.W., SCHMOKER, C.J., SCHENK, G.F., & ULMISHEK, T.S. 2005. Global resource estimates from total petroleum systems. *American Association of Petroleum Geologists Memoir*, **86**, 1–334.

AINSWORTH, R.B., VAKARELOV, B.K. & NANSON, R.A. 2011. Dynamic spatial and temporal prediction of changes in depositional processes on clastic shorelines: toward improved subsurface uncertainty reduction and management. *American Association of Petroleum Geologists Bulletin*, **95**, 267–297, doi: 10.1306/06301010036.

AINSWORTH, R.B., VAKARELOV, B.K., LEE, C., MACEACHERN, J.A., MONTGOMERY, A.E., RICCI, L.P. & DASHTGARD, S.E. 2015. Architecture and evolution of a regressive, tide-influenced marginal marine succession, Drumheller, Alberta, Canada. *Journal of Sedimentary Research*, **85**, 596–625, doi: http://dx.doi.org/10.2110/jsr.2015.33.

ALLEN, J.L. & JOHNSON, C.L. 2010a. Facies control on sandstone composition (and influence of statistical methods on interpretations) in the John Henry Member, Straight Cliffs Formation, southern Utah, USA. *Sedimentary Geology*, **230**, 60–76, doi: 10.1016/j.sedgeo.2010.06.023.

ALLEN, J.L. & JOHNSON, C.L. 2010b. Sedimentary facies, paleoenvironments and relative sea level changes in the John Henry Member, Cretaceous Straight Cliffs Formation, southern Utah, USA. *In*: Carney, S.M., Tabet, D.E. & Johnson, C.L. (eds) *Geology of South-Central Utah*. Salt Lake City, Utah Geological Association Publication, 225–247.

ALLEN, J.L. & JOHNSON, C.L. 2011. Architecture and formation of transgressive-regressive cycles in marginal marine strata of the John Henry Member, Straight Cliffs Formation, Upper Cretaceous of southern Utah, USA. *Sedimentology*, **58**, 1486–1513, doi: 10.1111/j.1365-3091.2010.01223.x.

ALLEN, J.R.L. 1966. On bed forms and paleocurrents. *Sedimentology*, **6**, 153.

AMBROSE, W.A. & AYERS, W.B. 2007. Geologic controls on transgressive-regressive cycles in the upper Pictured Cliffs Sandstone and coal geometry in the lower Fruitland Formation, northern San Juan Basin, New Mexico and Colorado. *American Association of Petroleum Geologists Bulletin*, **91**, 1099–1122, doi:

10.1306/03080706040.

ANDERSON, J.B., RODRIGUEZ, A.B., MILLIKEN, K.T. & TAVIANI, M. 2008. The Holocene evolution of the Galveston estuary complex, Texas: evidence for rapid change in estuarine environments. *In*: Anderson, J.B. & Rodriguez, A.B. (eds) *Response of Upper Gulf Coast Estuaries to Holocene Climate Change and Sea-Level Rise*. Geological Society of America Special Papers, **443**, 89–104, doi: 10.1130/2008.2443(06).

ANTIA, J. & FIELDING, C.R. 2011. Sequence stratigraphy of a condensed low-accommodation succession: Lower Upper Cretaceous Dakota Sandstone, Henry Mountains, southeastern Utah. *American Association of Petroleum Geologists Bulletin*, **95**, 413–447, doi: 10.1306/06301009182.

ARNOTT, R.W.C. 1995. The parasequence definition-are transgressive deposits inadequately addressed? *Journal of Sedimentary Research*, **B65**, 1–6, doi: 10.1306/D42681D0-2B26-11D7-8648000102C1865D.

ATHY, L.F. 1930. Density, porosity, and compaction of sedimentary rocks. *American Association of Petroleum Geologists Bulletin*, **14**, 194–200, doi: 10.1306/3D93289E-16B1-11D7-8645000102C1865D.

BARNES, R.S.K. 1980. *Coastal Lagoons: The Natural History of a Neglected Habitat*. Cambridge England, Cambridge University Press, 106.

BARWIS, J.H. & HAYES, M.O. 1985. Antidunes on modern and ancient washover fans. *Journal of Sedimentary Research*, **55**, 907–916, doi: 10.1306/212F883C-2B24-11D7-8648000102C1865D.

BECKER, M.A., WELLNER, R.W., MALLERY, C.S. & CHAMBERLAIN, J.A. 2010. Chondrichthyans from the lower Ferron Sandstone Member of the Mancos Shale (Upper Cretaceous: Middle Turonian) of Emery and Carbon Countires Utah, USA . *Journal of Paleontology*, **84**, 248–266, doi: 10.1666/09-053r.1.

BELAÚSTEGUI, Z. & DE GIBERT, J.M. 2013. Bow-shaped, concentrically laminated polychaete burrows: a *Cylindrichnus concentricus* ichnofabric from the Miocene of Tarragona, NE Spain. *Palaeogeography, Palaeoclimatology, Palaeoecology*, **381-382**, 119–127, doi: 10.1016/j.palaeo.2013.04.021.

BHATTACHARYA, J.P. 2003. Deltas and estuaries. *In*: Middleton, G.V. (ed) *Encyclopedia of Sedimentology*. Kluwer Academic, 145–152.

BHATTACHARYA, J.P. 2010. Deltas. *In*: James, N.P. & Dalrymple, R.W. (eds) *Facies Models 4*. St. John's, Newfoundland, Geolgical Society of Canada, 233–264.

BHATTACHARYA, J.P. & GIOSAN, L. 2003. Wave-influenced deltas: geomorphological

implications for facies reconstruction. *Sedimentology*, **50**, 187–210, doi: 10.1046/j.1365-3091.2003.00545.x.

BHATTACHARYA, J.P. & MACEACHERN, J.A. 2009. Hyperpycnal rivers and prodeltaic shelves in the Cretaceous Seaway of North America. *Journal of Sedimentary Research*, **79**, 184–209, doi: 10.2110/jsr.2009.026.

BHATTACHARYA, J.P. & WALKER, R.G. 1991. River- and wave-dominated systems of the Upper Cretaceous Dunvegan Formation, northwestern Alberta. *Bulletin of Canadian Petroleum Geology*, **39**, 165–191.

BLOOM, A.L. 1964. Peat accumulation and compaction in a Connecticut coastal marsh. *Journal of Sedimentary Petrology*, **34**, 599–603, doi: 10.1306/74D710F5-2B21-11D7-8648000102C1865D.

BLUM, M.D. & ASLAN, A. 2006. Signatures of climate vs. sea-level change within incised valley-fill successions: Quaternary examples from the Texas Gulf Coast. *Sedimentary Geology*, **190**, 177-211, doi: 10.1016/j.sedgeo.2006.05.024.

BOBB, M.C. 1991. *The Calico Bed, Upper Cretaceous, Southern Utah: A Fluvial Sheet Deposit in the Western Interior Foreland Basin and Its Relationship to Eustasy and Tectonics*. MS thesis,University of Colorado, Boulder, CO.

BOOTHROYD, J.C., FRIEDRICH, N.E. & MCGINN, S.R. 1985. Geology of microtidal coastal lagoons: Rhode Island. *Marine Geology*, **63**, 35–76, doi: http://dx.doi.org/10.1016/0025-3227(85)90079-9.

BOYD, R. 2010. Transgressive wave-dominated coasts. *In*: James, N.P. & Dalrymple, R.W. (eds) *Facies Models 4*. St. John's, Newfoundland, Geological Association of Canada, 265–294.

BOYD, R., DALRYMPLE, R.W., ZAITLIN, B.A. & DALRYMPLE, M. 2006. Estuarine and incised-valley facies models. *In*: Posamentier, H.W. & Walker, R.G. (eds) *Facies Models Revisited*. SEPM Special Publication, **84**, 171–235, doi: 10.2110/pec.06.84.

BRITISH GEOTECHNICAL SOCIETY. 1975. *Settlement of Structures*. London, Pentech Press, 811.

BULLIMORE, S.A., HELLAND-HANSEN, W., HENRIKSEN, S. & STEEL, R.J. 2008. Shoreline trajectory and its impact on coastal depositional environments: an example from the Upper Cretaceous Mesaverde Group, northwestern Colorado, U.S.A. *In*: Hampson, G.J. (ed) *Recent Advances in Models of Siliciclastic Shallow-Marine Stratigraphy*. SEPM Special Publication, **90**, 209–236.

CARTER, C.H. 1978. A regressive barrier and barrier-protected deposit: depositional environments and geographic setting of the Late Tertiary Cohansey Sand. *Journal of*

Sedimentary Research, **48**, 933–949, doi: 10.1306/212F75AE-2B24-11D7-8648000102C1865D.

CATTANEO, A. & STEEL, R.J. 2003. Transgressive deposits: a review of their variability. *Earth-Science Reviews*, **62**, 187–228, doi: 10.1016/S0012-8252(02)00134-4.

CHARVIN, K., HAMPSON, G.J., GALLAGHER, K.L. & LABOURDETTE, R. 2010. Intra-parasequence architecture of an interpreted asymmetrical wave-dominated delta. *Sedimentology*, **57**, 760–785, doi: 10.1111/j.1365-3091.2009.01118.x.

CHENTNIK, B.M. 2014. *Valleys, Estuaries, and Lagoons: Paleoenvironments and Regressive-Transgressive Architecture of the Upper Cretaceous Straight Cliffs Formation*. MS thesis, University of Utah, Salt Lake City, UT.

CHENTNIK, B.M., JOHNSON, C.L., MULHERN, J.S. & STRIGHT, L.E. 2015. Valleys, estuaries, and lagoons: paleoenvironments and regressive-transgressive architecture of the Upper Cretaceous Straight Cliffs Formation. *Journal of Sedimentary Research,* **85**, 1166–1196.

CLIFTON, H.E. 2006. A reexamination of facies models for clastic shorelines. *In*: Posamentier, H.G. & Walker, R.G. (eds) *Facies Models Revisited*. SEPM Special Publication, **84**, 293–337.

CLOETINGH, S. & HAQ, B.U. 2015. Inherited landscapes and sea level change. *Science*, **347**, 1258375, doi: 10.1126/science.1258375.

COLLINSON, M.E. & SCOTT, A.C. 1987. Implications of vegetational change through the geological record on models for coal-forming environments. *Geological Society, London, Special Publications*, **32**, 67–85, doi: 10.1144/GSL.SP.1987.032.01.06.

COOPER, J.A.G. 1993. Sedimentation in a river dominated estuary. *Sedimentology*, **40**, 979–1017, doi: 10.1111/j.1365-3091.1993.tb01372.x.

CUMBAA, S.L., SHIMADA, K. & COOK, T.D. 2010. Mid-Cenomanian vertebrate faunas of the Western Interior Seaway of North America and their evolutionary, paleobiogeographical, and paleoecological implications. *Palaeogeography, Palaeoclimatology, Palaeoecology*, **295**, 199–214, doi: 10.1016/j.palaeo.2010.05.038.

CURRAY, J.R. 1964. Transgressions and regressions. *In*: Miller, R.L. (ed) *Papers in Marine Geology, Shepard Commemorative Volume*. New York, Macmillan, 175–203.

CURRIE, B.S. 2002. Structural configuration of the early Cretaceous Cordilleran forland-basin system and Sevier thrust system, Utah and Colorado. *The Journal of Geology*, **110**, 697–718.

DALRYMPLE, R.W. 2006. Incised valleys in time and space: an introduction to the volume and an examination of the controls on valley formation and filling. *In*: Dalrymple, R.W., Leckie, D.A. & Tillman, R.W. (eds) *Incised Valleys in Time and Space*. SEPM Special Publication, **85**, 5–12.

DALRYMPLE, R.W. 2010. Tidal depositional systems. *In*: James, N.P. & Dalrymple, R.W. (eds) *Facies Models 4*. St. John's, Newfoundland, Geological Association of Canada, 201–232.

DALRYMPLE, R.W. & CHOI, K. 2007. Morphologic and facies trends through the fluvial–marine transition in tide-dominated depositional systems: a schematic framework for environmental and sequence-stratigraphic interpretation. *Earth-Science Reviews*, **81**, 135–174, doi: 10.1016/j.earscirev.2006.10.002.

DALRYMPLE, R.W. & RHODES, R.N. 1995. Estuarine dunes and bars. *Developments in Sedimentology*, **53**, 359–422, doi: 10.1016/S0070-4571(05)80033-0.

DALRYMPLE, R.W., ZAITLIN, B.A. & BOYD, R. 1992. Estuarine facies models: conceptual basis and stratigraphic implications. *Journal of Sedimentary Research*, **62**, 1130–1146, doi: 10.1306/D4267A69-2B26-11D7-8648000102C1865D.

DALRYMPLE, R.W., MACKAY, D.A., ICHASO, A.A. & CHOI, K.S. 2012. Processes, morphodynamics, and facies of tide-dominated estuaries. *In*: Davis Jr, R.A. & Dalrymple, R.W. (eds) *Principles of Tidal Sedimentology*. Dordrecht, Springer Netherlands, 79–107.

DASHTGARD, S.E., GINGRAS, M.K. & MACEACHERN, J.A. 2009. Tidally modulated shorefaces. *Journal of Sedimentary Research*, **79**, 793–807, doi: 10.2110/jsr.2009.084.

DASHTGARD, S.E., MACEACHERN, J.A., FREY, S.E. & GINGRAS, M.K. 2012. Tidal effects on the shoreface: towards a conceptual framework. *Sedimentary Geology*, **279**, 42–61, doi: http://dx.doi.org/10.1016/j.sedgeo.2010.09.006.

DAVIES, J.L. 1964. A morphogenic approach to world shorelines. *Zeitschrift für Geomorphologie*, **8**, 127–142.

DAVIES, R., HOWELL, J., BOYD, R., FLINT, S. & DIESSEL, C. 2006. High-resolution sequence-stratigraphic correlation between shallow-marine and terrestrial strata: examples from the Sunnyside Member of the Cretaceous Blackhawk Formation, Book Cliffs, eastern Utah. *American Association of Petroleum Geologists Bulletin*, **90**, 1121–1140, doi: 10.1306/02210604077.

DAVIS, G.H. 1999. *Structural Geology of the Colorado Plateau Region of Southern Utah: With Special Emphasis on Deformation Bands*. Geological Society of America Special Paper, **342,** 157.

DAVIS, G.H. AND BUMP, A.P. 2009. Structural geologic evolution of the Colorado Plateau. *In*: Kay, S.M., Ramos, V.A., and Dickinson, W.R. (eds) *Back-bone of the Americas: Shallow Subduction, Plateau Uplift, and Ridge and Terrane Collision*. Geological Society of America, Memoir, **204**, 99-124.

DAVIS JR., R.A. 2013. A new look at barrier-inlet morphodynamics. *Journal of Coastal Research, Special Issue*, **69**, 1–12, doi: 10.2112/SI_69_2.

DAVIS JR., R.A. 2012. Tidal signatures and their preservation potential in stratigraphic sequences. *In*: Davis Jr., R. A. & Dalrymple, R. W. (eds) *Principles of Tidal Sedimentology*. Dordrecht, Springer Netherlands, 35–55.

DAVIS JR., R.A. 1994. Barrier island systems- a geologic overview. *In*: Davis Jr., R. A. (ed) *Geology of Holocene Barrier Island Systems*. Berlin, Springer-Verlag, 1–46.

DAVIS JR., R.A. & CLIFTON, H.E. 1987. Sea-level change and the preservation potential of wave-dominated and tide-dominated coastal sequences. *In*: Nummedal, D., Pilkey, O. H. & Howard, J. D. (eds) *Sea-Level Fluctuation and Coastal Evolution*. SEPM Special Publication, **41**, 167–178.

DAVIS JR., R.A. & HAYES, M.O. 1984. What is a wave-dominated coast? *Marine Geology*, **60**, 313–329, doi: http://dx.doi.org/10.1016/0025-3227(84)90155-5.

DAY, J.H. 1980. What is an estuary? *South African Journal of Science*, **76**, 198.

DAY, J.H. 1981. The nature, origin, and classification of estuaries. *In*: Day, J.H. (ed) *Estuarine Ecology: With Particular Reference to Southern Africa*. Rotterdam, Balkema, 1–6.

DECELLES, P.G. 2004. Late Jurassic to Eocene evolution of the Cordilleran thrust belt and foreland basin system, western, U.S.A. *American Journal of Science*, **304**, 105–168, doi: 10.2475/ajs.304.2.105.

DECELLES, P.G. 2012. Foreland basin systems revisited: variation in response to tectonic settings. *In*: Busby, C. & Azor, A. (eds) *Tectonics of Sedimentary Basins: Recent Advances*. Hoboken, Blackwell Publishing, 405–427.

DECELLES, P.G. & COOGAN, J.C. 2006. Regional structure and kinematic history of the Sevier fold-and-thrust belt, central Utah. *Geological Society of America Bulletin*, **118**, 841–864, doi: 10.1130/b25759.1.

DECELLES, P.G. & GILES, K. A. 1996. Foreland basin systems. *Basin Research*, **8**, 105–123, doi: 10.1046/j.1365-2117.1996.01491.x.

DECELLES, P.G., LAWTON, T.F. & MITRA, G. 1995. Thrust timing, growth of structural culminations, and synorogenic sedimentation in the type Sevier orogenic belt,

western United States. *Geology*, **23**, 699–702, doi: 10.1130/0091-7613(1995)023<0699:TTGOSC>2.3.CO;2.

DEMAREST, J. & KRAFT, J.C. 1987. Stratigraphic record of Quaternary sea levels: implications for more ancient strata. *In*: Nummedal, D., Pilkey, O.H. & Howard, J.D. (eds) *Sea-Level Fluctuation and Coastal Evolution*. SEPM Special Publication, **41**, 223–239, doi: 10.2110/pec.87.41.0223.

DEVINE, P.E. 1991. Transgressive origin of channeled estuarine deposits in the Point Lookout Sandstone, northwestern New Mexico: a model for Upper Cretaceous, cyclic regressive parasequences of the U.S. western interior. *American Association of Petroleum Geologists Bulletin*, **75**, 1039–1063.

DICKINSON, W.R., KLUTE, M. A., HAYES, M.J., JANECKE, S.U., LUNDIN, E.R. & OLIVARES, M.D. 1988. Paleogeographic and paleotectonic setting of Laramide sedimentary basins in the central Rocky Mountain region: alternative interpretation and reply -- Cather et al. 102 (2): 256 -- GSA Bulletin. *Geological Soceity of America Bulletin*, **100**, 1023, doi: 10.1130/0016-7606(1990)102<0256.

DOELLING, H.H. & WILLIS, G.C. 1999. Interim geologic map of the Escalante and parts of the Loa and Hite Crossing 30’ X 60' Quadranges, Garfield and Kane Counties, Utah. *Open File Report 368*.

DOELLING, H.H., BLACKETT, R.E., HAMBLIN, A.H., POWELL, J.D. & POLLOCK, G.L. 2000. Geology of Grand Staircase-Escalante National Monument, Utah. *In*: Sprinkel, D.A., Chidsey T.C., & Anderson, P.B. (eds) *Geology of Utah’s Parks and Monuments*. Utah Geological Association Publication, **28**, 189–231.

DOLSON, J., MULLER, D., EVETTS, M.J. & STEIN, J.A. 1991. Regional paleotopographic trends and production, Muddy Sandstone (Lower Cretaceous), central and northern Rocky Mountains. *American Association of Petroleum Geologists Bulletin*, **75**, 409–435.

DOOLING, P.R. 2013. *Tidal Facies, Stratigraphic Architecture, and Along-Strike Variability of a High Energy, Transgressive Shoreline, Late Cretaceous, Kaiparowits Plateau, Southern Utah*. MS thesis, University of Utah, Salt Lake City, UT.

DROSER, M.L. & BOTTJER, D.J. 1989. Ichnofabric of sandstones deposited in high-energy nearshore environments measurements and utilization. *Palaios*, **4**, 598–604.

DUKE, W.L. 1985. Hummocky cross-stratification, tropical hurricanes and intense winter storms. *Sedimentology*, **32**, 167–194.

DUMAS, S. 2005. Experiments on oscillatory-flow and combined-flow bed forms: implications for interpreting parts of the shallow-marine sedimentary record.

Journal of Sedimentary Research, **75**, 501–513, doi: 10.2110/jsr.2005.039.

DUMAS, S. & ARNOTT, R.W.C. 2006. Origin of hummocky and swaley cross-stratification - the controlling influence of unidirectional current strength and aggradation rate. *Geology*, **34**, 1073–1076, doi: 10.1130/G22930A.1.

DYMAN, T.S., COBBAN, W.A., ET AL. 2002. Upper Cretaceous marine and brackish water strata at Grand Staircase-Escalante National Monument, Utah: Geological Society of America Field Trip Road Log, May 2002.

DZUYNSKI, S. & SMITH, A.J. 1963. Convolute lamination, its origin, preservation, and directional significance. *Journal of Sedimentary Research*, **33**, 616–627, doi: 10.1306/74D70ED4-2B21-11D7-8648000102C1865D.

EATON, J.G. 1991. Biostratigraphic framework for the Upper Cretaceous rocks of the Kaiparowits Plateau, southern Utah. *In*: Nations, J. D. & Eaton, J. G. (eds) *Stratigraphy, Depositional Environments, and Sedimentary Tectonics of the Western Margin, Cretaceous Western Interior Seaway*. Geological Society of America, Special Paper, **260**, 47–63, doi: 10.1130/SPE260.

EATON, J.G. & NATIONS, J.D. 1991. Introduction; Tectonic setting along the margin of the Cretaceous Western Interior Seaway, southwestern Utah and northern Arizona. *In*: Nations, J. D. & Eaton, J. G. (eds) *Stratigraphy, Depositional Environments, and Sedimentary Tectonics of the Western Margin, Cretaceous Western Interior Seaway*. Geological Society of America, Special Paper, **260**, 1-8, doi: 10.1130/SPE260-p1.

EKDALE, A.A. & HARDING, S.C. 2015. *Cylindrichnus concentricus* toots in Howard, 1966 (trace fossil) in its type locality, upper Cretaceous, Wyoming. *Annales Societatis Geologorum Poloniae*, **85**, 427-432.

ELLIOTT, M. & MCLUSKY, D.S. 2002. The need for definitions in understanding estuaries. *Estuarine, Coastal and Shelf Science*, **55**, 815–827, doi: 10.1006/ecss.2002.1031.

EMBRY, A.F. & JOHANNESSEN, E.P. 1993. T-R sequence stratigraphy, facies analysis and reservoir distribution in the uppermost Triassic-Lower Jurassic succession, western Sverdrup Basin, Arctic Canada. *In*: Vorren, T. O., Bergsager, E., Dahl-Stamnes, O. A., Holter, E., Johansen, B., Lie, E. & Lund, T. B. (eds) *Arctic Geology and Petroleum Potential*. Norwegian Petroleum Society, Special Publication, **2**, 121–146.

EMERY, D. & MYERS, K.J. (eds). 1996. *Sequence Stratigraphy*. Oxford, Blackwell Science, 297.

ERICKSEN, M.C. & SLINGERLAND, R. 1990. Numerical simulations of tidal and wind-driven circulation in the Cretaceous Interior Seaway of North America. *Geological*

Society of America Bulletin, **102**, 1499–1516, doi: 10.1130/0016-7606(1990)102<1499:nsotaw>2.3.co;2.

FENIES, H. & TASTET, J. 1998. Facies and architecture of an estuarine tidal bar (the Trompeloup bar, Gironde Estuary, SW France). *Marine Geology*, **150**, 149–169, doi: http://dx.doi.org/10.1016/S0025-3227(98)00059-0.

FIELDING, C.R., TRUEMAN, J.D. & ALEXANDER, J. 2005. Sharp-based, flood-dominated mouth bar sands from the Burdekin River Delta of northeastern Australia: extending the spectrum of mouth-bar facies, geometry, and stacking patterns. *Journal of Sedimentary Research*, **75**, 55–66, doi: 10.2110/jsr.2005.006.

FITZGERALD, D.M., BUYNEVICH, I. & HEIN, C. 2012. Morphodynamics and facies architecture of tidal inlets and tidal deltas. *In*: Davis Jr., R.A. & Dalrymple, R.W. (eds) *Principles of Tidal Sedimentology*. Dordrecht, Springer Netherlands, 301–333, doi: 10.1007/978-94-007-0123-6.

FREY, R.W. 1990. Trace fossils and hummocky cross-stratification, Upper Cretaceous of Utah. *Palaios*, **5**, 203–218.

FRICKE, H.C., FOREMAN, B.Z. & SEWALL, J.O. 2010. Integrated climate model-oxygen isotope evidence for a North American monsoon during the Late Cretaceous. *Earth and Planetary Science Letters*, **289**, 11–21, doi: 10.1016/j.epsl.2009.10.018.

GALLIN, W.N., JOHNSON, C.L. & ALLEN, J.L. 2010. Fluvial and marginal marine architecture of the John Henry Member, Straight Cliffs Formation, Kelly Grade of the Kaiparowits Plateau, south-central Utah. *In*: Carney, S. M., Tabet, D. E. & Johnson, C. L. (eds) *Geology of South-Central Utah*. Salt Lake City, Utah Geological Association, 248–275.

GALLOWAY, W.E. 1975. Process framework for describing the morphologic and stratigraphic evolution of deltaic depositional systems. *In*: Broussard, M. L. (ed) *Deltas: Models for Exploration*. Houston, Texas, Houston Geological Society, 86–98.

GALLOWAY, W.E. 1989. Genetic stratigraphic sequences in basin analysis I: architecture and genesis of flooding-surface bounded depositional units. *American Association of Petroleum Geologists Bulletin*, **73**, 125–142, doi: 10.1306/703C9AF5-1707-11D7-8645000102C1865D.

GANI, M.R. & BHATTACHARYA, J.P. 2007. Basic building blocks and process variability of a Cretaceous delta: internal facies architecture reveals a more dynamic interaction of river, wave, and tidal processes than is indicated by external shape. *Journal of Sedimentary Research*, **77**, 284–302, doi: 10.2110/jsr.2007.023.

GAYES, P.T. 1983. *Primary consolidation and subsidence in transgressive barrier island*

systems. MS thesis, Pennsylvania State University, University Park, PA.

GEORGE, D.A. & HILL, P.S. 2008. Wave climate, sediment supply and the depth of the sand-mud transition: a global survey. *Marine Geology*, **254**, 121–128, doi: 10.1016/j.margeo.2008.05.005.

GINGRAS, M.K., MACEACHERN, J.A. & PEMBERTON, S.G. 1998. A comparative analysis of the ichnology of wave- and river-dominated allomembers of the Upper Cretaceous Dunvegan Formation. *Bulletin of Canadian Petroleum Geology*, **46**, 51–73.

GOLDSTRAND, P.M. 1994. Tectonic development of Upper Cretaceous to Eocene strata of southwestern Utah. *Geological Society of America Bulletin*, **106**, 145–154, doi: 10.1130/0016-7606(1994)106<0145:TDOUCT>2.3.CO;2.

GONZALEZ, R., DIAS, J.A. & FERREIRA, Ó. 2001. Recent rapid evolution of the Guadiana Estuary mouth (southwestern Iberian Peninsula). In: *International Coastal Symposium (ICS 2000): Challenges for the 21st Century in Coastal Sciences, Engineering, and Environment.* Journal of Coastal Research, Special Issue, **34**, 516–527.

GOOLEY, J.T., JOHNSON, C.L. & PETTINGA, L.A. in press. Spatial and temporal variation of fluvial architecture within a prograding clastic wedge of the Late Cretaceous Western Interior Basin (Kaiparowits Plateau), USA. *Journal of Sedimentary Research*, accepted November, 2015.

GRAHAM, G.H., JACKSON, M.D. & HAMPSON, G.J. 2015. Three-dimensional modeling of clinoforms in shallow-marine reservoirs: part 1. concepts and application. *American Association of Petroleum Geologists Bulletin*, **99**, 1013–1047, doi: 10.1306/01191513190.

GUBER, A.L. & SLINGERLAND, R. 1981. Compaction and lateral flow as processes in barrier island and associated environments. *In*: Slingerland, R., Guber, A.L. & Hanson, H.W. (eds) *Field Guide to Selected Coastal Geologic Problems on the Central Delmarva Penninsula, Eight Annual Assateague Shelf and Shore Workshop*. Penn State University, 14.

HAMPSON, G.J. 2010. Sediment dispersal and quantitative stratigraphic architecture across an ancient shelf. *Sedimentology*, **57**, 96–141, doi: 10.1111/j.1365-3091.2009.01093.x.

HAMPSON, G.J. & STORMS, J.E.A. 2003. Geomorphological and sequence stratigraphic variability in wave-dominated, shoreface-shelf parasequences. *Sedimentology*, **50**, 667–701, doi: 10.1046/j.1365-3091.2003.00570.x.

HANCOCK, J.M. & KAUFFMAN, E.G. 1979. The great transgressions of the Late

Cretaceous. *Journal of the Geological Society*, **136**, 175–186, doi: 10.1144/gsjgs.136.2.0175.

HAQ, B.U., HARDENBOL, J. & VAIL, P.R. 1987. Chronology of fluctuating sea levels since the Triassic. *Science*, **235**, 1156–1167, doi: 10.1126/science.235.4793.1156.

HASSAN, S.M., STEEL, R.J., EL BARKOOKY, A., HAMDAN, M., OLARIU, C. & HELPER, M.A. 2012. Stacked, Lower Miocene tide-dominated estuary deposits in a transgressive succession, Western Desert, Egypt. *Sedimentary Geology*, **282**, 241–255, doi: http://dx.doi.org/10.1016/j.sedgeo.2012.09.013.

HAYES, M.O. 1979. Barrier island morphology as a function of tidal and wave regime. *In*: Leatherman, S.P. (ed) *Barrier Islands from the Gulf of Mexico to the Gulf of St. Lawrence*. New York, Academic Press, 1–28.

HAYES, M.O. 1994. The Georgia Bight barrier system. *In*: Davis, R.A. (ed) *Geology of Holocene Barrier Island Systems*. Berlin, Springer-Verlag, 233–304.

HELLAND-HANSEN, W. & GJELBERG, J.G. 1994. Conceptual basis and variability in sequence stratigraphy: a different perspective. *Sedimentary Geology*, **92**, 31–52, doi: 10.1016/0037-0738(94)90053-1.

HELLAND-HANSEN, W. & HAMPSON, G.J. 2009. Trajectory analysis: Concepts and applications. *Basin Research*, **21**, 454–483, doi: 10.1111/j.1365-2117.2009.00425.x.

HELLAND-HANSEN, W. & MARTINSEN, O.J. 1996. Shoreline trajectories and sequences: description of variable deposisional-dip scenarios. *Journal of Sedimentary Research*, **66**, 670–688, doi: 10.1306/D42683DD-2B26-11D7-8648000102C1865D.

HENRIKSEN, S., HAMPSON, G.J., HELLAND-HANSEN, W., JOHANNESSEN, E.P. & STEEL, R.J. 2009. Shelf edge and shoreline trajectories, a dynamic approach to stratigraphic analysis. *Basin Research*, **21**, 445–453, doi: 10.1111/j.1365-2117.2009.00432.x.

HETTINGER, R.D. 2000. Chapter J: A summary of coal distribution and geology in the Kaiparowits Plateau, Utah. *In*: Krischbaum, M.A., Roberts, L.N.R. & Biewick, L.R.H. (eds) *Geologic Assessment of Coal in the Colorado Plateau: Arizona, Colorado, New Mexico, and Utah*. U.S. Geological Survey Professional Paper 1625-B, J1–J17.

HETTINGER, R.D., MCCABE, P.J. & SHANLEY, K.W. 1993. Detailed facies anatomy of transgressive and highstand systems tracts from the Upper Cretaceous of southern Utah, U.S.A. *In*: Weimer, R.J. & Posamentier, H.W. (eds) *Siliciclastic Sequence Stratigraphy: Recent Developments and Applications*. American Association of Petroleum Geologists Memoir, **58**, 235–257.

HETTINGER, R.D., ROBERTS, L.N.R., BIEWICK, L.R.H. & KIRSCHBAUM, M.A. 2009.

Geologic overview and resource assessment of coal in the Kaiparowits Plateau, southern Utah. *In*: Kirschbaum, M.A., Roberts, L.N.R. & Biewick, L.R.H. (eds) *Geologic Assessment of Coal in the Colorado Plateau: Arizona, Colorado, New Mexico, and Utah*. Denver, Colorado, U.S. Geological Survey Professional Paper **1625-B**, 83.

HILL, P.S., FOX, J.M., ET AL. 2007. Sediment delivery to the seabed on continental margins. *In*: *Continental Margin Sedimentation*. Blackwell Publishing Ltd., Oxford, 49–99, doi: 10.1002/9781444304398.ch2.

HINTZE, L.F. 1988. *Geologic History of Utah*. Provo, Brigham Young University, 202.

HOLZ, M., VIEIRA, P.E. & KALKREUTH, W. 2000. The early Permian coal-bearing succession of the Paraná Basin in southernmost Brazil: depositional model and sequence stratigraphy. *Revista Brasileira de Geiosciencias*, **30**, 424–426.

HOLZ, M., KALKREUTH, W. & BANERJEE, I. 2002. Sequence stratigraphy of paralic coal-bearing strata: an overview. *International Journal of Coal Geology*, **48**, 147–179, doi: http://dx.doi.org/10.1016/S0166-5162(01)00056-8.

HUBBARD, S.M., GINGRAS, M.K., PEMBERTON, S.G. & THOMAS, M.B. 2002. Variability in wave-dominated estuary sandstones: implications on subsurface reservoir development. *Bulletin of Canadian Petroleum Geology*, **50**, 118–137, doi: 10.2113/50.1.118.

HUDOCK, J.W., FLAIG, P.P. & WOOD, L.J. 2014. Washover fans: a modern geomorphologic analysis and proposed classification scheme to improve reservoir models. *Journal of Sedimentary Research*, **84**, 854–865.

HUGHES, Z.J. 2012. Tidal channels on tidal flats and marshes. *In*: Davis Jr., R.A. & Dalrymple, R.W. (eds) *Principles of Tidal Sedimentology*. Dordrecht, Springer Netherlands, 269–300, doi: 10.1007/978-94-007-0123-6_11.

HUME, T.M. & HERDENDORF, C.E. 1988. A geomorphic classification of estuaries and its application to coastal resource management—a New Zealand example. *Ocean and Shoreline Management*, **11**, 249–274, doi: http://dx.doi.org/10.1016/0951-8312(88)90022-7.

ICHASO, A.A. & DALRYMPLE, R.W. 2009. Tide- and wave-generated fluid mud deposits in the Tilje Formation (Jurassic), offshore Norway. *Geology*, **37**, 539–542, doi: 10.1130/G25481A.1.

ISMAT, Z. & MITRA, G. 2001. Folding by cataclastic flow at shallow crustal levels in the Canyon Range, Sevier orogenic belt, west-central Utah. *Journal of Structural Geology*, **23**, 355–378, doi: 10.1016/S0191-8141(00)00101-2.

JAMES, N. & DALRYMPLE, R.W. (eds). 2010. *Facies Models 4*. St. John's, Newfoundland, Geological Society of Canada, 586.

JINNAH, Z.A. & ROBERTS, E.M. 2011. Facies associations, paleoenvironment, and base-level changes in the Upper Cretaceous Wahweap Formation, Utah, U.S.A. *Journal of Sedimentary Research*, **81**, 266–283, doi: 10.2110/jsr.2011.22.

JINNAH, Z.A., ROBERTS, E.M., DEINO, A.L., LARSEN, J.S., LINK, P.K. & FANNING, C.M. 2009. New 40Ar-39Ar and detrital zircon U-Pb ages for the Upper Cretaceous Wahweap and Kaiparowits Formations on the Kaiparowits Plateau, Utah: implications for regional correlation, provenance, and biostratigraphy. *Cretaceous Research*, **30**, 287–299, doi: 10.1016/j.cretres.2008.07.012.

JOECKEL, R.M. & KORUS, J.T. 2012. Bayhead delta interpretation of an Upper Pennsylvanian sheetlike sandbody and the broader understanding of transgressive deposits in cyclothems. *Sedimentary Geology*, **275-276**, 22–37, doi: 10.1016/j.sedgeo.2012.07.002.

JORDAN, T.E. 1981. Thrust loads and foreland basin evolution, Cretaceous, Western United States. *American Association of Petroleum Geologists Bulletin*, **65**, 2506–2520.

KAMOLA, D.L., & Van Wagoner, J.C. 1995. Stratigraphy and facies architecture of parasequences with examples from the Spring Canyon Member, Blackhawk Formation, Utah *In*: Van Wagoner, J.C. & Bertram, G.T. (eds) *Sequence Stratigraphy of Foreland Basin Deposits*. American Association of Petroleum Geologists Memior, **64**, 27–54.

KAUERRAUF, A.I. & HANTSCHEL, T. 2009. *Fundamentals of Basin and Petroleum Systems Modeling*. Berlin, Springer-Verlag, 476.

KAUFFMAN, E.G. 1977. Geological and biological overview: Western Interior Cretaceous Basin. *Mountain Geologist*, **14**, 75–99.

KIEFT, R.L., HAMPSON, G.J., JACKSON, C.A.L. & LARSEN, E. 2011. Stratigraphic architecture of a net-transgressive marginal- to shallow-marine succession: Upper Almond Formation, Rock Springs Uplift, Wyoming, U.S.A. *Journal of Sedimentary Research*, **81**, 513–533, doi: 10.2110/jsr.2011.44.

KIRKLAND, J.I., EATON, J.G. & BRINKMAN, D.B. 2013. Elasmobranchs from Upper Cretaceous freshwater facies in southern Utah. *In*: Titus, A.L. & Loewen, M.A. (eds) *At the Top of the Grand Staircase: The Late Cretaceous of Southern Utah*. Bloomington, Indiana University Press, 153–194.

KJERFVE, B. 1986. Comparative oceanography of coastal lagoons. *In*: *Estuarine Variability*. Academic Press, 63–81.

KJERFVE, B. & MAGILL, K.E. 1989. Geographic and hydrodynamic characteristics of shallow coastal lagoons. *Marine Geology*, **88**, 187–199, doi: http://dx.doi.org/10.1016/0025-3227(89)90097-2.

KOOI, H. & DE VRIES, J.J. 1998. Land subsidence and hydrodynamic compaction of sedimentary basins. *Hydrology and Earth System Sciences*, **2**, 159–171, doi: 10.5194/hess-2-159-1998.

KVALE, E.P. 2012. Tidal constituents of modern and ancient tidal rhythmites: criteria for recognition and analyses. *In*: Davis, R.A. & Dalrymple, R.W. (eds) *Principles of Tidal Sedimentology*. Dordrecht, Springer Netherlands, 1–17.

LARSEN, J.S. 2007. *Facies and Provenance of the Pine Hollow Formation: Implications for Sevier Foreland Basin Evolution and the Paleocene Climate of Southern Utah*. MS thesis, Idaho State University, Pocatello, ID.

LARSEN, J.S., LINK, P.K., ROBERTS, E.M., TAPANILA, L. & FANNING, C.M. 2010. Cyclic stratigraphy of the Paleogene Pine Hollow Formation and detrital zircon provenance of Campanian to Eocene sandstones of the Kaiparowits and Table Cliffs Basins, south-central Utah. *In*: Carney, S.M., Tabet, D.E. & Johnson, C.L. (eds) *Geology of South-Central Utah*. Utah Geological Association Publication, 39, 194–214.

LAWTON, T.F. & BRADFORD, B.A. 2011. Correlation and provenance of Upper Cretaceous (Campanian) fluvial strata, Utah, U.S.A., from zircon U-Pb geochronology and petrography. *Journal of Sedimentary Research*, **81**, 495–512, doi: 10.2110/jsr.2011.45.

LAWTON, T.F., POLLOCK, S.L. & ROBINSON, R.A.J. 2003. Integrating sandstone petrology and nonmarine sequence stratigraphy: application to the Late Cretaceous fluvial systems of southwestern Utah, USA. *Journal of Sedimentary Research*, **73**, 389–406, doi: 10.1306/100702730389.

LAWTON, T.F., SCHELLENBACH, W.L. & NUGENT, A.E. 2014. Late Cretaceous fluvial-megafan and axial-river systems in the southern Cordilleran foreland basin: Drip Tank Member of Straight Cliffs Formation and adjacent strata, southern Utah, U.S.A. *Journal of Sedimentary Research*, **84**, 407–434.

LEIER, A.L., DECELLES, P.G. & PELLETIER, J.D. 2005. Mountains, monsoons, and megafans. *Geology*, **33**, 289–292, doi: 10.1130/G21228.1.

LESSA, G.C., MEYERS, S.R. & MARONE, E. 1998. Holocene stratigraphy in the Paranagua Bay estuary, southern Brazil. *Journal of Sedimentary Research*, **68**, 1060–1076, doi: 10.2110/jsr.68.1060.

LI, W., BHATTACHARYA, J.P., ZHU, Y., GARZA, D. & BLANKENSHIP, E. 2011. Evaluating delta asymmetry using three-dimensional facies architecture and ichnological

analysis, Ferron 'Notom Delta', Capital Reef, Utah, USA. *Sedimentology*, **58**, 478–507, doi: 10.1111/j.1365-3091.2010.01172.x.

LIU, S., NUMMEDAL, D. & LIU, L. 2011. Migration of dynamic subsidence across the Late Cretaceous United States Western Interior Basin in response to Farallon Plate subduction. *Geology*, **39**, 555–558, doi: 10.1130/G31692.1.

LIU, S., NUMMEDAL, D. & GURNIS, M. 2014. Dynamic versus flexural controls of Late Cretaceous Western Interior Basin, USA. *Earth and Planetary Science Letters*, **389**, 221–229, doi: 10.1016/j.epsl.2014.01.006.

LONG, A.J., WALLER, M.P., & STUPPLES, P. 2006, Driving mechanisms of coastal change: peat compaction and the destruction of late Holocene coastal wetlands. *Marine Geology*, **225**, 63–84, doi: 10.1016/j.margeo.2005.09.004.

LONGHITANO, S.G., MELLERE, D., STEEL, R.J. & AINSWORTH, R.B. 2012. Tidal depositional systems in the rock record: a review and new insights. *Sedimentary Geology*, **279**, 2–22, doi: 10.1016/j.sedgeo.2012.03.024.

MACEACHERN, J.A. & PEMBERTON, S.G.Y. 1992. Ichnological aspects of Cretaceous shoreface successions and shoreface variability in the Western Interior Seaway of North America. *In*: Pemberton, S.G. (ed) *Applications of Ichnology to Petroleum Exploration*. Society of Sedimentary Geology Core Workshop, **17**, 57–84.

MACEACHERN, J. A., ZAITLIN, B.A., PEMBERTON, S.G. & FIELD, J. 1998. High-resolution sequence stratigraphy of early transgressive deposits, Viking Formation, Joffre Field, Alberta, Canada. *American Association of Petroleum Geologists Bulletin*, **82**, 729–756, doi: 10.1306/1D9BC5E3-172D-11D7-8645000102C1865D.

MACEACHERN, J. A., PEMBERTON, G.S., GINGRAS, M.K. & BANN, K. 2010. Ichnology and facies models. *In*: James, N.P. & Dalrymple, R.W. (eds) *Facies Models 4*. St. John's, Newfoundland, Geological Association of Canada, 19-58.

MASSELINK, G. & PULEO, J.A. 2006. Swash-zone morphodynamics. *Continental Shelf Research*, **26**, 661–680, doi: http://dx.doi.org/10.1016/j.csr.2006.01.015.

MCCABE, P. J. 1987. Facies studies of coal and coal-bearing strata. *Geological Society, London, Special Publications*, **32**, 51–66, doi: 10.1144/GSL.SP.1987.032.01.05.

MCCABE, P. J. & SHANLEY, K.W. 1992. Organic control on shoreface stacking patterns: bogged down in the mire. *Geology*, **20**, 741–744, doi: 10.1130/0091-7613(1992)020<0741:OCOSSP>2.3.CO;2.

MCCUBBIN, D. G. 1982. Barrier-island and strand plain facies. *In*: Scholle, P.A. & Spearing, D. (eds) *Sandstone Depositional Environments*. American Association of Petroleum Geologists Memior, **31**, 247–279.

MCEWEN, M.C. 1969. Sedimentary Facies of the Modern Trinity Delta. *In*: *Galveston Bay Geology: Holocene Geology of the Galveston Bay Area*. Houston Geological Society, 53–77.

MCGOOKEY, D.P., HAUN, J.P., HEELE, L.A., GOODELL, H.G., MCCUBBIN, D.G., WEIMER, R.J. & WULF, G.R. 1972. Cretaceous Systems. *In*: *Geologic Atlas of the Rocky Mountain Region*. Rocky Mountain Association of Geologists, 190–233.

MCQUEEN, H.W.S. & BEAUMONT, C. 1989. Mechanical models of tilted block basins. *In*: Price, R.A. (ed) *Origin and Evolution of Sedimentary Basins and Their Energy and Mineral Resources*. Washington, DC, American Geophysical Union, Geophysical Monograph, 65–71, doi: 10.1029/GM048p0065.

MECKEL, T.A., TEN BRINK, U.S. & WILLIAMS, S.J. 2006. Current subsidence rates due to compaction of Holocene sediments in southern Louisiana. *Geophysical Research Letters*, **33**, 1–5, doi: 10.1029/2006GL026300.

MECKEL, T.A., TEN BRINK, U.S. & WILLIAMS, S.J. 2007. Sediment compaction rates and subsidence in deltaic plains: numerical constraints and stratigraphic influences. *Basin Research*, **19**, 19–31, doi: 10.1111/j.1365-2117.2006.00310.x.

MELLERE, D., Zecchin, M. & Perale, C. 2005. T Stratigraphy and sedimentology of fault-controlled backstepping shorefaces, middle Pliocene of Crotone Basin, southern Italy. *Sedimentary Geology*, **176**, 281–303, doi: 10.1016/j.sedgeo.2005.01.010.

MIALL, A.D. 1974. Paleocurrent analysis of alluvial sediments: a discussion of directional variance and vector magnitude. *Journal of Sedimentary Research*, **44**, 1174–1185, doi: 10.1306/212F6C6C-2B24-11D7-8648000102C1865D.

MILLER, K.G., KOMINZ, M.A., ET AL. 2005. The Phanerozoic record of global sea-level change. *Science*, **310**, 1293–1298, doi: 10.1126/science.1116412.

MILLI, S., D'AMBROGI, C., ET AL. 2013. The transition from wave-dominated estuary to wave-dominated delta: the Late Quaternary stratigraphic architecture of Tiber River deltaic succession (Italy). *Sedimentary Geology*, **284–285**, 159–180, doi: http://dx.doi.org/10.1016/j.sedgeo.2012.12.003.

MITROVICA, J., BEAUMONT, C. & JARVIS, G. 1989. Tilting of continental interiors by the dynamical effects of subduction. *Tectonics*, **8**, 1079–1094.

MUTO, T. & STEEL, R.J. 1997. Principles of regression and transgression: the nature of the interplay between accommodation and sediment supply. *Journal of Sedimentary Research*, **67**, 994–1000, doi: 10.1306/D42686A8-2B26-11D7-8648000102C1865D.

NADON, G.C. 1998. Magnitude and timing of peat-to-coal compaction. *Geology*, **26**, 727–

730, doi: 10.1130/0091-7613(1998)026<0727:matopt>2.3.co;2.

NICHOLS, M.M. 1989. Sediment accumulation rates and relative sea-level rise in lagoons. *Marine Geology*, **88**, 201–219.

NICHOLS, M.M. & BIGGS, R.B. 1985. Estuaries. *In*: Davis, R.A. (ed) *Coastal Sedimentary Environments*. Berlin, Springer-Verlag, 77–186.

OLARIU, M.I., CARVAJAL, C.R., OLARIU, C. & STEEL, R.J. 2012. Deltaic process and architectural evolution during cross-shelf transits, Maastrichtian Fox Hills Formation, Washakie Basin, Wyoming. *American Assocation of Petroleum Geologists Bulletin*, **96**, 1931–1956, doi: 10.1306/03261211119.

OLARIU, C., STEEL, R.J., DALRYMPLE, R.W. & GINGRAS, M.K. 2012. Tidal dunes versus tidal bars: the sedimentological and architectural characteristics of compound dunes in a tidal seaway, the lower Baronia Sandstone (Lower Eocene), Ager Basin, Spain. *Sedimentary Geology*, **279**, 134–155, doi: 10.1016/j.sedgeo.2012.07.018.

OLSEN, T.R., MELLERE, D. & OLSEN, T. 1999. Facies architecture and geometry of landward-stepping shoreface tongues: the Upper Cretaceous Cliff House Sandstone (Mancos Canyon, south-west Colorado). *Sedimentology*, **46**, 603–625, doi: 10.1046/j.1365-3091.1999.00234.x.

PAINTER, C.S. & CARRAPA, B. 2013. Flexural versus dynamic processes of subsidence in the North American Cordillera foreland basin. *Geophysical Research Letters*, **40**, 4249–4253, doi: 10.1002/grl.50831.

PAINTER, C.S., YORK-SOWECKE, C.C. & CARRAPA, B. 2013. Sequence stratigraphy of the Upper Cretaceous Sego Sandstone Member reveals spatio-temporal changes in depositional processes, Northwest Colorado, U.S.A. *Journal of Sedimentary Research*, **83**, 323–338, doi: 10.2110/jsr.2013.21.

PANG, M. & NUMMEDAL, D. 1995. Flexural subsidence and basement tectonics of the Cretaceous Western Interior basin, United States. *Geology*, **23**, 173–176, doi: 10.1130/0091-7613(1995)023<0173:FSABTO>2.3.CO;2.

PATCHINEELAM, S.M., KJERFVE, B. & GARDNER, L.R. 1999. A preliminary sediment budget for the Winyah Bay estuary, South Carolina, USA. *Marine Geology*, **162**, 133–144, doi: 10.1016/S0025-3227(99)00059-6.

PETERSON, F. 1969a. Cretaceous sedimentation and tectonism in the southeastern Kaiparowits region, Utah. *United States Department of the Interior Geologic Survey,* Open File Report, **69**.

PETERSON, F. 1969b. Four new members of the Upper Cretaceous Straight Cliffs Formation in the southeastern Kaiparowits Region, Kane County, Utah. *Geological*

Survey Bulletin, J1–J28.

PLINK-BJÖRKLUND, P. 2008. Wave-to-tide facies change in a Campanian shoreline complex, Chimney Rock Tongue, Wyoming-Utah, U.S.A. *In*: Hampson, G.J. (ed) *Recent Advances in Models of Siliciclastic Shallow-Marine Stratigraphy*. SEPM Special Publication, **90**, 265–291.

PLINT, A.G. 2010. Wave-and storm-dominated shoreline and shallow-marine systems. *In*: James, N. P. & Dalrymple, R. W. (eds) *Facies Models 4*. St. John's, Newfoundland, Geolgical Society of Canada, 167–199.

POSAMENTIER, H.W. & ALLEN, G.P. 1993. Variability of the sequence stratigraphic model: effects of local basin factors. *Sedimentary Geology*, **86**, 91–109, doi: http://dx.doi.org/10.1016/0037-0738(93)90135-R.

POSAMENTIER, H.W. & ALLEN, G.P. 1999. *Siliciclastic Sequence Stratigraphy: Concepts and Applications*: SEPM Concepts in Sedimenology and Paleontology, **7**. Tulsa, SEPM Society for Sedimentary Geology.

POSAMENTIER, H.W., JERVEY, M.T. & VAIL, P.R. 1988. Eustatic controls on clastic deposition I - conceptual framework. *In*: Wilgus, C.K., Hastings, B.S., Kendall, C.G.S.C., Posamentier, H.W., Ross, C.A. & Van Wagoner, J.C. (eds) *Sea-Level Changes: An Integrated Approach*. SEPM Special Publication, **42**, 109–124.

POTTER, I.C., CHUWEN, B.M., HOEKSEMA, S.D. & ELLIOTT, M. 2010. The concept of an estuary: a definition that incorporates systems which can become closed to the ocean and hypersaline. *Estuarine, Coastal and Shelf Science*, **87**, 497–500, doi: 10.1016/j.ecss.2010.01.021.

PRITCHARD, D.W. 1967. What is an estuary? physical viewpoint. *In*: Lauff, G.H. (ed) *Estuaries*. Washington, DC, American Association for the Advancement of Science Publication, **83**, 3–5.

RAMPINO, M.R. & SANDERS, J.E. 1980. WEvolution of the barrier: islands of southern Long Island, New York *Seidmentology*, **28**, 37–47, doi: 10.1111/j.1365-3091.1981.tb01661.x.

READING, H.G. & COLLINSON, J.D. 1996. *Clastic Coasts*, 3rd ed. Oxford, Blackwell Science.

REINSON, G.E. 1992. Transgressive barrier island and estuarine systems. *In*: Walker, R.G. & James, N. P. (eds) *Facies Models: Response to Sea-Level Changes*. St. John's, Newfoundland, Geological Society of Canada, 179–194.

REDDERING, J.S. V. 1980. What is an estuary? *South African Journal of Science*, **76**, 341.

REYNOLDS, A.D. 1999. Dimensions of paralic sandstone bodies. *American Association of Petroleum Geologists Bulletin*, **83**, 211–229, doi: 10.1306/00AA9A48-1730-11D7-8645000102C1865D.

REYNOLDS, D.J., STECKLER, M.S. & COAKLEY, B.J. 1991. The role of the sediment load in sequence stratigraphy: the influence of flexural isostasy and compaction. *Journal of Geophysical Research: Solid Earth*, **96**, 6931–6949, doi: 10.1029/90jb01914.

ROBERTS, L.N.R. & KIRSCHBAUM, M.A. 1995. Paleogeography of the Late Cretaceous of the Western Interior of middle North America- coal distribution and sediment accumulation. *U.S. Geological Survey Professional Paper*, **1561**, 116.

ROEHLER, H.W. 1988. The Pintail coal bed and barrier bar G - a model for coal of barrier bar - lagoon origin, Upper Cretaceous Almond Formation, Rock Springs Coal Field, Wyoming. *U.S. Geological Survey Professional Paper*, **1398**.

ROSATI, J.D. 2009. *Barrier Island Migration over a Consolidating Substrate*. PhD dissertation, Louisiana State University, Baton Rouge, LA.

ROSATI, J.D., DEAN, R.G. & STONE, G.W. 2010. A cross-shore model of barrier island migration over a compressible substrate. *Marine Geology*, **271**, 1–16, doi: http://dx.doi.org/10.1016/j.margeo.2010.01.005.

RYER, T.A. & LANGER, A.W. 1980. Thickness change involved in the peat-to-coal transformation for a bituminous coal of Cretaceous age in central Utah. *Journal of Sedimentary Petrology*, **50**, 987–992, doi: 10.1306/212F7B44-2B24-11D7-8648000102C1865D.

SADLER, P.M. 1981. Sediment accumulation rates and the completeness of stratigraphic sections. *The Journal of Geology*, **89**, 569–584, doi: 10.2307/30062397.

SADLER, P.M. 1999. The influence of hiatuses on sediment accumulation rates. *GeoReserch Forum*, **5**, 15–40.

SAITO, Y. 1994. Shelf sequence and characteristic bounding surfaces in a wave-dominated setting: Latest Pleistocene-Holocene examples from northeast Japan. *Marine Geology*, **120**, 105–127, doi: http://dx.doi.org/10.1016/0025-3227(94)90080-9.

SALEM, A.C. 2009. *Mesozoic Tectonics of the Maria Fold and Thrust Belt and McCoy Basin, Southeastern California*. PhD dissertation, Arizona State University, Tempe, AZ.

SALZMANN, L., GREEN, A. & COOPER, J.A.G. 2013. Submerged barrier shoreline sequences on a high energy, steep and narrow shelf. *Marine Geology*, **346**, 366–374, doi: 10.1016/j.margeo.2013.10.003.

SARGENT, K.A. & HANSEN, D.E. 1982. Bedrock geologic map of the Kaiparowits coal-basin area, Utah. *U.S. Geological Survey*, Miscellaneous Investigations Map, **I-1033-I**.

SCHIEBER, J. & SOUTHARD, J.B. 2009. Bedload transport of mud by floccule ripples—direct observation of ripple migration processes and their implications. *Geology*, **37**, 483–486, doi: 10.1130/g25319a.1.

SCHIEBER, J., SOUTHARD, J. & THAISEN, K. 2007. Accretion of mudstone beds from migrating floccule ripples. *Science*, **318**, 1760–1763, doi: 10.1126/science.1147001.

SCHLAGER, W. 1993. Accommodation and supply—a dual control on stratigraphic sequences. *Sedimentary Geology*, **86**, 111–136, doi: http://dx.doi.org/10.1016/0037-0738(93)90136-S.

SCHWARTZ, R.K. 1982. Bedform and stratification characteristics of some modern small-scale washover sand bodies. *Sedimentology*, **29**, 835–849, doi: 10.1111/j.1365-3091.1982.tb00087.x.

SEDGWICK, P.E. & DAVIS JR, R.A. 2003. Stratigraphy of washover deposits in Florida: implications for recognition in the stratigraphic record. *Marine Geology*, **200**, 31–48, doi: http://dx.doi.org/10.1016/S0025-3227(03)00163-4.

SEIDLER, L. & STEEL, R. 2001. Pinch-out style and position of tidally influenced strata in a regressive–transgressive wave-dominated deltaic sandbody, Twentymile Sandstone, Mesaverde Group, NW Colorado. *Sedimentology*, **48**, 399–414, doi: 10.1046/j.1365-3091.2001.00370.x.

SHANLEY, K.W. & MCCABE, P.J. 1991. Predicting facies architecture through sequence stratigraphy - an example from the Kaiparowits Plateau, Utah. *Geology*, **19**, 742–745, doi: 10.1130/0091-7613(1991)019<0742.

SHANLEY, K.W. & MCCABE, P.J. 1993. Alluvial architecture in a sequence stratigraphic framework: a case history from the Upper Cretaceous of southern Utah, USA. *Special Publication of the International Association of Sedimentologists*, **15**, 21–56.

SHANLEY, K.W. & MCCABE, P.J. 1994. Perspectives on the sequence stratigraphy of continental strata. *American Assocation of Petroleum Geologists Bulletin*, **78**, 544–568.

SHANLEY, K.W. & MCCABE, P.J. 1995. Sequence stratigraphy of Turonian – Santonian strata, Kaiparowits Plateau, southern Utah, U.S.A.: implications for regional correlation and foreland basin evolution. *In*: Van Wagoner, J.C. & Bertram, G.T. (eds) *Sequence Stratigraphy of Foreland Basin Deposits*. American Association of Petroleum Geologists Memoir, **64**, 103–136.

SIXSMITH, P.J., HAMPSON, G.J., GUPTA, S., JOHNSON, H.D. & FOFANA, J.F. 2008. Facies architecture of a net transgressive sandstone reservoir analog: the Cretaceous Hosta Tongue, New Mexico. *American Association of Petroleum Geologists Bulletin*, **92**, 513–547, doi: 10.1306/01020807017.

SLATER, R.D. 1985. A numerical model of tides in the Cretaceous Seaway of North America. *The Journal of Geology*, **93**, 333–345, doi: 10.2307/30085018.

SLINGERLAND, R. & KEEN, T. 1999. Sediment transport in the Western Interior Seaway of North America: predictions from a climate-ocean-sediment model. *In*: Bergman, K.A. & Snedden, J.W. (eds) *Isolated Shallow Marine Sandodies: Sequence Stratigraphic Analysis and Sedimentologic Interpretation*. SEPM Special Publication, **64**, 179–190.

SLINGERLAND, R., KUMP, L.R., ARTHUR, M.A., FAWCETT, P.J., SAGEMAN, B.B. & BARRON, E.J. 1996. Estuarine circulation in the Turonian Western Interior Seaway of North America. *Geological Society of America Bulletin*, **108**, 941–952, doi: 10.1130/0016-7606(1996)108<0941:ecittw>2.3.co;2.

SNEDDEN, J.W. & KERSEY, D.G. 1981. Origin of the San Miguel lignite deposit and associated lithofacies, Jackson Group, south Texas. *American Association of Petroleum Geologists Bulletin*, **65**, 1099–1109, doi: 10.1306/03B59602-16D1-11D7-8645000102C1865D.

SOMMERFIELD, C.K. 2006. On sediment accumulation rates and stratigraphic completeness: lessons from Holocene ocean margins. *Continental Shelf Research*, **26**, 2225–2240, doi: http://dx.doi.org/10.1016/j.csr.2006.07.015.

SOUTHARD, J.B., LAMBIE, J.M., FEDERICO, D.C., PILE, H.T. & WEIDMAN, C.R. 1990. Experiments on bed configurations in fine sands under bidirectional purely oscillatory flow, and the origin of hummocky cross-stratification. *Journal of Sedimentary Research*, **60**, 1–17, doi: 10.1306/212F90F7-2B24-11D7-8648000102C1865D.

SOUZA-FILHO, P.W.M., LESSA, G.C., COHEN, M.C.L., COSTA, F.R. & LARA, R.J. 2009. The subsiding macrotidal barrier estuarine system of the eastern Amazon Coast, northern Brazil. *In*: *Geology and Geomorphology of Holocene Coastal Barriers of Brazil SE - 11*. Springer Berlin Heidelberg, Lecture Notes in Earth Sciences, 347–375, doi: 10.1007/978-3-540-44771-9_11.

SWIFT, D.J.P. 1968. Coastal erosion and transgressive stratigraphy. *The Journal of Geology*, **76**, 444–456, doi: 10.1086/627342.

SZWARC, T.S., JOHNSON, C.L., STRIGHT, L.E. & MCFARLANE, C.M. 2014. Interactions between axial and transverse drainage systems in the Late Cretaceous Cordilleran foreland basin: Evidence from detrital zircons in the Straight Cliffs Formation,

southern Utah. *Geological Society of America Bulletin*, **127**, 372–392, doi: 10.1130/B31039.1.

TAYLOR, A.M. & GOLDRING, R. 1993. Description and analysis of bioturbation and ichnofabric. *Journal of the Geological Society*, **150**, 141–148, doi: 10.1144/gsjgs.150.1.0141.

TAYLOR, W.J. 1993. Stratigraphic and lithologic analysis of the Claron Formation in southwestern Utah. *Miscellaneous Publication Utah Geologic Survey*, **93**.

TERZAGHI, K. 1943. *Theoretical Soil Mechanics*. New York, Wiley, 510.

THORNE, J.A. & SWIFT, D.J.P. 1991. Sedimentation on continental margins; VI, A regime model for depositional sequences, their component systems tracts, and bounding surfaces. *In*: Swift, D.J.P., Oertel, G.F., Tillman, R.W. & Thorne, J.A. (eds) *Shelf Sand and Sandstone Bodies: Geometry, Facies and Sequence Stratigraphy*. International Association of Sedimentology, **14**, 189–255.

TINDALL, S.E. & DAVIS, G.H. 1999. Monocline development by oblique-slip fault-propagation folding: The East Kaibab monocline, Colorado Plateau, Utah. *Journal of Structural Geology*, **21**, 1303–1320, doi: 10.1016/S0191-8141(99)00089-9.

TINDALL, S.E., STORM, L.P., JENESKY, T.A. & SIMPSON, E.L. 2010. Growth faults in the Kaiparowits Basin, Utah, pinpoint initial Laramide deformation in the western Colorado Plateau. *Lithosphere*, **2**, 221–231, doi: 10.1130/L79.1.

TÖRNQVIST, T.E., WALLACE, D.J., ET AL. 2008. Mississippi Delta subsidence primarily caused by compaction of Holocene strata. *Nature Geoscience*, **1**, 173–176, doi: 10.1038/ngeo129.

TYE, R.S., HEWLETT, J.S., THOMPSON, P.R. & GOODMAN, D.K. 1999. Intergrated stratigrahic and depositional-facies analysis of parasequences in a transgressive systems tract. *In*: Weimer, R.J. & Posamentier, H.W. (eds) *Siliciclastic Sequence Stratigraphy: Recent Developments and Applications*. American Association of Petroleum Geologists Memior, **58**, 99–133.

VAIL, P.R. & MITCHUM, R.M. 1979. Global cycles of relative changes of sea level from seismic stratigraphy. *In*: Watkins, J.S., Montadert, L. & Dickerson, P.W. (eds) *Geological and Geophysical Investigations of Continental Margins*. American Association of Petroleum Geologists Memior, **29**, 469–472.

VAIL, P.R., MITCHUM JR., R.M. & THOMPSON III, S. 1977. Seismic stratigraphy and global changes of sea level, Part 3: Relative changes of sea level from coastal onlap. *In*: Payton, C.E. (ed) *Seismic Stratigraphy: Applications to Hydrocarbon Exploration*. American Association of Petroleum Geologists Memior, **26**, 99–116.

VALASEK, D. 1995. The Tocito Sandstone in a sequence stratigraphic framework: an example of landward-stepping small-scale genetic sequences. *In*: Van Wagoner, J.C. & Bertram, G.T. (eds) *Sequence Stratigraphy of Foreland Basin Deposits*. American Association of Petroleum Geologists Memoir, **64**, 349–369.

VAKARELOV, B.K. & AINSWORTH, R.B. 2013. A hierarchical approach to architectural classification in marginal-marine systems: bridging the gap between sedimentology and sequence stratigraphy. *American Association of Petroleum Geologists Bulletin*, **97**, 1121–1161, doi: 10.1306/11011212024.

VAKARELOV, B.K., AINSWORTH, R.B. & MACEACHERN, J.A. 2011. Recognition of wave-dominated, tide-influenced shoreline systems in the rock record: variations from a microtidal shoreline model. *Sedimentary Geology*, **279**, 23–41, doi: 10.1016/j.sedgeo.2011.03.004.

VAN ASSELEN, S. 2011. The contribution of peat compaction to total basin subsidence: implications for the provision of accommodation space in organic-rich deltas. *Basin Research*, **23**, 239–255, doi: 10.1111/j.1365-2117.2010.00482.x.

VAN HEERDEN, I. & ROBERTS, H.H. 1988. Facies development of Atchafalaya Delta, Louisiana: a modern bayhead delta. *American Assocation of Petroleum Geologists Bulletin*, **72**, 439–453.

VAN WAGONER, J.C., POSAMENTIER, H.W., MITCHUM, R.M., VAIL, P.R., SARG, J.F., LOUTIT, T.S. & HARDENBOL, J. 1988. An overview of the fundamentals of sequence stratigraphy and key definitions. *In*: Wilgus, C.K., Posamentier, H.W., Ross, C.K. & Kendall, C.G. (eds) *Sea-Level Changes: An Integrated Approach*. SEPM Special Publication, **42**, 39–45.

VAN WAGONER, J.C., MITCHUM, R.M., CAMPION, K.M. & RAHMANIAN, V.D. 1990. Siliciclastic sequence stratigraphy in well logs, cores, and outcrops: concepts for high-resolution correlation of time and facies. *In*: Van Wagoner, J.C., Mitchum, R.M., Campion, K.M. & Rahmanian, V.D. (eds) *Methods in Exploration Series 7: Siliciclastic Sequence Stratigraphy in Well Logs, Cores, and Outcrops: Concepts for High-Resolution Correlation of Time and Facies*. American Association of Petroleum Geologists, 1–51.

VANINETTI, G.E. 1979. *Coal Stratigraphy of the John Henry Member of the Straight Cliffs Formation, Kaiparowits Plateau, Utah*. MS thesis, University of Utah, Salt Lake City, UT.

WADSWORTH, J., DIESSEL, C. & BOYD, R. 2010. The sequence stratigraphic significance of paralic coal and its use as an indicator of accommodation space in terrestrial sediments. *In*: Ratcliffe, K. & Zaitlin, B.A. (eds) *Application of Modern Stratigraphic Techniques: Theory and Case Histories*. SEPM Special Publication, **94**, 201–219, doi: 10.2110/sepmsp.094.201.

WALKER, R.G. & PLINT, A.G. 1992. Wave- and storm-dominated shallow marine systems. *In*: Walker, R.G. & James, N.P. (eds) *Facies Models: A Response to Sea-Level Changes*. St. John's, Newfoundland, Geological Association of Canada, 219–238.

WEIMER, R.J. 1960. Upper Cretaceous stratigraphy, Rocky Mountain area. *American Assocation of Petroleum Geologists Bulletin*, **44**, 1–20, doi: 10.1126/science.51.1323.468.

WELLER, J.M. 1959. The compaction of sediment. *American Association of Petroleum Geologists Bulletin*, **51**, 468–470, doi: 10.1126/science.58.1489.27.

WHITE, T., FURLONG, K. & ARTHUR, M. 2002. Forebulge migration in the Cretaceous Western Interior Basin of the central United States. *Basin Research*, **14**, 43–54, doi: 10.1046/j.1365-2117.2002.00165.x.

WILLIS, A.J. & MOSLOW, T.F. 1994. Stratigraphic setting of transgressive barrier-island reservoirs with an example from the Triassic Halfway Formation, Wembley Field, Alberta, Canada. *American Assocation of Petroleum Geologists Bulletin*, **78**, 775–791.

WRIGHT, L.D. & SHORT, A.D. 1984. Morphodynamic variability of surf zones and beaches: a synthesis. *Marine Geology*, **56**, 93–118, doi: http://dx.doi.org/10.1016/0025-3227(84)90008-2.

YORK, C.C., PAINTER, C.S. & CARRAPA, B. 2011. Sedimentological characterization of the Sego Sandstone (NW Colorado, USA): a new scheme to recognize ancient flood-tidal-delta deposits and implications for reservoir potential. *Journal of Sedimentary Research*, **81**, 401–419, doi: 10.2110/jsr.2011.35.

YOSHIDA, S., JOHNSON, H.D., PYE, K. & DIXON, R.J. 2004. Transgressive changes from tidal estuarine to marine embayment depositional systems: the Lower Cretaceous Woburn Sands of southern England and comparison with Holocene analogs. *American Association of Petroleum Geologists Bulletin*, **88**, 1433–1460, doi: 10.1306/05140403075.

YOSHIDA, S., STEEL, R.J. & DALRYMPLE, R.W. 2007. Changes in depositional processes-an ingredient in a new generation of sequence-stratigraphic models. *Journal of Sedimentary Research*, **77**, 447–460, doi: 10.2110/jsr.2007.048.

ZAITLIN, B.A. & SHULTZ, B.C. 1990. Wave-influenced estuarine sand body, Senlac Heavy Oil Pool, Saskatchewan, Canada. *In*: Barwis, J.H., McPherson, J.G. & Studlick, J.R.J. (eds) *Sandstone Petroleum Reservoirs*. New York, Springer-Verlag, 363–387.

ZECCHIN, M. 2007. The architectural variability of small-scale cycles in shelf and ramp

clastic systems: the controlling factors. *Earth Science Reviews*, **84**, 21–55, doi: 10.1016/j.earscirev.2007.05.003.

ZECCHIN, M. 2010. Towrds the strandardization of sequence stratigraphy: is the parasequence concept to be redefined or abandoned? *Earth Science Reviews*, **102**, 117–119, doi:10.1016/j.earscirev.2010.03.004

Figure 1.1. (**a**) Regional map of the Kaiparowits Plateau of southern Utah. Outcrops of the Straight Cliffs Formation are shaded gray, and locations of previous studies focused on the John Henry Member are labeled. Arrows indicate the general proximal to distal facies relationships in the John Henry Member, ranging from fluvial on the western margin to marine on the eastern margin, with tidal and paralic facies in between. Abbreviations: CNTB-Central Nevada Thrust Belt, SFTB-Sevier fold-thrust belt, WIS-Western Interior Seaway, MTB-Maria Thrust Belt. Location of northern Kaiparowits Plateau geological map (Fig. 1.1B) and preliminary stratigraphic correlation lines (Figs. 1.11 & 1.14) are shown. Modified from Szwarc *et al.* (2014) and Chentnik *et al.* (2015). (**b**) Simplified geological map of the Buck Hollow field area showing all four members of the Straight Cliffs Formation exposed in an along-strike orientation. Black lines show the locations of measured sections and the location of the correlation line used in Figure 1.4. Modified from Doelling & Willis (1999).

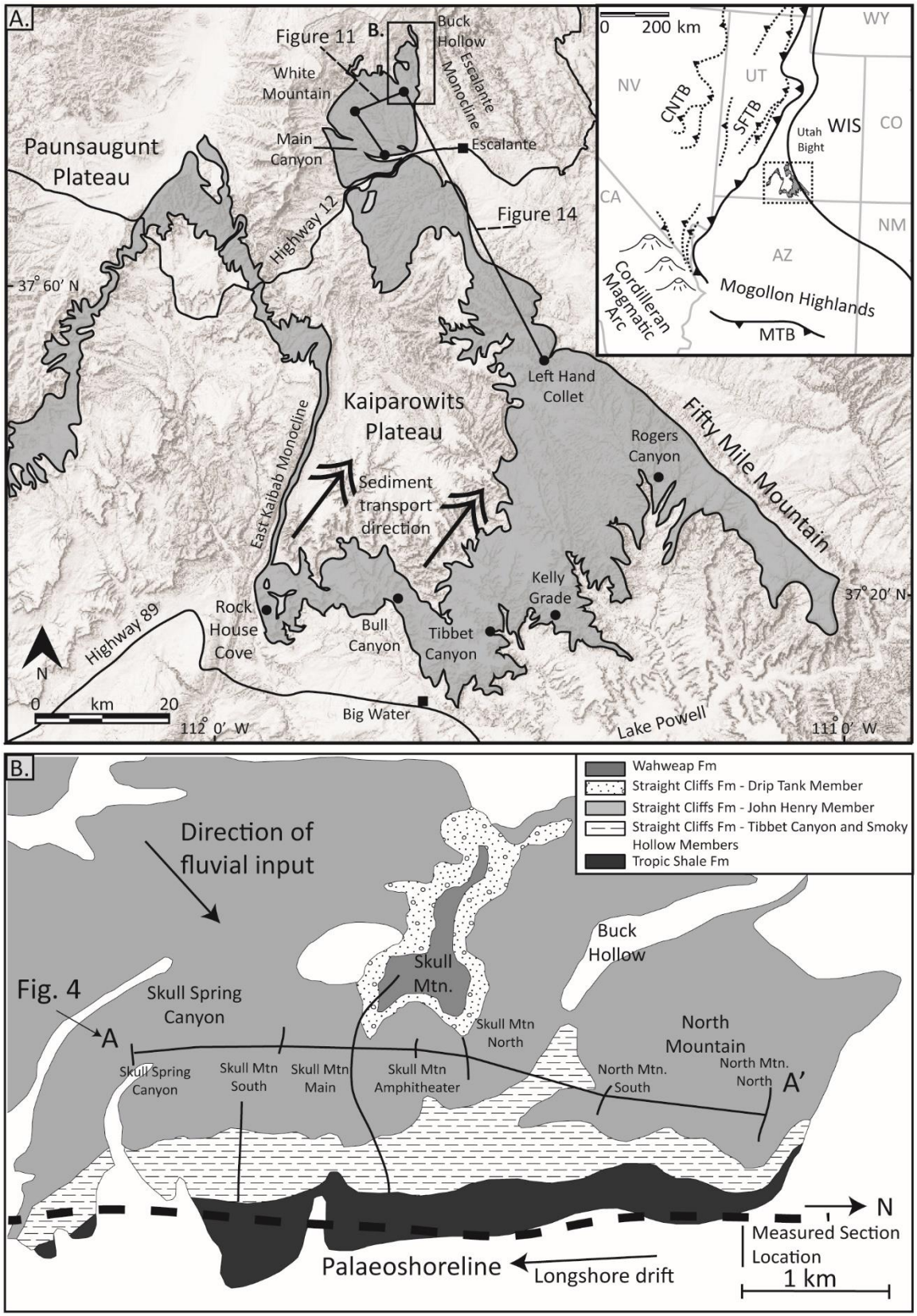
A.
B.
Figure 11
Buck Hollow
White Mountain
Escalante Monocline
Main Canyon
Escalante
Paunsaugunt Plateau
Figure 14
Highway 12
37° 60′ N
Kaiparowits Plateau
Left Hand Collet
Fifty Mile Mountain
Rogers Canyon
East Kaibab Monocline
Sediment transport direction
Kelly Grade
37° 20′ N
Rock House Cove
Bull Canyon
Tibbet Canyon
Highway 89
N
0 km 20
112° 0′ W
Big Water
Lake Powell
111° 0′ W
0 200 km
WY
NV
UT
CO
CA
NM
AZ
CNTB
SFTB
Utah Bight
WIS
Cordilleran Magmatic Arc
Mogollon Highlands
MTB
Wahweap Fm
Straight Cliffs Fm - Drip Tank Member
Straight Cliffs Fm - John Henry Member
Straight Cliffs Fm - Tibbet Canyon and Smoky Hollow Members
Tropic Shale Fm
Direction of fluvial input
Fig. 4
A
Skull Spring Canyon
Skull Mtn.
Buck Hollow
Skull Mtn North
North Mountain
Skull Spring Canyon
Skull Mtn South
Skull Mtn Main
Skull Mtn Amphitheater
North Mtn. South
North Mtn. North
A′
N
Measured Section Location
Palaeoshoreline
Longshore drift
1 km

Figure 1.2. Stratigraphic summary chart of the Turonian-Campanian Straight Cliffs Formation, including previous lithostratigraphic and sequence stratigraphic interpretations. Seven marine sandstone packages were named "A-G" by Peterson (1969*a*), and these pinch out landward into coal zones and coastal plain facies. Relative shoreline movements are based on shoreface pinchouts and marginal marine facies distributions at Left Hand Collet, Rogers Canyon, Main Canyon, and Buck Hollow. Also included are original and updated sequence stratigraphic interpretations for the Straight Cliffs Formation. Abbreviations: SB - sequence boundary; LJHMSB - Lower John Henry Member Sequence Boundary; Fm. – formation; JHM - John Henry Member. Modified from Chentnik *et al.* (2015).

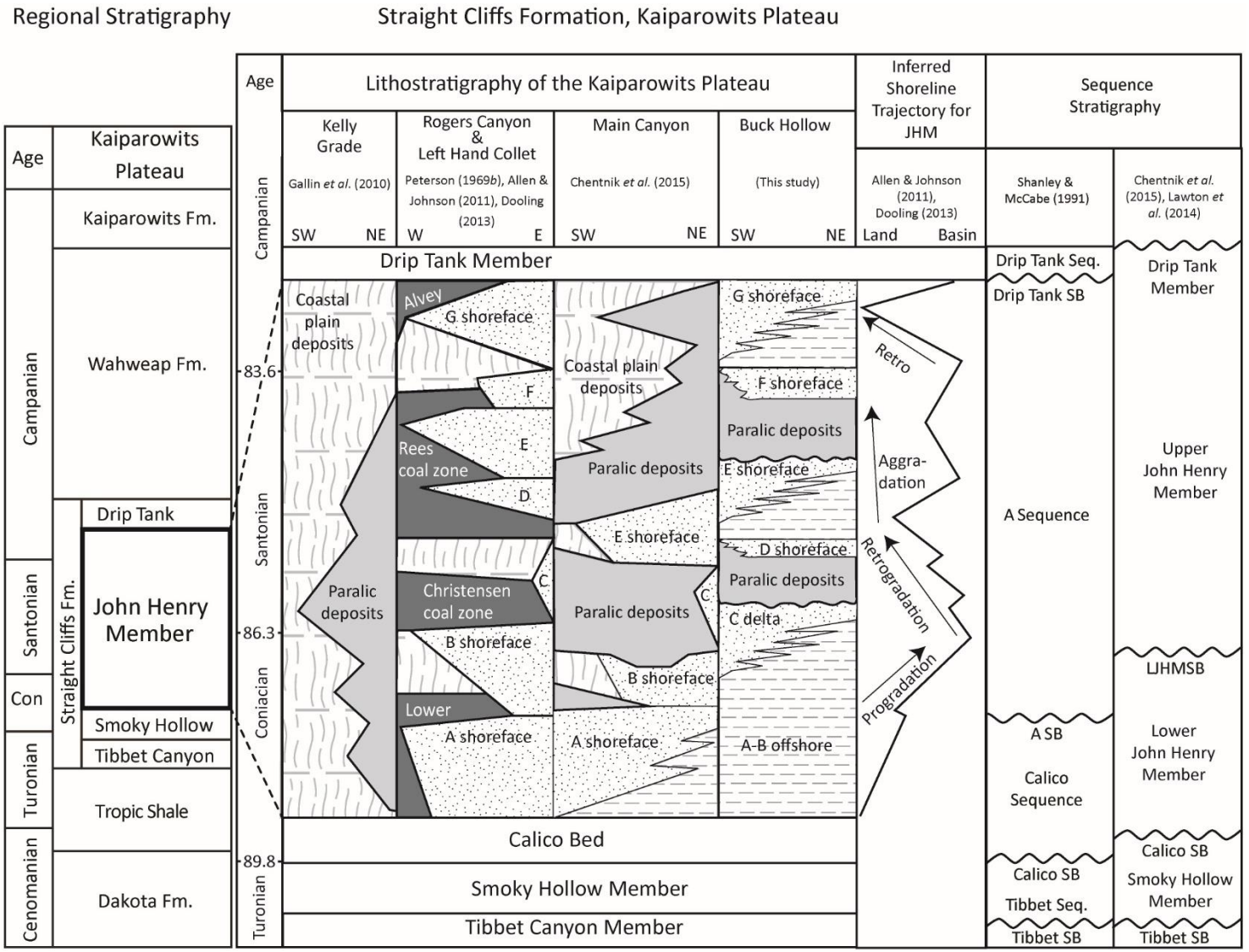
Regional Stratigraphy
Straight Cliffs Formation, Kaiparowits Plateau
Age
Kaiparowits Plateau
Campanian
Kaiparowits Fm.
Wahweap Fm.
Santonian
Drip Tank
Straight Cliffs Fm.
John Henry Member
Con
Smoky Hollow
Turonian
Tibbet Canyon
Tropic Shale
Cenomanian
Dakota Fm.
Age
Lithostratigraphy of the Kaiparowits Plateau
Kelly Grade
Gallin et al. (2010)
SW NE
Rogers Canyon & Left Hand Collet
Peterson (1969b), Allen & Johnson (2011), Dooling (2013)
W E
Main Canyon
Chentnik et al. (2015)
SW NE
Buck Hollow
(This study)
SW NE
Inferred Shoreline Trajectory for JHM
Allen & Johnson (2011), Dooling (2013)
Land Basin
Sequence Stratigraphy
Shanley & McCabe (1991)
Chentnik et al. (2015), Lawton et al. (2014)
Campanian
Santonian
Coniacian
Turonian
83.6
86.3
89.8
Drip Tank Member
Coastal plain deposits
Alvey
G shoreface
F
E
Rees coal zone
D
Paralic deposits
Christensen coal zone
C
B shoreface
Lower
A shoreface
Coastal plain deposits
Paralic deposits
E shoreface
C
Paralic deposits
B shoreface
A shoreface
G shoreface
F shoreface
Paralic deposits
E shoreface
D shoreface
Paralic deposits
C delta
A-B offshore
Retro
Aggra-dation
Retrogradation
Progradation
Calico Bed
Smoky Hollow Member
Tibbet Canyon Member
Drip Tank Seq.
Drip Tank SB
A Sequence
A SB
Calico Sequence
Calico SB
Tibbet Seq.
Tibbet SB
Drip Tank Member
Upper John Henry Member
LJHMSB
Lower John Henry Member
Calico SB
Smoky Hollow Member
Tibbet SB

Figure 1.3. Outcrop photos of the Buck Hollow field area. (**a**) An oblique photopan looking north at the along-strike outcrop exposures in Buck Hollow. (**b**) Photo of the John Henry Member of the Straight Cliffs Formation exposed on the southern limb of Skull Mountain in the Buck Hollow field area. The intervals of the John Henry Member ("A-G") are labeled. Major surfaces are marked and the column indicates the broad depositional environments preserved in each interval.

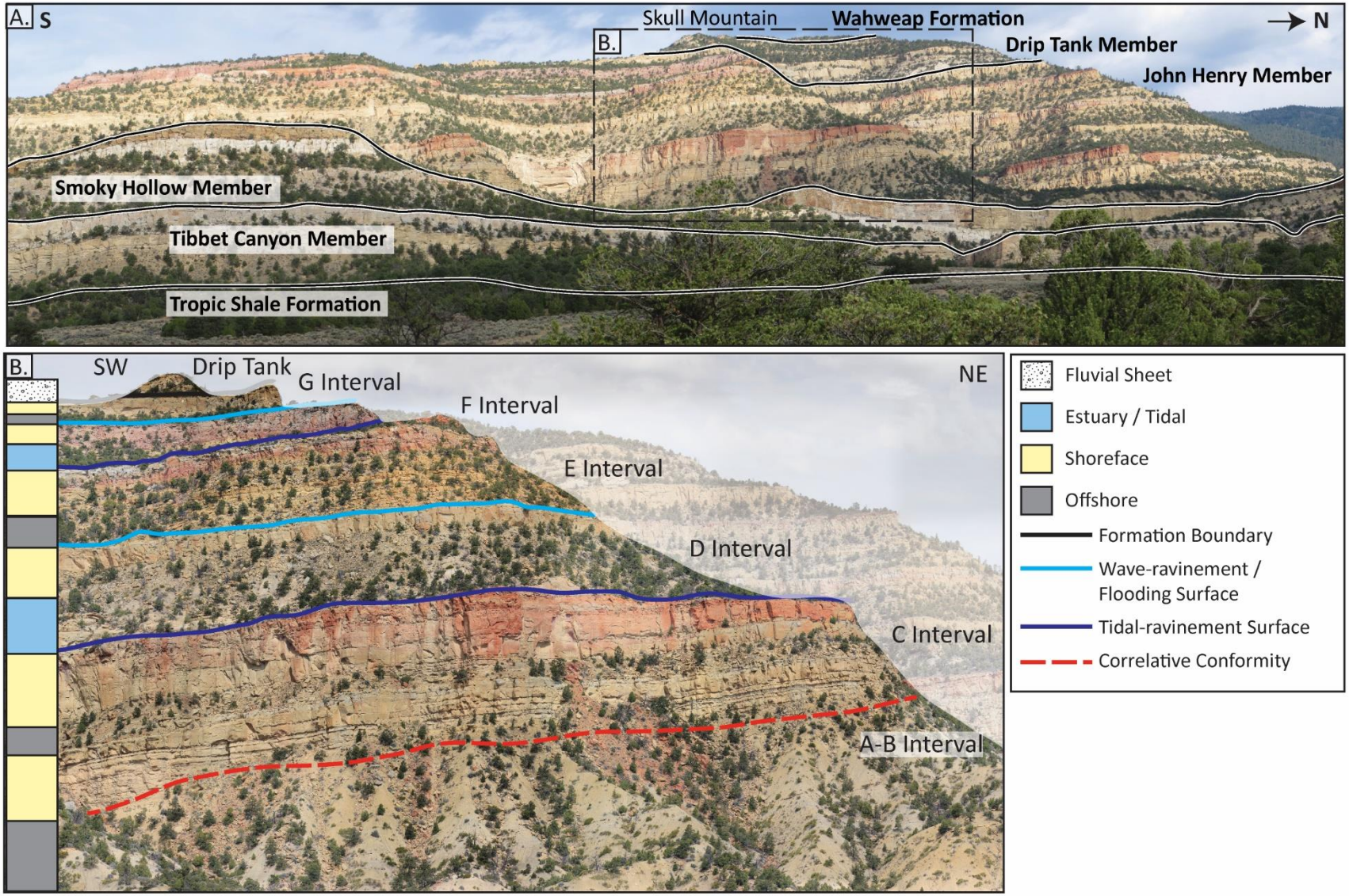
A.
S
Skull Mountain
Wahweap Formation
N
B.
Drip Tank Member
John Henry Member
Smoky Hollow Member
Tibbet Canyon Member
Tropic Shale Formation
B.
SW
Drip Tank
G Interval
F Interval
E Interval
D Interval
C Interval
A-B Interval
NE
Fluvial Sheet
Estuary / Tidal
Shoreface
Offshore
Formation Boundary
Wave-ravinement / Flooding Surface
Tidal-ravinement Surface
Correlative Conformity

Figure 1.4. Stratigraphic correlation of the Buck Hollow field area. Cross section line and measured section locations are shown in Figure 1.1B. Black triangles mark the R-T cycles. Also noted are the intervals depicted by the palaeogeographic maps in Figure 1.12. Abbreviations: DLSF - distal lower shoreface; PLSF - proximal lower shoreface; USF- upper shoreface; DF- delta front; pCf - process change from wave- to fluvial-dominated processes; tRs- tidal-ravinement surface; wRs/FS - wave-ravinement/flooding surface; SU- subaerial unconformity; CC - correlative conformity; TA - trough-axes; AS - accretion sets.

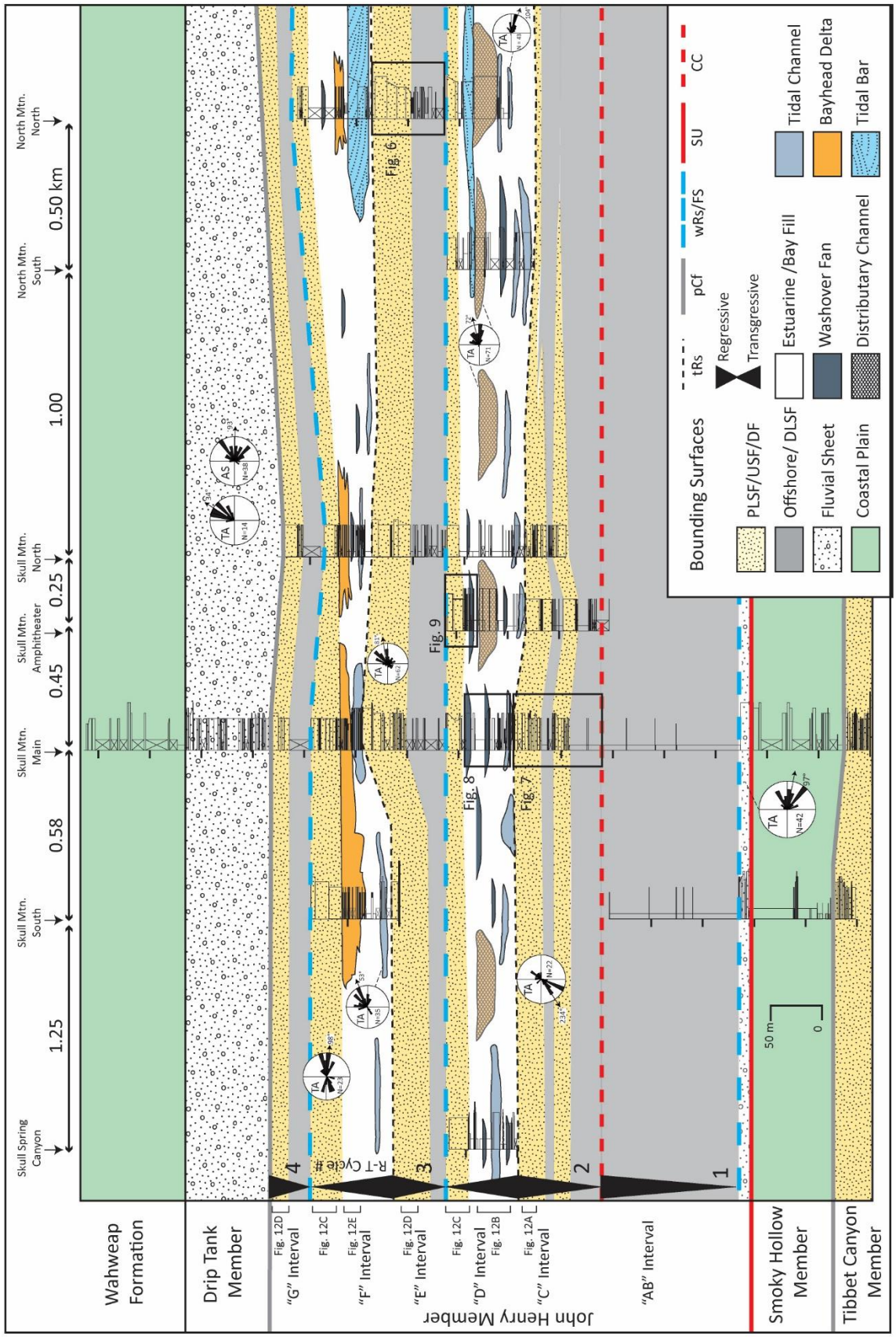
Skull Spring Canyon
Skull Mtn. South
Skull Mtn. Main
Skull Mtn. Amphitheater
Skull Mtn. North
North Mtn. South
North Mtn. North
1.25
0.58
0.45
0.25
1.00
0.50 km
Wahweap Formation
Drip Tank Member
John Henry Member
Smoky Hollow Member
Tibbet Canyon Member
"G" Interval
"F" Interval
"E" Interval
"D" Interval
"C" Interval
"AB" Interval
Fig. 12D
Fig. 12C
Fig. 12E
Fig. 12D
Fig. 12C
Fig. 12B
Fig. 12A
R-T Cycle #
4
3
2
1
Fig. 6
Fig. 7
Fig. 8
Fig. 9
50 m
0
Bounding Surfaces
tRs
pCf
wRs/FS
SU
CC
Regressive
Transgressive
PLSF/USF/DF
Offshore/ DLSF
Fluvial Sheet
Coastal Plain
Estuarine /Bay Fill
Washover Fan
Distributary Channel
Tidal Channel
Bayhead Delta
Tidal Bar

Figure 1.5. Biostratigraphic summary data for Buck Hollow plotted beside the Skull Mountain Main measured section (location in Fig. 1.1B). Sample locations are marked with stars, colored by location. Interpreted palaeoenvironment track is divided into four sub-environments. The curves of the key fossil groups represent total count of specimens per sample. Location of $^{40}Ar/^{39}Ar$ dated bentonite sample is marked by a yellow circle. Abbreviation: EOD - environment of deposition; DLSF - distal lower shoreface.

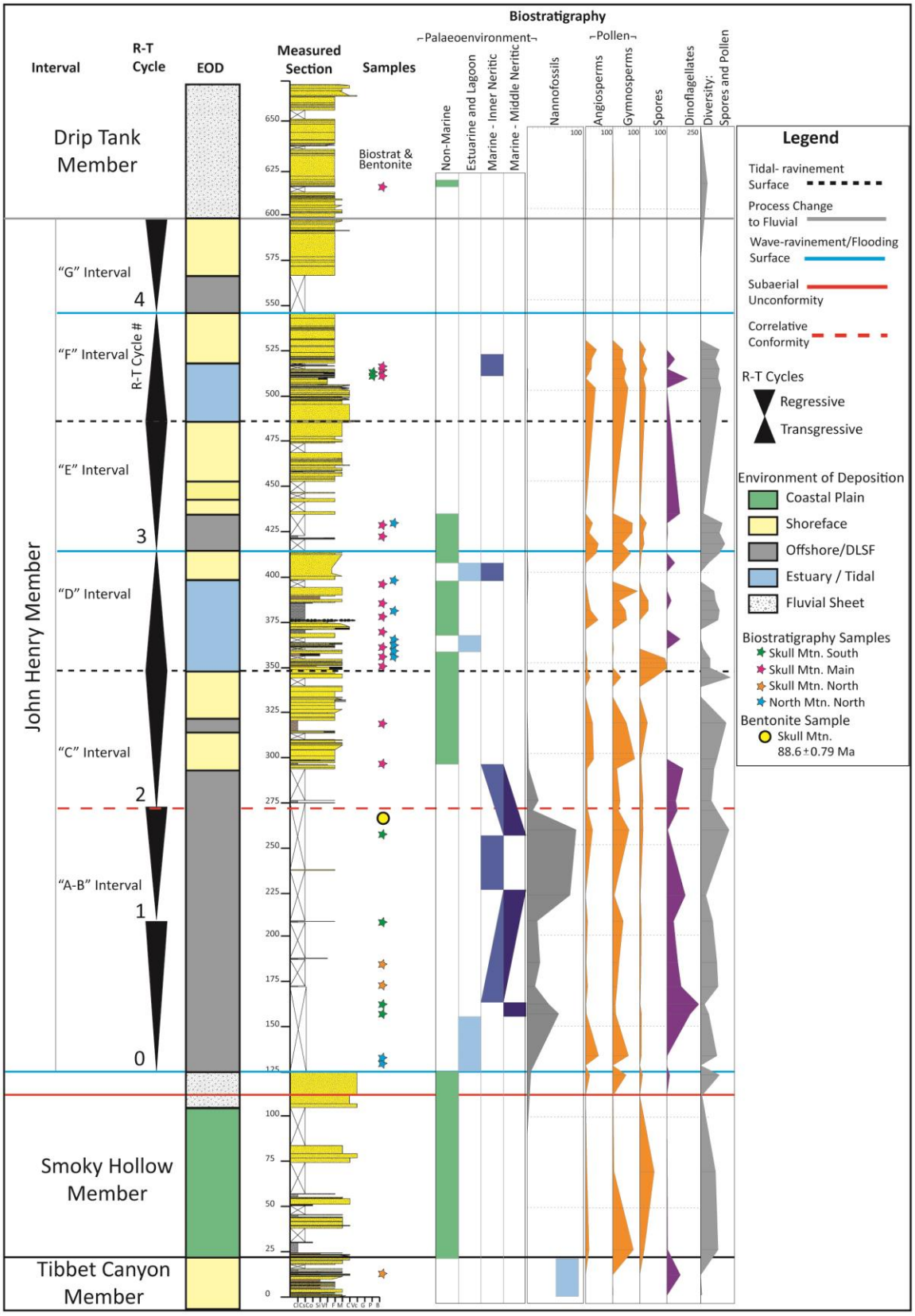
Biostratigraphy
Palaeoenvironment
Pollen
Interval
R-T Cycle
EOD
Measured Section
Samples
Non-Marine
Estuarine and Lagoon
Marine - Inner Neritic
Marine - Middle Neritic
Nannofossils
Angiosperms
Gymnosperms
Spores
Dinoflagellates
Diversity: Spores and Pollen
Drip Tank Member
Biostrat & Bentonite
"G" Interval
"F" Interval
"E" Interval
"D" Interval
"C" Interval
"A-B" Interval
R-T Cycle #
John Henry Member
Smoky Hollow Member
Tibbet Canyon Member
Legend
Tidal- ravinement Surface
Process Change to Fluvial
Wave-ravinement/Flooding Surface
Subaerial Unconformity
Correlative Conformity
R-T Cycles
Regressive
Transgressive
Environment of Deposition
Coastal Plain
Shoreface
Offshore/DLSF
Estuary / Tidal
Fluvial Sheet
Biostratigraphy Samples
Skull Mtn. South
Skull Mtn. Main
Skull Mtn. North
North Mtn. North
Bentonite Sample
Skull Mtn. 88.6±0.79 Ma

Figure 1.6. Representative measured section and field photos of the wave-dominated shoreface facies association (FA1): (**a**) Representative measured section of the shoreface facies association. The lower John Henry Member is characterised by coarsening-upwards parasequences stacked progradationally. Section is the "E" interval of the North Mountain North section (Fig. 1.4); (**b**) Interbedded mudstone and sandstone layers (LF2); (**c**) Representative outcrop showing stacked hummocky, swaley (LF3) and trough cross-stratified sandstone beds (LF4); (**d**) *Ophiomorpha nodosa;* (**e**) *Arenicolites*; (**f**) *Palaeophycus;* (**g**) *Cylindrichnus concentricus;* (**h**) Swaley cross-stratification (LF3); (**i**) Hummocky cross-stratification (LF3); (**j**) Gray fissile mudstones (LF1); (**k**) Three progradationally stacked shoreface parasequences from the "E" interval at Buck Hollow. Abbreviations: SF- shoreface; FA- facies association.

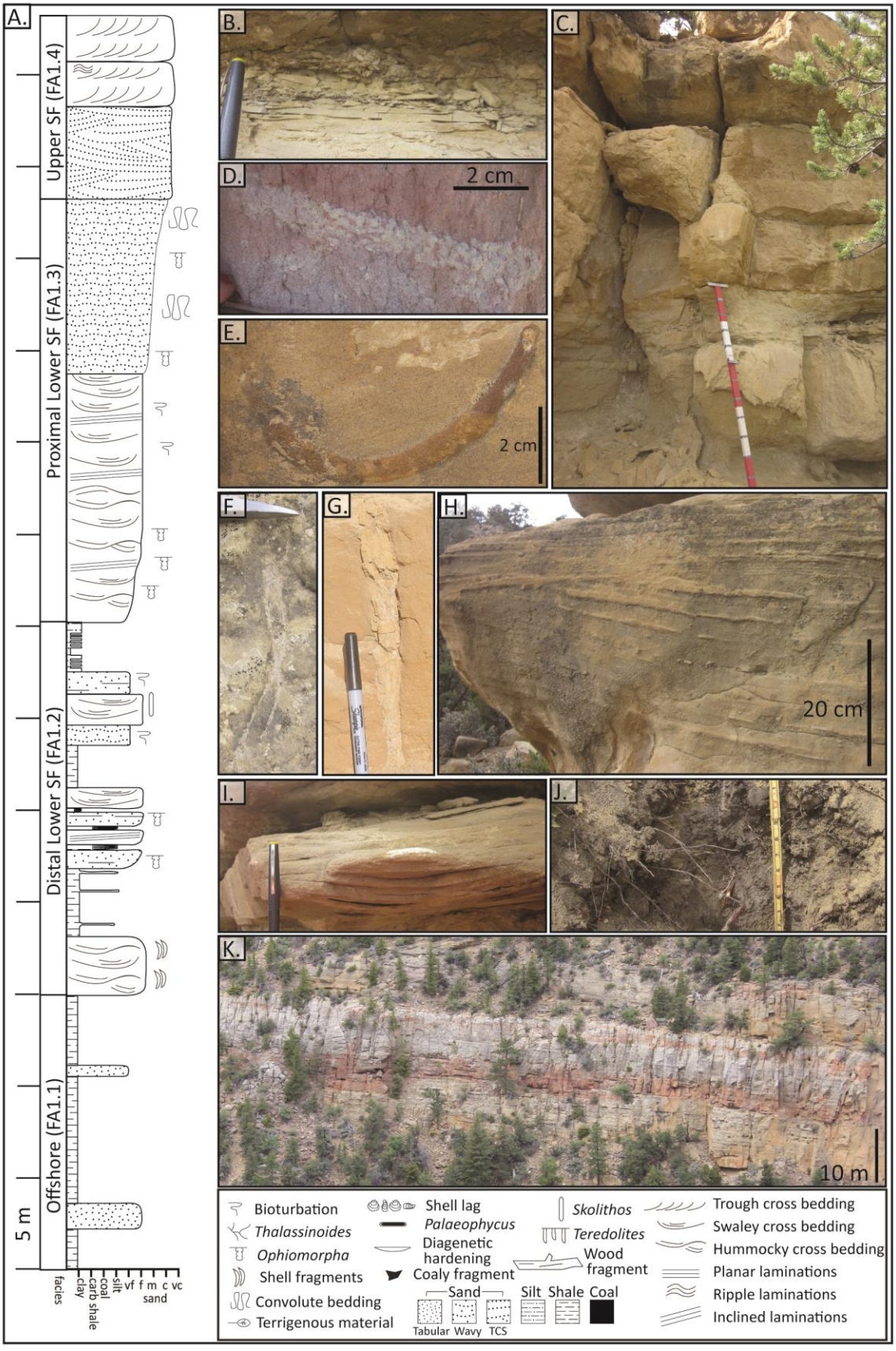
A.
Upper SF (FA1.4)
Proximal Lower SF (FA1.3)
Distal Lower SF (FA1.2)
Offshore (FA1.1)
5 m
facies
clay
carb shale
coal
silt
vf f m c vc
sand
B.
C.
D.
2 cm
E.
2 cm
F.
G.
H.
20 cm
I.
J.
K.
10 m
Bioturbation
Thalassinoides
Ophiomorpha
Shell fragments
Convolute bedding
Terrigenous material
Shell lag
Palaeophycus
Diagenetic hardening
Coaly fragment
Skolithos
Teredolites
Wood fragment
Sand
Tabular
Wavy
TCS
Silt
Shale
Coal
Trough cross bedding
Swaley cross bedding
Hummocky cross bedding
Planar laminations
Ripple laminations
Inclined laminations

Figure 1.7. Field photos and measured section representing the wave-dominated delta facies association (FA2): (**a**) Representative measured section of a delta succession. Section is the "C" interval from the Skull Mountain Main section (Figs. 1.4, 1.11 & 1.14); (**b**) Delta front facies (LF3 & LF4), with wavy bedding (**c**); (**d**) The lower delta front contains swaley cross-stratification (LF3), suggesting wave influence; (**e**) Inoceramid fragment; (**f**) Outcrop photo of the lower delta front showing interbedded mudstones and sandstones (LF2 & LF3); (**g**) Muddy interbedded interval from the delta front showing disturbed beds; (**h**) Shell impression; (**i**) Leaf impression showing proximity to fluvial output; (**j**) Outcrop photo showing progradationally stacked delta successions truncated by tidal ravinement. Legend in Figure 1.6.

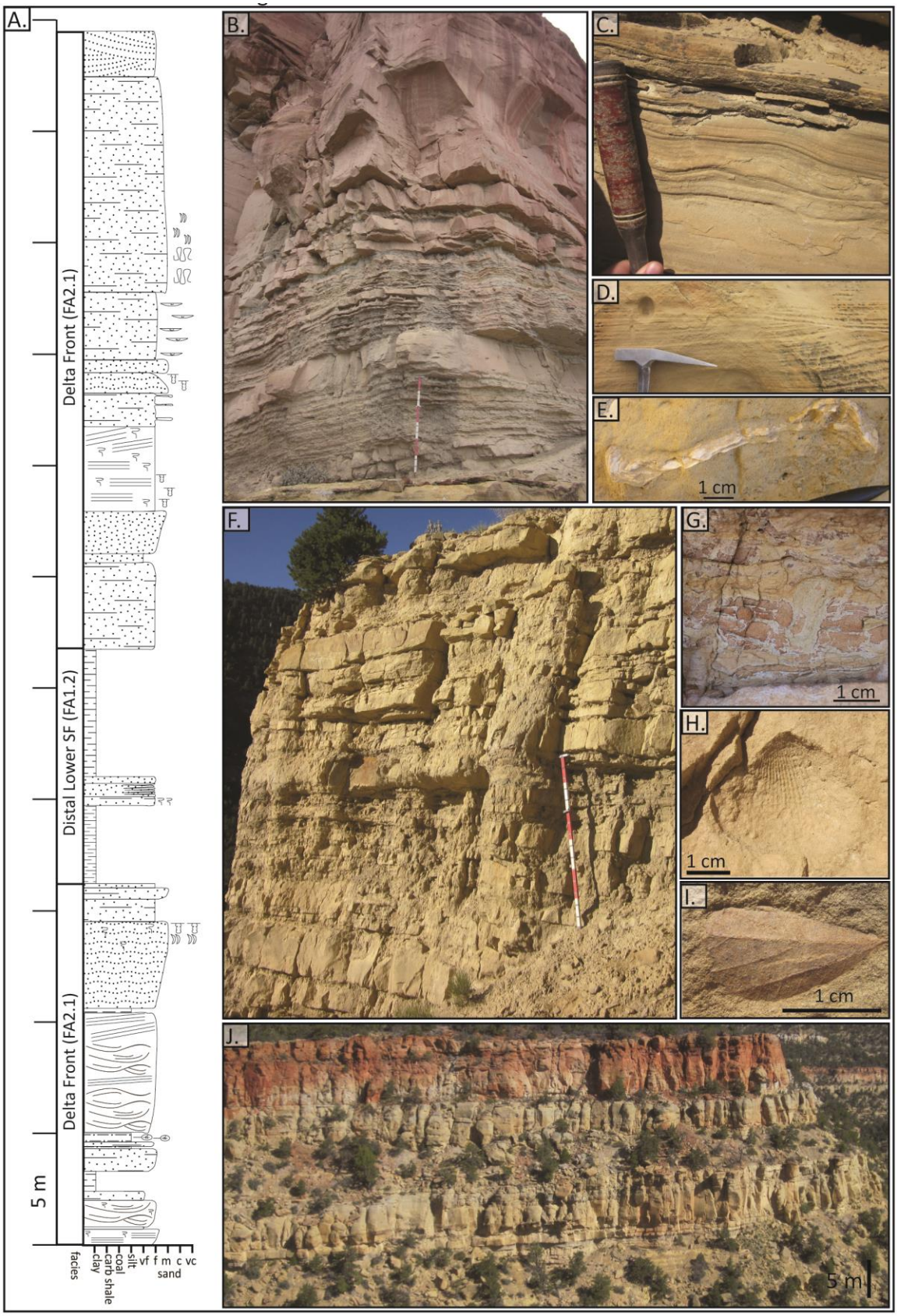
A.
Delta Front (FA2.1)
Distal Lower SF (FA1.2)
Delta Front (FA2.1)
5 m
facies
clay
carb shale
coal
silt
vf f m c vc
sand
B.
C.
D.
E.
1 cm
F.
G.
1 cm
H.
1 cm
I.
1 cm
J.
5 m

Figure 1.8. Field photos illustrating the diversity of estuarine facies (FA3) preserved in Buck Hollow: (**a**) Representative measured section for the estuarine facies association. Section is the lower "D" interval from the Skull Mountain Main section (Figs. 1.4, 1.11 & 1.14); (**b**) *Thalassinoides* burrows on a bedding plane of a bayhead delta sandstone bed; (**c**) Washover fan outcrop (LF9) with an outline around a concentration of shell fragments in the upper part of the fan (LF8); (**d**) *Palaeophycus* fossil from a washover fan outcrop; (**e**) Carbonaceous shale and coal at the base of a washover fan outcrop; (**f**) Vertical trace fossils (*Skolithos*) from the interbedded portion off a bayhead delta outcrop; (**g**) Convolute bedding from a bayhead delta outcrop; (**h**) Ammonite impression from a bayhead delta outcrop; (**i**) Outcrop image of a bayhead showing the wavy and interbedded nature of the beds (LF14); (**j**) Impression of plant material from carbonaceous mudstones (LF6) within the bayhead delta deposits; (**k**) Sharks' tooth from a bayhead delta deposit; (**l**) *Cylindrichnus concentricus* from a bayhead delta outcrop; (**m**) Shell fragments from a washover fan outcrop (LF8); (**n**) *Cylindrichnus concentricus* from a distributary channel; (**o**) Distributary channel outcrop (LF10) with metre-scale channels separated by a coarse-grained matrix with abundant mudstone clasts; (**p**) Terrigenous material from a distributary channel outcrop (LF10); (**q**) Large mudstone clasts within a coarse-grained sandstone matrix from the interchannel portion of a distributary channel outcrop (LF10); (**r**) *Teredolites* from an interchannel portion of a distributary channel outcrop. Legend in Figure 1.6.

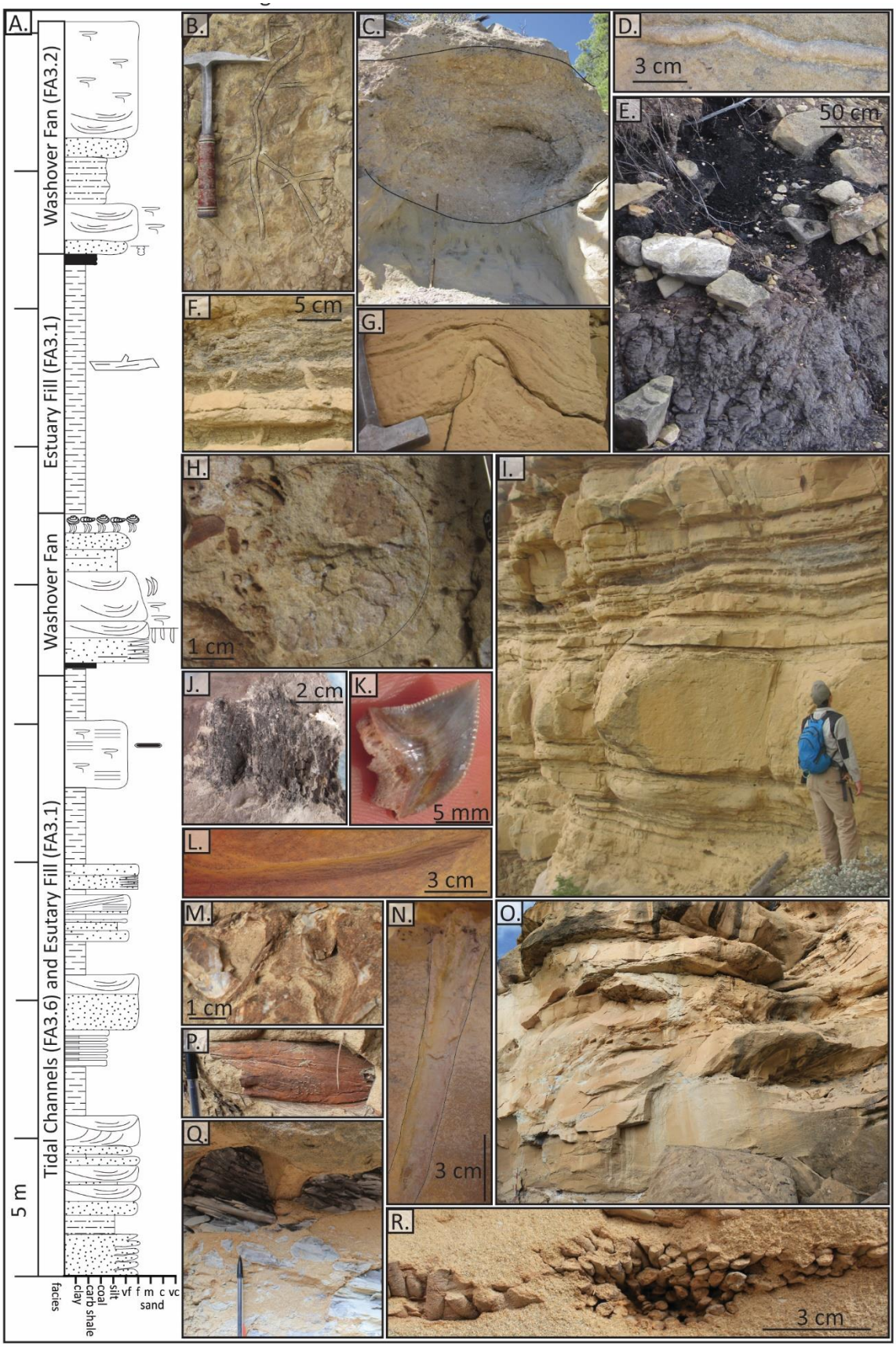
A.
5 m
Washover Fan (FA3.2)
Estuary Fill (FA3.1)
Washover Fan
Tidal Channels (FA3.6) and Esutary Fill (FA3.1)
facies
clay
carb shale
coal
silt
vf f m c vc
sand
B.
C.
D.
3 cm
E.
50 cm
F.
5 cm
G.
H.
1 cm
I.
J.
2 cm
K.
5 mm
L.
3 cm
M.
1 cm
N.
3 cm
O.
P.
Q.
R.
3 cm

Figure 1.9. Field photos illustrating the tidal (FA3) and barrier island facies present in Buck Hollow: (**a**) Representative measured section showing estuarine facies overlain by a barrier island shoreface. Section is the upper "D" interval from the Skull Mountain Amphitheater section (Fig. 1.4); (**b**) Tidal channels (LF11); (**c**) Interbedded interval composed of laminated mudstones (LF7) and coarse-grained sandstone lenses (LF16). Mudstones contain abundant leaf and plant impression. Sandstone lenses are ~1-10 cm thick and contain small coal and mud rip-up fragments; (**d**) Tidal bars with lateral accretion master surfaces (LF13); (**e**) *Palaeophycus* from a tidal bar; (**f**) *Thalassinoides* preserved within a coal bed at the base of a tidal bar; (**g**) Tidal bar showing *Palaeophycus*, *Cylindrichnus*, and *Ophiomorpha*; (**h**) Rhizoliths from a tidal bar; (**i**) *Diplocraterion* from a tidal bar; (**j**) Estuary and barrier island outcrop showing the sharp juxtaposition of barrier island shoreface sandstones on top of interbedded estuary fill. Legend in Figure 1.6.

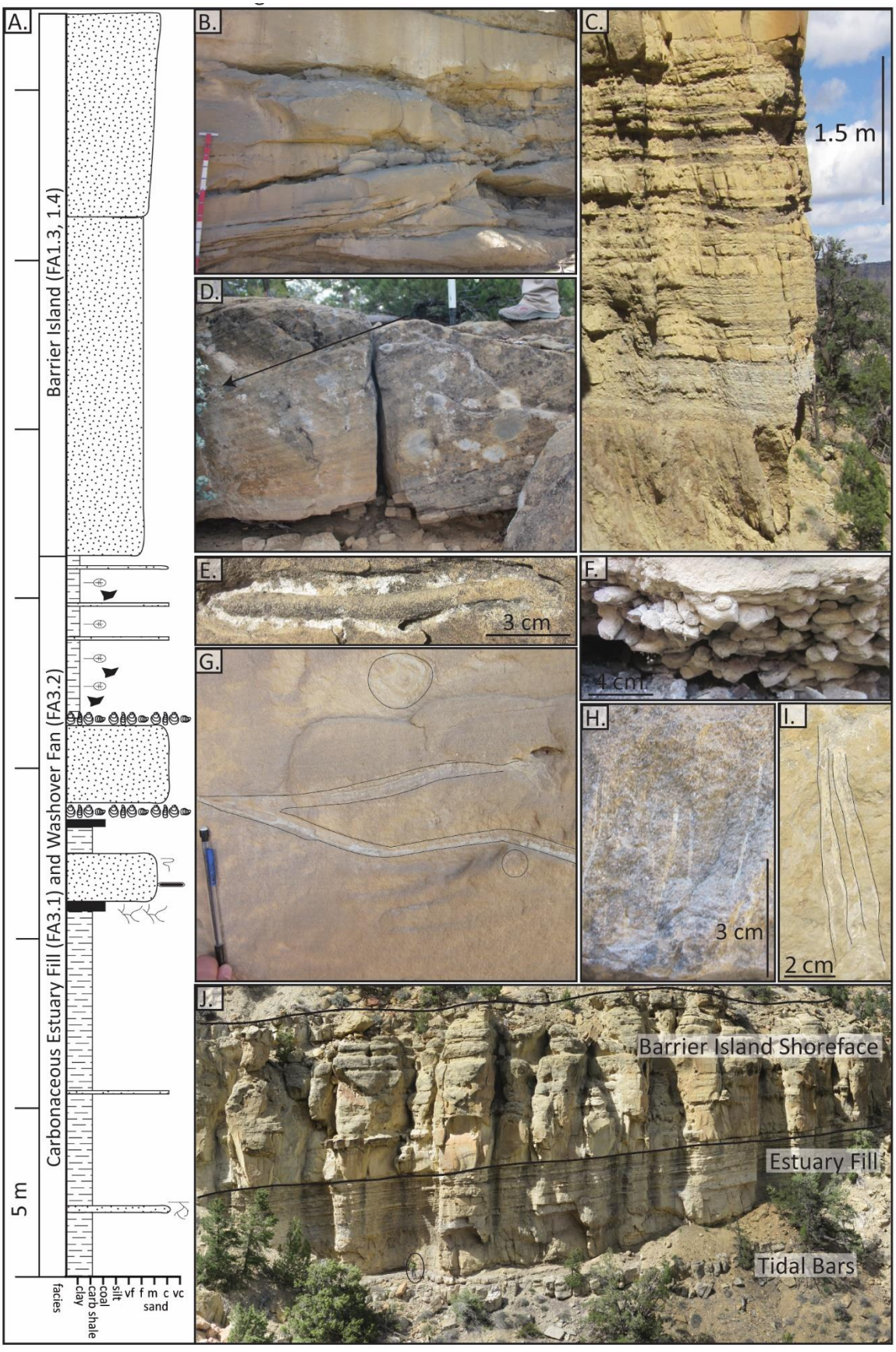
A.
Barrier Island (FA1.3, 1.4)
Carbonaceous Estuary Fill (FA3.1) and Washover Fan (FA3.2)
5 m
facies
clay
carb shale
coal
silt
vf f m c vc
sand
B.
C.
1.5 m
D.
E.
3 cm
F.
4 cm
G.
H.
3 cm
I.
2 cm
J.
Barrier Island Shoreface
Estuary Fill
Tidal Bars

Figure 1.10. Schematic stratigraphic columns showing the decompacted and compacted (italics) thicknesses of representative measured sections for Buck Hollow and Main Canyon. Decompaction values were generated through one-dimensional basin modeling. See Table 1.3 for model inputs.

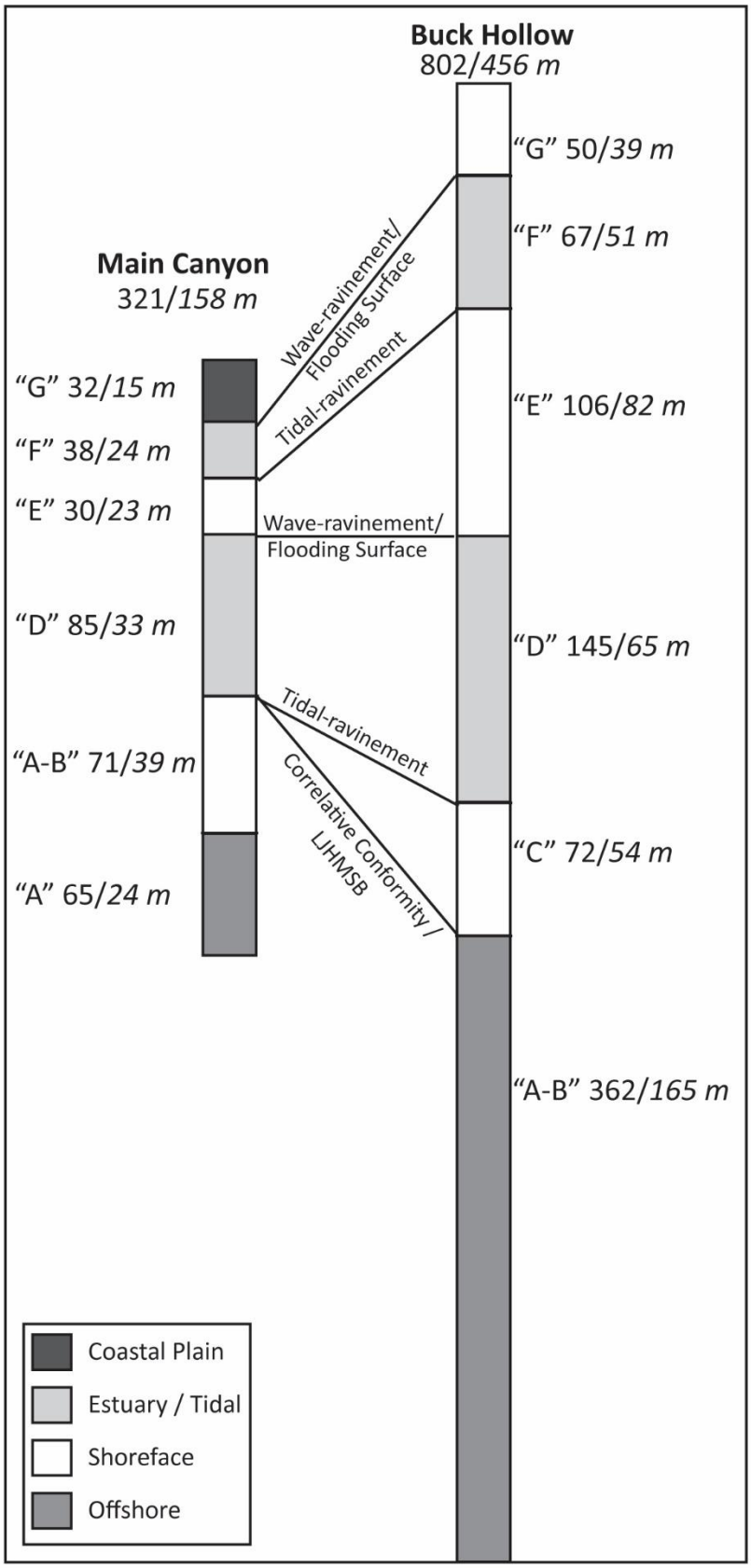
Buck Hollow
802/456 m
"G" 50/39 m
"F" 67/51 m
"E" 106/82 m
"D" 145/65 m
"C" 72/54 m
"A-B" 362/165 m
Main Canyon
321/158 m
"G" 32/15 m
"F" 38/24 m
"E" 30/23 m
"D" 85/33 m
"A-B" 71/39 m
"A" 65/24 m
Wave-ravinement/ Flooding Surface
Tidal-ravinement
Wave-ravinement/ Flooding Surface
Tidal-ravinement
Correlative Conformity / LJHMSB
Coastal Plain
Estuary / Tidal
Shoreface
Offshore

Figure 1.11. Regional stratigraphic correlation from southwest to northeast across the northern Kaiparowits Plateau from Main Canyon and Buck Hollow. Correlation location shown on Figure 1. Abbreviations: TCM - Tibbet Canyon Member; SHM - Smoky Hollow Member; JHM - John Henry Member; DTM- Drip Tank Member; DLSF - distal lower shoreface; pCf - process change from tide- to fluvial-dominated processes; tRs- tidal-ravinement surface; wRs/FS - wave-ravinement/flooding surface; SU/mRs/tRs - combined subaerial unconformity, maximum regressive surface, and tidal- ravinement surface; LJHMSB - lower John Henry Member sequence boundary. Modified from Chentnik *et al.* (2015).

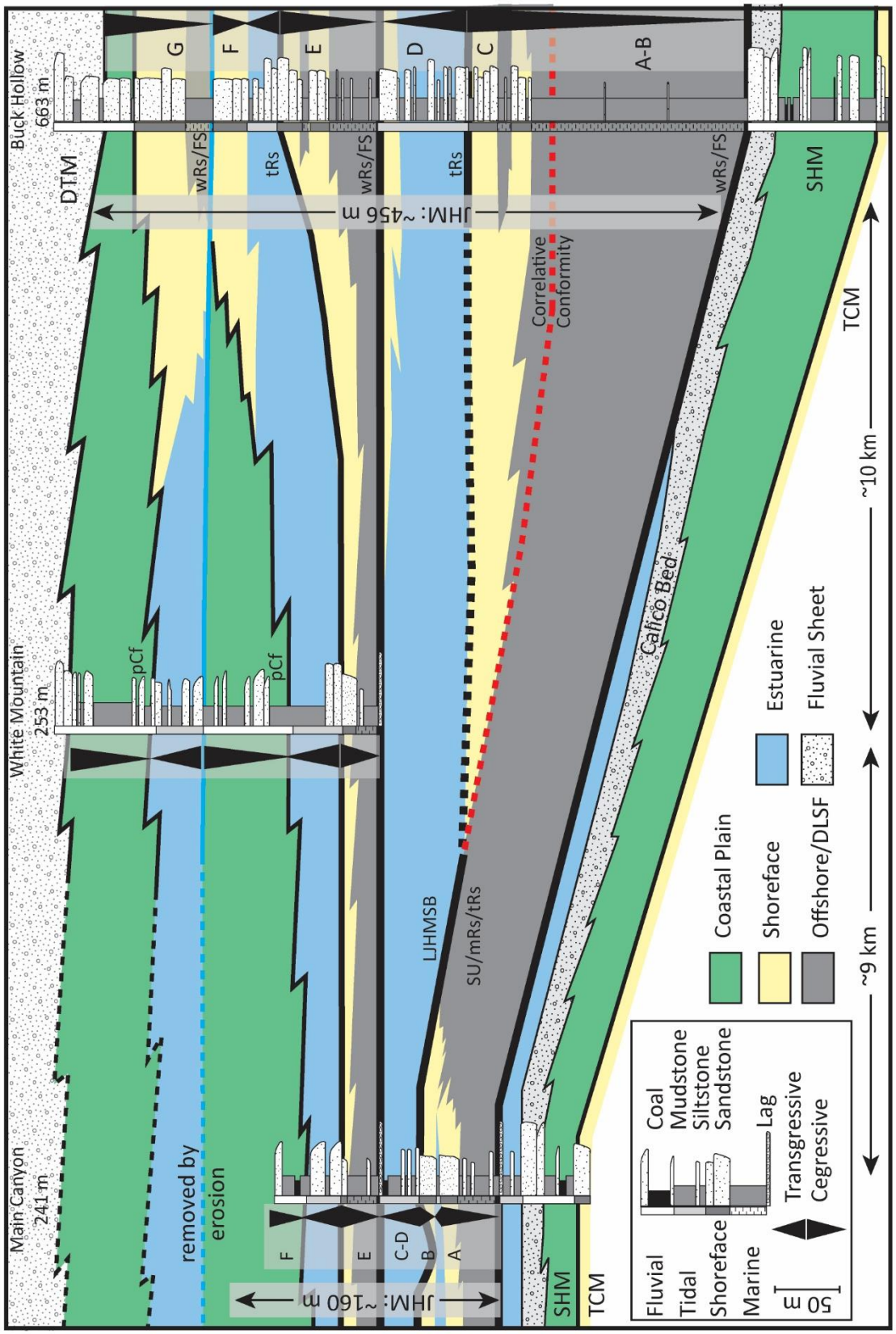
Buck Hollow
663 m
White Mountain
253 m
Main Canyon
241 m
DTM
G
F
E
D
C
A-B
wRs/FS
tRs
wRs/FS
tRs
wRs/FS
JHM: ~456 m
Correlative
Conformity
pCf
pCf
removed by
erosion
LJHMSB
SU/mRs/tRs
Calico Bed
SHM
TCM
F
E
C-D
B
A
JHM: ~160 m
SHM
TCM
~9 km
~10 km
Coastal Plain
Shoreface
Offshore/DLSF
Estuarine
Fluvial Sheet
Fluvial
Tidal
Shoreface
Marine
Coal
Mudstone
Siltstone
Sandstone
Lag
Transgressive
Cegressive
50 m

Figure 1.12. Schematic palaeogeographic maps for Buck Hollow showing the distribution of depositional environments through time. Black circles mark points controlled by measured section observations. These points are spaced laterally based on the Buck Hollow measured section correlation line shown at the bottom (cf. A-A' Figs. 1.1B & 1.4). The points are positioned on the maps to indicate the facies preserved in each measured section. The approximate stratigraphic level of each interval depicted is shown in Figure 1.4. (**a**) Wave-dominated delta progradation is characterised by direct fluvial output to the shoreline, shore-parallel mouth bars, and shorefaces. (**b**) Wave-dominated estuary settings include washover fans, flood tidal deltas, longitudinal tidal bars, central estuary, and marsh/swamp environments. (**c**) Barrier island settings are characterised by a tidal inlet and shoreface environments that are detached from the mainland. (**d**) Wave-dominated shoreface settings are attached to the mainland. (**e**) Proximal wave-dominated estuaries are characterised by bayhead delta and central estuary environments.

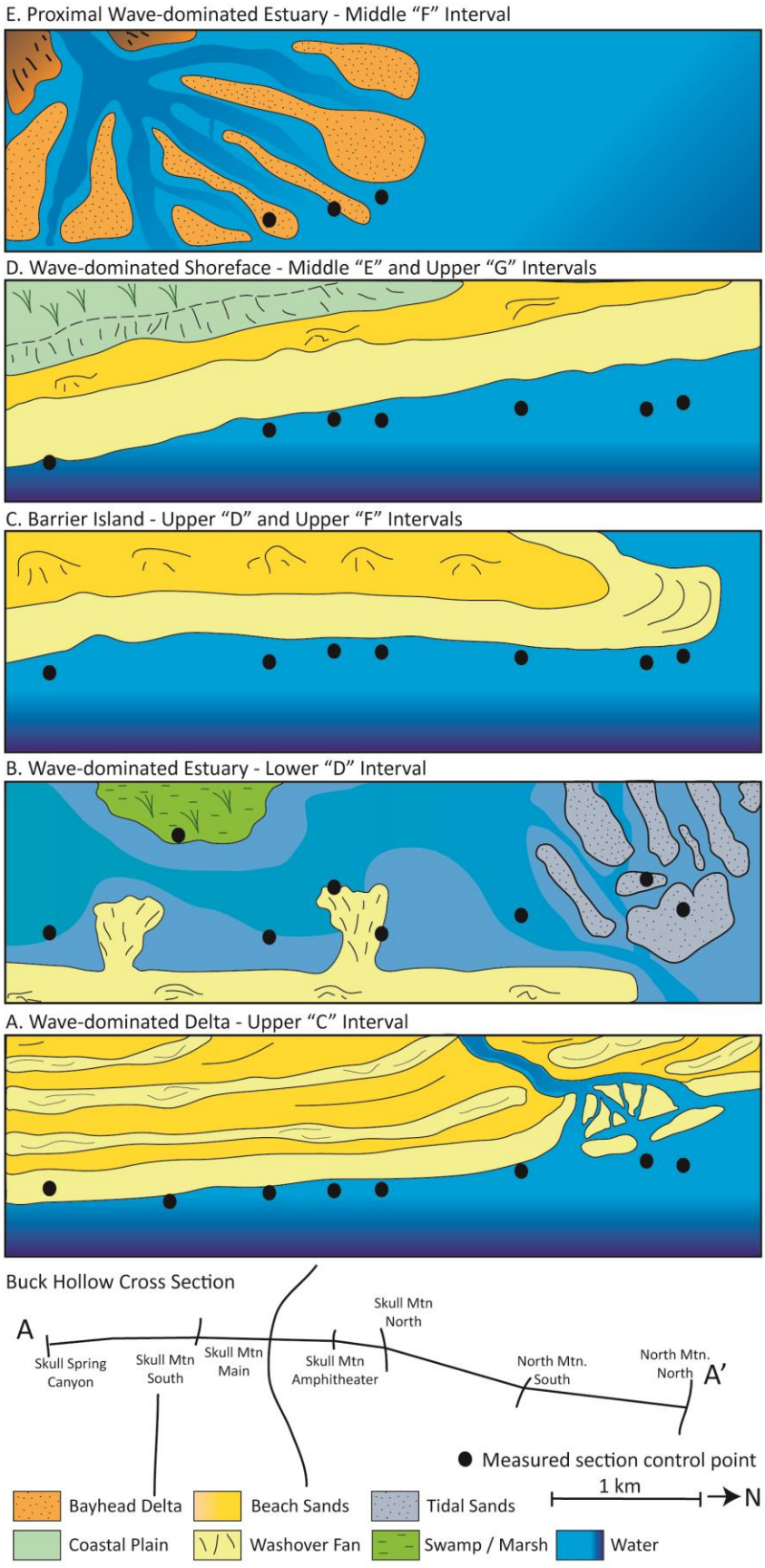
E. Proximal Wave-dominated Estuary - Middle "F" Interval
D. Wave-dominated Shoreface - Middle "E" and Upper "G" Intervals
C. Barrier Island - Upper "D" and Upper "F" Intervals
B. Wave-dominated Estuary - Lower "D" Interval
A. Wave-dominated Delta - Upper "C" Interval
Buck Hollow Cross Section
A
Skull Spring Canyon
Skull Mtn South
Skull Mtn Main
Skull Mtn Amphitheater
Skull Mtn North
North Mtn. South
North Mtn. North
A'
Measured section control point
1 km
N
Bayhead Delta
Beach Sands
Tidal Sands
Coastal Plain
Washover Fan
Swamp / Marsh
Water

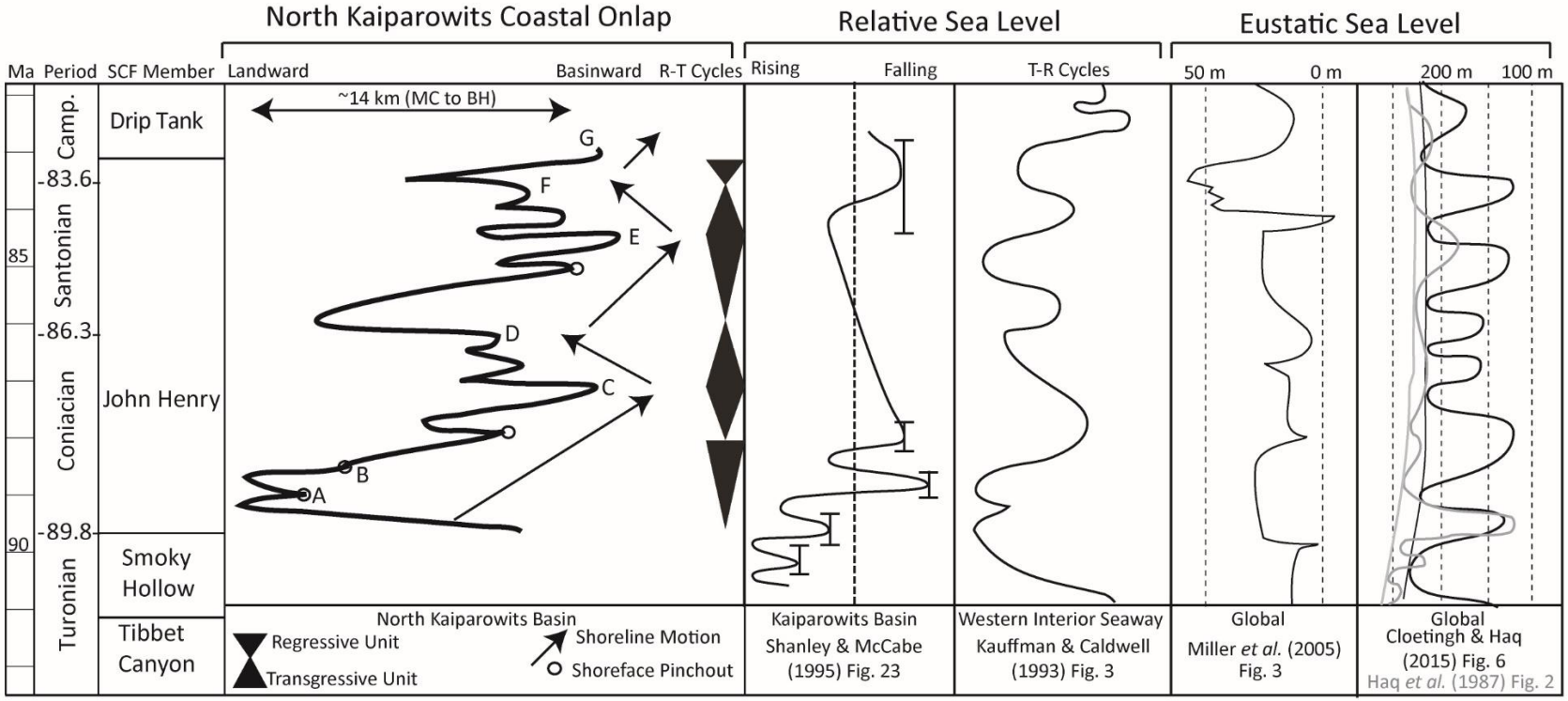

Figure 1.13. Coastal onlap, relative sea level, and global eustatic sea level curves for the Turonian to Campanian. North Kaiparowits coastal onlap curve estimates the relative shifts in the shoreline position based on the stratigraphy at Buck Hollow and Main Canyon and down-dip shoreface pinchouts (into offshore marine) where identified. Vertical bars in the Kaiparowits Plateau curve represent the estimates of uncertainty in the age dates of the sequence boundaries designated by Shanley & McCabe (1995). Abbreviations: Camp.- Campanian; SCF - Straight Cliffs Formation; MC - Main Canyon; BH - Buck Hollow; R-T - regressive-transgressive.

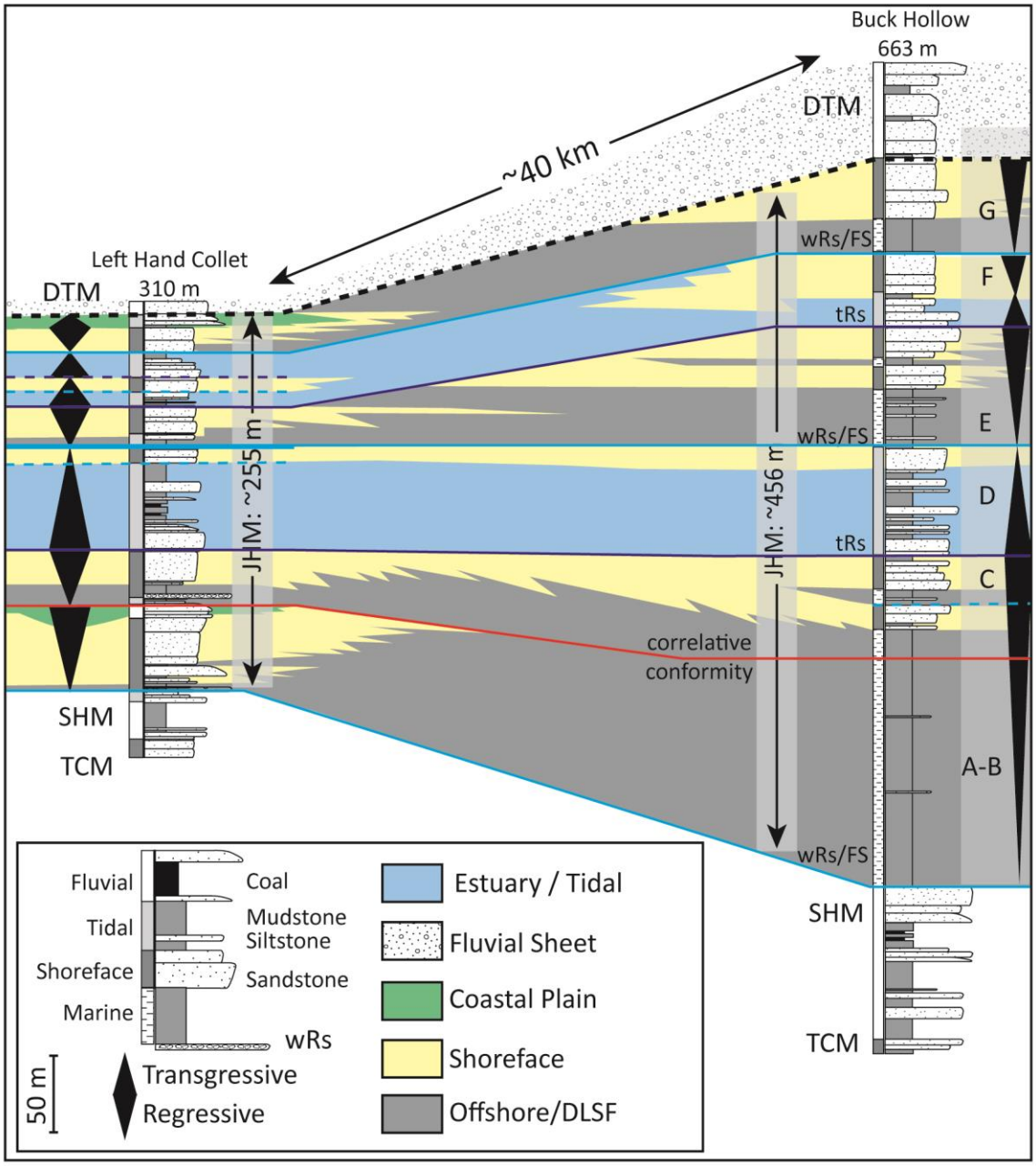

Figure 1.14. Stratigraphic correlation between Left Hand Collet (Dooling 2013) and Buck Hollow, correlation location shown on Figure 1.1. Abbreviations: TCM - Tibbet Canyon Member; SHM - Smoky Hollow Member; JHM - John Henry Member; DTM - Drip Tank Member; wRs/FS - wave-ravinement/flooding surface; tRs - tidal-ravinement surface; DLSF - distal lower shoreface.

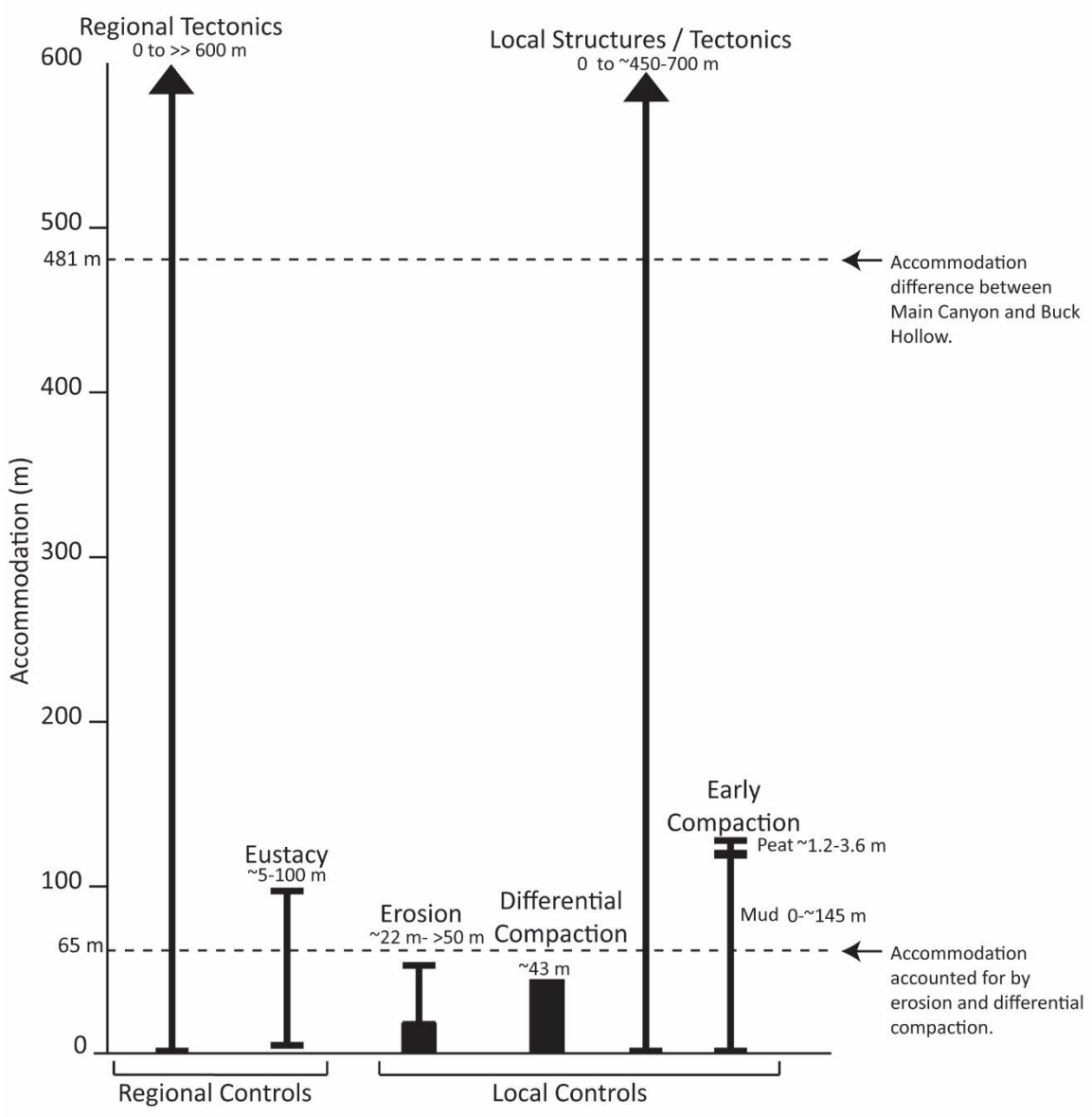

Figure 1.15. Schematic plot showing estimates of possible controls on accommodation. The accommodation generated by regional tectonics at the ~10 My time scale could range to over 600 m (Currie 2002). Eustatic variation of ~5-100 m occurred during John Henry Member deposition (Haq *et al.* 1987; Miller *et al.* 2005; Cloetingh & Haq 2015). Upper arrow notes the total decompacted thickness difference between Buck Hollow and Main Canyon (481 m). Lower arrow notes combined accommodation difference (65 m) accounted for by erosion (22 m) measured from outcrop (Chentnik *et al.* 2015) and post depositional differential compaction (43 m) calculated through back-stripping (black boxes). Estimates for early compaction were made by applying modern rates of early compaction (Table 1.7) to the thickness values from Buck Hollow (see text). The estimate of the potential accommodation generated by local structures and tectonics (~450-700 m) was determined by applying expansion values (2.8x) from nearby faulting (Tindall *et al.* 2010) to the John Henry Member at Main Canyon and Left Hand Collet.

Table 1.1
Lithofacies Descriptions

Lithofacies	Lithofacies Description and Architecture	Trace/Body Fossils
LF1– gray mudstone	Wavy-laminated mudstones, generally gray colored and fissile. Clay-rich with a minor silty component.	Small shell fragments, inoceramid and oyster shell fragments. BI = 0-1
LF2– Interbedded light brown-gray mudstone, siltstone, fine-grained sandstone	Planar-laminated mudstones and siltstones, 1-10 cm thick, with rare symmetrical wave ripples. Sandstone beds are 0.2-1 m thick, sharp-based, and contain abundant hummocky cross-stratification (HCS). Packages coarsen upward from silt to very fine-grained sandstone in 0.5-4 m sections.	Small shell fragments, Thalassinoides, Planolites. BI = 0-3
LF3– Hummocky and swaley cross-stratified sandstone	Outcrop-forming very fine- to fine-grained sandstones, form sharp-based coarsening-upward packages, separated by finer-grained sandstones or marine mudstones. Amalgamated sandstone units can be >25 m thick and laterally continuous >10 km. HCS and swaley-cross stratification (SCS) are abundant. Locally, SCS grades into zones of planar laminations that are gently inclined to the east.	Minor inoceramid and oyster shell fragments. Ophiomorpha, Thalassinoides, Skolithos. BI = 0-3
LF4– Trough cross-stratified sandstone and planar bedded sandstone	Cliff forming fine to medium-grained sandstones. Abundant trough cross-stratification (TCS). Internally bedding is blocky and consists of thick (>1 m) sandstone beds with occasional mud (~5 cm) interbeds.	Small shell fragments. Ophiomorpha. BI = 0-3
LF5– Homogeneous and planar bedded medium grained sandstone	Planar bedded to massive medium-grained sandstone. Rare trough cross-stratification.	Rare shell fragments. BI = 0-1
LF6 - Carbonaceous mudstone and coal	Massive and planar-laminated siltstones and mudstones with minor interbeds of very fine-grained ripple-laminated sandstones and coal. The organic content of carbonaceous shales increases vertically at the bed scale, with thin (typically <0.5 m) coals typically occurring as capping units. Siltstone and rippled sandstones are most commonly observed at the bases of sandstone bodies.	Root traces were the only fossils observed. BI = 0-1
LF7– Interlaminated light and dark gray mudstone	Blocky, wavy-interbedded mudstones with mm-scale laminations of alternating light and dark gray mudstones. Common (<1 cm thick) coarse-grained sandstone layers.	Skolithos filled with coarse grained orange sandstone BI= 0-2
LF8– Shell hash conglomerate	Small, laterally discontinuous .2-2 m beds of shell fragments within a coarse-grained sandstone matrix. Shell fragments range from whole to broken and weathered. Fragment sizes range from 0.5-15 cm long.	Oyster shells. BI=0

LF9– Isolated medium grained sandstone lense	Lens-shaped, medium-grained sandstone deposits with internal trough cross-stratification. Generally, white to yellow colored. Pockets of convolute bedding and soft sediment deformation. Prevalent oyster shell fragments, often large sized (>15 cm), grouped into lags and lenses. Sporadic large (>20 cm) pockets of Teredolites.	Prevalent shell fragments, often large (>15 cm) sized, grouped into lenses and lags. Mollusks and inoceramids. Teredolites, Skolithos, Palaeophycus, Ophiomorpha BI = 0-3
LF10– Amalgamated trough cross-bedded sandstone with mudstone rip-up clasts	Cliff forming, amalgamated, trough cross-stratified, channelised coarse-grained sandstones with rare pebbles. Generally, orange colored. Channelised beds cut into matrix supported intervals with highly variably sized mud clasts (.5-25 cm). Some mud clasts show internal lamination. Matrix is composed of coarse-grained, cemented sandstone.	Leaf fossils. Teredolites. Oyster fragments. BI=0-2
LF11– Channelised, bidirectional sandstone	Laterally confined sigmoidal bars and channel-shaped sandstones. Sandstones typically fine upwards and contain primary sedimentary structures of: low-angle planar laminations, wavy-lenticular-flaser bedding, convolute beds, bidirectional, planar, and trough cross-stratification with double mud drapes and abundant reactivation surfaces.	Inoceramid and oyster shell fragments, Trace fossils are scarce but include: Skolithos, and Planolites. BI = 0-3
LF12–Tabular, bidirectional cross-stratified sandstone	Medium-grained, well-sorted sandstones contain abundant reactivation surfaces, planar, trough, sigmoidal, and herringbone cross-stratification, mud and carbonaceous draped cross-sets, and ball-pillow and flame soft-sediment deformation features.	Shell fragments of inoceramid and oysters fragments are common, with minor amounts of terrestrial plant debris observed scattered throughout. Palaeophycus and Diplocraterion. BI = 0-1
LF13–High-angle laminated sandstone	Medium-grained sandstones with high-angle accretion sets and trough cross-stratification. Beds range in thickness from 0.-1.5 m. Some convolute bedding visible toward the top.	Occasional shell fragment. BI = 0
LF14– Inclined heterolithic strata	Thinly interbedded very fine-grained sandstone and mudstone. Inclined beds are between 0. -1.5 m thick, and laterally interfinger with medium-grained sandstone deposits, carbonaceous shales, terrestrial, material visible within layers. Double mud drapes occur along foresets of low-angle trough cross-stratification within sandstones.	Shell and wood fragments were found with marine trace fossils, ammonite impression, sharks' teeth; Planolites, Cylindrichnus, Thalassinoides and Skolithos. BI = 0-3
LF15–Heavily bioturbated sandstone	Cliff forming fine-grained sandstones (~1 -3 m thick) intervals of heavy bioturbation.	Occasional shell fragments and sharks' teeth. Trace fossils almost exclusively Ophiomorpha. BI = 3-6
LF16– Homogenous, tabular sandstone	Homogenous, tabular fine- to medium-grained sandstones.	Occasional shell fragments and mudstone clasts concentrated along bedding laminations. BI = 0

Bioturbation Index (BI) follows the scheme of Taylor & Goldring (1993).

Table 1.2
Description of Facies Associations for Buck Hollow

LFs	Description	FA	EOD	Justification
Facies Association Group 1 – Wave-dominated Shoreface (Fig. 1.6)				
LF1, LF2	Recessed and partly covered intervals composed of planar to wavy bedded, fissile, gray mudstones (LF1) and interbedded mudstones and sandstones (LF2; Fig. 1.6J) with occasional Inoceramid and oyster shell fragments. Thin sandstones (LF3) display hummocky cross stratification (HCS) and are occasionally bioturbated (Thalassinoides).	1.1	Offshore	These mudstones are interpreted as offshore strata (Plint 2010) deposited below storm weather wave base (>30; George & Hill 2008), likely transported via hyperpycnal flows (Hillet al. 2007; Bhattacharya & MacEachern 2009).
LF1, LF2, LF3	Mudstones deposits (LF1) grading verticallyinto interbedded with millimetre scale laminated mudstones and sandstones (LF2) and hummocky and swaley cross-stratified sandstone beds (LF3) 2-50 cm thick.	1.2	Distal lower shoreface	These hummocky and swaley cross-stratified interbedded sandstones record shelfal transport and reworking during storms (Duke 1985; Southard et al. 1990; Dumas 2005; Dumas & Arnott 2006)suggesting deposition in a distal lower shoreface environment (Clifton 2006).
LF3, LF4 LF1	Hummocky and swaley cross-stratified sandstone beds (LF3) .1 -1 m thick grading into planar laminated and trough cross -stratified sandstone beds (LF4; Fig. 1.6H,I). Sandstones separated by mm -cm scale mudstone layers (LF1).	1.3	Proximal lower shoreface	These sandy deposits show evidence of both oscillatory and geostrophic flows, suggesting deposition below fair-weather wave base in the proximal lower shoreface (Reading & Collinson 1996) known to contain Cylindrichnus concentricus(Frey 1990).
LF4, LF1	Blocky bedded (0.5-2 m thick) fine- to medium -grained, trough cross - stratified and planar -bedded sandstones containing Skolithosand Ophiomorpha (LF4). Beds are laterally continuous and separated by thin (<1 cm thick) interbeds of fissile, laminated, gray mudstones (LF1).	1.4	Upper shoreface	The higher energy indicators, such as Ophiomorpha (Droser & Bottjer 1989), within these deposits suggest deposition in the upper shoreface above fair -weather wave base (Plint 2010).
LF5	Single bed 1 -2 m thick bed of planar laminated medium -grained sandstone (LF5) with occasional shell fragments in some locations.	1.5	Foreshore	These planar laminated sandstones are foreshore strata deposited in the swash zone (Wright & Short 1984;Masselink & Puleo 2006; Plint 2010).
Facies Association Group Two – Wave-dominated Delta (Fig. 1.7)				
LF3, LF4, LF1	Sharp-based, gently inclined (<5°), hummocky and swaley cross-stratified sandstones (LF3) and trough cross -bedded and planar fine - to medium- grained sandstones (LF4). Sands contain Ophiomorpha, shell fragments (Fig. 1.7E), and leaf impressions (Fig. 1.7I). Beds are tabular and increase in size from .1-2 m thick (Fig. 1.7B). Mudstone interbeds are laterally discontinuous and vary in thickness (.1 -1 cm; Fig. 1.7B).	2.1	Delta front	The sharp-based nature of the sandstone packages, inclination of bedding, and terrigenous material suggest deposition in mouth bars in a delta front with sediment supplied by nearby distributary channels (Walker & Plint 1992; Gingras et al. 1998). Dominance of trough cross -bedded sandstones suggests unidirectional current flow in the upper delta front (Charvinet al. 2010).
Facies Association Group Three – Wave-dominated Estuary (Figs. 1.8 & 1.9)				
LF6, LF1, LF7	Carbonaceous mudstones and siltstones, often capped by .1 -1 m coal beds (Fig. 1.8E). Carbonaceous mudstones and siltstones have a high sulphur content, abundant plant material, and contain sporadic shell fragments. Interval is predominantly covered and erodes into blocky fragments, suggesting wavy rather than fissile bedding. Tends to create intervals .2-5 m thick. Intervals are eroded by higher energy facies.	3.1	Proximal carbonaceous estuary fill	These carbonaceous intervals are interpreted as deposition within a low energy back-barrier estuary or bay with flanking swamps or tidal marsh areas, which provided the terrigenous material (Snedden & Kersey 1981; Holzet al. 2000). Carbonaceous shales grade vertically into coals, suggesting the coals are wetting upwards and transgressive (Wadsworth et al. 2010).
LF9, LF5, LF8,	Lens shaped medium -grained sandstone deposits with internal trough cross-stratification (LF9). Sandstone have pockets of convolute bedding and soft sediment deformation. Prevalent oyster shell fragments, often large sized (>15 cm), grouped into lags and lenses (LF8; Fig. 1.8C). Interval is heavilybioturbated and contains Ophiomorpha,	3.2	Washover fans	These deposits are washover fans , which display upper plane bed sedimentation (Barwis & Hayes 1985) with trough and ripple cross - stratification formed by runoff channels (McCubbin 1982; Schwartz 1982). Marine trace fossils suggest deposition within the subaqueous back-barrier.

	Palaeophycus (Fig. 1.8D), and occasional large (>20cm) pockets of Teredolites.		
LF14, LF15, LF16, LF7	Sandstone dominated outcrop (~3.5 m thick) with a variety of internal facies stacked into 1-50 cm thick beds composed of inclined heterolithic strata (LF14), homogenous sandstone beds (LF16), heavily bioturbated beds (LF15), convolute bedding, and laminated mudstones (LF7;Fig. 1.8I). Biotubration is prevalent throughout the interval, with burrows both concentrated on bedding planes (Thalassinoides; Fig. 1.8B), within beds (Cylindrichnus concentricus;Fig. 1.8L), and cross-cutting strata (Skolithos; Fig. 1.8F). Occasional shell fragments, sharks' teeth (Fig. 1.8K), ammonite impressions (Fig. 1.8H), and gastropod shells found.	3.3	Bayhead delta	These stacked, slightly inclined, heterolithic, upward coarsening sands are interpreted as the distal expression of a bayhead delta (Joeckel & Korus 2012) Convolute bedding suggests loading and dewatering during deposition (Dzuynski & Smith 1963) Sharks' teeth are indicative of an estuarine, marine-influenced setting (Becker et al. 2010; Cumbaa et al. 2010; Kirklandet al. 2013). Cylindrichnus concentricus is consistent with shallow marine deposition (Belaústegui & de Gibert 2013; Ekdale & Harding 2015)
LF10, LF6, LF7	Large (30 m thick), amalgamated, lenticular, coarse to medium grained, erosive sandstone deposits (LF10;Fig. 1.8O) cut through carbonaceous mudstones and coals (LF6). Between the individual channels within the larger amalgamated intervals, large (>10 cm) mudclasts (Fig. 1.8Q) are visible in a coarse-grained matrix. Wood material (Fig. 1.8P), leaf fossils,Teredolites (Fig. 1.8R), and shell fragments (Fig. 1.8M) are preserved. Continuous, laminated mudstone layers (LF7) separate the channelised facies.	3.4	Distributary channel	These stacked, amalgamated sand lenses are interpreted as distributary channels entering an estuary. The matrix and mud rip up clast layers that create the interbeds between the channels sands represent reworking of estuarine bay fill. Continuous mud layers are interpreted to be fluid-mud deposits (Ichaso & Dalrymple, 2009). Both terrestrial (wood fragments and plant material) and marine (Teredolites and shell fragments) are visible within these deposits.
LF7, LF11	Slope forming deposits of blocky, wavy-interbedded mudstones with millimetre scale laminations of alternating light and dark gray mud (LF7). Occasional (~1cm) coarse-grained sandstone layers and round burrows, ~3-8 mm in diameter, filled with coarse-grained sandstone. Isolated channelised sandstone lenses (LF11) are confined with these fine-grained deposits. Intervals are non-continuous and isolated.	3.5	Tide-dominated central estuary bay fill	These fine-grained, laminated facies represent deposition within the central basin of an estuary (Kvale 2012) Coarse-grained sand interlaminations are the result of storm washover into the central bay. Isolated tidal channels cut through this bay fill.
LF11	Lens shaped outcrops of medium-grained sandstones (LF11) with trough cross-stratification, bidirectional cross-stratification and double mud drapes (Fig. 1.9B).	3.6	Tidal channels	These tidal channel deposits are fairly common, particularly at the base of the transgressive intervals likely because they have a relatively high preservation potential (Davis 2012)
LF13, LF12	Medium-grained sandstones with trough cross-stratification and bidirectional cross-stratification (LF13, LF12) anddistinct, bed scale, angled lateral accretion master surfaces (Fig. 1.9D). Interference ripples visible on master bedding planes. Forms laterally extensive 3-15 m thick white sheets that can be traced for over 10 km. This facies can have either an erosional base with 1-2 m of relief or conformably overlie shoreface deposits. Occasional trace fossils (Diplocraterion, Palaeophycus, and Teredolites) visible (Fig. 1.9E,F,G,I).	3.7	Tidal bars	The visible lateral accretion master surfaces within these trough and planar cross-bedded sandstones suggest these features tidal bars (Dalrymple & Choi 2007; Olariuet al. 2012) which form in the constricted part of the estuary experiencing a high tidal flow regime (Dalrymple & Rhodes 1995) The clean nature of the sand stone suggests these deposits are either estuarine tidal bars or tidal delta bars (Dalrymple et al. 1992) rather than muddier bayhead delta tidal bars (Fenies & Tastet 1998).
LF16, LF7	Stacked, tabular, westward inclined fine- to medium-grained sandstone beds (LF16) which vary in thickness laterally. Some beds show 10-30 cm of incision into underlying beds and well-indurated shell fragment lags along the basal incision surface. Some metre thick beds are homogenous with abundant mudstone clasts. Mudstone interbeds separating sandstones are gray and fissile (LF7).	3.8	Flood-tidal delta	The westward (landward) stacked, gently-dipping beds within this interval suggest flood-tidal delta deposition (Fitzgeraldet al. 2012). Storm action gives deposits lobate shape (Boothroyd et al. 1985).

Table 1.3
Basin Modeling Parameters

Interval	Original Thickness (m)	Decompacted Thickness (m)	Age (Ma)	Lithology	References
Claron Fm.	640		40.0-34.0	Limestone (shaly)	(Taylor 1993; Goldstrand 1994; Larsen 2007)
Pine Hollow Fm.	137		62.0-55.0	Shale (organic lean, sandy)	(Larsen 2007; Larsen *et al.* 2010)
Cannan Peak Fm.	274		70.5-62.0	Conglomerate (typical)	(Larsen *et al.* 2010)
Kaiparowits Fm.	726		76.1-74.7	Shale (organic lean, sandy)	(Eaton 1991; Lawton & Bradford 2011)
Wahweap Fm.	231		81.8-76.1	Sandstone (clay rich)	(Lawton *et al.* 2003, 2014; Jinnah *et al.* 2009; Larsen *et al.* 2010; Jinnah & Roberts 2011)
SCF Drip Tank	65		82.8-81.8	Sandstone (quartzite, typical)	(Szwarc *et al.* 2014)
SCF JHM "G"	39	50	83.5-82.8	Sandstone (typical)	
SCF JHM "F"	30	39	84.0-83.5	Sandstone (typical)	
SCF JHM "F"	21	28	84.5-84.0	Sandstone (subarkose, clay rich)	
SCF JHM "E"	82	106	85.5-84.5	Sandstone (typical)	
SCF JHM "D"	16	21	86.0-85.5	Sandstone (typical)	
SCF JHM "D"	3	12	86.2-86.0	Coal (pure)	
SCF JHM "D"	46	112	86.8-86.2	Shale (organic lean, silty)	
SCF JHM "C"	54	72	88.5-86.8	Sandstone (quartzite, typical)	$^{40}Ar/^{39}Ar$ date (this study)
SCF JHM "A-B"	165	362	89.1-88.5	Shale (organic rich, typical)	$^{40}Ar/^{39}Ar$ date (this study)
SCF SHM	102		93.2-89.1	Sandstone (clay rich)	(J. Primm pers. comm. 2016)
SCF TCM	22		95.0-93.2	Sandstone (typical)	(J. Primm pers. comm. 2016)
Tropic Shale	190		98.0-95.0	Shale (typical)	(Eaton 1991)
Dakota and Cedar Mountain Fms.	57		100-98.0	Sandstone (typical)	(Eaton 1991; Dyman *et al.* 2002)

General references: Hintze 1988; Eaton 1991; Doelling & Willis 1999; Doelling *et al.* 2000; Hettinger *et al.* 2009.

Table 1.4
Coal Lithology Sensitivity Analysis Results

Lithology	Decompacted Thickness (m)
Coal (pure)	12
Coal (with impurities)	11
Shale (organic rich, 20% TOC)	9
Shale (organic rich, 8% TOC)	9
Shale (organic rich, typical)	9
Shale (black)	9
Coal (silty)	9

Table 1.5
Sedimentation Rates for the Straight Cliffs Formation

	JHM Thickness (m)	Duration of deposition (My)	Sedimentation Rate (m / My)
Buck Hollow (Szwarc *et al.* 2014; this study)			
Compacted – Measured Section Thicknesses			
Low Case	456	8.5	53.6
Middle Case	456	6.3	72.4
High Case	456	4.1	111.2
Decompacted – Calculated Thicknesses			
Low Case	802	8.5	94.4
Middle Case	802	6.3	127.3
High Case	802	4.1	195.6
Main Canyon (Chentnik *et al.* 2015)			
Compacted – Measured Section Thicknesses			
Low Case	158	8.5	18.6
Middle Case	158	6.3	25.1
High Case	158	4.1	38.5
Decompacted – Calculated Thicknesses			
Low Case	321	8.5	38.8
Middle Case	321	6.3	50.9
High Case	321	4.1	78.3
Rogers Canyon (Allen & Johnson 2011)			
Compacted – Measured Section Thicknesses			
Low Case	265	5	53.5
High Case	265	4.5	58.8
Left Hand Collet (Dooling 2013)			
Compacted – Measured Section Thicknesses			
	281	5	56.2
Kaiparowits Basin – (Shanley & McCabe 1995)			
Compacted Subsidence			25.56

Table 1.6
Sedimentation Rates for the Western Interior Seaway

Authors	Duration (my)	Thickness (m)	Rate (m/my)
York *et al.* (2011)	2.5	60	24
Sixsmith *et al.* (2008)	0.8	45	56
Valasek (1995)	0.3	10	33
Antia & Fielding (2011)	1	38	38

Table 1.7
Early Compaction Calculations

Location / Study	Substrate	Original Thickness (m)	Thickness Change (m)	Time Interval (years)	Rate (mm/yr)	% Compaction
Assawoman Island, Virginia (Guber & Slingerland 1981; Gayes 1983; Rosati et al. 2010)*	Back barrier silty mudstones		1.0-1.2	40	25.0	
Theoretical Calculations (Terzaghi 1943, p. 265-296)	Silty clay	14	.31	47	6.6	2.2%
Rhine-Muse delta, North Sea (van Asselen 2011)	Peat	10	3	~100	0.6	30 %
Romney Marsh, southeast England, UK (Long et al. 2006)	Peat		3	~750		
Hammock River Marsh, Connecticut (Bloom 1964)	Sedge-peat	10.6		7,000		13-44 %
Bayou Lafourche, Mississippi Delta, Louisiana (Tornqvist et al. 2008)	Peat, clay and silt	<40		~10,000	0.5-5.0	

*Example adjusted for relative sea level rise of 2 mm/yr.

2. BARRIER ISLAND FACIES MODELS AND RECOGNITION CRITERIA

Abstract

Excellent outcrop exposures of the paralic Upper Cretaceous Straight Cliffs Formation of southern Utah provide an opportunity to update facies models and recognition criteria for barrier island deposits. Three main architectural elements (shorefaces, tidal inlets, and tidal channels) occur independently or in combination to create barrier island deposits. Barrier island shorefaces record progradation, while barrier island tidal inlets record lateral migration, and barrier island tidal channels record aggradation within the tidal inlet. Four facies associations (FA) are used to describe and characterize these barrier island architectural elements. Barrier islands occur in association with back-barrier fill (FA1) and internally contain lower and upper shoreface (FA2), high-energy upper shoreface (FA3), and tidal channel facies (FA4). Barrier islands bound lagoons or estuaries, and are distinguished from other shoreface deposits by their internal facies and geometry, association with back-barrier facies, and position within transgressive successions. Tidal processes, in particular tidal inlet migration and reworking of the upper shoreface, also distinguish barrier island successions. Existing barrier island facies models are largely based on modern observations. While this approach highlights the heterogeneous and dynamic nature of barrier island systems, it overlooks processes tied to geologic time scales, such as multidirectional motion, erosion,

and reworking, and their expressions in preserved barrier island strata. Accordingly, this study uses characteristic outcrop expressions to update models for barrier island motion and preservation to include geologic time-scale processes.

Introduction

Barrier islands comprise 10% of modern coastlines (Stutz and Pilkey, 2011), making them prominent coastal features. They are home to growing coastal populations and expanding infrastructure (Zhang and Leatherman, 2011), but are threatened by increasing storm prevalence and magnitude, and rising sea levels driven by global warming (Leatherman, 1983; Zhang et al., 2002; Moore et al., 2010; Masselink and van Heteren, 2014). Thus research focuses on island motion, dynamics, and sediment budgets, to help better understand how barrier islands move naturally and respond to anthropogenic alteration (Fisher and Dolan, 1977; Short, 1999; Dronkers, 2005; Stutz and Pilkey, 2005; Dyke, 2007; Anthony, 2009; Kana et al., 2011; Lentz and Hapke, 2011; Davis Jr., 2013). When carefully integrated with lessons learned from modern systems (Oost et al., 2012), examples from the rock record can further illustrate how barrier islands reflect changes in relative sea level through geologic time, including predicting facies and architecture.

Ancient barrier island systems create large petroleum reservoirs (Davies et al., 1971; Galloway, 1986; Cheel and Leckie, 1990) and form an important part of the transgressive geologic record (Cattaneo and Steel, 2003). Despite their significance, preserved barrier islands are not commonly interpreted, and facies models are notably lacking in comparison to other sedimentary environments, particularly with regard to

recognition criteria (Boyd, 2010). The last major conceptual models for interpretation were published in the 1980s and early 1990s (Reinson, 1979; Reinson, 1984; Schatzinger et al., 1989; Reinson, 1992). As a result, many interpretations lump barrier islands into shoreface environments, potentially missing important clues to depositional history, sand-body distribution, etc. (Olsen et al., 1999; Mellere et al., 2005; Allen and Johnson, 2011; Antia et al., 2011; Kieft et al., 2011).

The development of sequence stratigraphy may have inadvertently limited ancient barrier island interpretations. Traditional sequence stratigraphic models emphasize ravinement during transgression (Vail et al., 1977; Posamentier et al., 1988; Van Wagoner et al., 1988). Important modifications recognize greater preservation potential in high accommodation settings, where barrier islands can step up and over back-barrier deposits (Roehler, 1988; Painter et al., 2013; Mulhern and Johnson, 2016). While there are conceptual models and modern examples of how barrier islands can be preserved (Curray, 1964; Swift, 1968; Rampino and Sanders, 1980; De Falco et al., 2015), these ideas become complicated when considered in a sequence stratigraphic context (Devine, 1991; Sixsmith et al., 2008). Furthermore, guidelines and criteria for recognizing ancient barrier islands (Galloway, 1986; Reinson, 1992) lag behind our understanding of other transgressive features that are more commonly included in sequence stratigraphic models, such as incised valleys and estuaries (Dalrymple et al., 1992; Zaitlin et al., 1994).

One challenge to recognizing barrier island deposits is the close spatial and temporal link to sedimentologically distinct subenvironments. Barrier islands are elongate, shore-parallel bodies of unconsolidated sediment separated from an adjacent landmass by a body of water (Fig. 2.1; Oertel, 1985; Davis Jr., 1994; Otvos, 2012). The

island is a distinct feature within the broader barrier island system, which includes sub-environments such as the back-barrier, flood- and ebb-tidal deltas, and washover fans (Fig. 2.1). Tidal inlets are the spaces or voids separating barrier island deposits. If preserved, the barrier island is the largest sandstone body within a barrier island system, so accurate predictions of these dimensions and extent are central to reservoir characterization and net-to-gross calculations. Grouping, simplification, and misinterpretation of subenvironments in an ancient barrier island system could lead to inaccurate environmental or sequence stratigraphic interpretations, and/or reservoir characteristics.

A final challenge in the interpretation of ancient barrier island deposits is the fact that existing models are largely based on examples from the modern (Fig. 2.1b). Stratigraphic sections through modern examples (Shepard and Moore, 1955; Hoyt and Henry Jr., 1965; Kumar and Sanders, 1974; Thom, 1984; Moslow and Tye, 1985), particularly an early study of Galveston Island (Bernard et al., 1962), are directly used as predictive models for interpreting preserved strata. However, this tie to the modern has not been rigorously tested, and furthermore it introduces an inherent bias because modern system observation is limited to short time scales whereas ancient systems time-average geologic processes (Storms et al., 2002).

One effect of the difference in time scales between ancient barrier island deposits and analogous modern systems is an inconsistency in how barrier island motion is identified and used in classification. Barrier islands are ephemeral, constantly moving features. In the modern, different directions of short-term, local island motion yield different barrier island geometries (Fig. 2.2; Dickinson et al., 1972). Modern barrier

islands are classified based on their relative motion, i.e., progradational (basinward motion), retrogradational (landward motion), and/or aggradational (vertical motion; Fig. 2.2; Galloway and Hobday, 1983; Galloway, 1986; Davis Jr., 1994). These three island types (Fig. 2.2) are the foundation for ancient barrier island facies models (Reinson, 1979; Reinson, 1984; Schatzinger et al., 1989; Reinson, 1992), which are difficult to apply to the ancient because they do not account for erosion, reworking, ravinement, motion, and stacking at geologic time scales. Consequently, modern island geometries and features may not be directly translated into the rock record.

Thus, there is a need for re-examining and updating facies models to guide the interpretation of ancient barrier island deposits, and improving our understanding of their preservation dynamics. Outcrops of barrier island deposits from the Upper Cretaceous Straight Cliffs Formation of southern Utah, with kms-long lateral exposures that are 10s-100s of m thick, provide an excellent opportunity to study barrier islands in detail. Measured sections of three typical barrier island successions, termed architectural elements, show the internal facies and geometry of barrier islands in outcrop. The lateral and vertical arrangement of these architectural elements lends new insight into barrier island dynamics and preservation at geologic timescales.

Geologic Background and Methods

Outcrop observations from the Cretaceous Straight Cliffs Formation in the Kaiparowits Plateau document the facies of barrier island deposits (Fig. 2.3). Located in the foreland basin of the Cordilleran Sevier fold-and-thrust belt, the northern Kaiparowits Plateau experienced unusually high rates of sediment supply and accommodation during

deposition of the Coniacian–early Campanian John Henry Member of the Straight Cliffs Formation. These conditions led to the preservation of stacked, fourth-order, regressive-transgressive, shallow marine successions (Allen and Johnson, 2011). This study focuses on outcrops of the John Henry Member at Buck Hollow and Alvey Wash near Escalante, Utah, where stacked barrier island successions are preserved over a ~150-250 m-thick section of ~4 my of deposition (Fig. 2.3; Mulhern and Johnson, 2016).

Previous studies from the John Henry Member provide a sedimentological and sequence stratigraphic framework of the Straight Cliffs Formation in the northern Kaiparowits Plateau (Peterson, 1969; Hettinger et al., 1993; Shanley and McCabe, 1995; Chentnik et al., 2015). The paleoshoreline trend ran roughly north-northwest to south-southeast. Therefore depositional strike parallels the eastern edge of the plateau (Fig. 2.3a). The John Henry Member is the thickest member of the Straight Cliffs Formation and is broken into eight intervals defined by the main shoreline successions exposed along 50 Mile Mountain, lettered A through G (Peterson, 1969). The John Henry Member was the focus of early sequence stratigraphic studies, which linked terrestrial and marine depositional environments (Shanley and McCabe, 1995). Detailed stratigraphic analysis recognizes four regressive-transgressive cycles in the John Henry Member, particularly regional transgression during the C -D and E-F intervals, which favored deposition and preservation of the barrier island systems documented here (Fig. 2.3c; Allen and Johnson, 2011; Dooling, 2013; Chentnik et al., 2015; Mulhern and Johnson, 2016).

Measured sections and aerial photography data from Buck Hollow and Alvey Wash (Fig. 2.3a) were used to document and interpret barrier island facies from within the John Henry Member. Buck Hollow (Fig. 2.3a) consists of a ~7 km long along-strike

outcrop exposure, with ~456 m of total JHM section (Mulhern and Johnson, 2016). Alvey Wash is located along Smoky Mountain Road, 5 km south of Escalante, Utah (Fig. 2.3a) and consists of a ~6 km along-strike canyon with parallel outcrop exposures on both sides as well as east-west oriented side canyons providing dip exposures, and ~330 m of John Henry Member strata. Combined, these two areas provide excellent case-study of barrier island facies in outcrop.

Results

John Henry Member barrier island deposits are characterized by four facies associations (Table 2.1), described and interpreted below. Typical stacking patterns of these facies associations define three main barrier island architectural elements, which can occur independently or in combination. A variety of architectural geometries and stratigraphic relationships are documented, to illustrate barrier island motion and preservation.

Facies Associations

Facies Association 1 (FA1)

Description. *Carbonaceous Mudstones, Fine-Grained Sandstones, and Coals*. This facies is composed of brown and gray carbonaceous mudstones that grade vertically into coals over 5- >20 m-thick intervals (Fig. 2.4h,j). The mudstones are wavy-bedded and contain abundant plant fossils (Fig. 2.4f), terrigenous material, coal fragments, and oyster shell fragments (Fig. 2.4c,e). The mudstone intervals are dissected by lens-shaped, fine- and medium-grained sandstones (0.02-0.30 m thick; Fig. 2.4i), which pinch out

laterally over 0.5-2.0 m (Fig. 2.4a). Shell fragments are distributed sporadically throughout the mudstones or gathered into layers and clusters (Fig. 2.4c). Coals are 0.05-2.0 m thick. The upper surface of coal beds has locally abundant *Thalassinoides* burrows (Fig. 2.4d,g). Coals and mudstones locally contain flaser to lenticular bedding (Fig. 2.4b). Mudstones contain a palynoflora (*Quadripollis krempii*) and dinoflagellates (*Spiniferites ramosus* and *Palaeohystrichophora infusoridides*; Mulhern and Johnson, 2016; Pocknall et al., 2016).

Interpretation. *Back-Barrier Fill*. These fine-grained mudstones and coals suggest deposition within a protected back-barrier setting. Barrier islands can bound both lagoons and wave-dominated estuaries. Therefore the term back-barrier is used henceforth to describe both settings. Coals and abundant terrigenous material (Fig. 2.4f) along with oyster shell fragments (Fig. 2.4e) suggest both terrestrial and marine influence (Kieft et al., 2011; Painter et al., 2013; Chentnik et al., 2015). Flaser to lenticular bedding suggests tidal reworking (Fig. 2.4b; Reineck and Singh, 1980; Dalrymple, 2010). Medium-grained, wavy, lens-shape, sandstone beds which interfinger with the mudstones (Fig. 2.4a,i) are interpreted as the distal expression of storm-driven washover fans. Vertical gradation from carbonaceous mudstone to coal (Fig. 2.4j) suggests cyclic wetting upwards (Wadsworth et al., 2010). *Thalassinoides* burrows typically found at the top of the coals indicate marine influence and thus a relative deepening or transgression (Fig. 2.4d,g; Savrda, 1991; Carvalho et al., 2007). The thin-walled nature and low abundance of peridinioid dinoflagellates suggests brackish water conditions (Pocknall et al., 2016). Back-barrier facies are included in the facies descriptions outlined here because they are central to identifying barrier island deposits. They are not, however,

actually part of the barrier island itself.

Facies Association 2 (FA2)

Description. *Fine- to Medium-Grained, Tabular Sandstones*. This facies is composed of fine-grained, 0.1-1 m thick, tabular sandstone beds containing hummocky and swaley cross-stratification (Fig. 2.5a). These beds continuously grade vertically into medium-grained, 0.5-1.5 m thick, tabular sandstone beds containing low-angle trough cross-stratification, and planar bedding. These notably 'blocky' sandstone beds stack vertically to form tabular, laterally continuous outcrops (>30 m wide; Fig. 2.5f). In some areas, the internal character of these beds alternates from laminated and/or homogenous to completely bioturbated (Fig. 2.5e). Bioturbated layers contain abundant and pervasive *Ophiomorpha nodosa* (Fig. 2.5b,c,d).

Interpretation. *Lower and Upper Shoreface*. These sandstones are interpreted as lower and upper shoreface deposits. Lower shoreface strata are recognized by the presence of hummocky and swaley cross-stratification (Fig. 2.5f; Dumas, 2005; Dumas and Arnott, 2006), confirming storm-influenced deposition below fair-weather wave base. These storm-dominated facies grade vertically into wave-dominated facies, evidenced by the gradual transition to medium-grained, trough cross-stratification and planar laminated sandstones. These wave energy indicators suggest deposition above fair-weather wave base in an upper shoreface environment (Reading and Collinson, 1996; Plint, 2010). *Ophiomorpha nodosa* (Fig. 2.5b,c,d) is common in shoreface settings (Frey and Howard, 1985; Droser and Bottjer, 1989). Alternating laminated and heavily bioturbated bedding (Fig. 2.5e,f), also called 'lam-scram' (MacEachern and Pemberton,

1992; Bann and Fielding, 2004; Pemberton et al., 2012), indicates periods of rapid deposition, creating laminated and homogenous layers, followed by periods of quiescence during which the sands are bioturbated (Fig. 2.5c). The presence of both storm and wave influence makes this facies association distinctive.

Facies Association 3 (FA3)

Description. *Medium-Grained, Cross-Stratified Sandstone*. This facies is composed of medium-grained sandstone beds with abundant trough-cross stratification, accretion sets (Fig. 2.6a,d), ripple laminations (Fig. 2.6e), and bidirectional paleocurrent indicators (Table 2.1). Medium-sized sand grains concentrate along stratification laminations, adding to the laminated texture of this facies. The beds are 0.1-0.5 m thick and generally lack bioturbation, but occasionally this laminated facies cuts into bioturbated layers (Fig. 2.6b). Beds contain sporadic shell fragments <1 cm in diameter. These beds stack to form blocky outcrops (Fig. 2.6c). These deposits do not show any evidence of internal dissection or lens-shaped sandstone bodies (Fig. 2.6c).

Interpretation. *High -Energy Upper Shoreface*. The medium-grain size and abundance of accretion sets (Fig. 2.6a,d) and ripples suggests deposition in a high-energy setting, dominated by tide and current energy (Fig. 2.6e; Allen, 1982; Boothroyd, 1985; Longhitano et al., 2012). Accretion sets have a dominant direction in some areas, suggesting current influence. In other areas bidirectional paleocurrent indicators suggest tidal influence (Table 2.1: Dooling, 2013; Chentnik et al., 2015). The alternation of medium and fine grains along laminations also suggest rhythmic tidal influence. These beds lack bioturbation, further indicating high-energy deposition (Hubbard et al., 2002;

Dashtgard et al., 2009; Steel et al., 2012). The abundance of high-angle trough cross-stratification and accretion sets (Fig. 2.6d) distinguishes this high-energy upper shoreface from the upper shoreface of facies association 2, which is dominated by wide (>0.15 m), more sporadic, trough-cross stratification (Fig. 2.5). These high-energy upper shoreface deposits lack hummocky and swaley cross-stratification indicative of lower shoreface settings.

Facies Association 4 (FA4)

Description. *Lens-Forming, Fine-Grained Sandstone*. This interval is composed of laterally discontinuous, lens-shaped bedforms (0.5-2.0 m thick; Fig. 2.7a) of fine- and medium-grained sandstone with erosive bases, cross-cutting each other over 1-10 m laterally (Fig. 2.7h). These sand bodies are highly variable, forming both tabular and lens-shaped beds with a variety of internal bedforms and patterns including abundant trough cross-stratification, ripple laminations (Fig. 2.7f), accretion set packages (1-5 cm thick; Fig. 2.7i), bidirectional cross-stratification (Fig. 2.7j), and convolute bedding (Fig. 2.7e). Mudstone clasts (2-15 mm long) and shell fragments line the basal surfaces and are arranged along bedding planes within sand-bodies. Shell impressions (Fig. 2.7b), shell fragments, double mud drapes (Fig. 2.7i,j), and bioturbation are present (Fig. 2.7c,d,g). The basal surface of some sandstone bodies is heavily bioturbated with *Gastrocheanolites* (Fig. 2.7d,g).

Interpretation. *Tidal Channels*. These variable sandstones are interpreted as tidal channels. Erosive basal surfaces (Fig. 2.7a), internal cross-cutting (Fig. 2.7h), and high-angle trough cross-stratification suggest channelized flow. Bidirectional accretion sets

and double mud drapes (Fig. 2.7i,j) are indicative of tidal processes (Barwis and Hayes, 1979; Hayes, 1980; Nio and Yang, 1991; Longhitano et al., 2012). Brackish trace fossils (*Teredolites* (Fig. 2.7c) and *Gastrocheanolites* (Fig. 2.7d,g)) and shell impressions (Fig. 2.7b) indicate deposition in an area with both marine and fresh water input. Mudstone rip-up clasts suggest erosion and reworking of underlying or adjacent material. Convolute bedding suggests dewatering and rapid deposition (Dzuynski and Smith, 1963).

Architectural Elements

The four facies associations described above stack in distinct ways to create three barrier island architectural elements, which we document using measured sections (Fig. 2.8) and outcrop photos (Fig. 2.9) and summarize in Figure 2.10.

Type 1: Barrier Island Shoreface

Description. Barrier island shoreface elements are composed of 1- >10 m of carbonaceous mudstone of back-barrier fill (FA1), overlain by a sharp-based, cliff-forming sandstone interval of lower and upper shoreface (FA2 and FA3, respectively; Fig. 2.8a). The mudstone units vary in thickness and internal composition laterally (Fig. 2.9a,b). In some locations the mudstones are homogenous, whereas others are interbedded with sandstone layers (Fig. 2.4a,i), and some grade vertically into coals (Fig. 2.4j). A sharp contact separates these finer-grained facies from an overlying, blocky, cliff-forming, fine- to medium-grained, lower shoreface sandstone unit (>5 m thick; FA2; Fig. 2.9a,b), which is typically laterally continuous over >2 km. The uppermost portion of the cliff-forming interval contains beds 0.2-1 m thick with high-angle trough cross-

stratification with bidirectional paleocurrent indicators (FA3; Fig. 2.8a).

Interpretation. Barrier island shoreface elements (Figs. 2.8a and 2.9a,b) preserve the lower and upper shoreface (FA2) and high-energy upper shoreface (FA3) directly atop back-barrier facies (FA1). In these examples, the offshore and distal lower shoreface are not preserved. Instead, proximal lower shoreface deposits directly overlies carbonaceous back-barrier fill and coals (Fig. 2.9a,b). The sharp base and alternating bioturbated and laminated intervals suggest rapid and episodic deposition (MacEachern and Pemberton, 1992; Bann and Fielding, 2004; Pemberton et al., 2012). Bidirectional paleocurrent indicators in the uppermost portion of the sequence suggest tidal reworking (Fig. 2.8a).

Type 2: Barrier Island Tidal Inlet

Description. These elements (Fig. 2.8b) are composed of carbonaceous mudstones (FA1) overlain by erosive-based, cliff-forming sandstone units (>5 m thick) composed of trough cross-stratified medium- to coarse-grained sandstone beds (0.20-0.50 m thick) lacking bioturbation (FA3). The sandstone dominated interval is blocky and tabular (Fig. 2.9c), with internal beds (0.5-1 m thick) composed of trough cross-stratification, mainly unidirectional accretion sets, convolute bedding, ripple laminations, homogenous bedding, and clear bidirectional paleocurrent indicators (Figs. 2.6 and 2.8b).

Interpretation. Barrier island tidal inlet elements (Fig. 2.8b) are composed of high-energy shoreface sands (FA3) stacked vertically to create laterally continuous sandstone sheets (Fig. 2.9c) overlying back-barrier deposits (FA5). These deposits record the preservation of a barrier island laterally migrating into the void of a tidal inlet

(Reddering, 1983; Anthony et al., 1996), leading to the preservation of upper shoreface sandstones reworked by high-energy tidal and current processes (Fig. 2.8b). The large, blocky, substantial (>5 m thick) outcrops (Fig. 2.9c) formed by these deposits suggest they are not channelized or fan-shaped. Rather these deposits are notably laterally extensive (>4 km) similar to tidal inlet outcrops described previously (Uhlir et al., 1988). Outcrops with south-directed (shore-parallel), unidirectional accretion sets (Fig. 2.6a) and ripples (Fig. 2.6e) support a dominant direction of lateral accretion driven by long-shore currents, while bidirectional flow indicators show tidal reworking (Fig. 2.8b; Dooling, 2013; Chentnik et al., 2015). These deposits may have low angle (<3°) lateral accretion clinoform surfaces (e.g., Siringan and Anderson, 1993) not recognizable in outcrop exposures of <1 km lateral distance. The blocky, amalgamated character of these outcrops (Figs. 2.6c and 2.9c) likely comes from the stacking and migration of multiple tidal inlet depositional events (Heron Jr. et al., 1984).

Type 3: Barrier Island Tidal Channels

Description. These elements are composed of interfingered intervals of carbonaceous mudstones and coals (FA1) cut into by lens-shaped outcrops (>5 m tall, >10 m wide; Fig. 2.9d). These finer-grained intervals have abundant carbonaceous and terrigenous material (FA1). The thickness of these mudstone-dominated intervals varies as they are eroded by the sandstone-dominated intervals. Internally, the sand dominated intervals are composed of lens-shaped, fine- to medium- grained sandstone beds (FA4; Fig. 2.8c) which locally fine upwards. These beds are 0.5-2.0 m thick and contain trough cross-stratification, double mud drapes, ripple laminations, brackish trace fossils, and

shell impressions (FA4; Fig. 2.7).

Interpretation. These lens-shaped sand-dominated outcrops are interpreted as tidal channel barrier island elements (Fig. 2.8c). They are composed of vertically and laterally stacked tidal channels (FA4; Fig. 2.9c) sometimes interbedded with backbarrier fill (FA1; Fig. 2.8c; Tye and Moslow, 1993). Neither dunes nor bars (Olariu et al., 2012), these outcrops are interpreted as channels based on the lens-shape and erosive characteristics of the internal beds forms (Fig. 2.7a,h), as well as abundant trough-cross stratification. The combination of channel features and tidal indicators (bidirectional accretion sets and mud drapes; Fig. 2.8c) make these deposits similar to other tidal inlet channel fill successions (Willis and Moslow, 1994a; Kieft et al., 2011) and modern channelized inlet fill (Kumar and Sanders, 1974; Israel et al., 1987).

These tidal channel deposits can be distinguished from tidal inlet deposits by their internal geometry and mud content. Barrier island tidal inlet deposits (described above; Fig. 2.9c) are more blocky and uniform, lacking channel-form geometries and back-barrier interbeds seen in tidal channel deposits (Fig. 2.9d). Furthermore, barrier island tidal channel deposits likely record deposition in the more central portion of the inlet, rather than the margin (Heron Jr. et al., 1984).

Outcrop Geometries

The 3 barrier island architectural elements are summarized in Figure 2.10. Outcrop examples of the Straight Cliffs Formation from Alvey Wash and Buck Hollow show the lateral and vertical variability within barrier island strata (Figs. 2.11-2.13) deposited during a relatively short (~4 my) time period (C-F intervals; Fig. 2.2c), and

within a small region (~20 km^2, Escalante area combined; Fig. 2.3). The variability of barrier island facies within the Straight Cliffs highlights the range of ways these deposits can be preserved and creates an initial foundation, which can be updated as more examples are recognized.

Lateral Facies Patterns

The three barrier island elements can occur in a variety of lateral (along-strike; Figs. 2.11-2.13) and shore-perpendicular (dip-direction; Fig. 2.12b) arrangements. Barrier island shoreface elements grade laterally into correlative tidal channel elements in Alvey Wash (Fig. 2.11), as has been widely recognized in other examples (Davies and Ethridge, 1971; Davies, 1978; Flores, 1978; Self et al., 1986). The preservation of barrier island tidal channel facies, rather than laterally migrating tidal inlet facies, suggests that the inlet was either stationary or relatively short-lived. In Buck Hollow, barrier island shoreface deposits are laterally continuous along strike to the south (>5 km; Fig. 2.13) but grade into barrier island tidal inlet deposits along strike to the north (~1 km north of Fig. 2.12 location). This lateral facies change is similar to subsurface examples which also show lateral transition between tidal channel and tidal inlet deposits (Galloway, 1986; Hubbard et al., 2002). This gradation indicates the closing of a tidal inlet through lateral migration and infilling. Barrier island tidal inlet deposits are consistent and laterally continuous along strike in Alvey Wash (>4 km; Fig. 2.12a), extending the length of the outcrop exposure (>1.82 km). This suggests tidal inlet infilling via lateral migration across the Alvey Wash field area (~5 km by ~1 km).

Barrier island tidal inlet deposits also show distinct dip-direction lateral continuity

(>1 km; Fig. 2.12b). This shore-perpendicular lateral continuity could result from compound barrier island motion, as shore-perpendicular and lateral motion occur simultaneously (Heron Jr. et al., 1984). During oblique motion, sand stored in flood- and ebb-tidal deltas can be reworked into the barrier island proper. Similarly, barrier island shoreface examples are laterally continuous in the dip direction across the outcrop exposure (Fig. 2.12b). This indicates shore-perpendicular progradation of the island system. Other barrier island shoreface deposits are seen pinching out in the updip-direction (Fig. 2.12b) where they interfinger with back-barrier fill facies, suggesting preservation of the updip part of the island.

Vertical Stacking Patterns

Barrier island deposits also show a variety of vertical stacking patterns. The outcrops at Buck Hollow preserve barrier islands during the transgressive portion of two regressive-transgressive cycles, which are likely are relatively short, ~1 Ma each (based on 4 main regressive-transgressive cycles over ~4 my deposition), and dominated by back-barrier fill deposition (Fig. 2.13; Mulhern and Johnson, 2016). Barrier island shoreface deposits likely record relatively rapid deposition at the end of periods of back-barrier infilling. Both examples of barrier island shorefaces in Buck Hollow are sharp-based cliffs directly overlying back-barrier deposits (Fig. 2.13). Regionally significant flooding surfaces truncate the upper portion of the barrier islands, separating them from overlying offshore marine facies. These Buck Hollow barrier island shoreface deposits formed during regional transgression and correlate to an incised valley fill succession ~15 km updip (Chentnik et al., 2015).

The John Henry Member at Alvey Wash preserves a relatively stationary, aggradationally stacked, barrier island and back-barrier system deposited during the same time period as at Buck Hollow. This portion of the basin underwent smaller scale shifts in the relative position of the shoreline, resulting in a long-standing back-barrier system with more complex and variable stacking patterns (Figs. 2.11 and 2.12). In Alvey Wash, some barrier island shoreface deposits are overlain by carbonaceous back-barrier fill followed by a barrier island tidal inlet succession (Figs. 2.11 and 2.12). Other barrier island shorefaces are stacked vertically, separated by back-barrier fill (Fig. 2.12). Higher in the section, a barrier island shoreface is capped with barrier island tidal inlet deposits (Fig. 2.12b). Literature examples also show other barrier island stacking patterns such as barrier island shoreface deposits directly overlying a deltaic sequence (McCubbin, 1982) and strandplain shoreface deposits overlain by barrier island tidal inlets (Cheel and Leckie, 1990). Combined, these examples show that the three barrier island architectural elements defined here can be found in a variety of lateral and vertical patterns, underscoring the dynamic nature of barrier island systems.

Discussion

Comparison to Tidal Subenvironments

The classification of barrier island deposits presented here implies that deposition that occurred in the tidal inlet becomes part of the barrier island deposit. In modern systems, a tidal inlet is a channel, or void, filled with water, separating two barrier islands (Fig. 2.1). Tidal inlets can be sediment conduits, sources, or sinks, depending on the dynamics of the individual barrier island system (Oertel, 1988). Modern tidal inlets are

filled laterally with sand welded onto the island during down-drift migration, closing and opening as islands shift, particularly during storms (Hoyt and Henry Jr., 1965; Susman and Heron, 1979; Hayes and FitzGerald, 2013; Seminack and Buynevich, 2013). Inlet filling and migration is preserved as laterally building and vertically aggrading deposits (barrier island tidal inlet and channel successions, respectively), connecting or replacing adjacent barrier islands (Fig. 2.1; Moslow and Tye, 1985; Tye and Moslow, 1993; Seminack and Buynevich, 2013). Because of this complex motion, we argue that sandstones deposited within the tidal inlet are part of the preserved barrier island. All three barrier island architectural elements (Fig. 2.10) can be preserved within a single barrier island deposit.

This interpretation differs from some previous work, which considered tidal inlets separately from barrier island shoreface deposits (Heward, 1981; Hubbard et al., 2002). The separation of tidal inlets from barrier island shoreface deposits is mainly driven by modern observations (Hayes, 1980; Hayes and FitzGerald, 2013), but this overlooks the fact that the two are linked at geologic timescales and therefore may not be distinguishable from one another (Barwis and Makurath, 1978). Instead, we suggest that they are end-member architectural elements seen within broader barrier island deposits. This reduces the complexity of early interpretations, which observed similar facies, but struggled to articulate lateral variability within barrier island systems (e.g., Caplan and Moslow, 1999). Considering tidal inlet and tidal channel elements as parts of the barrier island itself provides a process-based explanation for tidal sandstones with sheet-like geometries (e.g., “tidal sheets” of Sixsmith et al., 2008).

Barrier island tidal channels record channelized deposition within the inlet, likely

through vertical aggradation during periods of localized high accommodation and inlet deepening. These deposits vary from barrier island tidal inlet architectural elements, which record the lateral extension of the barrier island shoreface into the tidal inlet. Tidal channels are located close to, or contiguous with, barrier island shoreface or tidal delta deposits (FitzGerald et al., 2012). This position, close to the open ocean, makes them distinct from deltaic tidal channels and back-barrier tidal channels, which are deposited in more proximal areas of the back-barrier (Flores, 1978). Barrier island tidal channels are distinct from deltaic tidal channels because they are not associated with prodelta or delta front facies (Rahmani, 1988). They are distinct from tidal channels within the back-barrier (e.g., open estuarine or lagoonal tidal channels) because they do not show the systematic shallowing-upward patterns characteristic of back-barrier tidal channels (Hughes, 2012), and are not associated with more proximal tidal facies such as tidal flats, bars, or tidally-influenced fluvial deposits (Dalrymple and Choi, 2007). Barrier island tidal channel deposits show less bioturbation than estuarine sand bars (Antia et al., 2011).

The barrier island elements and deposits described herein are distinct from other subenvironments within the barrier island system. The geometries and stacking patterns of barrier island elements distinguish them from flood-tidal deltas, ebb-tidal deltas, and washover fans, which can be preserved in conjunction with barrier island facies (Donselaar, 1984). Many of these elements are preserved within the back-barrier intervals preserved at Alvey Wash and Buck Hollow. Back-barrier fill (FA1) includes scattered washover fans and tidal channels as well as occasional tidal delta deposits (Mulhern and Johnson, 2016). Flood-tidal delta deposits in Main Canyon are identified based on their landward directed paleocurrent directions and limited lateral extent (Chentnik et al.,

2015). Examples of flood- and ebb- tidal deltas have internal facies patterns similar to barrier island tidal inlet successions, showing trough cross-stratification and accretion sets (Hayes, 1980; Boothroyd, 1985; Reinson, 1992; Hubbard et al., 2002). The key difference between tidal deltas and barrier island tidal inlet successions is the degree of interbedding with back-barrier facies (Heron Jr. et al., 1984; Hubbard et al., 2002). Flood-tidal delta and ebb-tidal delta facies show more internal heterogeneity than barrier island tidal inlet successions, as they interfinger with back-barrier and open-marine mudstones (Israel et al., 1987; Siringan and Anderson, 1993; FitzGerald et al., 2012). Barrier island tidal channels do show some interbedding with back-barrier facies (Fig. 2.7). However, the channelized nature of barrier island tidal channel successions distinguishes them from tabular tidal delta and washover fan deposits (Schwartz, 1982; Sedgwick and Davis Jr., 2003).

Washover fans and tidal deltas can also be distinguished by their fan-shaped geometries (Finley, 1978; Hayes, 1980; Szpakiewicz et al., 1991; Hudock et al., 2014). These deposits tend to form isolated lens-shaped outcrops while barrier islands have blocky, tabular, laterally continuous, sheet-like geometries (Fig. 2.9c). Flood-tidal deltas can stack and build into sheets depending on their proximity to the tidal inlet (Donselaar, 1984). However, the lateral continuity of these sheets is likely less extensive than barrier island tidal inlet deposits (Fig. 2.12; Barwis, 1990; Murakoshi and Masuda, 1991).

Comparison to Previous Models

The three barrier island elements discussed here both align with, and deviate from, existing barrier island facies models (Schatzinger et al., 1989; Reinson, 1992).

Barrier island shoreface deposits (Type 1) are similar to the facies model called "Regressive (Prograding) Barrier Model" of Reinson (1992, Fig. 2.9), which is based on modern examples. Both have the same internal facies (lower and upper shoreface). The key difference is that the preserved ancient examples from the Straight Cliffs Formation have a sharp-base and overlie back-barrier deposits (Figs. 2.8 and 2.9; Land, 1972; Roehler, 1988). The existing facies models are based on modern observations (Davies, 1978) and do not extend below the lower shoreface.

Barrier island tidal inlet deposits (Type 2) are similar to previously-described "Inlet Channel Sequences" (Moslow and Tye, 1985; Reinson, 1992, Fig. 2.10). Both show cross-bedded medium-grained sandstones with planar laminations and shell fragments. Preserved barrier island tidal inlet deposits lack the roots seen in the dune facies at the top of the model succession. Existing models for deposition within tidal inlets are focused on short-term location and channelized deposition (Moslow and Tye, 1985; Reinson, 1992, Fig. 2.10), and do not consider the long-term stratigraphic expression of lateral accretion and welding.

Barrier island tidal channels (Type 3) are similar to the "Barrier-inlet model" of Reinson (1992, Fig. 2.9). However, the specific subenvironments mentioned in the model (deep channel, shallow channel, welded ridge, spit beach, dune) are not recognized in outcrop. These models are based on modern examples (Kumar and Sanders, 1974) which may under-represent the reworking that could take place at geologic time-scales. Instead, barrier island tidal channel successions the Straight Cliffs Formation are highly variable, stacking both vertically and laterally and cross-cutting other barrier island facies. Consistent shallowing-upwards patterns are not seen across individual outcrops. Rather,

highly variable tidal channels are stacked vertically.

Deposits similar to the "Transgressive Barrier Model" (Reinson, 1984; Reinson, 1992, Fig. 2.9) have not been observed in the Straight Cliffs Formation. This model shows lagoon, flood-tidal delta, washover, channel, marsh and dune facies stacked vertically and was derived from observations of thin, landward-moving, modern islands dominated by washover processes (Leatherman, 1979; Heron Jr. et al., 1984). In these examples, washover processes control deposition within the body of the barrier island. Ancient examples interpreted using this model are identified by washover facies (Galloway, 1986; Willis and Moslow, 1994b) and barrier islands building landward over correlative back-barrier deposits (Hobday and Orme, 1974; Hobday and Jackson, 1979; Willis and Moslow, 1994b). These processes explain early interpretations describing transgressive sheet sands (Hollenshead and Pritchard, 1960; Heward, 1981) or shoestring sands (Bass, 1934). These strata would be expected to have subtle, land-directed erosional surfaces. Reworking and ravinement may make washover-dominated barrier island shoreface successions difficult to preserve and/or interpret. Washover fans occur within back-barrier intervals of the Straight Cliffs Formation, but washover processes are not dominant within any of the barrier island architectural elements described above.

Barrier Island Motion and Preservation

Current understanding of barrier island motion and preservation comes mainly from modern studies and observations, the complexity of which presents a major challenge for interpreting ancient barrier island deposits. Of particular importance is the distinction between barrier island motion and preservation, and how these concepts differ

across modern to ancient time scales. Over short time scales (generally <10,000 years) modern barrier islands can move in all directions (Fig. 2.2). They prograde (Bernard et al., 1962) and aggrade (Simms et al., 2006) through processes similar to regular shoreface development (Clifton, 2006). Two contrasting models exist for modern barrier island retrogradation: rollover and back-stepping (Fig. 2.15; Curray, 1964). Rollover occurs via overwash and storm reworking during continuous transgression, leaving behind only a transgressive lag of winnowed material (Fig. 2.15a; Swift, 1968; Dillon, 1970; Belknap and Kraft, 1981; Swift et al., 1991; Timmons et al., 2010). The alternative model suggests that barrier islands move through back-stepping, or in-place drowning, in which the island rapidly relocates in a landward position (Swift, 1975; Rampino and Sanders, 1980; Boyd and Penland, 1984; De Falco et al., 2015). These models have been extrapolated and applied to explain ancient barrier island preservation (Devine, 1991).

In a sequence stratigraphic sense, barrier islands tend to develop during periods of regional relative sea level rise, placing them within transgressive successions. Because of this tendency, the two conceptual models for modern barrier island retrogradational motion (Fig. 2.15; rollover and back-stepping) have been posed as conflicting models to explain barrier island preservation (Devine, 1991). We argue that, over long time scales (0.1-1 my), rollover and back-stepping merge together to explain barrier island preservation and the stacking of multiple individual barrier island deposits.

Geologic scale back-stepping explains the preservation of thick, stacked, barrier islands which show local, internal progradational or aggradational facies patterns (Fig. 2.15b; Sabins Jr, 1963; Land, 1972; Bridges, 1976; Roehler, 1988; Roy et al., 1994; Sixsmith et al., 2008). Rollover explains the preservation of thin deposits with evidence

of washover (Hobday and Orme, 1974; Hobday and Jackson, 1979; Willis and Moslow, 1994b). Yet, when considered at geologic time scales, the two models merge together because they are both dependent on the rate of relative sea level rise, regardless of the short-term motion of the island system. Rapid transgression limits overwash (Swift, 1968), preventing ravinement, and ultimately leading to in-place drowning, or back-stepping. Consequently, when longer time-scales are considered, rollover and back-stepping blend together and all three modern island types (aggradational, progradational, retrogradational) can be preserved with sufficient accommodation. Barrier islands can locally move landward through rollover but are preserved through rapid transgression and back-stepping. While this disconnect between relative sea level change and barrier island motions has been recognized and modeled (Storms et al., 2002), this is the first time they are incorporated into barrier island preservation models.

The preservation of prograding barrier islands through back-stepping implies that barrier island motion can be independent from the relative shoreline motion. Islands can build basinward while the shoreline steps landward, as occurs in both modern and ancient systems. For example, Galveston Island is prograding (Bernard et al., 1962; Morton, 1994) while the Gulf Coast is undergoing transgression (Milliken et al., 2008). Ancient barrier island deposits show progradation within transgressive successions, displaying Waltherian stacking patterns (Middleton, 1973), with more proximal facies (upper shoreface) over more distal facies (lower shoreface). This commonly occurs in the Straight Cliffs examples, where barrier island shoreface examples internally prograde, with shallowing upwards successions from lower to upper shoreface (Fig. 2.8a). This progradation occurs within the regionally transgressive D and F intervals of the John

Henry Member (Fig. 2.3b; Chentnik et al., 2015; Mulhern and Johnson, 2016). This concept is not new: local progradation during regional transgression creates retrogradational stacking patterns in sequence stratigraphic models (Posamentier and Allen, 1999). However, applying this concept of disconnect between local deposition and regional stacking patterns to barrier island environments explains the preservation of thick shoreface deposits during transgression, and allows for more plausible and consistent interpretations.

Summary of Barrier Island Recognition Criteria

The barrier island facies, architectural elements, and deposits documented here can be distinguished from other shoreface types as well as other transgressive sub-environments based on three main criteria: (1) proximity to back-barrier deposits, (2) internal facies, and (3) stratigraphic position. These criteria are focused on observations that can be made in outcrop, rather than compositional properties, which were used as early barrier island recognition criteria (Berg and Davies, 1968; Berg, 1970).

1. Proximity to Back-Barrier Deposits

The barrier island deposits of the Straight Cliffs Formation are found overlying or between back-barrier intervals, within broadly transgressive successions (Fig. 2.13). Although back-barrier deposits are not actually part of the barrier island itself, they are included in the descriptions herein because they help recognize and differentiate barrier island deposits. In the modern, barrier islands are sand bodies that bound lagoons and/or estuaries. Therefore, the presence of a shoreface either directly overlying or time-

correlative to back-barrier deposits, suggests a possible barrier island environment. In contrast, strandplains lack back-barriers (Galloway, 1986), and instead, fluvial and coastal plain facies are the correlative up-dip time-equivalent facies to strandplain shoreface deposits (Clifton, 2006). Similarly, deltas are associated with delta plains, coastal plain, and fluvial systems, rather than back-barriers (Cotter, 1975; Bhattacharya and Giosan, 2003; Hampson and Howell, 2005). While the examples from Alvey Wash and Buck Hollow are directly overlying back barrier deposits (Figs. 2.8 and 2.9), barrier islands can also be time-correlative with back-barrier facies (Boyd and Dyer, 1964; Bibler and Schmitt, 1986; Davies et al., 2006).

Back-barrier deposits can be difficult to interpret from outcrop, and with only cursory investigation, can be confused with both offshore or shelfal marine mudstone deposits and coastal plain deposits. Back-barrier facies can be distinguished from coaly coastal plain deposits by the presence of shell fragments, particularly oyster shells, and by marine trace fossils, such as *Thalassinoides*, which can burrow into the upper layer of back-barrier fill following a marine incursion (Savrda, 1991; Carvalho et al., 2007). Back-barrier deposits can show gradationally increasing carbonaceous material vertically, and are capped with coals, suggesting wetting-upward cycles (Wadsworth et al., 2010). In contrast, coastal plain coal cycles are linked to floodplain dynamics such as avulsion and channel abandonment, and more likely to preserve root traces (McCabe, 1987; Kieft et al., 2011). Offshore and shelfal marine mudstones tend to be gray to black, clay rich, mm-scale planar to wavy laminated mudstones (Macquaker et al., 2007) which can contain marine shell fragments such as Inoceramids, depending on depositional age. They typically lack abundant carbonaceous or terrigenous material, coals, and oyster shells.

Biostratigraphy (e.g., pollen, nannofossils, dinoflagellates, and foraminifera) can be used to identify open-marine, brackish, and fresh water conditions based on the type and abundance of fossils preserved (Leckie, 1987; Eaton, 1991; Tibert and Leckie, 2004).

2. Geometry and Internal Facies

Barrier island shorefaces show more internal variability than other shoreface successions because they are deposited rapidly and are more likely to be reworked. Barrier island shoreface deposits are sharp-based shorefaces with storm indicators (hummocky and swaley cross-stratification; Dumas and Arnott, 2006) as well as evidence of rapid deposition (homogenous beds, alternating bioturbated and laminated beds). Offshore and distal lower shoreface deposits are not typically preserved (Fig. 2.8), as they more commonly are in deltaic and strandplain shorefaces (Reading and Collinson, 1996). At the outcrop scale, barrier island shoreface deposits can be less laterally continuous and more heterolithic than strandplain shorefaces. Along-strike the different barrier island successions can grade into one another. The degree of reworking and variability is likely a function of the available accommodation, rate of relative sea level change, and the local hydrodynamic regime (wave, tidal, storm, and current energy).

A sharp-based shoreface geometry is indicative of, but not exclusive to, barrier islands: it also occurs in deltaic deposits, as a result of high sediment supply and rapid progradation (Pattison, 1995; Willis and Gabel, 2001; Bhattacharya and Giosan, 2003). Delta-influenced shorefaces may show a greater amount of terrigenous material and also may be associated with episodic waning flow events (e.g., Bouma sequences) and clinoform geometries (Bhattacharya, 2010; Olariu et al., 2010; Feldman et al., 2014),

which helps to distinguish them from barrier islands. Forced regression also can place sharp-based shoreface successions directly over more distal marine facies (Posamentier et al., 1992; Plint, 2010, Fig. 2.20). As a result, the sharp-based barrier island deposits should be considered in the context of other recognition criteria and indicators.

High-energy upper shoreface deposits (FA3) at the top of barrier island shoreface successions (Fig. 2.8a) can be confused with tidal bars or tidal channels, which can erode into shoreface deposits via tidal ravinement (Fig. 2.14). High-energy upper shoreface deposits associated with barrier islands are vertically continuous, grading upward from the underlying shoreface (Fig. 2.14a). These beds are part of the blocky sandstone outcrop expression and are laterally continuous. They contain high-energy bed forms including distinct, high-angle accretion sets, and small scale (0.05 m tall), high-angle trough cross-stratification. In contrast, tidal channels and tidal bars tend to have erosive bases, cutting down into underlying deposits and creating a tidal ravinement surface, which forms a distinct break in the outcrop (Fig. 2.14b). These deposits can be part of the same cliff band as the shoreface below, but more often they are recessed back, creating a discontinuous layer. Internally, tidal channels and bars contain stacked accretion sets with bidirectional paleocurrent indicators (Fig. 2.8) in addition to multidirectional trough-cross stratification (Chentnik et al., 2015; Mulhern and Johnson, 2016). High-energy upper shoreface deposits show a gradational increase in signals of tidal energy in the upper portion of the shoreface, but lack evidence of basal tidal ravinement.

3. Sequence-Stratigraphic Position

Barrier islands are thick (>5 m) sandstone deposits within regional transgressive successions, and therefore can be identified by their sequence stratigraphic relationships. By definition, barrier islands are separated from the shoreline by a back-barrier lagoon or estuary (Oertel, 1985). This makes ancient barrier islands "transgressive," in the geologic sense, because lagoons and estuaries are inherently transgressive features (Davies, 1978; Kraft et al., 1987). Lagoons form by flooding of coastal plain or strandplain environments during relative sea level rise (Barnes, 1980; Martin and Dominguez, 1994). As lagoons are infilled, coals and back-barrier deposits can record the regressive turn around (Sixsmith et al., 2008; Allen and Johnson, 2011). Similarly, estuaries are flooded river valleys (Dalrymple et al., 1992; 2012). Once an estuary is a net-exporter of sediment to the coastline, it infills and records the regressive turn around, becoming a delta (Dalrymple, 2006). Barrier islands are associated with preserved lagoon and estuary facies, and therefore can be identified by their position within transgressive cycles, often close to the transgressive – regressive turn around. For example, the barrier island shoreface deposits of Buck Hollow are within transgressive intervals, above regressive-transgressive turn-arounds, and below major wave-ravinement surfaces and/or maximum flooding surfaces (Fig. 2.13; Mulhern and Johnson, 2016).

While examples from the Straight Cliffs Formation may not encompass all of the possible variability, excellent outcrop exposure and preservation provide a new foundation for understanding the most commonly preserved types in barrier island deposits. High accommodation and long-lived paralic environments of the Straight Cliffs Formation created optimal preservation conditions for barrier islands, allowing for facies

models to be updated, developed, and described. Barrier islands in other localities may vary in thickness, lateral extent, or the way the architectural elements combine. Nevertheless the internal facies and recognition criteria presented here provide a basis for distinguishing barrier islands from other depositional environments.

Conclusions

Barrier island deposits are composed of four facies associations (back-barrier fill, shoreface, high-energy shoreface, and tidal channels), which stack to create three barrier island architectural elements. Barrier island shorefaces preserve lower and upper shoreface strata over back-barrier fill, recording progradational island motion. Barrier island tidal inlets are composed of high-energy upper shoreface deposits, recording the lateral migration of a barrier island through time. Barrier island tidal channels record vertical aggradation within tidal inlets. Barrier islands can be recognized through three key criteria: proximity to back-barrier facies, internal facies patterns, and sequence stratigraphic position. Barrier islands are associated with back-barriers (lagoons or wave-dominated estuaries) and therefore are inherently preserved within transgressive successions, distinguishing them from regressive strandplain or deltaic shorefaces. The successions documented here depart from existing models, which were based on modern observations, and instead incorporate multidirectional island motion, ravinement, erosion, and reworking. Defining these three types of barrier island deposits implies that modern tidal inlet processes are time-integrated and that deposits preserved within tidal inlets are part of the barrier island succession. Barrier island motion can be independent of the regional shoreline trajectory. Consequently, barrier island deposits can record local

progradational, aggradational, retrogradational, or lateral motion within transgressive successions. Understanding of modern barrier islands has progressed beyond these three motion types. However, these new ideas have not been integrated into existing barrier island facies models. The barrier island deposits within the Straight Cliffs Formation provide an updated understanding of barrier island facies, motion, and preservation, facilitating future interpretations.

References

Allen, J.R.L., 1982, Simple models for the shape and symmetry of tidal sand waves: (1) statically stable equilibrium forms: Marine Geology, v. 48, no. 1, p. 31–49, doi: http://dx.doi.org/10.1016/0025-3227(82)90128-1.

Allen, J.L., and Johnson, C.L., 2011, Architecture and formation of transgressive-regressive cycles in marginal marine strata of the John Henry Member, Straight Cliffs Formation, Upper Cretaceous of southern Utah, USA: Sedimentology, v. 58, no. 6, p. 1486–1513, doi: 10.1111/j.1365-3091.2010.01223.x.

Anthony, E.J., 2009, Shore processes and their palaeoenvironmental applications: Elsevier, Amsterdam.

Anthony, E.J., Lang, J., and Oyede, L.M., 1996, Sedimentation in a tropical, microtidal, wave-dominated coastal-plain estuary: Sedimentology, v. 43, no. 4, p. 665–675, doi: 10.1111/j.1365-3091.1996.tb02019.x.

Antia, J., Fielding, C.R., and Joeckel, R.M., 2011, Multiple cycles of wave-dominated estuarine deposits in low-accommodation settings, Cretaceous J sandstone, northwestern Nebraska: American Association of Petroleum Geologists Bulletin, v. 95, no. 7, p. 1227–1256, doi: 10.1306/11051009105.

Bann, K.L., and Fielding, C.R., 2004, An integrated ichnological and sedimentological comparison of non-deltaic shoreface and subaqueous delta deposits in Permian reservoir units of Australia, *in* McIlroy, D.M. ed., The Application of Ichnology to Palaeoenvironmental and Stratigraphic Analysis, Geological Society, London, Special Publication, 228, London, p. 273–310.

Barnes, R.S.K., 1980, Coastal lagoons: the natural history of a neglected habitat: Cambridge University Press, Cambridge.

Barwis, J.H., 1990, Flood-tidal delta reservoirs, Medora-Dickinson trend, North Dakota,

in Barwis, J.H., McPherson, J.G., and Studlick, J.R.J. eds., Sandstone Petroleum Reservoirs, Springer-Verlag, New York, p. 389–412.

Barwis, J.H., and Hayes, M.O., 1979, Regional patterns of modern barrier island and tidal inlet deposits as applied to paleoenvironmental studies, *in* Ferm, J.C., Horne, J.C., Weisenfluh, G.A., and Staub, J.R. eds., Carboniferous depositional environments in the Appalachian region, University of South Carolina Geology Department, Columbia, S.C., p. 472–498.

Barwis, J.H., and Makurath, J.H., 1978, Recognition of ancient tidal inlet sequences: an example from the Upper Silurian Keyser Limestone in Virginia: Sedimentology, v. 25, no. 1, p. 61–82, doi: 10.1111/j.1365-3091.1978.tb00301.x.

Bass, N.W., 1934, Origin of Bartlesville shoestring sands, Greenwood and Butler Counties, Kansas: American Assocation of Petroleum Geologists Bulletin, v. 18, no. 10, p. 1313–1345.

Belknap, D.F., and Kraft, J.C., 1981, Preservation potential of transgressive coastal lithosomes on the U.S. Atlantic shelf: Marine Geology, v. 42, no. 1–4, p. 429–442, doi: http://dx.doi.org/10.1016/0025-3227(81)90173-0.

Berg, R., 1970, Identification of sedimentary environments in reservoir sandstones: Transactions of the Gulf Coast Assication of Geological Societies, v. 20, p. 137–143.

Berg, R., and Davies, D., 1968, Origin of Lower Cretaceous Muddy Sandstone at Bell Creek Field, Montana: American Association of Petroleum Geologists Bulletin, v. 52, no. 10, p. 1888–1898, doi: 10.1306/5D25C53B-16C1-11D7-8645000102C1865D.

Bernard, H.A., LeBlanc, R.J., and Major, C.F., 1962, Recent and Pleistocene geology of southeast Texas, Field excursion no. 3, *in* Rainwater, E.H. and Zingula, R.P. eds., Geology of the Gulf Coast and Central Texas and Guidebook of Excursions, Houston Geological Society, Houston, Texas, p. 175–224.

Bernard, H.A., Major, C.F., Parrott, B.S., and Le Blanc, R.J., 1970, Recent sediments of southeast Texas: a field guide to the Brazos alluvial and deltaic plains and the Galveston barrier island complex: Bureau of Economic Geology, University of Texas at Austin, Austin.

Bhattacharya, J.P., 2010, Deltas, *in* James, N.P. and Dalrymple, R.W. eds., Facies Models 4, Geological Society of Canada, St. John's, Newfoundland, p. 233–264.

Bhattacharya, J.P., and Giosan, L., 2003, Wave-influenced deltas: geomorphological implications for facies reconstruction: Sedimentology, v. 50, no. 1, p. 187–210, doi: 10.1046/j.1365-3091.2003.00545.x.

Bibler, C.J., and Schmitt, J.G., 1986, Barrier-island coastline deposition and

paleogeographic implications of the Upper Cretaceous Horsethief Formation, Northern Disturbed Belt, Montana: The Mountain Geologist, v. 23, no. 4, p. 113–127.

Boothroyd, J.C., 1985, Tidal inlets and tidal deltas, *in* Davis Jr., R.A. ed., Coastal Sedimentary Environments, Springer-Verlag, New York, p. 445–532.

Boyd, R., 2010, Transgressive wave-dominated coasts, *in* James, N.P. and Dalrymple, R.W. eds., Facies Models 4, Geological Association of Canada, St. John's, Newfoundland, p. 265–294.

Boyd, D.R., and Dyer, B.F., 1964, Frio barrier bar system of south Texas: Transactions - Gulf Coast Association of Geological Societies, v. 14, p. 309–322.

Boyd, R., and Penland, S., 1984, Shoreface translation and the Holocene stratigraphic record: examples from Nova Scotia, the Mississippi Delta and eastern Australia: Marine Geology, v. 60, no. 1, p. 391–412, doi: http://dx.doi.org/10.1016/0025-3227(84)90159-2.

Bridges, P.H., 1976, Lower Silurian transgressive barrier islands, southwest Wales: Sedimentology, v. 23, no. 3, p. 347, doi: 10.1111/j.1365-3091.1976.tb00054.x.

Caplan, M.L., and Moslow, T.F., 1999, Depositional origin and facies variability of a Middle Triassic barrier island complex, Peejay Field, northeastern British Columbia: American Association of Petroleum Geologists Bulletin, v. 83, no. 1, p. 128–154, doi: 10.1306/00AA9A20-1730-11D7-8645000102C1865D.

Carvalho, C.N. de, Viegas, P.A., and Cachao, M., 2007, Thalassinoides and its producer: populations of Mecochirus buried within their burrow systems, Boca de Chapim Formation (Lower Cretaceous), Portugal: Palaios, v. 22, no. 1, p. 104–109, doi: 10.2110/palo.2006.p06-011r.

Cattaneo, A., and Steel, R.J., 2003, Transgressive deposits: a review of their variability: Earth-Science Reviews, v. 62, no. 3–4, p. 187–228, doi: 10.1016/s0012-8252(02)00134-4.

Cheel, R.J., and Leckie, D.A., 1990, A tidal-inlet complex in the Cretaceous epeiric sea of North America: Virgelle Member, Milk River Formation, southern Alberta, Canada: Sedimentology, v. 37, no. 1, p. 67–81, doi: 10.1111/j.1365-3091.1990.tb01983.x.

Chentnik, B.M., Johnson, C.L., Mulhern, J.S., and Stright, L.E., 2015, Valleys, estuaries, and lagoons: paleoenvironments and regressive-transgressive architecture of the Upper Cretaceous Straight Cliffs Formation: Journal of Sedimentary Research, v. 85, no. 10, p. 1166–1196, doi: 10.2110/jsr.2015.70.

Clifton, H.E., 2006, A reexamination of facies models for clastic shorelines, *in* Posamentier, H.G. and Walker, R.G. eds., Facies Models Revisited, SEPM Special

Publication, 84, p. 293–337.

Cotter, E., 1975, Deltaic deposits in the Upper Cretaceous Ferron Sandstone, Utah, *in* Broussard, M. Lou ed., Deltas: Models for Exploration, Houston Geological Society, Houston, p. 471–484.

Curray, J.R., 1964, Transgressions and regressions, *in* Miller, R.L. ed., Papers in Marine Geology, Shepard Commemorative Volume, Macmillan Company, New York, p. 175–203.

Dalrymple, R.W., 2006, Incised valleys in time and space: an introduction to the volume and an examination of the controls on valley formation and filling, *in* Dalrymple, R.W., Leckie, D.A., and Tillman, R.W. eds., Incised Valleys in Time and Space, SEPM Special Publication, 85, p. 5–12.

Dalrymple, R.W., 2010, Tidal depositional systems, *in* James, N.P. and Dalrymple, R.W. eds., Facies Models 4, Geological Association of Canada, St. John's, Newfoundland, p. 201–232.

Dalrymple, R.W., and Choi, K., 2007, Morphologic and facies trends through the fluvial–marine transition in tide-dominated depositional systems: a schematic framework for environmental and sequence-stratigraphic interpretation: Earth-Science Reviews, v. 81, no. 3–4, p. 135–174, doi: 10.1016/j.earscirev.2006.10.002.

Dalrymple, R.W., Mackay, D.A., Ichaso, A.A., and Choi, K.S., 2012, Processes, morphodynamics, and facies of tide-dominated estuaries, *in* Davis Jr, R.A. and Dalrymple, R.W. eds., Principles of Tidal Sedimentology, Springer Netherlands, Dordrecht, p. 79–107.

Dalrymple, R.W., Zaitlin, B.A., and Boyd, R.R., 1992, Estuarine facies models: conceptual basis and stratigraphic implications: Journal of Sedimentary Petrology, v. 62, no. 6, p. 1130–1146, doi: 10.1306/D4267A69-2B26-11D7-8648000102C1865D.

Dashtgard, S.E., Gingras, M.K., and MacEachern, J.A., 2009, Tidally modulated shorefaces: Journal of Sedimentary Research, v. 79, no. 11, p. 793–807, doi: 10.2110/jsr.2009.084.

Davies, D.K., 1978, Models and concepts for exploration in barrier islands, *in* Saxena, R.S. ed., Gulf Coast Association of Geological Societies, New Orleans, LA, p. 159–197.

Davies, D.K., and Ethridge, F.G., 1971, The Claiborne group of central Texas: Transactions - Gulf Coast Association of Geological Societies, v. 21, p. 115–124.

Davies, D., Ethridge, F., and Berg, R., 1971, Recognition of barrier environments: American Association of Petroleum Geologists Bulletin, v. 4, no. 4, p. 550–565.

Davies, R., Howell, J., Boyd, R., Flint, S., and Diessel, C., 2006, High-resolution

sequence-stratigraphic correlation between shallow-marine and terrestrial strata: examples from the Sunnyside Member of the Cretaceous Blackhawk Formation, Book Cliffs, eastern Utah: American Association of Petroleum Geologists Bulletin, v. 90, no. 7, p. 1121–1140, doi: 10.1306/02210604077.

Davis Jr., R.A., 2013, A new look at barrier-inlet morphodynamics: Journal of Coastal Research, Special Issue, v. 69, p. 1–12, doi: 10.2112/SI_69_2.

Davis Jr., R.A., 1994, Barrier island systems- a geologic overview, *in* Davis Jr., R.A. ed., Geology of Holocene Barrier Island Systems, Springer-Verlag, Berlin, p. 1–46.

Devine, P.E., 1991, Transgressive origin of channeled estuarine deposits in the Point Lookout Sandstone, northwestern New Mexico: a model for Upper Cretaceous, cyclic regressive parasequences of the U.S. Western Interior: American Association of Petroleum Geologists Bulletin, v. 75, no. 6, p. 1039–1063, doi: 10.1306/0C9B28C1-1710-11D7-8645000102C1865D.

Dickinson, K.A., Berryhill, H.L., and Holmes, C.W., 1972, Criteria for recognizing ancient barrier coastlines, *in* Rigby, J.K. and Hamblin, W.K. eds., Recognition of Ancient Sedimentary Environments, SEPM, Special Publication 16, p. 108–145.

Dillon, W.P., 1970, Submergence effects on a Rhode Island barrier and lagoon and inferences on migration of barriers: The Journal of Geology, v. 78, no. 1, p. 94–106.

Donselaar, M.E., 1984, Flood tidal delta sedimentation in the Late Cretaceous Menefee Formation (Mesaverde Group), San Juan Basin, northwest New Mexico: Geologie en Mijnbouw, v. 63, no. 3, p. 323–331.

Dooling, P.R., 2013, Tidal Facies, Stratigraphic Architecture, and Along-Strike Variability of a High Energy, Transgressive Shoreline, Late Cretaceous, Kaiparowits Plateau, Southern Utah [M.Sc] [Thesis]: University of Utah, 135 p.

Dronkers, J.J., 2005, Dynamics of coastal systems: World Scientific, Singapore.

Droser, M.L., and Bottjer, D.J., 1989, Ichnofabric of sandstones deposited in high-energy nearshore environments measurements and utilization: Palaios, v. 4, no. 6, p. 598–604.

Dumas, S., 2005, Experiments on oscillatory-flow and combined-flow bed forms: implications for interpreting parts of the shallow-marine sedimentary record: Journal of Sedimentary Research, v. 75, no. 3, p. 501–513, doi: 10.2110/jsr.2005.039.

Dumas, S., and Arnott, R.W.C., 2006, Origin of hummocky and swaley cross-stratification - the controlling influence of unidirectional current strength and aggradation rate: Geology, v. 34, no. 12, p. 1073–1076, doi: 10.1130/G22930A.1.

Dyke, P.P.G., 2007, Modeling coastal and offshore processes: Imperial College Press, London.

Dzuynski, S., and Smith, A.J., 1963, Convolute lamination, its origin, preservation, and directional significance: Journal of Sedimentary Research, v. 33, no. 3, p. 616–627, doi: 10.1306/74D70ED4-2B21-11D7-8648000102C1865D.

Eaton, J.G., 1991, Biostratigraphic framework for the Upper Cretaceous rocks of the Kaiparowits Plateau, southern Utah, *in* Nations, J.D. and Eaton, J.G. eds., Stratigraphy, depositional environments, and sedimentary tectonics of the western margin, Cretaceous Western Interior Seaway, Geological Society of America, Special Paper, 260, p. 47–63.

De Falco, G., Antonioli, F., Fontolan, G., Lo Presti, V., Simeone, S., and Tonielli, R., 2015, Early cementation and accommodation space dictate the evolution of an overstepping barrier system during the Holocene: Marine Geology, v. 369, p. 52–66, doi: 10.1016/j.margeo.2015.08.002.

Feldman, H.R., Fabijanic, J.M., Faulkner, B.L., and Rudolph, K.W., 2014, Lithofacies, parasequence stacking, and depositional architecture of wave- to tide-dominated shorelines in the Frontier Formation, western Wyoming, U.S.A: Journal of Sedimentary Research, v. 84, no. 8, p. 694–717, doi: 10.2110/jsr.2014.53.

Finley, R.J., 1978, Ebb-tidal delta morphology and sediment supply in relation to seasonal wave energy flux, North Inlet, South Carolina: Journal of Sedimentary Petrology, v. 48, no. 1, p. 227–238, doi: 10.1306/212F743C-2B24-11D7-8648000102C1865D.

Fisher, J.S., and Dolan, R. (Eds.), 1977, Beach processes and coastal hydrodynamics: Dowden, Hutchinson & Ross, Stroudsburg, PA.

Fisk, H.N., 1959, Padre Island and the Laguna Madre Flats, coastal south Texas: , p. 103–151.

FitzGerald, D.M., Buynevich, I., and Hein, C., 2012, Morphodynamics and facies architecture of tidal inlets and tidal deltas, *in* Davis Jr, R.A. and Dalrymple, R.W. eds., Principles of Tidal Sedimentology, Springer Netherlands, Dordrecht, p. 301–333.

Flores, R.M., 1978, Barrier and back-barrier environments of deposition of the Upper Cretaceous Almond Formation, Rock Springs Uplift, Wyoming: The Mountain Geologist, v. 15, no. 2, p. 57–65.

Frey, R.W., and Howard, J.D., 1985, Trace fossils from the Panther Member, Star Point Formation (Upper Cretaceous), Coal Creek Canyon, Utah: Journal of Paleontology, v. 59, no. 2, p. 370–404.

Galloway, W.E., 1986, Reservoir facies architecture of microtidal barrier systems: American Association of Petroleum Geologists Bulletin, v. 70, no. 7, p. 787–808, doi: 10.1306/9488634E-1704-11D7-8645000102C1865D.

Galloway, W.E., and Hobday, D.K. (Eds.), 1983, Terrigenous clastic depositional systems: applications to petroleum, coal, and uranium exploration: Springer-Verlag, New York.

Hampson, G.J., and Howell, J.A., 2005, Sedimentologic and geomorphic characterization of ancient wave-dominated deltaic shorelines: Upper Cretaceous Blackhawk Formation, Book Cliffs, Utah, U.S.A, *in* Giosan, L. and Bhattacharya, J.P. eds., River deltas; concepts, models, and examples, SEPM Special Publication, 83, p. 133–154.

Hayes, M.O., 1980, General morphology and sediment patterns in tidal inlets: Sedimentary Geology, v. 26, no. 1–3, p. 139–156, doi: 10.1016/0037-0738(80)90009-3.

Hayes, M.O., and FitzGerald, D.M., 2013, Origin, evolution, and classification of tidal inlets: Journal of Coastal Research, v. 69, p. 14–33, doi: 10.2112/SI_69_3.

Heron Jr., S.D., Moslow, T.F., Berelson, W.M., Herbert, J.R., Steele III, G.A., and Susman, K.R., 1984, Holocene sedimentation of a wave-dominated barrier island shoreline: Cape Lookout, North Carolina: Marine Geology, v. 60, no. 1–4, p. 413–434, doi: http://dx.doi.org/10.1016/0025-3227(84)90160-9.

Hettinger, R.D., McCabe, P.J., and Shanley, K.W., 1993, Detailed facies anatomy of aransgressive and highstand systems sracts from the Upper Cretaceous of Southern Utah, U.S.A., *in* Weimer, R.J. and Posamentier, H.W. eds., Siliciclastic Sequence Stratigraphy: Recent Developments and Applications, American Association of Petroleum Geologists Memior, 58, p. 235–257.

Heward, A.P., 1981, A review of wave-dominated clastic shoreline deposits: Earth-Science Reviews, v. 17, no. 3, p. 223–276, doi: http://dx.doi.org/10.1016/0012-8252(81)90022-2.

Hobday, D.K., and Jackson, M.P.A., 1979, Transgressive shore zone sedimentation and syndepositional deformation in the Pleistocene of Zululand, South Africa: Journal of Sedimentary Research, v. 49, no. 1, p. 145–158, doi: 10.1306/212F76DA-2B24-11D7-8648000102C1865D.

Hobday, D.K., and Orme, A.R., 1974, The Port Durnford Formation: Verhandelinge van die Geologiese Vereniging van Suid Afrika, v. 77, no. 2, p. 141–149.

Hollenshead, C.T., and Pritchard, R.I., 1960, Geometry of producing Mesaverde sandstones, San Juan Basin, *in* Peterson, J.A. and Osmond, J.C. eds., Geometry of Sandstone Bodies, American Association of Petroleum Geologists Special Publication, 22, p. 98–118.

Hoyt, J., and Henry Jr., V.J., 1965, Significance of inlet sedimentation in the recognition of ancient barrier islands, *in* DeVoto, R.H. and Bitter, R.K. eds., Sedimentation of Late Cretaceous and Tertiary Outcrops, Rock Springs Uplift, Ninteenth Annual

Field Conference Guidebook, Wyoming Geological Association, p. 190–194.

Hubbard, S.M., Gingras, M.K., Pemberton, S.G., and Thomas, M.B., 2002, Variability in wave-dominated estuary sandstones: implications on subsurface reservoir development: Bulletin of Canadian Petroleum Geology, v. 50, no. 1, p. 118–137, doi: 10.2113/50.1.118.

Hudock, J.W., Flaig, P.P., and Wood, L.J., 2014, Washover fans: a modern geomorphologic analysis and proposed classification scheme to improve reservoir models: Journal of Sedimentary Research, v. 84, p. 854–865.

Hughes, Z.J., 2012, Tidal channels on tidal flats and marshes, *in* Davis Jr., R.A. and Dalrymple, R.W. eds., Principles of Tidal Sedimentology, Springer Netherlands, Dordrecht, p. 269–300.

Israel, A.M., Ethridge, F.G., and Estes, E.L., 1987, A sedimentologic description of a microtidal, flood-tidal delta, San Luis Pass, Texas: Journal of Sedimentary Research, v. 57, no. 2, p. 288–300, doi: 10.1306/212f8b07-2b24-11d7-8648000102c1865d.

Kana, T.W., Rosati, J.D., and Traynum, S.B., 2011, Lack of evidence for onshore sediment transport from deep water at decadal time scales: Fire Island, New York: Journal of Coastal Research, v. 59, no. 1961, p. 61–75, doi: 10.2112/SI59-007.1.

Kieft, R.L., Hampson, G.J., Jackson, C.A.L., and Larsen, E., 2011, Stratigraphic architecture of a net-transgressive marginal- to shallow-marine succession: Upper Almond Formation, Rock Springs Uplift, Wyoming, U.S.A.: Journal of Sedimentary Research, v. 81, no. 7, p. 513–533, doi: 10.2110/jsr.2011.44.

Kraft, J.C., Chrzastowski, M.J., Belknap, D.F., Toscano, M.A., and Fletcher III, C.H., 1987, The transgressive barrier-lagoon coast of Delaware: morphostratigraphy, sedimentary sequences and responses to relative rise in sea level, *in* Nummedal, D., Pilkey, O.H., and Howard, J.D. eds., Sea-level Fluctuation and Coastal Evolution, SEPM Special Publication, 41, p. 129–143.

Kraft, J.C., and John, C.J., 1979, Lateral and vertical facies relations of transgresslve barrier: American Assocation of Petroleum Geologists Bulletin, v. 63, no. 12, p. 2145–2163.

Kumar, N., and Sanders, J.E., 1974, Inlet sequence: a vertical succession of sedimentary structures and textures created by the lateral migration of tidal inlets: Sedimentology, v. 21, no. 4, p. 491–532, doi: 10.1111/j.1365-3091.1974.tb01788.x.

Land, C.B., 1972, Stratigraphy of Fox Hills Sandstone and associated formations, Rock Springs uplift and Wamsutter Arch area, Sweetwater County, Wyoming: a shoreline-estuary sandstone model for the Late Cretaceous: Colorado School of Mines, [Golden.

Leatherman, S.P., 1983, Barrier island evolution in response to sea level rise: a

discussion: Journal of Sedimentary Petrology, v. 53, no. 3, p. 1026–1033.

Leatherman, S.P., 1979, Migration of Assateague Island, Maryland, by inlet and overwash processes: Geology, v. 7, no. 2, p. 104–107, doi: 10.1130/0091-7613(1979)7<104:MOAIMB>2.0.CO;2.

Leckie, R.M., 1987, Paleoecology of mid-Cretaceous planktonic foraminifera: a comparison of open ocean and epicontinental sea assemblages: Micropaleontology, v. 33, no. 2, p. 164–176, doi: 10.2307/1485491.

Lentz, E.E., and Hapke, C.J., 2011, Geologic framework influences on the geomorphology of an anthropogenically modified barrier island: Assessment of dune/beach changes at Fire Island, New York: Geomorphology, v. 126, no. 1–2, p. 82–96, doi: http://dx.doi.org/10.1016/j.geomorph.2010.10.032.

Longhitano, S.G., Mellere, D., Steel, R.J., and Ainsworth, R.B., 2012, Tidal depositional systems in the rock record: a review and new insights: Sedimentary Geology, v. 279, p. 2–22, doi: 10.1016/j.sedgeo.2012.03.024.

MacEachern, J.A., and Pemberton, S.G., 1992, Ichnological aspects of Cretaceous shoreface successions and shoreface variability in the Western Interior Seaway of North America, *in* Pemberton, S.G. ed., Applications of Ichnology to Petroleum Exploration, Society of Sedimentary Geology Core Workshop, 17, p. 57–84.

Macquaker, J.H.S., Taylor, K.G., and Gawthorpe, R.L., 2007, High-resolution facies analyses of mudstones: implications for paleoenvironmental and sequence stratigraphic interpretations of offshore ancient mud-dominated successions: Journal of Sedimentary Research, v. 77, no. 4, p. 324–339, doi: 10.2110/jsr.2007.029.

Martin, L., and Dominguez, J.M.L., 1994, Chapter 3 Geological history of coastal lagoons, *in* Kjerfve, B. ed., Coastal Lagoon Processes, Elsevier, Amsterdam, p. 41–68.

Masselink, G., and van Heteren, S., 2014, Response of wave-dominated and mixed-energy barriers to storms: Marine Geology, v. 352, p. 321–347, doi: 10.1016/j.margeo.2013.11.004.

McCabe, P.J., 1987, Facies studies of coal and coal-bearing strata, *in* Scott, A.C. ed., Coal and Coal-bearing Strata: Recent Advances, Geological Society, London, Special Publications, 32, p. 51–66.

McCubbin, D.G., 1982, Barrier-island and strand plain facies, *in* Scholle, P.A. and Spearing, D. eds., Sandstone Depositional Environments, American Association of Petroleum Geologists Memior, 31, p. 247–279.

Mellere, D., Zecchin, M., and Perale, C., 2005, Stratigraphy and sedimentology of fault-controlled backstepping shorefaces, middle Pliocene of Crotone Basin, Southern Italy: Sedimentary Geology, v. 176, no. 3–4, p. 281–303, doi:

10.1016/j.sedgeo.2005.01.010.

Middleton, G. V, 1973, Johannes Walther's Law of the correlation of facies: Geological Society of America Bulletin, v. 84, no. 3, p. 979, doi: 10.1130/0016-7606(1973)84<979:JWLOTC>2.0.CO;2.

Milliken, K.T., Anderson, J.B., and Rodriguez, A.B., 2008, A new composite Holocene sea-level curve for the northern Gulf of Mexico, *in* Anderson, J.B. and Rodriguez, A.B. eds., Response of Upper Gulf Coast Estuaries to Holocene Climate Change and Sea-Level Rise, Geological Society of America, Special Paper 443, p. 1–11.

Moore, L.J., List, J.H., Williams, S.J., and Stolper, D., 2010, Complexities in barrier island response to sea level rise: insights from numerical model experiments, North Carolina Outer Banks: Journal of Geophysical Research: Earth Surface, v. 115, no. F030004, p. 1–27, doi: 10.1029/2009JF001299.

Morton, R.A., 1994, Texas barriers, *in* Davis Jr., R.A. ed., Geology of Holocene Barrier Island Systems, Springer-Verlag, Berlin, p. 75–114.

Moslow, T.F., 1984, Barrier island shoreline systems, *in* CN27: Depositional Models of Shelf and Shoreline Sandstones, p. 5–15.

Moslow, T.F., and Tye, R.S., 1985, Recognition and characterization of Holocene tidal inlet sequences: Marine Geology, v. 63, no. 1–4, p. 129–151, doi: http://dx.doi.org/10.1016/0025-3227(85)90081-7.

Mulhern, J.S., and Johnson, C.L., 2016, Time–space variability of paralic strata deposited in a high accommodation, high sediment supply setting: example from the Cretaceous of Utah, *in* Hampson, G.J., Reynolds, A.D., Kostic, B., and Wells, M.R. eds., Geological Society, London, Special Publications, Geological Society, London, Special Publication, 444.

Murakoshi, N., and Masuda, F., 1991, A depositional model for a flood-tidal delta and washover sands in the late Pleistocene, *in* Smith, D.G., Reinson, G.E., Zaitlin, B.A., and Rahmani, R.A. eds., Clastic Tidal Sedimentology, Canadian Society of Petroleum Geologists, Memoir 16, p. 219–226.

Nio, S.-D., and Yang, C.-S., 1991, Diagnostic attributes of clastic tidal deposits, *in* Smith, D.G., Reinson, G.E., Zaitlin, B.A., and Rahmani, R.A. eds., Clastic Tidal Sedimentology, Canadian Society of Petroleum Geologists, Memior 16, p. 3–28.

Oertel, G.F., 1988, Processes of sediment exchange between tidal inlets, ebb deltas and barrier islands, *in* Aubrey, D.G. and Weishar, L. eds., Hydrodynamics and Sediment Dynamics of Tidal Inlets, Springer-Verlag, New York, p. 297–318.

Oertel, G.F., 1985, The barrier island system: Marine Geology, v. 63, no. 1, p. 1–18, doi: 10.1016/0025-3227(85)90077-5.

Olariu, C., Steel, R.J., Dalrymple, R.W., and Gingras, M.K., 2012, Tidal dunes versus tidal bars: the sedimentological and architectural characteristics of compound dunes in a tidal seaway, the lower Baronia Sandstone (Lower Eocene), Ager Basin, Spain: Sedimentary Geology, v. 279, no. 0, p. 134–155, doi: 10.1016/j.sedgeo.2012.07.018.

Olariu, C., Steel, R.J., and Petter, A.L., 2010, Delta-front hyperpycnal bed geometry and implications for reservoir modeling: Cretaceous Panther Tongue delta, Book Cliffs, Utah: American Assocation of Petroleum Geologists Bulletin, v. 94, no. 6, p. 819–845, doi: 10.1306/11020909072.

Olsen, T.R., Mellere, D., and Olsen, T., 1999, Facies architecture and geometry of landward-stepping shoreface tongues: the Upper Cretaceous Cliff House Sandstone (Mancos Canyon, south-west Colorado): Sedimentology, v. 46, no. 4, p. 603–625, doi: 10.1046/j.1365-3091.1999.00234.x.

Oost, A.P., Hoekstra, P., Wiersma, A., Flemming, B., Lammerts, E.J., Pejrup, M., Hofstede, J., van der Valk, B., Kiden, P., Bartholdy, J., van der Berg, M.W., Vos, P.C., de Vries, S., and Wang, Z.B., 2012, Barrier island management: lessons from the past and directions for the future: Ocean & Coastal Management, v. 68, p. 18–38, doi: 10.1016/j.ocecoaman.2012.07.010.

Otvos, E.G., 2012, Coastal barriers - nomenclature, processes, and classification issues: Geomorphology, v. 139–140, no. 0, p. 39–52, doi: 10.1016/j.geomorph.2011.10.037.

Painter, C.S., York-Sowecke, C.C., and Carrapa, B., 2013, Sequence stratigraphy of the Upper Cretaceous Sego Sandstone Member reveals spatio-temporal changes in depositional processes, northwest Colorado, U.S.A: Journal of Sedimentary Research, v. 83, no. 4, p. 323–338, doi: 10.2110/jsr.2013.21.

Pattison, S.A.J., 1995, Sequence stratigraphic significance of sharp-based lowstand shoreface deposits, Kenilworth Member, Book Cliffs, Utah: American Assocation of Petroleum Geologists Bulletin, v. 79, no. 3, p. 444–462, doi: 10.1306/8D2B155C-171E-11D7-8645000102C1865D.

Pemberton, S.G., MacEachern, J.A., Dashtgard, S.E., Bann, K.L., Gingras, M.K., and Zonneveld, J.-P., 2012, 19. Shorefaces, *in* Knaust, D. and Bromley, R.G. eds., Trace Fossils as Indicators of Sedimentary Environments, Elsevier BV, Amsterdam, p. 563–606.

Peterson, F., 1969, Four new members of the Upper Cretaceous Straight Cliffs Formation in the southeastern Kaiparowits Region, Kane County, Utah: Geological Survey Bulletin, v. 1274–J, p. J1–J28.

Plint, A.G., 2010, Wave-and storm-dominated shoreline and shallow-marine systems, *in* James, N.P. and Dalrymple, R.W. eds., Facies Models 4, Geological Society of Canada, St. John's, Newfoundland, p. 167–199.

Pocknall, D., Johnson, C.L., Mulhern, J.S., and Johnson, C., 2016, Palynology of non-

marine and marine strata of the Straight Cliffs Formation (Coniacian-Campanian), Kaiparowits Plateau, Utah, *in* Program and Abstracts, Joint Meeting of The Society for Organic Petrology, International Committee for Coal and Organic Petrology, and AASP – The Palynological Society, September 18-23, Houston Texas, p. 95.

Posamentier, H.W., Allen, G.P., James, D.P., and Tesson, M., 1992, Forced regressions in a sequence stratigraphic framework: concepts, examples, and exploration significance: American Association of Petroleum Geologists Bulletin, v. 76, no. 11, p. 1687–1709.

Posamentier, H.W., Jervey, M.T., and Vail, P.R., 1988, Eustatic controls on clastic deposition I - conceptual framework, *in* Wilgus, C.K., Hastings, B.S., Posamentier, H.W., Van Wagoner, J.C., Ross, C.A., and Kendall, C.G.S.C. eds., Sea-level changes: an integrated approach, SEPM Special Publication, 42, p. 109–124.

Rahmani, R.A., 1988, Estuarine tidal channel and nearshore sedimentation of a Late Cretaceous epicontinental sea, Drumheller, Alberta, Canada, *in* de Boer, P.L., van Gelder, A., and Nio, S.D. eds., Tide-Influenced Sedimentary Environments and Facies, Reidel Publishing, Dordrecht, p. 433–474.

Rampino, M.R., and Sanders, J.E., 1980, Evolution of the barrier: islands of southern Long Island, New York: Sedimentology, v. 28, p. 37–47, doi: 10.1111/j.1365-3091.1981.tb01661.x.

Reading, H.G., and Collinson, J.D., 1996, Clastic coasts, *in* Reading, H.G. ed., Sedimentary Environments: Processes, Facies, and Stratigraphy, Blackwell Science, Oxford, p. 154–231.

Reddering, J.S. V, 1983, An inlet sequence produced by migration of a small microtidal inlet against longshore drift: the Keurbooms Inlet, South Africa: Sedimentology, v. 30, no. 2, p. 201–218, doi: 10.1111/j.1365-3091.1983.tb00665.x.

Reineck, H.-E., and Singh, I.B. (Eds.), 1980, Depositional sedimentary environments, with reference to terrigenous clastics: Springer-Verlag, Berlin.

Reinson, G.E., 1979, Barrier island systems, *in* Walker, R.G. ed., Facies Models, Geosciences Canada, Toronto, p. 57–74.

Reinson, G.E., 1984, Barrier-island and associated strand-plain systems, *in* Walker, R.G. ed., Facies Models, Geological Association of Canada, Toronto, p. 119–140.

Reinson, G.E., 1992, Transgressive barrier island and estuarine systems, *in* Walker, R.G. and James, N.P. eds., Facies Models: Response to Sea-Level Changes, Geological Association of Canada, St. John's, Newfoundland, p. 179–194.

Roehler, H.W., 1988, The Pintail coal bed and barrier bar G - a model for coal of barrier bar - lagoon origin, Upper Cretaceous Almond Formation, Rock Springs Coal Field, Wyoming: U.S. Geological Survey Professional Paper, v. 1398.

Roy, P.S., Cowell, P.J., Fernland, M.A., and Thom, B.G., 1994, Wave-dominated coasts, *in* Carter, R.W.G. and Woodroffe, C.D. eds., Coastal Evolution: Late Quaternary Shoreline Morphodynamics, Cambridge University Press, Cambridge, p. 121–186.

Sabins Jr, F.F., 1963, Anatomy of stratigraphic trap, Bisti field, New Mexico: American Assocation of Petroleum Geologists Bulletin, v. 47, no. 2, p. 193–228, doi: 10.1126/science.58.1489.27.

Savrda, C.E., 1991, Ichnology in sequence stratigraphic studies: an example from the Lower Paleocene of Alabama: Palaios, v. 6, p. 39–53.

Schatzinger, R.A., Szpakiewicz, M., and Sharma, B., 1989, Applicable correlations and overall characteristics of barrier island deposystems: Department of Energy Report No. NIPER-427, p. 1–39.

Schwartz, R.K., 1982, Bedform and stratification characteristics of some modern small-scale washover sand bodies: Sedimentology, v. 29, no. 6, p. 835–849, doi: 10.1111/j.1365-3091.1982.tb00087.x.

Sedgwick, P.E., and Davis Jr., R.A., 2003, Stratigraphy of washover deposits in Florida: implications for recognition in the stratigraphic record: Marine Geology, v. 200, no. 1–4, p. 31–48, doi: http://dx.doi.org/10.1016/S0025-3227(03)00163-4.

Self, G.A., Breard, S.Q., Rael, H.P., Stein, J.A., Thayer, P.A., Traugott, M.O., and Easom, W.D., 1986, Lockhart Crossing Field: New Wilcox Trend in Southeastern Louisiana: American Association of Petroleum Geologists Bulletin, v. 70, no. 5, p. 501–515.

Seminack, C.T., and Buynevich, I., 2013, Sedimentological and geophysical signatures of a relict tidal inlet complex along a wave-dominated barrier: Assteague Island, Maryland, USA: Journal of Sedimentary Research, v. 83, p. 132–144.

Shanley, K.W., and McCabe, P.J., 1995, Sequence stratigraphy of Turonian-Santonian strata, Kaiparowits Plateau, southern Utah, USA: implications for regional correlation and foreland basin evolution, *in* Van Wagoner, J.C. and Bertram, G.T. eds., Sequence Stratigraphy of Foreland Basin Deposits, American Association of Petroleum Geologists Memior, 64, p. 103–136.

Shepard, F.P., and Moore, D.G., 1955, Sediment zones bordering the barrier islands of central Texas coast, *in* Hough, J.L. and Menard, H.W. eds., Finding Ancient Shorelines, SEPM Special Publication, 3, p. 78–98.

Short, A.D. (Ed.), 1999, Handbook of Beach and Shoreface Morphodynamics: John Wiley & Sons, Chichester.

Simms, A.R., Anderson, J.B., and Blum, M., 2006, Barrier-island aggradation via inlet migration: Mustang Island, Texas: Sedimentary Geology, v. 187, no. 1–2, p. 105–125, doi: 10.1016/j.sedgeo.2005.12.023.

Siringan, F.P., and Anderson, J.B., 1993, Seismic facies, architecture, and evolution of the Bolivar Roads tidal inlet/delta complex, East Texas Gulf Coast: Journal of Sedimentary Petrology, v. 63, no. 5, p. 794–808, doi: 10.1306/D4267C08-2B26-11D7-8648000102C1865D.

Sixsmith, P.J., Hampson, G.J., Gupta, S., Johnson, H.D., and Fofana, J.F., 2008, Facies architecture of a net transgressive sandstone reservoir analog: the Cretaceous Hosta Tongue, New Mexico: American Assocation of Petroleum Geologists Bulletin, v. 92, no. 4, p. 513–547, doi: 10.1306/01020807017.

Steel, R.J., Plink-Bjorklund, P., and Aschoff, J., 2012, Tidal deposits of the Campanian Western Interior Seaway, Wyoming, Utah and Colorado, USA, *in* Davis, R.A. and Dalrymple, R.W. eds., Principles of Tidal Sedimentology, Springer Netherlands, Dordrecht, p. 437–471.

Storms, J.E.A., Weltje, G.J., van Dijke, J.J., Geel, C.R., and Kroonenberg, S.B., 2002, Process-response modeling of wave-dominated coastal systems: simulating evolution and stratigraphy on geological timescales: Journal of Sedimentary Research, v. 72, no. 2, p. 226–239, doi: 10.1306/052501720226.

Stutz, M.L., and Pilkey, O.H., 2011, Open-ocean barrier islands: global influence of climatic, oceanographic, and depositional settings: Journal of Coastal Research, v. 27, no. 2, p. 207–222, doi: 10.2112/09-1190.1.

Stutz, M.L., and Pilkey, O.H., 2005, The relative influence of humans on barrier islands: humans versus geomorphology: Reviews in Engineering Geology, v. 16, no. 12, p. 137–147, doi: 10.1130/2005.4016(12).

Susman, K.R., and Heron, S.D., 1979, Evolution of a barrier island, Shackleford Banks, Carteret County, North Carolina: Geological Society of America Bulletin, v. 90, no. 2, p. 205–215, doi: 10.1130/0016-7606(1979)90<205:EOABIS>2.0.CO;2.

Swift, D.J.P., 1975, Barrier-island genesis: evidence from the central Atlantic shelf, eastern U.S.A: Sedimentary Geology, v. 14, no. 1, p. 1–43.

Swift, D.J.P., 1968, Coastal erosion and transgressive stratigraphy: The Journal of Geology, v. 76, no. 4, p. 444–456, doi: 10.1086/627342.

Swift, D.J.P., Phillips, S., and Thorne, J.A., 1991, Sedimentation on continental margins, V: parasequences, *in* Swift, D.J.P., Oertel, G.F., Tillman, R.W., and Thorne, J.A. eds., Shelf Sand and Sandstone Bodies: Geometry, Facies and Sequence Stratigraphy, Special Publication of the International Association of Sedimentologists, 14, Oxford, p. 153–187.

Szpakiewicz, M., Schatzinger, R.A., Jackson, S., Sharma, B., and Honarpour, M., 1991, Selection and initial characterization of a second barrier island reservoir system and refining of methodology for characterization of shoreline barrier reservoirs: IIT Research Institute, National Institute for Petroleum and Energy Research, U.S.

Department of Energy, NIPER-484.

Thom, B.G., 1984, Sand barriers of eastern Australia: Gippsland - a case study, *in* Thom, B.G. ed., Coastal geomorphology in Australia, Australia: Acad. Press, Sydney, N.S.W., p. 233–261.

Tibert, N.E., and Leckie, R.M., 2004, High-resolution estuary sea level cycles from the Late Cretacous: amplitude constraints using agglutinated foraminifera: Journal of Foraminiferal Research, v. 34, no. 2, p. 130–143.

Timmons, E.A., Rodriguez, A.B., Mattheus, C.R., and DeWitt, R., 2010, Transition of a regressive to a transgressive barrier island due to back-barrier erosion, increased storminess, and low sediment supply: Bogue Banks, North Carolina, USA: Marine Geology, v. 278, no. 1–4, p. 100–114, doi: 10.1016/j.margeo.2010.09.006.

Tye, R., and Moslow, T., 1993, Tidal inlet reservoirs: insights from modern examples, *in* Rhodes, E.G. and Moslow, T.F. eds., Marine Clastic Reservoirs: Examples and Analogues, Springer-Verlag, New York, p. 77–100.

Uhlir, D.M., Akers, A., and Vondra, C.F., 1988, Tidal inlet sequence, Sundance Formation (Upper Jurassic), north-central Wyoming: Sedimentology, v. 35, no. 5, p. 739, doi: 10.1111/j.1365-3091.1988.tb01248.x.

Vail, P.R., Mitchum Jr., R.M., and Thompson III, S., 1977, Seismic stratigraphy and global changes of sea level, part 3: relative changes of sea level from coastal onlap, *in* Payton, C.E. ed., Seismic Stratigraphy: Applications to Hydrocarbon Exploration, American Association of Petroleum Geologists Memior, 26, p. 63–81.

Wadsworth, J., Diessel, C., and Boyd, R., 2010, The sequence stratigraphic significance of paralic coal and its use as an indicator of accommodation space in terrestrial sediments, *in* Ratcliffe, K. and Zaitlin, B.A. eds., Application of Modern Stratigraphic Techniques: Theory and Case Histories, SEPM Special Publication, 94, p. 201–219.

Van Wagoner, J.C., Posamentier, H.W., Mitchum, R.M., Vail, P.R., Sarg, J.F., Loutit, T.S., and Hardenbol, J., 1988, An overview of the fundamentals of sequence stratigraphy and key definitions, *in* Wilgus, C.K., Posamentier, H.W., Ross, C.K., and Kendall, C.G. eds., Sea-level Changes: An Integrated Approach, SEPM Special Publication, 42, Tulsa, p. 39–45.

Willis, B.J., and Gabel, S., 2001, Sharp-based, tide-dominated deltas of the Sego Sandstone, Book Cliffs, Utah, USA: Sedimentology, v. 48, no. 3, p. 479–506, doi: 10.1046/j.1365-3091.2001.00363.x.

Willis, A.J., and Moslow, T.F., 1994a, Sedimentology and stratigraphy of tidal inlet reservoirs in the Triassic Halfway Formation, Wembley Field, Alberta: Bulletin of Canadian Petroleum Geology, v. 42, no. 2, p. 245–262.

Willis, A.J., and Moslow, T.F., 1994b, Stratigraphic setting of transgressive barrier-island reservoirs with an example from the Triassic Halfway Formation, Wembley Field, Alberta, Canada: American Association of Petroleum Geologists Bulletin, v. 78, no. 5, p. 775–791, doi: 10.1306/A25FE3B5-171B-11D7-8645000102C1865D.

Zaitlin, B.A., Dalrymple, R.W., and Boyd, R., 1994, The stratigraphic organization of incised-valley systems associated with relative sea-level change, *in* Dalrymple, R.W., Boyd, R., and Zaitlin, B.A. eds., Incised-Valley Systems: Origin and Sedimentary Sequences, Society of Economic Paleontologists and Mineralogists Special Publication, 51, p. 45–60.

Zhang, K., Douglas, B., and Leatherman, S., 2002, Do storms cause long term beach erosion along the U.S. east barrier coast? The Journal of Geology, v. 110, no. 4, p. 493–502.

Zhang, K., and Leatherman, S., 2011, Barrier island population along the U.S. Atlantic and Gulf Coasts: Journal of Coastal Research, v. 272, no. 2, p. 356–363, doi: 10.2112/JCOASTRES-D-10-00126.1.

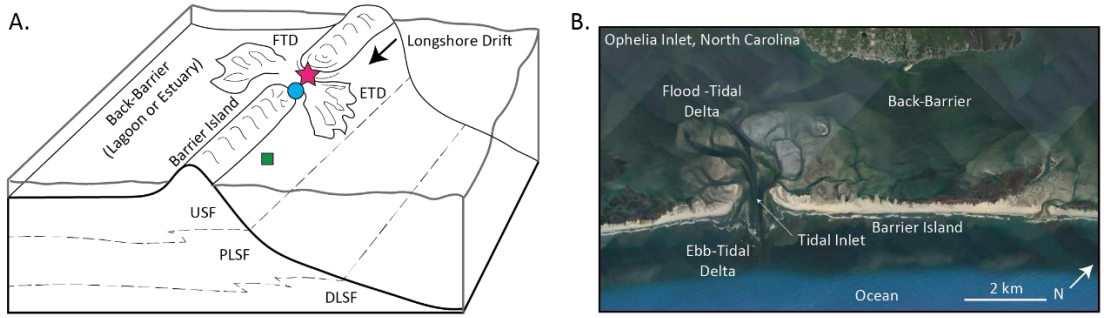

Figure 2.1. (A) Schematic, vertically-exaggerated block diagram and (B) Google Earth image showing the parts of the barrier island depositional system. Markers indicate the three architectural elements that the barrier island: barrier island shoreface (green square), barrier island tidal inlet (pink star), and barrier island tidal channels (blue circle). Abbreviations: FTD - flood-tidal delta; ETD - ebb-tidal delta; DLSF - distal lower shoreface; plsf - proximal lower shoreface; USF - upper shoreface.

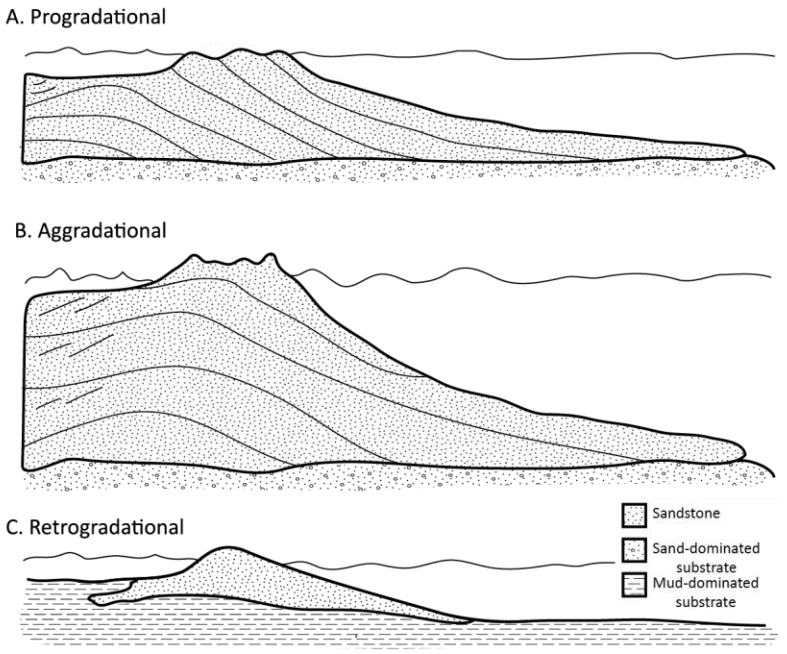

Figure 2.2. Schematic cross sections showing the three end-member types of modern barrier islands. (A) Progradational islands build seaward (Bernard et al., 1970). (B) Aggradational islands build vertically (Fisk, 1959; Morton, 1994). (C) Retrogradational islands move landward (Kraft and John, 1979). These sections are highly simplified, meant to show the overall difference in island geometry. Modified after Dickinson et al. (1972), Galloway and Hobday (1983), Moslow (1984), Galloway (1986), and Davis Jr. (1994).

Figure 2.3. (A) Regional map of the Kaiparowits Plateau of southern Utah. Outcrops of the Straight Cliffs Formation are shown in grey and the locations of previous studies focused on the John Henry Member are labelled. General proximal to distal facies relationships in the John Henry Member range from fluvial on the western margin to marine on the eastern margin, with tidal and paralic facies in between. Dashed lines show the region of barrier island (BI) deposition during the C-F intervals of the John Henry Member. (B) Location of the northern Kaiparowits Plateau geological map. (C) Stratigraphic column showing the age of the four members of the Straight Cliffs Formation. Coastal onlap curve for the northern Kaiparowits Plateau estimates the relative shifts in the shoreline position based on the stratigraphy at Buck Hollow and Main Canyon and down-dip shoreface pinch-outs (into offshore marine) where identified. Modified from Chentnik et al. (2015) and Mulhern and Johnson (2016). Abbreviations: CNTB, Central Nevada Thrust Belt; SFTB, Sevier fold-thrust belt; WIS, Western Interior Seaway; MTB, Maria Thrust Belt; Camp.-Campanian; SCF-Straight Cliffs Formation; MC - Main Canyon; BH - Buck Hollow; R-T – regressive-transgressive; BI-barrier island.

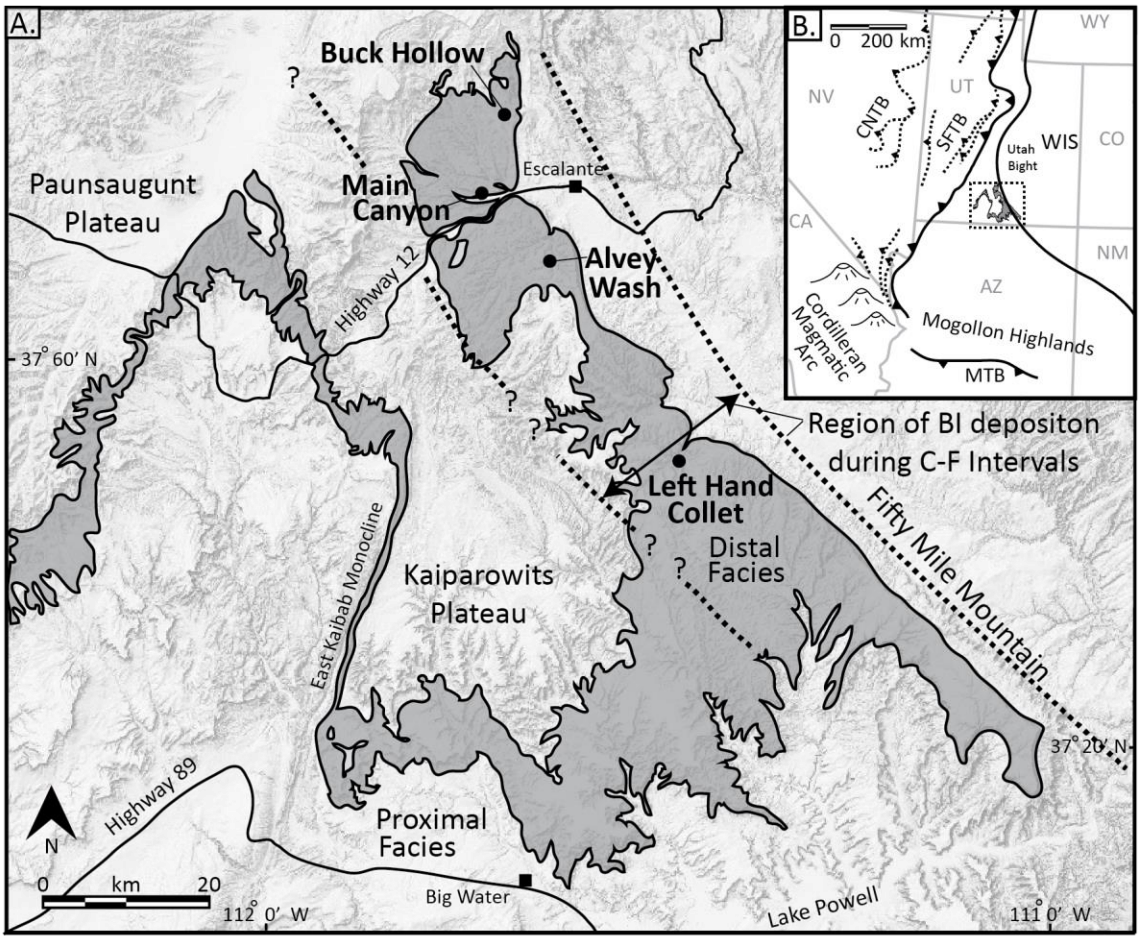
A.
Buck Hollow
Escalante
Main Canyon
Paunsaugunt Plateau
Alvey Wash
Highway 12
37° 60′ N
Region of BI depositon during C-F Intervals
Left Hand Collet
Distal Facies
Fifty Mile Mountain
East Kaibab Monocline
Kaiparowits Plateau
37° 20′ N
Highway 89
Proximal Facies
N
0 km 20
112° 0′ W
Big Water
Lake Powell
111° 0′ W
B.
0 200 km
WY
NV
UT
CO
CA
NM
AZ
CNTB
SFTB
WIS
Utah Bight
Cordilleran Magmatic Arc
Mogollon Highlands
MTB

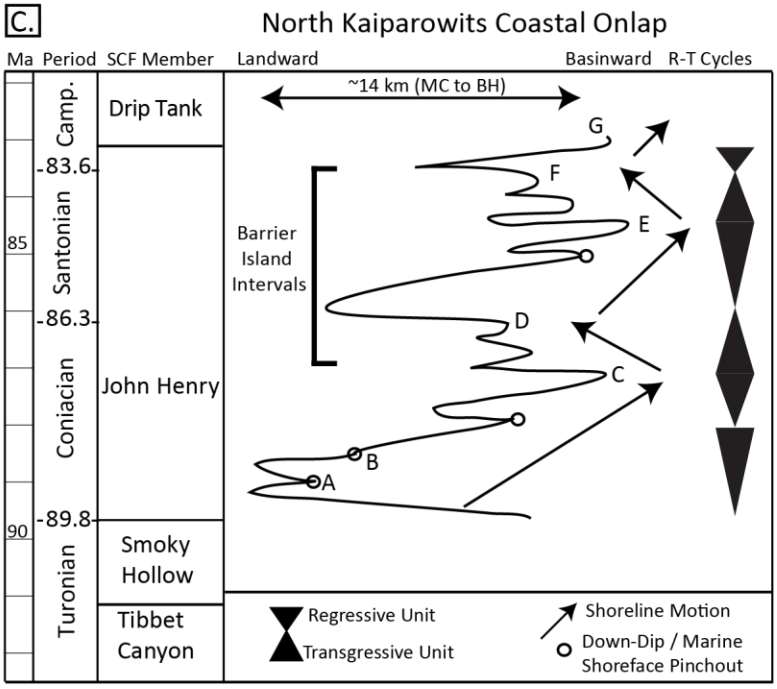
C.
North Kaiparowits Coastal Onlap
Ma
Period
SCF Member
Landward
Basinward
R-T Cycles
~14 km (MC to BH)
Camp.
Drip Tank
83.6
Santonian
85
Barrier Island Intervals
G
F
E
D
C
B
A
Coniacian
John Henry
86.3
89.8
90
Turonian
Smoky Hollow
Tibbet Canyon
Regressive Unit
Transgressive Unit
Shoreline Motion
Down-Dip / Marine Shoreface Pinchout

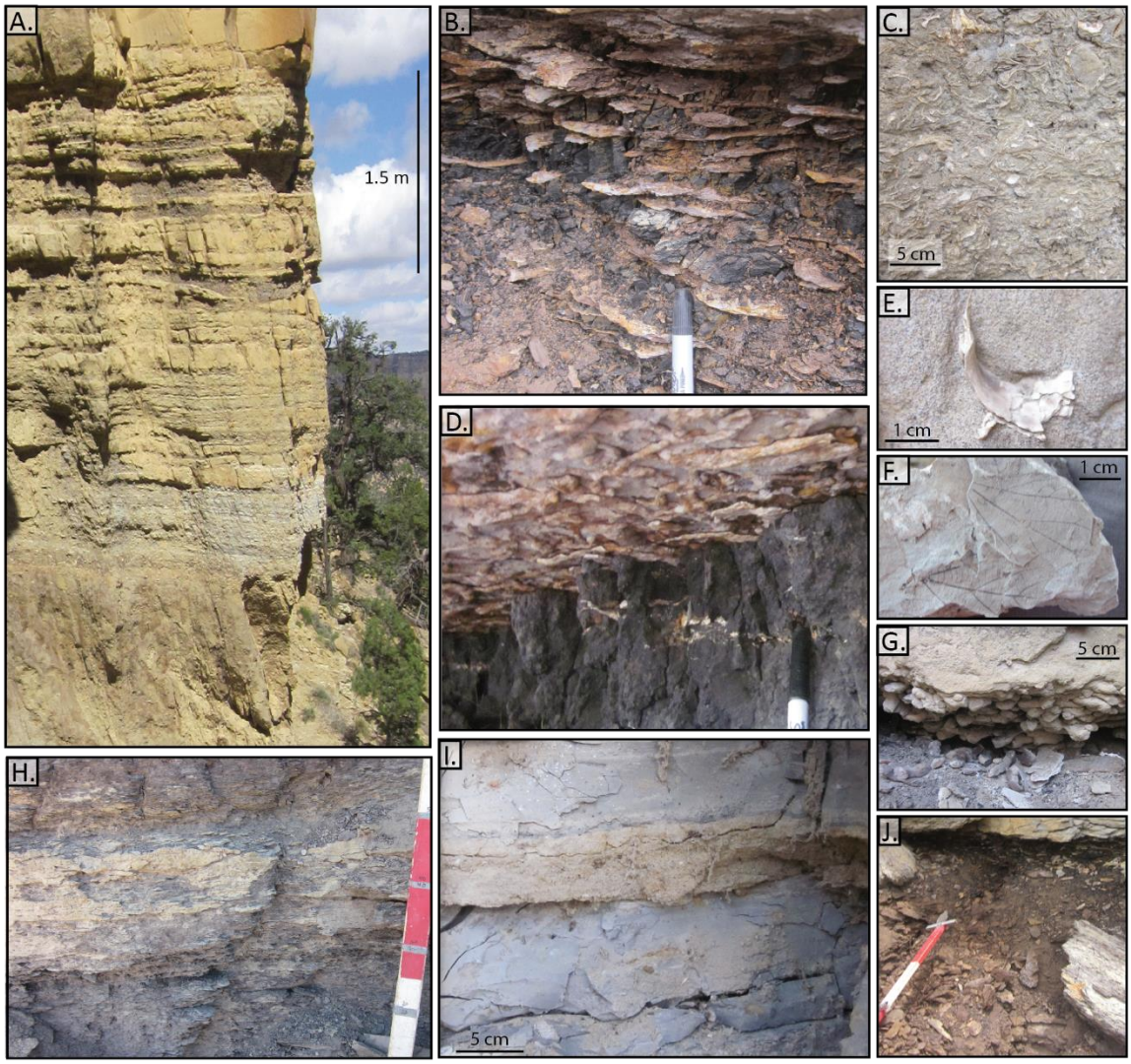

Figure 2.4. Facies Association 1: Back-Barrier Fill. (A) Outcrop photo of back-barrier fill with interbedded with sandstone lenses. (B) Coal reworked with flaser- to lenticular-bedded fine-grained sand lenses. (C) Shell fragments in a sand matrix. (D) *Thalassinoides* burrows on the base of a fine-grained sandstone bed overlying coal deposits. (E) Oyster shell fragment. (F) Leaf impressions. (G) *Thalassinoides* within coal at the base of a medium-grained sandstone. (H) Carbonaceous mudstone with fine- to medium-grained sandstone lenses. (I) Medium-grained sandstone bed within gray mudstone with abundant terrigenous material and leaf impressions. (J) Interval of brown carbonaceous mudstone grading vertically into coal.

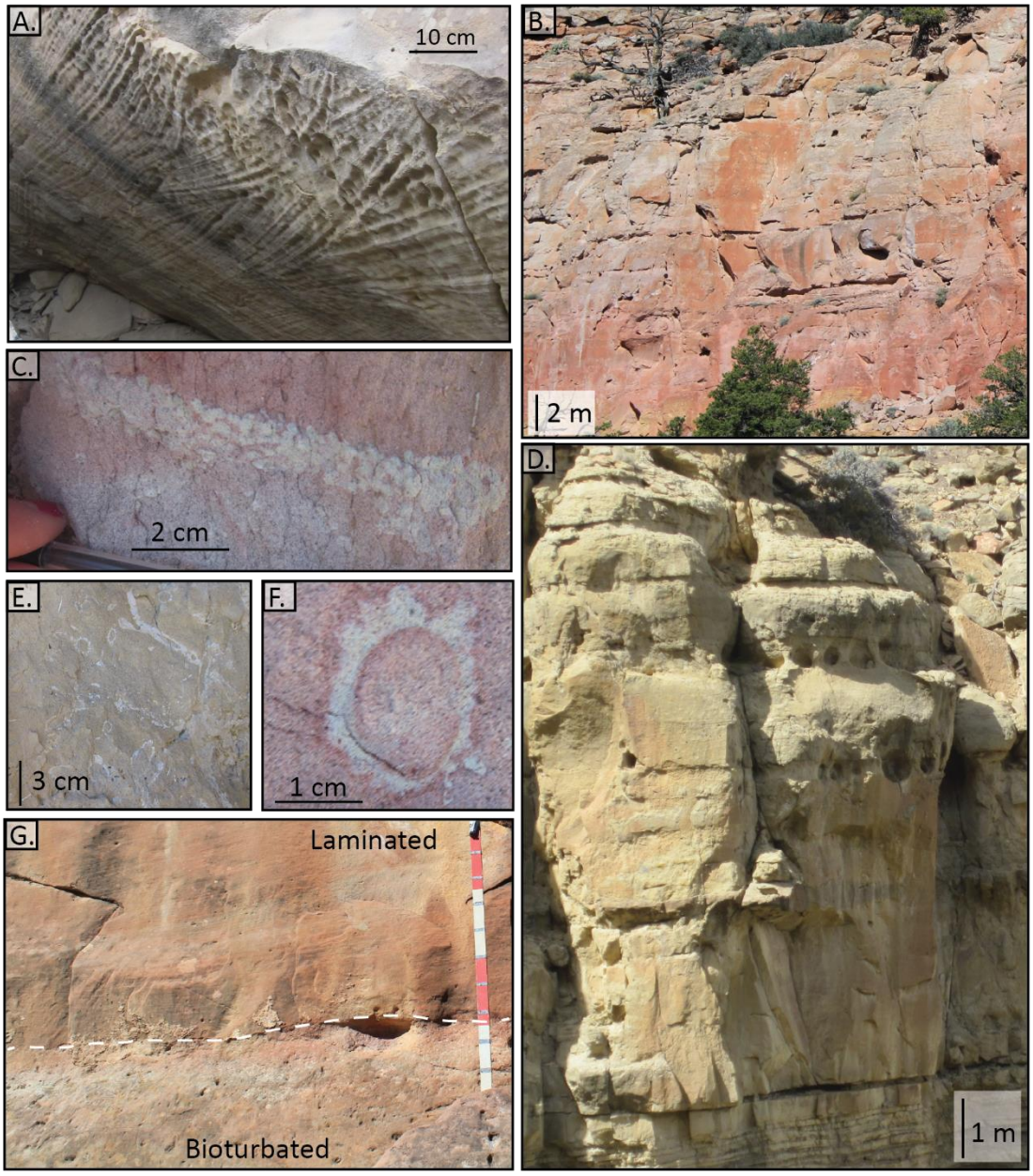

Figure 2.5. Facies Association 2: Lower and Upper Shoreface. (A) Hummocky and swaley cross-stratification in a down-dropped block. (B) Blocky outcrops with alternating layers of lamination and bioturbation. (C) *Ophiomorpha nodosa*. (D) Blocky, fine-grained sandstone with tabular laterally continuous beds. (E) Biotubated bed showing *Ophiomorpha nodosa*. (F) Cross-section through *Ophiomorpha nodosa.* (G) Contact between heavily bioturbated bed and overlying laminated bed.

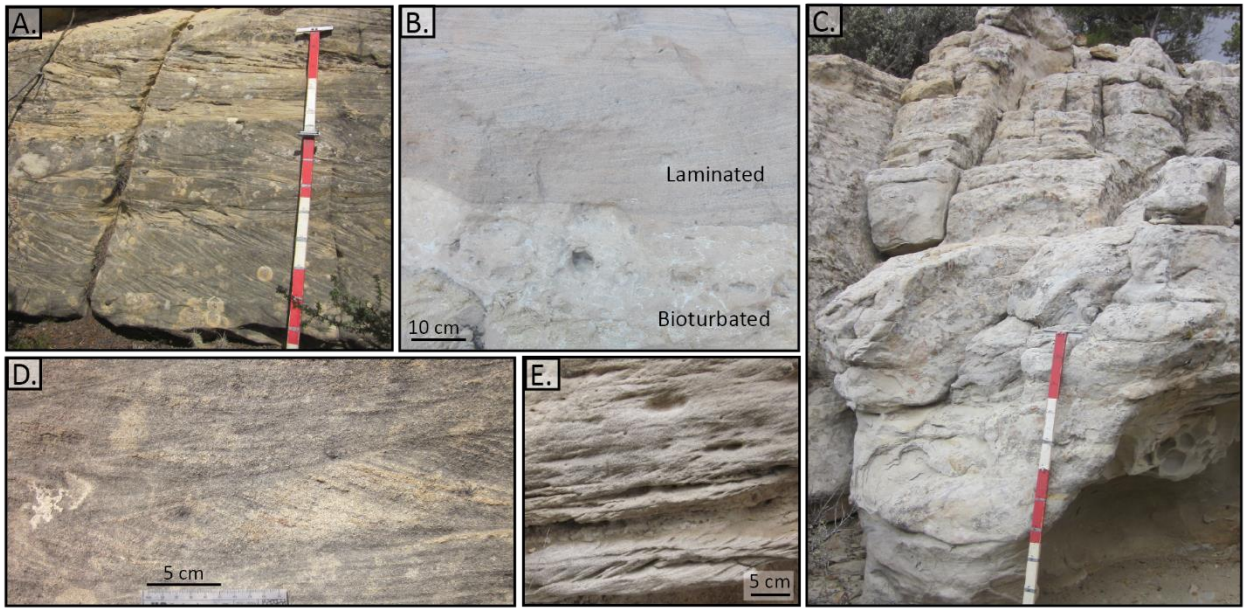

Figure 2.6. Facies Association 3: High-Energy Upper Shoreface. (A) Sandstone beds showing stacked accretion sets. (B) Medium-grained sandstone with clear accretion sets cutting into heavily bioturbated strata with clear *Ophiomorpha*. (C) Outcrop photo showing the block nature of tidal inlet barrier island deposits. (D) Sandstone with unidirectional accretion sets. (E) Ripple laminated sandstone.

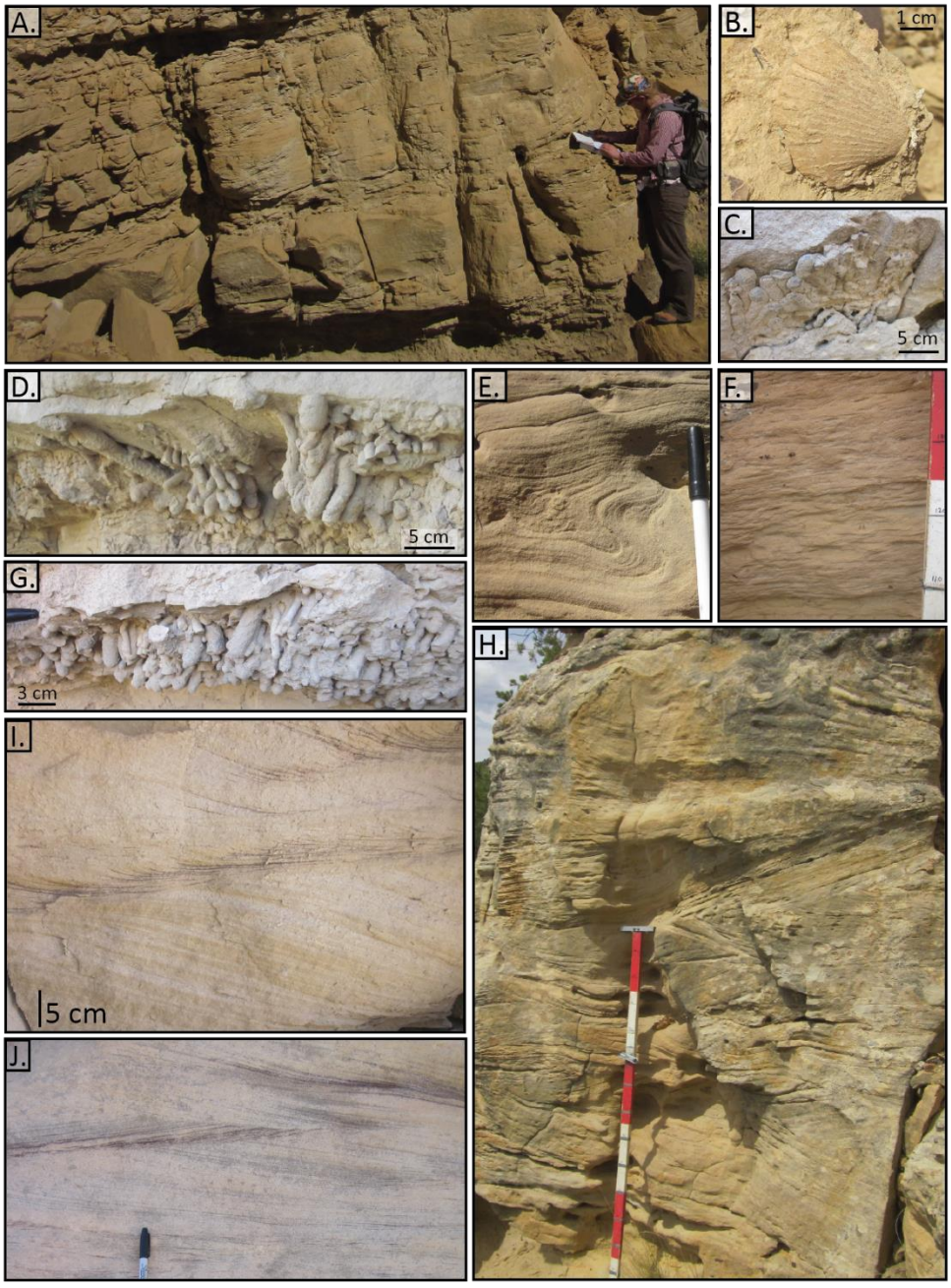

Figure 2.7. Facies Association 4: Tidal Channels. (A) Outcrop with an incisional base. (B) Shell impression. (C) *Teredolites*. (D) *Gastrocheanolites*. (E) Convolute bedding. (F) Ripple laminated bed. (G) *Gastrocheanolites*. (H) Outcrop photo showing the cross-cutting and convolute bedding. (I) Double mud drapes. (J) Bidirectional accretion sets with double mud drapes.

Figure 2.8. Measured sections of the (A) barrier island shoreface, (B) barrier island tidal inlet, and (C) barrier island tidal channel architectural elements, with representative paleocurrent measurement data from Buck Hollow and Main Canyon.

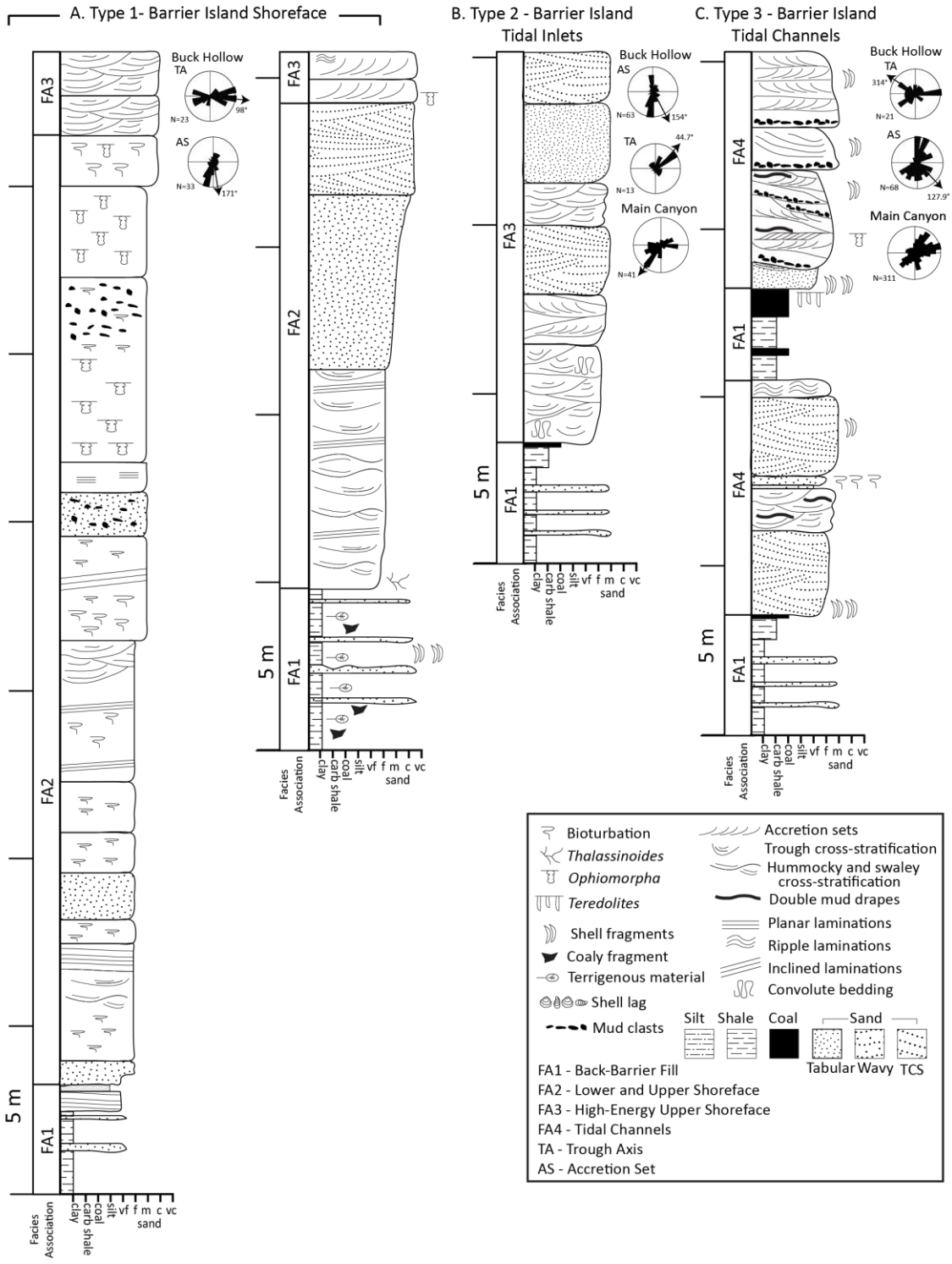
A. Type 1- Barrier Island Shoreface
B. Type 2 - Barrier Island Tidal Inlets
C. Type 3 - Barrier Island Tidal Channels
Buck Hollow
TA
AS
Main Canyon
FA1
FA2
FA3
FA4
5 m
Facies Association
clay
carb shale
coal
silt
vf f m c vc
sand
Bioturbation
Thalassinoides
Ophiomorpha
Teredolites
Shell fragments
Coaly fragment
Terrigenous material
Shell lag
Mud clasts
Accretion sets
Trough cross-stratification
Hummocky and swaley cross-stratification
Double mud drapes
Planar laminations
Ripple laminations
Inclined laminations
Convolute bedding
Silt
Shale
Coal
Sand
Tabular
Wavy
TCS
FA1 - Back-Barrier Fill
FA2 - Lower and Upper Shoreface
FA3 - High-Energy Upper Shoreface
FA4 - Tidal Channels
TA - Trough Axis
AS - Accretion Set

Figure 2.9. Outcrop photos showing (A) barrier island shoreface, (B) barrier island shoreface with alternating bioturbated and laminated beds, (C) barrier island tidal inlet, and (D) barrier island tidal channels. Facies associations (Table 2.1) are labeled in each photo include back-barrier fill (FA1), shoreface (FA2), high-energy upper shoreface (FA3), and tidal channels (FA4). Note the two scale bars showing the perspective in the barrier island tidal channel photo (D).

A. Type 1- Barrier Island Shoreface

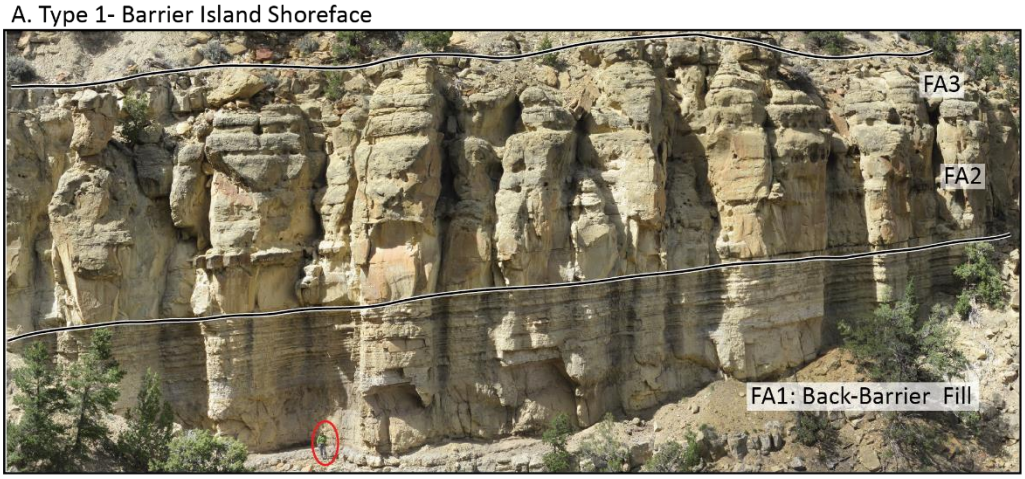

B. Type 1- Barrier Island Shoreface with Bioturbation

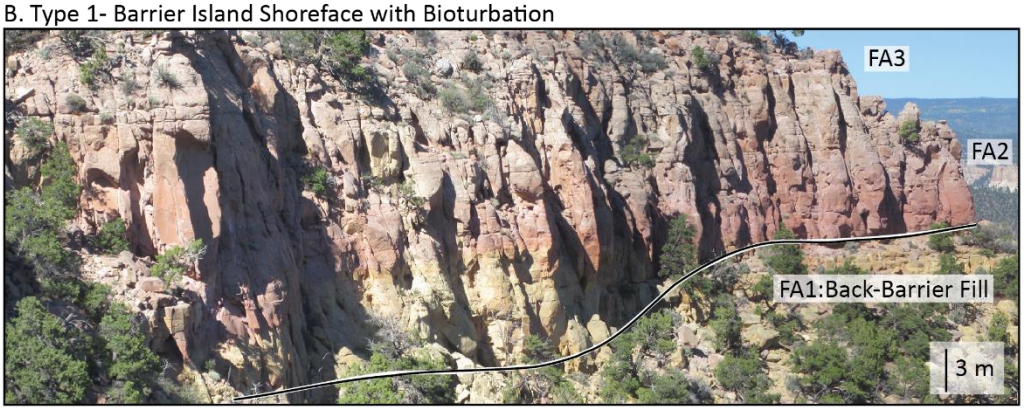

C. Type 2- Barrier Island Tidal Inlet

D. Type 3- Barrier Island Tidal Channels

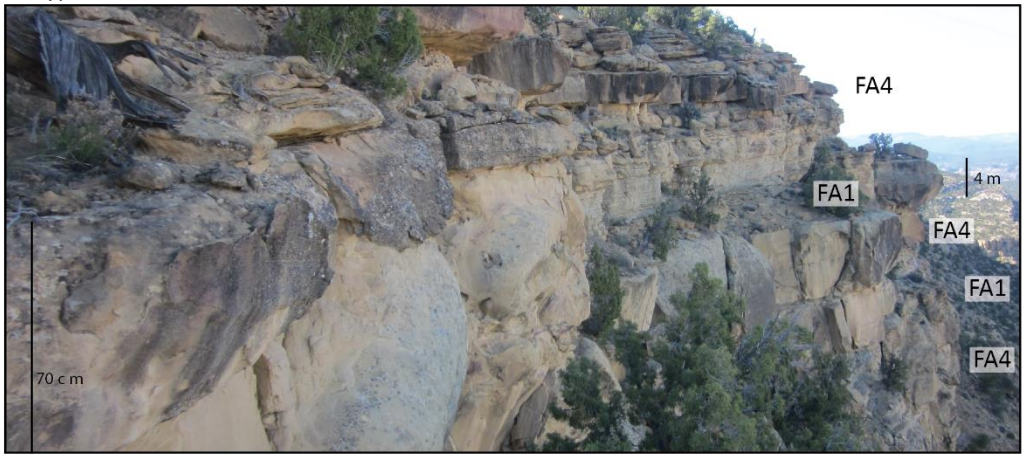

Figure 2.10. Summary of the three barrier island architectural elements showing the facies variation and one set of possible along-strike and dip-direction configurations. Abbreviations: BI SF – barrier island shoreface; BI TI – barrier island tidal inlet; BI TC – barrier island tidal channel.

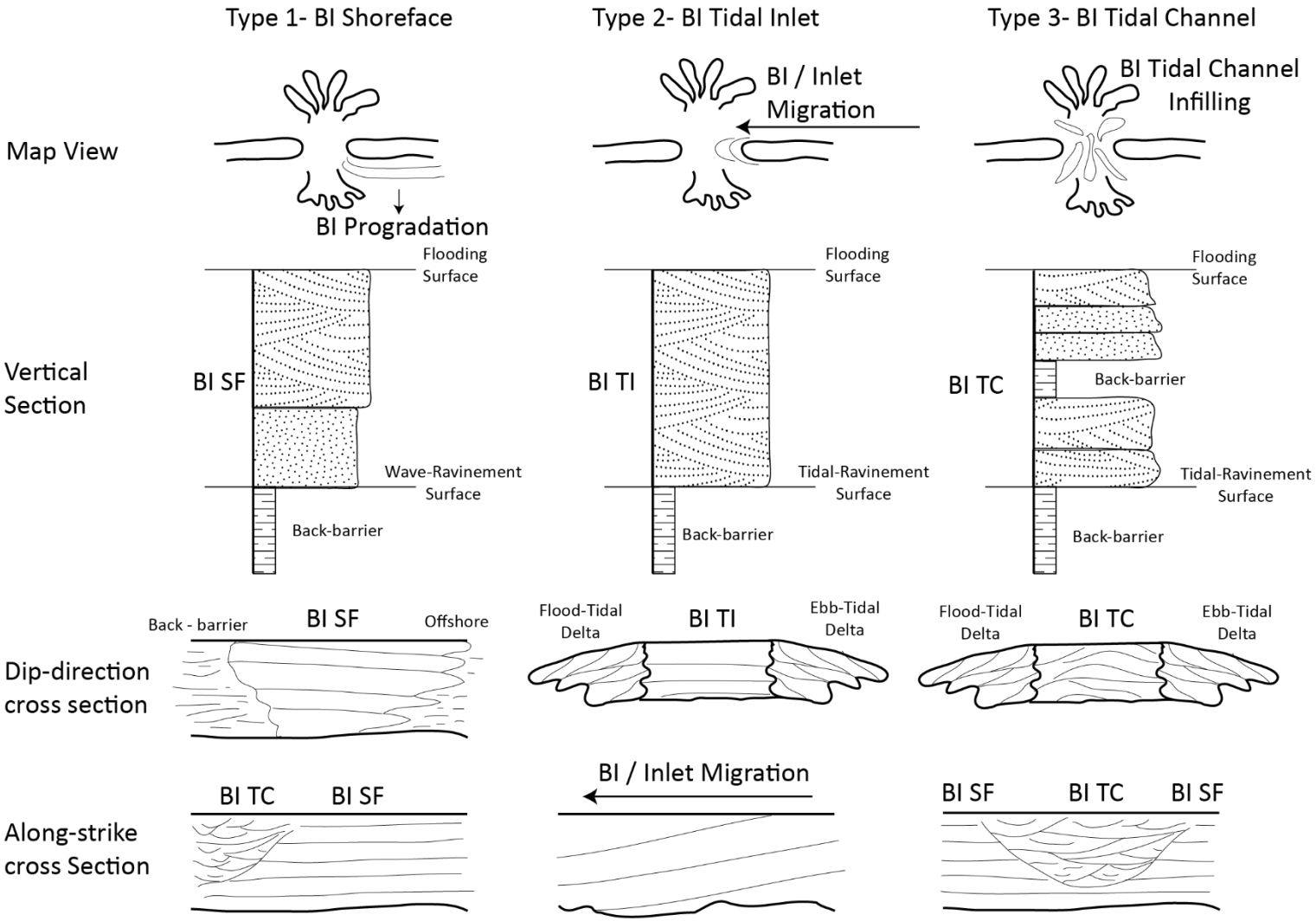
Type 1- BI Shoreface
Type 2- BI Tidal Inlet
Type 3- BI Tidal Channel
Map View
BI / Inlet Migration
BI Tidal Channel Infilling
BI Progradation
Vertical Section
Flooding Surface
BI SF
Wave-Ravinement Surface
Back-barrier
BI TI
Tidal-Ravinement Surface
BI TC
Dip-direction cross section
Back - barrier
Offshore
Flood-Tidal Delta
Ebb-Tidal Delta
Along-strike cross Section
BI / Inlet Migration

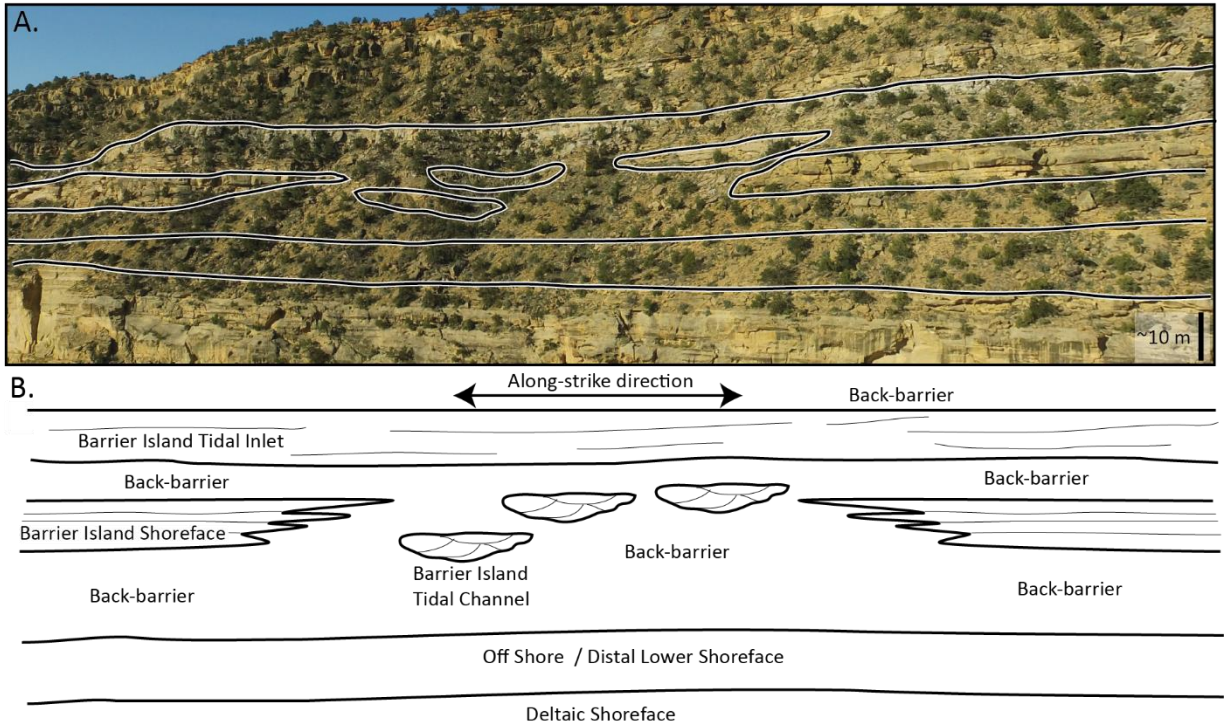

Figure 2.11. (A) Depositional strike orientated outcrop photo from Alvey Wash and schematic (B) interpretation showing a barrier island shoreface grading laterally into tidal channel deposits. This composite barrier island, composed of both barrier island shoreface and barrier island tidal channel elements, is overlain by an interval of back-barrier fill followed by a barrier island tidal inlet, which extends across the entire outcrop.

Figure 2.12. (A) Outcrop panel from Alvey Wash oriented oblique to depositional strike showing the lateral extent of a barrier island tidal inlet deposit (BI IT; red). Barrier island shoreface deposits (BI SF; blue), back-barrier (BB) fill, back-barrier tidal channels (BB TC), deltaic shoreface (DSF; green), and offshore (OS; black) deposits are also marked. Note scale bar changes with perspective as the photos were take obliquely. The entire exposure is roughly 1.8 km long. The vertical relief in the foreground is 190 m the vertical relief of the far left (north) side is 250 m. (B) Dip oriented outcrop panel from Alvey Wash showing a barrier island tidal inlet (BI TI; red) with sharp upper and lower contacts. A barrier island shoreface (BI SF; blue) pinches out in the middle of the outcrop. Towards the top there is a laterally continuous barrier island shoreface (BI SF; blue) overlain by another barrier island tidal inlet (BI TI; red). Back-barrier (BB) and back-barrier tidal channels (BB TC) are also marked. The exposure shown has ~200 m elevation change and is 0.6 km across.

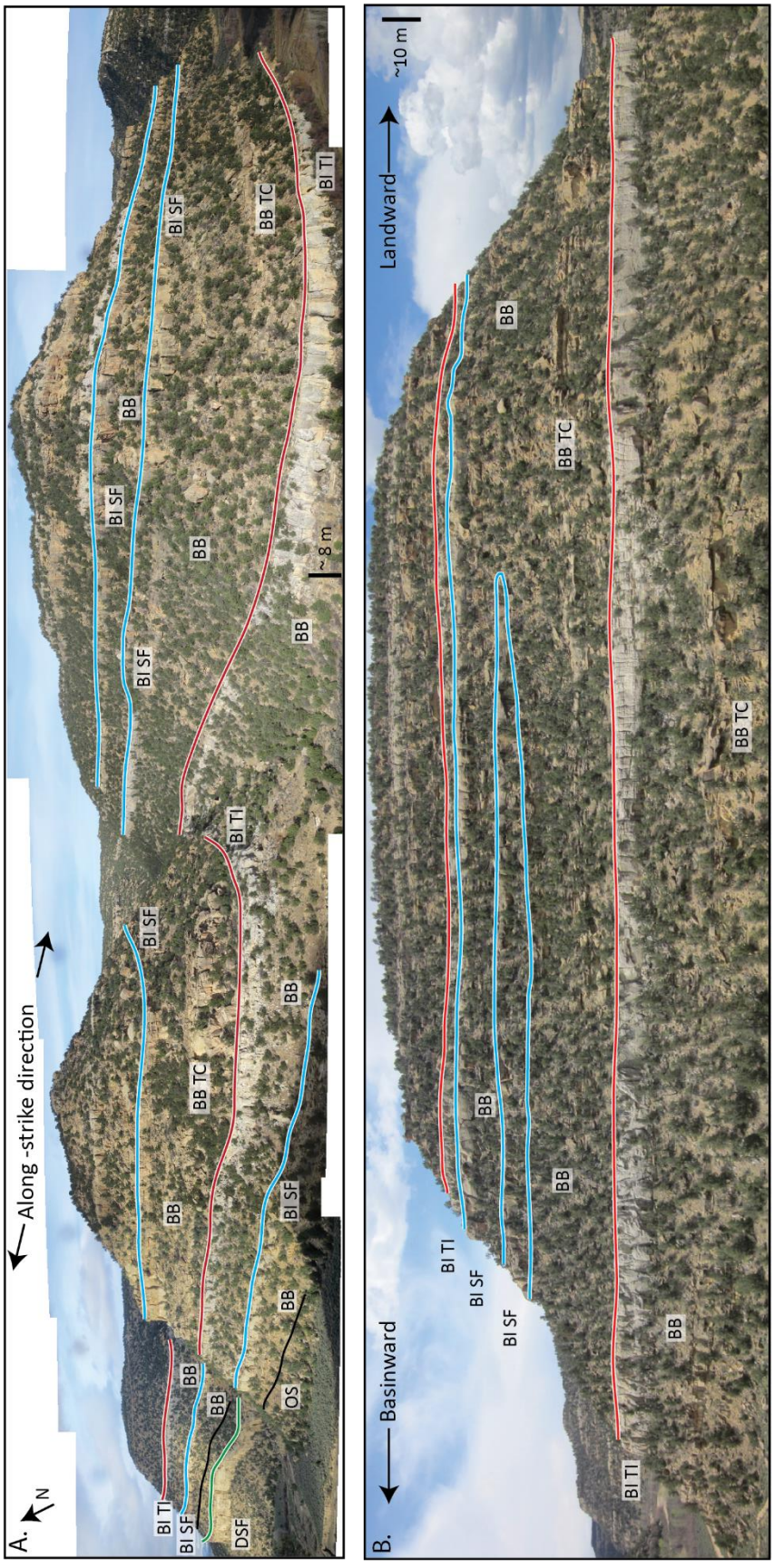
A.
N
Along -strike direction
BI TI
BI SF
DSF
BB
BB
BB TC
BI SF
BI TI
BB
BB
OS
BB
BI SF
BI SF
BB
BI SF
BB
BB TC
BI TI
~8 m
B.
Basinward
Landward
~10 m
BI TI
BI SF
BI SF
BB
BB
BB
BB TC
BB TC
BI TI

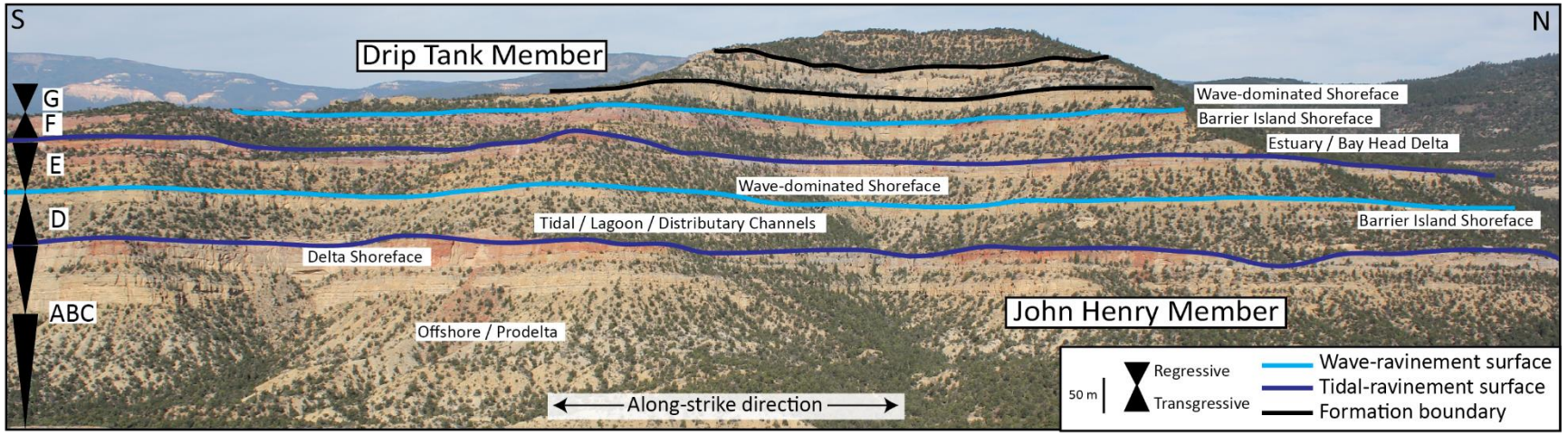

Figure 2.13. Interpreted aerial photography of an exposure parallel to depositional strike from Buck Hollow showing the relationship of barrier island shoreface deposits relative to other paralic environments. Barrier islands cap the D and F transgressive intervals. Outcrop panel is roughly 1.5 km wide in the strike direction (south to north), has 0.7 km of depth perspective (east to west direction) and shows ~400 m of elevation change.

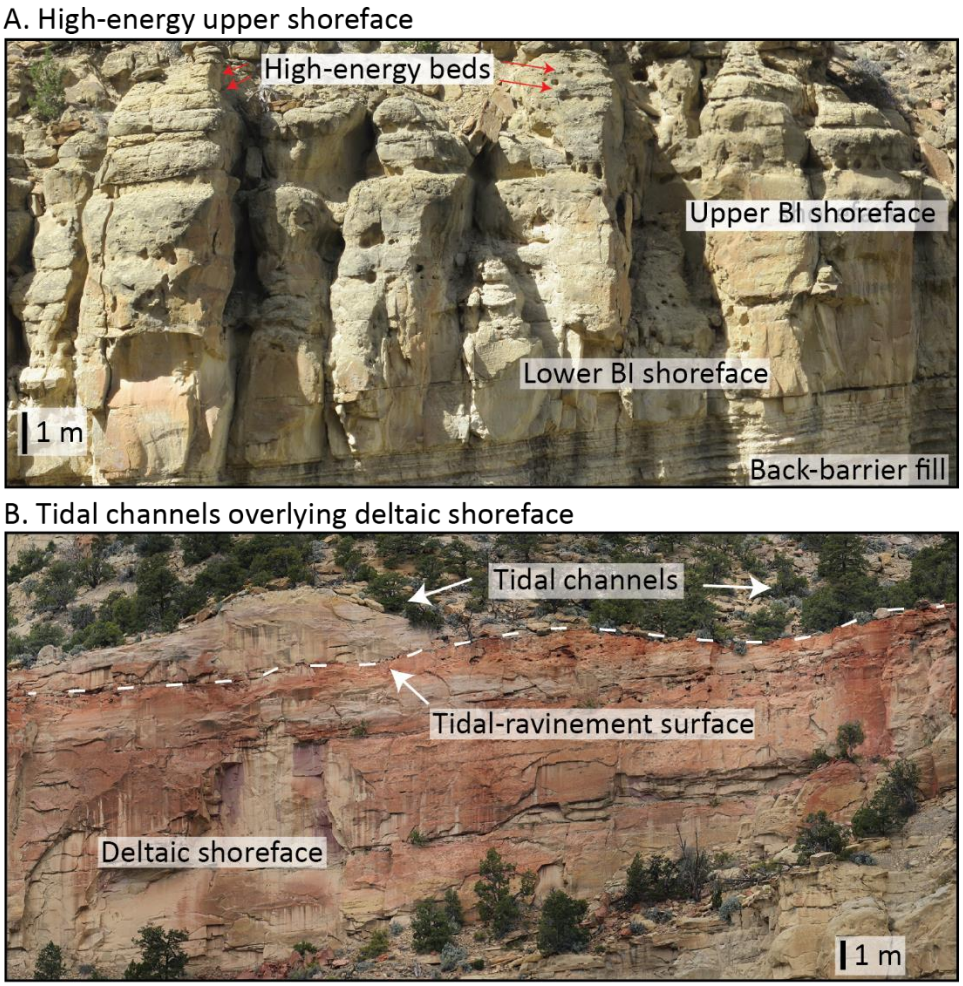

Figure 2.14. Comparison of (A) high-energy upper shoreface and (B) back-barrier tidal channels truncating an upper shoreface separated by a tidal-ravinement surface.

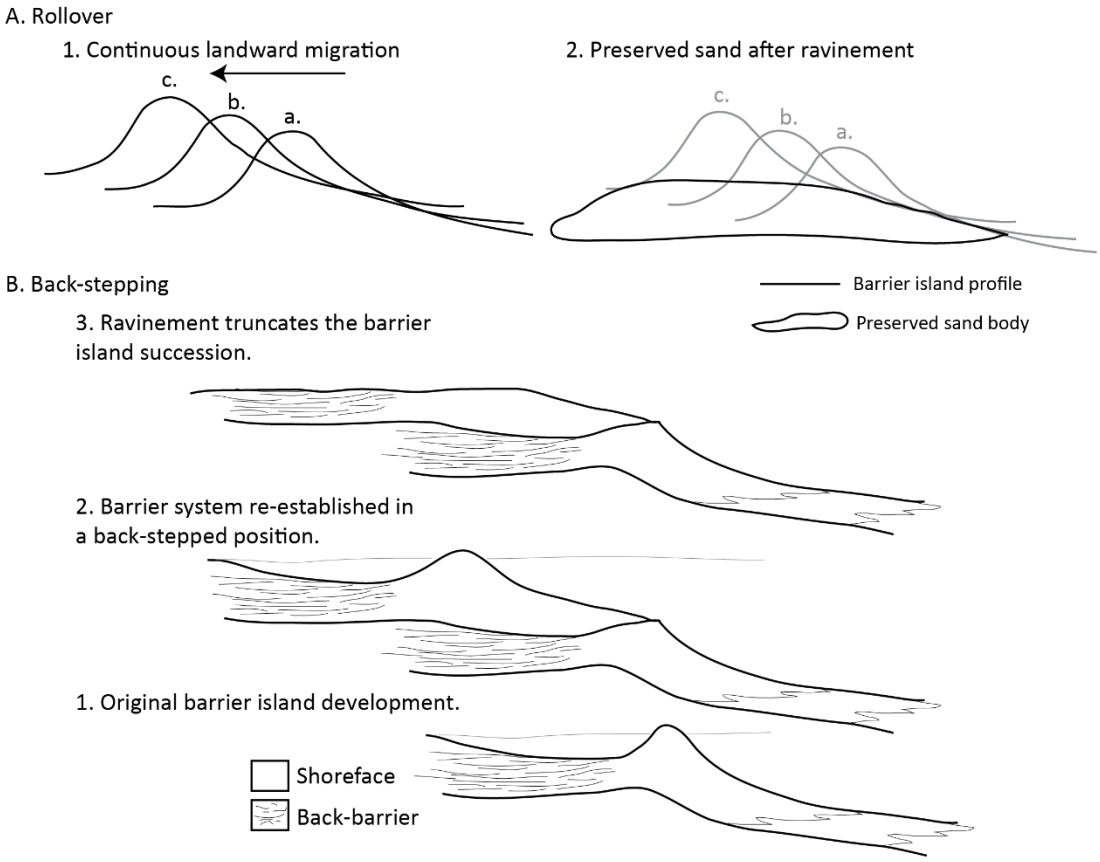

Figure 2.15. Schematic models for barrier island motion through rollover (A) and back-stepping (B) which shows a barrier island system back-stepping landward, re-establishing, and being truncated through ravinement.

Table 2.1: Facies Associations

	Description	Trace / Body Fossils	Paleocurrent Measurements	Interpretation
FA1- Carbonaceous Mudstones, Fine-Grained Sandstones, and Coals (Fig. 4)	Gray to brown, flaser to wavy bedded carbonaceous mudstones which grade vertically into coals. Mudstones are dissected by lens-shaped, fine- and medium-grained sandstone (2-30 cm thick), which pinch out laterally over 0.5-2.0 m.	Abundant plant material, oyster shell fragments *Thalassinoides* BI = 0-2, 6		Back-Barrier Fill
FA2 - Fine- to Medium-Grained, Tabular Sandstone (Fig. 5)	Sandstone beds 0.1-1 m thick containing hummocky and swaley cross-stratification, low-angle trough cross-stratification, and planar bedding. Internal character of these beds alternates between laminated and/or homogenous and completely bioturbated.	Sporadic shell fragments, *Ophiomorpha nodosa* BI =0-2, 6		Lower and Upper Shoreface
FA3- Medium-Grained, Cross-Stratified Sandstone (Fig. 6)	Medium-grained sandstone beds with abundant, bi-directional and uni-directional trough-cross stratification, accretion sets, and ripple laminations.	Sporadic shell fragments BI=0	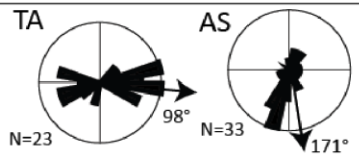	High-Energy Upper Shoreface
FA4 - Lens-Forming, Fine-Grained Sandstone (Fig. 7)	Lens-shaped bedforms (0.5-2.0 m thick) of fine- and medium-grained sandstone with erosive bases containing trough cross-stratification, ripple laminations, accretion sets, bi-directional cross-stratification, convolute bedding, double mud drapes, and mudclasts. Basal erosive surfaces have dense bioturbation (BI=6).	Shell impressions, shell fragments, *Thalassinoides*, *Gastrocheanolites* BI=0-2, 6	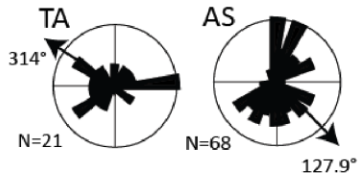	Tidal Channels

Bioturbation Index (BI) follows the scheme of Taylor and Goldring (1993).

3. COMPARING THE DIMENSIONS OF MODERN AND ANCIENT BARRIER ISLANDS TO UNDERSTAND CONTROLS ON PRESERVATION

Abstract

Modern barrier islands are commonly used as analogs for ancient systems, including predicting dimensions and characteristics of the rock record. However, ancient deposits are complicated by various geologic processes related to long-term motion and preservation. This study compares modern and ancient barrier island dimensions to investigate their scaling relationships and elucidate the challenges involved with analog comparisons. New database analysis compares the thickness (vertical), length (strike-direction), and width (dip-direction) of modern barrier islands (n=274) mapped from aerial imagery, to ancient barrier island dimensions (n=123) gathered from the literature. Ancient barrier islands are systematically 2-5x longer (p50 modern = 10.7 km; p50 ancient = 20.0 km), and 6-15x wider (p50 modern = 1.2 km; p50 ancient = 7.3 km) than modern islands. The size differences reflect vertical amalgamation, ancient barrier island growth by lateral accretion, and progradation. These geologic processes construct and preserve much larger ancient deposits, making modern analog selection difficult. Because ancient barrier islands are preserved at geologic time-scales, the stacking of multiple barrier island parasequences increases the thickness of amalgamated ancient examples (p50=45.72) relative to the modern (p50= 11). When amalgamated examples are

excluded, ancient length and width values remain larger than modern values, suggesting that barrier island deposits incorporate both shore-parallel and shore-perpendicular motion at geologic time scales. Both modern and ancient (single parasequence) barrier islands systems display length versus width scaling relationships with differing trends. This suggests that paleomorphodynamic scaling relationships could be developed through additional research and improved understanding of barrier island preservation. The measurement and comparison difficulties encountered in this initial comparison workflow suggest that detailed, subenvironment (e.g., upper shoreface) assessments are required to better constrain the processes linking modern and ancient barrier islands to enable the development of paleomorphodynamic relationships.

Introduction

Barrier islands are elongate coastal sandbodies which make up 10% of the world's coastlines (Hoyt, 1967; Oertel, 1985; Stutz and Pilkey, 2011). Morphodynamic aspects of modern barrier islands are thoroughly studied, largely due to their relevance to growing coastal populations and infrastructure (Fisher and Dolan, 1977; Short, 1999; Dronkers, 2005; Dyke, 2007; Anthony, 2009; Davis Jr., 2013; McBride et al., 2013). Well-studied examples from the U.S. Atlantic and Gulf coasts as well as the Dutch Wadden Sea create the foundation for existing barrier island facies models (Davies, 1978; Barwis and Hayes, 1979; Reinson, 1979; McCubbin, 1982), without extensive analysis of process and preservation differences between the modern and the ancient. Although detailed comparisons between modern sedimentary processes and preserved stratigraphy have been used to understand and quantify how modern sediments are translated into the rock

record in some environments (e.g., Bhattacharya and Tye, 2004; Lunt et al., 2013), these comparisons have not been investigated for barrier island systems.

Modern barrier islands are categorized based on their internal character as it relates to motion and growth, i.e., progradational (basinward motion), retrogradational (landward motion), and/or aggradational (vertical motion; Fig. 3.1; Galloway and Hobday, 1983; Galloway, 1986; Davis Jr., 1994a). These classifications are oversimplified because modern barrier islands move in the shore-parallel direction, as well as moving perpendicular to the shoreline (Fig. 3.2). Additionally, the localized island motion is often distinct from the broader motion of the shoreline. For example, modern barrier islands from the Wadden Sea (van Straaten, 1965; Johannessen et al., 2008; Johannessen et al., 2010) and Gulf of Mexico (Bernard et al., 1962; Morton, 1994) show progradation and aggradation during sea level rise due to local controlling factors such as shelf slope and sediment supply.

Despite these complexities, the local barrier island motion regime (progradation, retrogradation, and aggradation) became the foundation for existing barrier island facies models (Reinson, 1979, 1992; Reinson et al., 1988) and ancient interpretations, without acknowledging the time scale difference between the modern and the ancient. In the geologic record, motion terms are applied to broad stacking patterns as well as internal facies architecture. For example, bedforms and bed sets can prograde while an overall succession has a retrogradational shoreline trend and stacking pattern (Emery and Myers, 1996; Coe et al., 2003). This duality in terminology, combined with the complexities of barrier island motion, adds confusion to comparisons between modern and ancient barrier islands.

Understanding the processes controlling sand distribution in modern and ancient barrier island systems is the first step toward developing quantitative ways to scale and predict the dimensions of barrier island systems for morphodynamic modeling and subsurface predictions. Paleomorphodynamics is the broad term for the field of quantitative sedimentology that uses equations and empirical relationships to link and scale modern and ancient depositional systems (Syvitski and Milliman, 2007; Sømme et al., 2009; Blum et al., 2013). Although these relationships have been developed for fluvial (Mohrig et al., 2000; Parker, 2006; Hajek and Wolinsky, 2012; Milliken et al., 2012), deltaic (Edmonds and Slingerland, 2007; Jerolmack and Swenson, 2007), and deepwater (Pirmez and Imran, 2003; Covault et al., 2012) settings, parallel research in shallow marine, including barrier island, settings lags behind (cf. Hudock et al., 2014).

For barrier island systems, dimensional measurements, and the workflow needed to conduct them, are required to assess the feasibility of modern to ancient comparisons before paleomorphodynamic relationships can be generated. The goal of this paper is to provide a first order comparison of modern and ancient barrier island systems, using two new databases. Specifically, we compare the length, width, and thickness of modern and ancient barrier islands. This approach highlights some of the challenges of using modern barrier island measurement data, because truly analogous architectures are not necessarily preserved in the rock record due to processes like ravinement, reworking, and stacking through time. Inherent measurement inconsistencies and terminology problems are also revealed. Although complicated, these results create a starting point for future barrier island paleomorphodynamic analysis.

Methods

Database Development

Parallel databases that detail modern and ancient barrier island dimensions were developed for comparative analysis. Planform dimensions of modern barrier islands (n=274) were mapped using Google Earth aerial imagery and combined with measured thickness values from the literature (n=45). Barrier islands (visibly separated by water on all sides) and spits (partially attached; Oertel, 1985) were mapped by tracing each individual object at the water line along roughly 29,000 km of global coastlines (Fig. 3.3a). The spatial data were combined with thickness values gathered from the literature and measured from core, seismic, and ground penetrating radar studies of Holocene deposits as described below (e.g., Davis Jr., 1994b; Salzmann et al., 2013; Fruergaard et al., 2015).

Ancient barrier island dimensions were collected from an extensive literature review (n= 123 publications; Fig. 3.3b; Table 3.1). The database includes data from studies that use the term "barrier," or that suggest the preservation of barrier island deposits (Heward, 1981; Rawn-Schatzinger and Schatzinger, 1993). To establish internal consistency, the depositional environment of each example was assessed and reclassified as needed (Table 3.1). In straightforward examples, the extent of barrier island deposits was measured or recorded directly from the publication (e.g., Bridges, 1976; Franks, 1980). For more ambiguous examples, however, the sedimentology and geologic context was considered in detail (e.g., Berg, 1976; Guscott et al., 2003). Deposits were interpreted as barrier islands if the preserved shoreface was directly associated with estuarine, lagoon (Davies, 1978), or back barrier deposits as per widely-used definitions

(Oertel, 1985; Otvos, 2012).

Of the 123 total ancient examples documented, 83 were determined to be barrier island deposits (Table 3.1). Other studies were interpreted as back barriers (n=1), tidal inlets (n=3), tidal bars (n=2), spits (n=3), strand plains (n=3), and delta fronts (n=2), or were designated as uncertain (n=4). Duplicate studies of the same strata and locations (n=9) were included in the database, but only one value for each unique island deposit was used in this analysis. Barrier islands associated with deltas (n=13) are not included in this analysis because the proximity to deltaic processes likely influences the growth, shape, and preservation statistics of this subset of barrier island systems (Hoyt, 1969; Penland et al., 1988; Penland and Suter, 1989; Van Maren, 2005).

Measurements from ancient examples were estimated using scaled figures (e.g., measured sections and maps), or pulled from the text of each publication (following the methods of Reynolds, 1999). Key dimensions (length, width, and thickness) available from each study vary: the majority of examples (56%) have all spatial dimensions measured, 24% have thickness and width, and 14% have only thickness (Fig. 3.4). Image and source data, such as figure maps or cross-sections are stored within the database, as are key contextual metadata, including age, location, and nomenclature used to describe the deposits. Each study was given a confidence designation (1-high to 3-low), which indicates the quality of the available data and the confidence in the measurements, high (1) indicates clear and well-supported data, whereas low (3) indicates poorly-supported data or vague figures (Table 3.1).

A key challenge in this approach is that modern examples consist of a single island, while ancient examples can have multiple barrier island parasequences preserved

either stacked vertically or echelon (Fig. 3.5). Here the term parasequence is used to describe a single preserved barrier island shoreface succession, indicating the preservation of a distinct barrier island (cf. Van Wagoner et al., 1988; Arnott, 1995; Catuneanu et al., 2010). To investigate the importance of vertical amalgamation and barrier island stacking, examples with multiple barrier island parasequences were designated as amalgamated if the parasequences are in vertical contact with one another (Fig. 3.5a). When possible, the dimensions of individual island deposits within these amalgamated deposits were measured. If the individual parasequences were not clearly separated or measureable, the entire amalgamated succession was measured. Ancient examples are considered not amalgamated (Fig. 3.5b) if they contain only a single sequence, or if they contain multiple parasequences, which are not in contact with one another.

Measurement Comparisons

In developing this database, modern and ancient barrier islands were measured using the most straightforward methods and the most readily available data. However, the measurements made in the two realms are not directly analogous. Subaerial exposure of modern barrier islands is most conducive to measuring through global imagery (e.g., Google Earth). In contrast, the entire shoreface, rather than just the subaerial foreshore and dune, is most conducive to measuring ancient examples (Fig. 3.6), because the shoreface is commonly preserved, forms large outcrops (Allen and Johnson, 2011; Kieft et al., 2011), and creates distinct well-log patterns (Tizzard and Lerbekmo, 1975; Willis and Moslow, 1994). Our procedures for collecting database measurements are outlined

here (Fig. 3.6), the limitations and implications of which are explored in the discussion.

Modern lengths were measured along each island centerline in the shore-parallel direction from one tidal inlet to the next (Fig. 3.6a). Ancient lengths were measured from one end of the preserved shoreface to the other in the strike direction, potentially including or crossing the tidal inlet (Fig. 3.7). If a range of values was evident from the text or figures of a particular example, the range was recorded in the database and a representative value is used for analysis. Examples with tidal channel or tidal inlet deposits associated with the barrier island were included because these facies are often contiguous with the barrier island shoreface facies form part preserved barrier islands successions (Davies and Ethridge, 1971; Davies, 1978; Flores, 1978; Self et al., 1986).

Modern widths were measured in the shore-perpendicular direction in three locations along the length of the island, and averaged. These measurements document the subaerial extent of the island for a single snapshot in time, thus recording the topset width (Fig. 3.6b). In ancient examples, the extent of the preserved shoreface in the dip-direction was measured, documenting both topset and foreset widths (Fig. 3.6b). These measurements reflect the width of the whole island, rather than just the subaerial portion. It is not feasible to measure the subaerial potion of barrier island deposits because, if preserved, the foreshore requires detailed facies analysis to identify and is not often highlighted in literature examples. Inversely, subaqueous width measurements for the modern are not feasible at a global scale because they are inhibited by the scarcity of available data and the difficulty in defining, constraining, and documenting the back-barrier and shoreface boundary.

Modern thicknesses were measured vertically from the dune crest to the

underlying substrate (Fig. 3.6c). These values reflect the thickness of multiple shoreface subenvironments (i.e., dune, foreshore, upper shoreface) depending on the slope of the shoreface and the underlying shelf (Roy et al., 1994). Cores through some modern islands contain a range of depositional environments (e.g., Bernard et al., 1962), while others contain only thin upper shoreface deposits above underlying lagoonal facies (e.g., Belknap and Kraft, 1981). Ancient thicknesses were measured vertically through the sandstone portion of preserved barrier island deposits. These thickness measurements also represent variable subenvironments, depending on which portions of the barrier island are preserved (Fig. 3.6c). For example, some outcrops preserve only the upper shoreface (e.g., Mulhern and Johnson, 2016) while others record stacked offshore, lower shoreface, and middle shoreface successions (e.g., Løseth et al., 2009). For examples with multiple barrier island parasequences, the thickness of each individual sequence was measured when possible. In some cases only the thickness of the entire interval was available, these examples were given amalgamation designations (Fig. 3.5) to distinguish the type of measurements.

Although different portions of the barrier island are being measured in modern and ancient settings, the expression of progradation via either topset width (modern) or a dip-oriented shoreface width (ancient) represents a similar process, which is the underlying morphodynamic link between modern and ancient systems. Modern examples with the full island (topset and forest) documented bolster comparisons. Our attempt to quantify and compare barrier island features in this way provides an initial focus on the feasibility of such a comparison to begin with, and additionally insight into barrier island processes and preservation. Direct 1:1 relationships between modern and ancient

examples are not expected precisely because of nonstationality. If offsets between the two databases are systematic. However, then there could be predictive scaling relationships between the two.

Results

The ancient barrier island database highlights trends and problems with nomenclature as well as potential literature bias. Barrier island studies vary in frequency over time, with 39 studies between 1970-1979 compared to 20 studies between 1980-1989 (Fig. 3.8). Authors describe the deposits using 29 different terms (Fig. 3.8). Reported barrier island deposits occur mainly in passive margin (n=42) and retroarc foreland basin (n=58) settings, relative to other basins (forearc (n=2), rift (n=13), intracratonic (n=3), and aulacogen (n=4)). The majority of ancient barrier island examples are Mesozoic Western Interior Seaway deposits from the U.S. (n=32) and Canada (n=8; Fig. 3.10). A large number are also Tertiary Gulf of Mexico passive margin deposits (n=14 Fig. 3.10).

Kernel distributions (Fig. 3.11) of dimensional data show that modern and ancient barrier islands are not directly comparable. Ancient barrier islands are 2-5 times longer (p50 modern = 10.7 km; p50 ancient = 20.0 km), and 6-15 times wider (p50 modern = 1.2 km; p50 ancient = 7.3 km) than modern barrier islands. The median thickness values of the two datasets are similar (p50 modern = 11.0; p50 ancient = 15.2), however, the range of ancient thicknesses is three times greater than the modern range (Fig. 3.11c).

Because of these distinct size differences, modern examples were compared to ancient examples separated by vertical amalgamation. Ancient examples were split into

three groups (Fig. 3.5): vertically amalgamated ancient examples with multiple sequence measurements (Anc AMP), vertically amalgamated ancient examples with single sequence measurements (Anc ASP), and nonamalgamated ancient examples (Anc NA). Box-and-whisker plots (Fig. 3.12) show that vertically amalgamated ancient examples with multiple sequences (Anc AMP) are significantly thicker (5-10x) and wider (4-20x) than the other groups. Both types of amalgamated ancient examples, i.e., both multiple (Anc AMP p50=40.70 km) and single (Anc ASP p50=26.00 km) parasequence measurements, are longer than nonamalgamated ancient examples (Anc NA p50=14.7) and modern examples (p50=10.69; Fig. 3.12b).

Cross-plots (Fig. 3.13) were used compare modern dimensions to nonamalgamated and single parasequence amalgamated ancient examples. Cross-plotting thickness versus length (Fig. 3.13a) shows direct overlap between the modern and ancient with a single outlier. Cross-plotting thickness versus width (Fig. 3.13b) shows some overlap between the modern and the ancient, with the ancient examples skewed toward larger width values. Cross-plotting length versus width shows a distinct separation between modern and ancient values (Fig. 3.13c). The datasets have unique lines of best fit (Fig. 3.13c) with some overlap of their 90% confidence intervals. Scaling relationships exist between length and width for both modern (R^2=0.30) and the combined ancient single parasequence data (R^2=0.51). However, these unique modern and ancient lines of best fit do not intersect.

Discussion

Historical Context of Barrier Island Interpretations

Aggregating ancient barrier island examples from the literature sheds new light on interpretation trends through time. Explicit barrier island interpretations were common in the 1960s and 1970s, following a detailed characterization of Galveston Island by Bernard et al. (1962). Interestingly, this database shows that Galveston Island, one of the most heavily cited analogs for ancient barrier island deposits (Miller Jr., 1962; Shelton, 1967; Davies and Berg, 1969; Klein, 1974; Tizzard and Lerbekmo, 1975; Chiang, 1984), is large compared to the modern global dataset (Fig. 3.13c). Thus based on its large size, Galveston may not be an appropriate analog for many ancient examples, yet it forms the basis of many existing barrier island models (Davies et al., 1971; Davies, 1978; McCubbin, 1982; Reinson, 1992).

Barrier island interpretations declined slightly in the 1980s (Fig. 3.8) relative to the previous two decades, which may reflect the proliferation of sequence stratigraphic models. These models generally predict a condensed interval or lag deposits during transgression rather than barrier island preservation (Vail et al., 1977; Galloway and Hobday, 1983; Posamentier et al., 1988; Van Wagoner et al., 1988; Cattaneo and Steel, 2003). Consequently, some interpretations avoid barrier island terminology, using descriptive but less environmentally-specific shoreface nomenclature (Fig. 3.9; Allen and Johnson, 2011; Kieft et al., 2011). The development of sequence stratigraphy may have also prevented facies models for barrier island systems from being updated more recently (Boyd, 2010), partially explaining the variety in terminology that exists in the literature (Fig. 3.9). The database presented here suggests that barrier island deposits could be

under-represented in geologic studies of the last 30 years (Fig. 3.8), and that with improved facies models and consistent nomenclature, they can be appropriately interpreted moving forward.

Database Bias

The ancient systems documented here are overwhelmingly from the Cretaceous of North America (48%; Fig. 3.10). This bias may partly reflect exceptional accessibility of high-quality, Western Interior Seaway outcrops, as well as an abundance of subsurface data from coal and oil and gas exploration (Weimer, 1966; Berg, 1976; Hendricks, 1994; Olsen et al., 1999; Hubbard et al., 2002; Antia et al., 2011). The Western Interior Seaway developed in the high accommodation, high sediment supply setting of the Cordilleran foredeep (DeCelles, 2004) during a monsoonal greenhouse climate (Kauffman, 1977; Dennis et al., 2013). Temperate and high sediment supply settings are thought to be ideal for modern barrier island development (Hoyt, 1967; Weidie, 1968; Hayes, 1979; Otvos, 2012), which may also explain the abundance of Western Interior Seaway examples.

Modern coastlines create a natural laboratory for studying barrier islands, but they are not necessarily a representative of coastal landscapes through geologic time. For example, current transgressive/ highstand conditions within an interglacial period may not be ideal for ancient comparisons, particularly Late Cretaceous examples. By gathering barrier island examples into a database and considering the time-period and depositional conditions of each example, we can begin to assess changes in barrier island system through time as more data become available. This database is the first attempt to assess ancient barrier islands comparatively and lends insight into their dimensions and

variability.

Dimensional Comparisons

Using simple and straightforward measurement methods, these companion databases document that ancient islands are systematically longer, thicker, and wider than modern islands (Fig. 3.11) demonstrating quantitatively that ancient barrier island deposits characteristically preserve the accretion and stacking of individual islands through time. Some of the dimensional differences result from the stacking of multiple barrier island parasequences (Fig. 3.5). However, some could also indicate lateral or shore-perpendicular motion (Fig. 3.2). Modern barrier islands build landward, seaward, and vertically (Figs. 3.1 and 3.2). Vertically amalgamated examples are considered separately (Fig. 3.12) to understand much of the dimensional difference between modern and ancient barrier islands results from the stacking of multiple parasequences, versus the motion of a single preserved barrier island. These comparisons (Fig. 3.12) show that examples with multiple parasequences are larger (longer, wider, and thicker) than all other examples. This is a logical result given that multiple barrier islands can be stacked and preserved in conjunction with one another as the shoreline shifts over geologic timescales.

Understanding how the measurements of single ancient barrier islands compare to modern examples is more nuanced. Unfortunately, determining vertical amalgamation is not always straightforward: sometimes it is unclear whether the preserved sandstone deposits reflect one or multiple barrier island sequences (Fig. 3.14). Depending on how islands stack and the degree of ravinement, the preserved vertical sequence of an

amalgamated system may look similar to that of a single island or a prograding system (Fig. 3.14). To further complicate matters, barrier islands could be deposited rapidly, as most modern examples are thought to have established in the last 5,000 years (Stutz and Pilkey, 2011). Therefore, barrier island deposits may not display the clear coarsening and shallowing upward sequence normally indicative of shoreface deposition. Instead they may be more massive and undifferentiated.

Additionally, lateral facies variability, including the inclusion of tidal channels and tidal inlet facies within a barrier succession, can make it difficult to identify unique parasequences within barrier island deposits. These complications highlight the ways that barrier island motion and postdepositional processes determine barrier island dimensions. We have included the results from the whole dataset combined, as well as the dataset separated by amalgamation to provide the most detail possible. The complications surrounding barrier island amalgamation highlight some of the difficulty in developing a workflow for barrier island paleomorphodynamics. The prevalence of amalgamated barrier island examples provides data-based support for the well-established hypothesis that barrier island accretion and preservation are key considerations for barrier island system evolution (Dickinson et al., 1972; Barwis and Hayes, 1979; Reinson, 1992). Below we discuss both the full dataset results and the results separated by vertical amalgamation for each dimensional measurement (length, width, thickness) to consider the processes dictating those dimensions and the impact of barrier island motion and preservation processes.

Length

Ancient barrier island lengths are 2-5 times modern lengths (Fig. 3.11a) demonstrating that, as a whole, ancient islands preserve lateral migration at geologic time-scales. When separated by vertical amalgamation (Fig. 3.12a), comparisons show that both multiple (Anc AMP p50=40.70) and single (Anc ASP p50=26.00) sequence amalgamated ancient examples are longer than ancient nonamalgamated (Anc NA p50=22.28) and modern examples (p50=10.69). The long lengths of multiple parasequence amalgamated examples suggest that barrier island systems can preserve lateral, shore-parallel, stacking through time, meaning that, at geologic time-scales, the entire barrier sequence moves in the shore-parallel direction. This motion likely reflects shifts in the location of available accommodation.

The long lengths of single parasequence amalgamated ancient examples suggests that, in long-standing systems (indicated by the amalgamation), barrier islands move laterally. Modern barrier islands move in the shore-parallel direction through tidal inlet migration and island accretion driven by long-shore drift. Barrier island reworking through inlet generation, migration, and healing, is commonly observed in preserved deposits (Davies and Ethridge, 1971; Davies, 1978; Galloway, 1986; Self et al., 1986; Hendricks, 1994; Mulhern and Johnson, 2016) and is likely increasing the length single parasequence amalgamated examples. In addition to lateral migration, if an inlet infills with sand vertically, it can link two separate barriers into one larger one by combination. In some cases, migrating tidal inlet deposits comprise the primary barrier island succession, recording lateral motion of the island across the inlet channel through time (Moslow and Tye, 1985). Alternatively, in some modern examples, the shoreface can

extend across the inlet mouth, uninterrupted by inlet process, particularly on wave-dominated coasts where ebb-tidal deltas tend to be smaller and sand is readily reworked across the inlet mouth (Fig. 3.7; Hayes, 1979; FitzGerald et al., 2012). Similar processes could create long preserved barrier island deposits. The increased length of ancient examples suggests that ancient barrier island deposits are inherently time-transgressive, recording lateral island motion via tidal inlet migration, and it follows that both ancient islands as a whole, and more specially amalgamated ancient island measurements are longer than those of modern islands.

Modern (p50=10.69) and nonamalgamated ancient (Anc NA; p50=14.70) examples have fairly similar lengths (Fig. 3.12a). However the processes limiting island length in the modern and ancient are different. In modern systems, tidal inlets can limit barrier island length (Fig. 3.6a; Hayes, 1979), and inlet location and frequency can depend on a variety of factors including the tidal range, tidal prism, the location of storm scours or paleovalleys, longshore transport, and spit migration (Phleger, 1969; Hayes and FitzGerald, 2013). These limiting factors are less clear in the rock record, where measurements are derived from the preserved shoreface, which commonly grades laterally from shoreface to tidal facies (Fig. 3.7; Davies and Ethridge, 1971; Davies, 1978; Galloway, 1986; Self et al., 1986; Hendricks, 1994; Mulhern and Johnson, 2016). Thus a given inlet location may not be discernable in ancient barrier island systems, and certainly cannot be recognized without very detailed facies analysis (e.g., Reddering, 1983; Caplan and Moslow, 1999). Non-amalgamated ancient examples are more likely limited by the outcrop exposure or subsurface data available. Therefore, while modern and ancient nonamalgamated length values are similar, the range of values is large and

could be a reflection of the number of samples in the database, rather than an inherent sedimentary process, particularly because inlet motion and migration are likely increasing island length in the ancient.

Thickness

Ancient examples are thicker than modern examples (Fig. 3.11c). The median thickness values of the two datasets are similar (p50 modern = 11.0 m; p50 ancient =15.2 m; Fig. 3.11c). However the range of ancient barrier island thicknesses is three times greater than the modern range. Logically, vertically amalgamated islands with multiple parasequences (Anc AMP p50=45.72) measured are significantly thicker than other ancient (~6x) and modern (~10x) barrier islands (Fig. 3.12b), indicating that examples in which multiple islands are measured are thicker than examples in which only a single island is measured. The thickness of amalgamated multiple parasequence (Anc AMP) examples is likely a function of the available accommodation through time. In contrast, the other two groups of ancient examples (amalgamated single parasequence (Anc ASP) and nonamalgamated (Anc NA), are both similar to modern thicknesses. This is likely partially the result of available accommodation, but may also reflect similarity in the depth of closure between the modern and ancient.

In modern barrier island literature, the vertical thickness and limit of the barrier island shoreface is estimated using the depth of closure. The depth of closure is vertical height between the mean sea level and storm weather wave base (Fig. 3.15) or, more precisely, the depth below which no significant net sediment transport (Kraus, 1988). Because the depth of closure relates to levels of wave base it could be used to precisely

compare portions of modern and ancient barrier island shorefaces. Ancient upper shoreface thicknesses could be compared to inner depth of closure values. While conceptually straightforward, these comparisons would be difficult to execute because of limited data availability and ambiguity in the rock record. Inner and outer depth of closure measurements for a variety of modern islands would need to be compared to preserved upper shoreface or lower shoreface thicknesses. However, often in barrier island systems the shoreface is intersected by tidal channels (Davies and Ethridge, 1971; Roehler, 1988) or the boundary between the upper and lower shoreface is ambiguous or not reported by authors (Devine, 1991; Sixsmith et al., 2008). A variety of time-dependent equations estimate depth of closure for use in modern morphodynamics and hydrodynamics (Hallermeier and Nauman, 1978; Hallermeier, 1981; Birkemeier, 1985; Brutsché et al., 2014), empirically quantifying the limit of storm and wave processes on near shore sediments. These equations could be leveraged for future paleomorphodynamic comparisons of modern depth of closure values to specific portions of preserved barrier island deposits.

Width

Ancient barrier islands are 6-15 times wider (p50 modern = 1.2 km; p50 ancient = 7.3 km) than modern barrier islands (Fig. 3.11b). This large width difference is likely due to both measurement differences and amalgamation. Comparisons separated by amalgamation (Fig. 3.12c) show that ancient amalgamated examples with multiple parasequences measured (Anc AMP; p50=30.00 km) are significantly wider than other ancient examples (4-5x) and modern examples (23x). This suggests barrier islands move

and stack in the shore-perpendicular direction through geologic time. The remaining ancient examples (ancient amalgamated single parasequence examples (Anc ASP; p50=7.24 km) and ancient nonamalgamated examples (Anc NA; p50=4.08 km)) are both wider than modern examples (Mod; p50=1.19 km). This could be in part because of the way the width measurements were made. In modern settings, the subaerial topset defines the width; in ancient examples, both the topset width and the final foreset width combine to define the preserved width (Fig. 3.6b). In order to mirror the ancient width scale in the modern, both subaerial topset width and foreset length would need to be measured. Foreset data are quite rare from modern barrier systems, because core studies and data constraining modern barrier island clinothems are sparse. The few examples in the modern barrier island database (n=5) have foresets that are 1.2-4.0 times the topset width. Ancient examples are 3.4-6.1 times wider than modern examples (based on their mean values). This suggests that, while some of the difference between the modern and ancient is due to measurement methods, ancient examples also preserve some shore-perpendicular motion through time.

Modern barrier islands move basinward, landward, and vertically, creating three different barrier island geometries (Fig. 3.1). Equivalent motion of a single barrier island sequence also occurs in the ancient and is manifest in the internal facies patterns of preserved barrier island deposits. Some preserved examples show coarsening and shallowing upwards successions (Sabins Jr, 1963; Land, 1972; Bridges, 1976; Roehler, 1988; Roy et al., 1994; Sixsmith et al., 2008), indicating progradation of the shoreface via Walther's law (Middleton, 1973). Other examples show internal washover processes, suggesting retrogradation (Hobday and Orme, 1974; Hobday and Jackson, 1979; Willis

and Moslow, 1994). Because similar processes occur both in the modern and the ancient, the increased relative width of ancient examples suggests that ancient barrier islands are time-transgressive and that the deposit widths record motion at longer time scales than modern barrier island widths.

Paleomorphodynamic Implications

Cross-plots of length and width versus thickness (Fig. 3.13a,b) do not show systematic scaling relationships between modern and ancient examples, and therefore are not helpful in developing predictive modern to ancient relationships. Thickness similarities between ancient and modern examples could be a coincidental record of the range of local, example-specific controls on accommodation. Alternatively, the similarities could indicate a linked process-based control, such as depth of closure, pending future studies.

While thickness values may be similar, length and width differences between the two realms persist once multiple amalgamated parasequence examples are removed (Fig. 3.12a,c). Increased lengths and widths of ancient barrier islands suggest that preserved deposits are time-transgressive. Cross-plotting length versus width highlights the dimensional difference between modern and ancient barrier islands (single parasequence measurements only; Fig. 3.13c). The ancient barrier islands are skewed to longer and wider values relative to the modern examples. There is some overlap in the 90% confidence intervals, however, modern dimensions do not directly predict ancient dimensions because the trend lines of both datasets are offset. These trends lines are predictive (modern R^2= 0.30, ancient R^2=0.51) meaning that length predicts width and

vice versa for both systems for the two datasets independently, but not together.

In sum, future development of paleomorphodynamic relationships for barrier islands cannot escape the fundamental complication that ancient barrier islands preserve motion through time and postdepositional processes, which dictate their dimensions. In contrast to river systems, which are self-organized and display dynamic scaling (Sapozhnikov and Foufoula-Georgiou, 1997; Paola and Foufoula-Georgiou, 2001; Lane, 2006), the barrier island dynamics are time-scale dependent: processes occurring at short time scales vary from those occurring at geologic time scales. Consequently, ancient barrier island deposits cannot be linked to a single modern snapshot in time. This complexity will affect the way paleomorphodynamics can be developed for the shallow marine realm.

Nevertheless, this dataset outlines a workflow for quantifying ancient barrier islands and beginning modern to ancient comparisons. Although more examples are needed, gathering and measuring ancient barrier island dimensions constrains the range and distribution of dimensional values (Table 3.1; Figs. 3.11 and 3.12). These examples could be leveraged as analogs for modeling and subsurface predictions. The significant scaling relationships between length and width (Fig. 3.13c) suggest that rotation and translation could potentially be used to relate the two datasets, and define modern to ancient relationships, pending more data. This would allow for modern to ancient spatial predictions.

More broadly, the fields of nearshore hydrodynamics and numerical modeling can help to quantify and predict modern barrier island geometries, generating relationships that could be used in paleomorphodynamics. For example, depth of closure equations

(Hallermeier and Nauman, 1978; Brutsché et al., 2014) could be used to estimate wavebase and extrapolate shoreface thickness. Although imperfect (Cooper and Pilkey, 2004), equilibrium beach profile equations (Bruun, 1962) could be adapted and modified to estimate shelf morphology and slope to predict available accommodation. Tidal inlet depth (de Swart and Zimmerman, 2009), cross-sectional area (Gao and Collins, 1994; van de Kreeke, 2004), or symmetry (Hoyt and Henry Jr., 1965) calculations could be linked to island characteristics and morphology. Direct comparisons between specific modern and ancient subenvironments (i.e., upper shoreface) could also potentially aid in understanding scaling.

Conclusions

This first-order comparison of modern and ancient barrier island dimensions shows that ancient barrier island deposits are wider and longer than modern barrier islands, recording lateral and shore-perpendicular motion through time. Thickness differences suggest that ancient barrier island deposits can record vertical stacking of multiple barrier islands through time, emphasizing the role of accommodation in determining barrier island preservation potential. Available accommodation determines the thickness of ancient deposits, rather than the size of the paleo-island. Overall, the distinct differences in the aggregate modern and ancient barrier island dimensions suggest that modern analog dimensions should not be directly applied to ancient interpretations and predictions. However, there appear to be systematic shifts, suggesting that ancient barrier island deposits are time-transgressive. Thus these results are a first step towards understanding and quantifying the paleomorphodynamic relationships

between modern and ancient barrier islands. This dataset also highlights inconsistencies in barrier island terminology and facies models based on depositional trends, underscoring the need for updated barrier island facies models, and additional research into barrier island facies and preservation processes.

References

Allen, J.L., and Johnson, C.L., 2011, Architecture and formation of transgressive-regressive cycles in marginal marine strata of the John Henry Member, Straight Cliffs Formation, Upper Cretaceous of southern Utah, USA: Sedimentology, v. 58, no. 6, p. 1486–1513, doi: 10.1111/j.1365-3091.2010.01223.x.

Anthony, E.J., 2009, Shore processes and their palaeoenvironmental applications: Elsevier, Amsterdam.

Antia, J., Fielding, C.R., and Joeckel, R.M., 2011, Multiple cycles of wave-dominated estuarine deposits in low-accommodation settings, Cretaceous J sandstone, northwestern Nebraska: American Association of Petroleum Geologists Bulletin, v. 95, no. 7, p. 1227–1256, doi: 10.1306/11051009105.

Arnott, R.W.C., 1995, The parasequence definition--are transgressive deposits inadequately addressed? Journal of Sedimentary Research, v. 65, no. 1, p. 1–6, doi: 10.1306/D42681D0-2B26-11D7-8648000102C1865D.

Barwis, J.H., and Hayes, M.O., 1979, Regional patterns of modern barrier island and tidal inlet deposits as applied to paleoenvironmental studies, *in* Ferm, J.C., Horne, J.C., Weisenfluh, G.A., and Staub, J.R. eds., Carboniferous depositional environments in the Appalachian region, University of South Carolina Geology Department, Columbia, S.C., p. 472–498.

Belknap, D.F., and Kraft, J.C., 1981, Preservation potential of transgressive coastal lithosomes on the U.S. Atlantic shelf: Marine Geology, v. 42, no. 1–4, p. 429–442, doi: http://dx.doi.org/10.1016/0025-3227(81)90173-0.

Berg, R.R., 1976, Hilight muddy field-Lower Cretaceous transgressive deposits in the Powder River Basin, Wyoming: The Mountain Geologist, v. 13, no. 2, p. 33–45.

Bernard, H.A., LeBlanc, R.J., and Major, C.F., 1962, Recent and Pleistocene geology of southeast Texas, Field excursion no. 3, *in* Rainwater, E.H. and Zingula, R.P. eds., Geology of the Gulf Coast and Central Texas and Guidebook of Excursions, Houston Geological Society, Houston, Texas, p. 175–224.

Bhattacharya, J.P., and Tye, R.S., 2004, Searching for modern Ferron analogs and

application to subsurface interpretation, *in* Chidsey Jr., T.C., Adams, R.D., and Morris, T.H. eds., Regional to Wellbore Analog for Fluvial-Deltaic Reservoir Modeling: The Ferron Sandstone of Utah, American Association of Petroleum Geologists, Studies in Geology, 50, p. 39–58.

Birkemeier, W.A., 1985, Field data on seaward limit of profile change: Journal of Waterway, Port, Coastal, and Ocean Engineering, v. 111, no. 3, p. 598–602, doi: 10.1061/(ASCE)0733-950X(1985)111:3(598).

Blum, M., Martin, J., Milliken, K., and Garvin, M., 2013, Paleovalley systems: insights from Quaternary analogs and experiments: Earth-Science Reviews, v. 116, p. 128–169, doi: 10.1016/j.earscirev.2012.09.003.

Boyd, R., 2010, Transgressive wave-dominated coasts, *in* James, N.P. and Dalrymple, R.W. eds., Facies Models 4, Geological Association of Canada, St. John's, Newfoundland, p. 265–294.

Bridges, P.H., 1976, Lower Silurian transgressive barrier islands, southwest Wales: Sedimentology, v. 23, no. 3, p. 347, doi: 10.1111/j.1365-3091.1976.tb00054.x.

Brutsché, K.E., Rosati, J., Pollock, C.E., McFall, B.C., Iii, J.R., and Cheryl, E., 2014, Calculating depth of closure using WIS hindcast data: US Army Corps of Engineers, v. ERDC/CHL C, no. November, p. 1–10.

Bruun, P., 1962, Sea-level rise as a cause of shore erosion: Proceedings of the American Society of Civil Engineers, v. 88, p. 117–130.

Caplan, M.L., and Moslow, T.F., 1999, Depositional origin and facies variability of a Middle Triassic barrier island complex, Peejay Field, northeastern British Columbia: American Association of Petroleum Geologists Bulletin, v. 83, no. 1, p. 128–154, doi: 10.1306/00AA9A20-1730-11D7-8645000102C1865D.

Cattaneo, A., and Steel, R.J., 2003, Transgressive deposits: a review of their variability: Earth-Science Reviews, v. 62, no. 3–4, p. 187–228, doi: 10.1016/s0012-8252(02)00134-4.

Catuneanu, O., Bhattacharya, J.P., Blum, M.D., Dalrymple, R.W., Eriksson, P.G., Fielding, C.R., Fisher, W.L., Galloway, W.E., Gianolla, P., Gibling, M.R., Giles, K.A., Holbrook, J.M., Jordan, R., Kendall, C.G.S.C., et al., 2010, Sequence stratigraphy: common ground after three decades of development: first break, v. 28, no. 1717, p. 21–34, doi: 10.3997/1365-2397.2010002.

Chiang, K.K., 1984, The giant Hoadley gas field, south-central Alberta, *in* Masters, J.A. ed., Elmworth: Case Study of a Deep Basin Gas Field, American Association of Petroleum Geologists Memior, 38, p. 297–313.

Coe, A.L., Bosence, D.W., Church, K.D., Flint, S.S., Howell, J.A., and Wilson, R.C.L. (Eds.), 2003, The sedimentary record of sea-level change: Cambridge University

Press, Cambridge.

Cooper, J.A.G., and Pilkey, O.H., 2004, Sea-level rise and shoreline retreat: time to abandon the Bruun Rule: Global and Planetary Change, v. 43, no. 3–4, p. 157–171, doi: 10.1016/j.gloplacha.2004.07.001.

Covault, J.A., Shelef, E., Traer, M., Hubbard, S.M., Romans, B.W., and Fildani, A., 2012, Deep-water channel run-out length: insights from seafloor geomorphology: Journal of Sedimentary Research, v. 82, no. 1, p. 21–36, doi: 10.2110/jsr.2012.2.

Davies, D.K., 1978, Models and concepts for exploration in barrier islands, *in* Saxena, R.S. ed., Gulf Coast Association of Geological Societies, New Orleans, LA, p. 159–197.

Davies, D.K., and Berg, R.R., 1969, Sedimentary characteristics of Muddy barrier-bar reservoir and lagoonal trap at Bell Creek Field, *in* The Economic Geology of Eastern Montana and Adjacent Areas 20th Annual Conference 1969 Eastern Montana Symposium Oct 19-22, 1969, Montana Geological Society, Billings, p. 97–105.

Davies, D.K., and Ethridge, F.G., 1971, The Claiborne group of central Texas: Transactions - Gulf Coast Association of Geological Societies, v. 21, p. 115–124.

Davies, D., Ethridge, F., and Berg, R., 1971, Recognition of barrier environments: American Association of Petroleum Geologists Bulletin, v. 4, no. 4, p. 550–565.

Davis Jr., R.A., 2013, A new look at barrier-inlet morphodynamics: Journal of Coastal Research, Special Issue, v. 69, p. 1–12, doi: 10.2112/SI_69_2.

Davis Jr., R.A., 1994a, Barrier island systems- a geologic overview, *in* Davis Jr., R.A. ed., Geology of Holocene Barrier Island Systems, Springer-Verlag, Berlin, p. 1–46.

Davis Jr., R.A. (Ed.), 1994b, Geology of Holocene Barrier Island Systems: Berlin.

DeCelles, P.G., 2004, Late Jurassic to Eocene evolution of the Cordilleran thrust belt and foreland basin system, western, U.S.A: American Journal of Science, v. 304, no. 2, p. 105–168, doi: 10.2475/ajs.304.2.105.

Dennis, K.J.J., Cochran, J.K.K., Landman, N.H.H., and Schrag, D.P.P., 2013, The climate of the Late Cretaceous: new insights from the application of the carbonate clumped isotope thermometer to Western Interior Seaway macrofossil: Earth and Planetary Science Letters, v. 362, no. 0, p. 51–65, doi: http://dx.doi.org/10.1016/j.epsl.2012.11.036.

Devine, P.E., 1991, Transgressive origin of channeled estuarine deposits in the Point Lookout Sandstone, northwestern New Mexico: a model for Upper Cretaceous, cyclic regressive parasequences of the U.S. Western Interior: American Association of Petroleum Geologists Bulletin, v. 75, no. 6, p. 1039–1063, doi: 10.1306/0C9B28C1-1710-11D7-8645000102C1865D.

Dickinson, K.A., Berryhill, H.L., and Holmes, C.W., 1972, Criteria for recognizing ancient barrier coastlines, *in* Rigby, J.K. and Hamblin, W.K. eds., Recognition of Ancient Sedimentary Environments, SEPM, Special Publication 16, p. 108–145.

Dronkers, J.J., 2005, Dynamics of coastal systems: World Scientific, Singapore.

Dyke, P.P.G., 2007, Modeling coastal and offshore processes: Imperial College Press, London.

Edmonds, D.A., and Slingerland, R.L., 2007, Mechanics of river mouth bar formation: implications for the morphodynamics of delta distributary networks: Journal of Geophysical Research: Earth Surface, v. 112, no. 2, p. 1–14, doi: 10.1029/2006JF000574.

Emery, D., and Myers, K.J. (Eds.), 1996, Sequence Stratigraphy: Blackwell Science, Oxford.

Fisher, J.S., and Dolan, R. (Eds.), 1977, Beach processes and coastal hydrodynamics: Dowden, Hutchinson & Ross, Stroudsburg, PA.

FitzGerald, D.M., Buynevich, I., and Hein, C., 2012, Morphodynamics and facies architecture of tidal inlets and tidal deltas, *in* Davis Jr, R.A. and Dalrymple, R.W. eds., Principles of Tidal Sedimentology, Springer Netherlands, Dordrecht, p. 301–333.

Flores, R.M., 1978, Barrier and back-barrier environments of deposition of the Upper Cretaceous Almond Formation, Rock Springs Uplift, Wyoming: The Mountain Geologist, v. 15, no. 2, p. 57–65.

Franks, P.C., 1980, Models of marine transgression - example from Lower Cretaceous fluvial and paralic deposits, north-central Kansas: Geology, v. 8, no. 1, p. 56–61, doi: 10.1130/0091-7613(1980)8<56:MOMTEF>2.0.CO;2.

Fruergaard, M., Møller, I., Johannessen, P.N., Nielsen, L.H., Andersen, T.J., Nielsen, L., Sander, L., and Pejrup, M., 2015, Stratigraphy, evolution, and controls of a holocene transgressive – regressive barrier island under changing sea level: Danish North Sea coast: Journal of Sedimentary Research, v. 85, no. 7, p. 820–844.

Galloway, W.E., 1986, Reservoir facies architecture of microtidal barrier systems: American Association of Petroleum Geologists Bulletin, v. 70, no. 7, p. 787–808, doi: 10.1306/9488634E-1704-11D7-8645000102C1865D.

Galloway, W.E., and Hobday, D.K. (Eds.), 1983, Terrigenous clastic depositional systems: applications to petroleum, coal, and uranium exploration: Springer-Verlag, New York.

Gao, S., and Collins, M., 1994, Tidal inlet equilibrium, in relation to cross-sectional area and sediment transport patterns: Estuarine, Coastal and Shelf Science, v. 38, no. 2, p.

157–172, doi: http://dx.doi.org/10.1006/ecss.1994.1010.

Guscott, S., Russell, K., Thickpenny, A., and Poddubiuk, R., 2003, The Scott Field, Blocks 15/21a, 15/22, UK North Sea, *in* Gluyas, J.G. and Hichens, H.M. eds., United Kingdom Oil and Gas Fields Commemorative Millennium Volume, Geological Society, London, Memoirs, 20, p. 467–482.

Hajek, E.A., and Wolinsky, M.A., 2012, Simplified process modeling of river avulsion and alluvial architecture: connecting models and field data: Sedimentary Geology, v. 257–260, p. 1–30, doi: 10.1016/j.sedgeo.2011.09.005.

Hallermeier, R.J., 1981, A profile zonation for seasonal sand beaches from wave climate: Coastal Engineering, v. 4, p. 253–277, doi: http://dx.doi.org/10.1016/0378-3839(80)90022-8.

Hallermeier, R.J., and Nauman, K.E., 1978, Uses for a calculated limit depth to beach erosion, *in* Proceedings of the Coastal Engineering Conference, American Society of Civil Engineers, New York, NY, p. 1493–1512.

Hayes, M.O., 1979, Barrier island morphology as a function of tidal and wave regime, *in* Leatherman, S.P. ed., Barrier Islands from the Gulf of Mexico to the Gulf of St. Lawrence, Academic Press, New York, p. 1–28.

Hayes, M.O., and FitzGerald, D.M., 2013, Origin, evolution, and classification of tidal inlets: Journal of Coastal Research, v. 69, p. 14–33, doi: 10.2112/SI_69_3.

Hendricks, M.L., 1994, Ravinement surface control on hydrocarbon accumulation in transgressive systems tracts: Almond Formation, Green River Basin, Wyoming, *in* Dolson, J.C., Hendricks, M., and Westcott, W. eds., Unconformity Related Hydrocarbons in Sedimentary Sequences, Rocky Mountain Association of Geologists, p. 209–218.

Heward, A.P., 1981, A review of wave-dominated clastic shoreline deposits: Earth-Science Reviews, v. 17, no. 3, p. 223–276, doi: http://dx.doi.org/10.1016/0012-8252(81)90022-2.

Hobday, D.K., and Jackson, M.P.A., 1979, Transgressive shore zone sedimentation and syndepositional deformation in the Pleistocene of Zululand, South Africa: Journal of Sedimentary Research, v. 49, no. 1, p. 145–158, doi: 10.1306/212F76DA-2B24-11D7-8648000102C1865D.

Hobday, D.K., and Orme, A.R., 1974, The Port Durnford Formation: Verhandelinge van die Geologiese Vereniging van Suid Afrika, v. 77, no. 2, p. 141–149.

Hoyt, J.H., 1967, Barrier island formation: Geological Society of America Bulletin, v. 78, p. 1125–1136, doi: 10.1130/0016-7606(1967)78[1125:BIF]2.0.CO;2.

Hoyt, J.H., 1969, Chenier versus barrier, genetic and stratigraphic distinction: American

Association of Petroleum Geologists Bulletin, v. 53, no. 2, p. 299–306, doi: 10.1306/5D25C60D-16C1-11D7-8645000102C1865D.

Hoyt, J., and Henry Jr., V.J., 1965, Significance of inlet sedimentation in the recognition of ancient barrier islands, *in* DeVoto, R.H. and Bitter, R.K. eds., Sedimentation of Late Cretaceous and Tertiary Outcrops, Rock Springs Uplift, Ninteenth Annual Field Conference Guidebook, Wyoming Geological Association, p. 190–194.

Hubbard, S.M., Gingras, M.K., Pemberton, S.G., and Thomas, M.B., 2002, Variability in wave-dominated estuary sandstones: implications on subsurface reservoir development: Bulletin of Canadian Petroleum Geology, v. 50, no. 1, p. 118–137, doi: 10.2113/50.1.118.

Hudock, J.W., Flaig, P.P., and Wood, L.J., 2014, Washover fans: a modern geomorphologic analysis and proposed classification scheme to improve reservoir models: Journal of Sedimentary Research, v. 84, p. 854–865.

Jerolmack, D.J., and Swenson, J.B., 2007, Scaling relationships and evolution of distributary networks on wave-influenced deltas: Geophysical Research Letters, v. 34, no. 23, p. n/a-n/a, doi: 10.1029/2007GL031823.

Johannessen, P.N., Nielsen, L.H., and Nielsen, L., 2010, Architecture of an Upper Jurassic barrier island sandstone reservoir, Danish Central Graben: implications of a Holocene-Recent analogue from the Wadden Sea: Petroleum Geology Conference series, v. 7, p. 145–155, doi: 10.1144/0070145.

Johannessen, P.N., Nielsen, L.H., Nielsen, L.H., Moller, I., Pejrup, M., Andersen, T.J., Korshoj, J., Larsen, B., Piasecki, S., Møller, I., Pejrup, M., Andersen, T.J., Korshøj, J., Larsen, B., et al., 2008, Sedimentary facies and architecture of the Holocene to Recent Rømø barrier island in the Danish Wadden Sea island: Geological Survey of Denmark and Greenland Bulletin, v. 15, no. 2006, p. 49–52.

Kauffman, E.G., 1977, Geological and biological overview: Western Interior Cretaceous Basin: Mountain Geologist, v. 14, no. 3–4, p. 75–99.

Kieft, R.L., Hampson, G.J., Jackson, C.A.L., and Larsen, E., 2011, Stratigraphic architecture of a net-transgressive marginal- to shallow-marine succession: Upper Almond Formation, Rock Springs Uplift, Wyoming, U.S.A.: Journal of Sedimentary Research, v. 81, no. 7, p. 513–533, doi: 10.2110/jsr.2011.44.

Klein, G. deVries, 1974, Estimating water depths from analysis of barrier island and deltaic sedimentary sequences: Geology, v. 2, no. 8, p. 409–412, doi: 10.1130/0091-7613(1974)2<409:EWDFAO>2.0.CO;2.

Kraus, N.C., 1988, Inlet cross-sectional area calculated by process-based model: Coastal Engineering, p. 3265–3278.

van de Kreeke, J., 2004, Equilibrium and cross-sectional stability of tidal inlets:

application to the Frisian Inlet before and after basin reduction: Coastal Engineering, v. 51, no. 5–6, p. 337–350, doi: 10.1016/j.coastaleng.2004.05.002.

Land, C.B., 1972, Stratigraphy of Fox Hills Sandstone and associated formations, Rock Springs uplift and Wamsutter Arch area, Sweetwater County, Wyoming: a shoreline-estuary sandstone model for the Late Cretaceous: Colorado School of Mines, Golden, CO.

Lane, S.N., 2006, Approaching the system-scale understanding of braided river behaviour, *in* Sambrook Smith, G.H., Best, J.L., Bristow, C.S., and Petts, G.E. eds., Braided Rivers: Processes, Deposits, Ecology, and Management, Special Publication of the International Association of Sedimentologists, Oxford, p. 107–135.

Løseth, T.M., Ryseth, A.E., and Young, M., 2009, Sedimentology and sequence stratigraphy of the middle Jurassic Tarbert Formation, Oseberg South area (northern North Sea): Basin Research, v. 21, no. 5, p. 597–619, doi: 10.1111/j.1365-2117.2009.00421.x.

Lunt, I.A., Sambrook Smith, G.H., Best, J.L., Ashworth, P.J., Lane, S.N., and Simpson, C.J., 2013, Deposits of the sandy braided South Saskatchewan River: implications for the use of modern analogs in reconstructing channel dimensions in reservoir characterization: American Association of Petroleum Geologist Bulletin, v. 97, no. 4, p. 553–576, doi: 10.1306/09251211152.

van Maren, D.S., 2005, Barrier formation on an actively prograding delta system: the Red River Delta, Vietnam: Marine Geology, v. 224, no. 1–4, p. 123–143, doi: 10.1016/j.margeo.2005.07.008.

McBride, R.A., Anderson, J.B., Buynevich, I. V, Cleary, W., Fenster, M.S., FitzGerald, D.M., Harris, M.S., Hein, C.J., Klein, A.H.F., Liu, B., de Menezes, J.T., Pejrup, M., Riggs, S.R., Short, A.D., et al., 2013, Morphodynamics of barrier systems: a synthesis, *in* Sherman, D.J. ed., Treatise on Geomorphology: Volume 10 Coastal Geomorphology, Academic Press, San Diego, p. 166–244.

McCubbin, D.G., 1982, Barrier-island and strand plain facies, *in* Scholle, P.A. and Spearing, D. eds., Sandstone Depositional Environments, American Association of Petroleum Geologists Memior, 31, p. 247–279.

Middleton, G. V, 1973, Johannes Walther's Law of the correlation of facies: Geological Society of America Bulletin, v. 84, no. 3, p. 979, doi: 10.1130/0016-7606(1973)84<979:JWLOTC>2.0.CO;2.

Miller Jr., D.N., 1962, Patterns of barrier bar sedimentation and its similarity to Lower Cretaceous Fall River Stratigraphy, *in* Enyert, R.L. and Curry III, W.H. eds., Symposium of Early Cretaceous Rocks of Wyoming and Adjacent Areas 17th Annual Field Conference Guidebook, Wyoming Geological Association, p. 232–247.

Milliken, K., Blum, M., and Martin, J., 2012, Scaling relationships in fluvial depostional systems, *in* Search and Discovery Article #30245, American Association of Petroleum Geologists Annual Conference and Exhibition, Long Beach, California, April 22-25.

Mohrig, D., Heller, P.L., Paola, C., and Lyons, W.J., 2000, Interpreting avulsion process from ancient alluvial sequences: Guadalope-Matarranya system (northern Spain) and Wasatch Formation (western Colorado): Geological Society of America Bulletin, v. 112, no. 12, p. 1787–1803.

Morton, R.A., 1994, Texas barriers, *in* Davis Jr., R.A. ed., Geology of Holocene Barrier Island Systems, Springer-Verlag, Berlin, p. 75–114.

Moslow, T.F., and Tye, R.S., 1985, Recognition and characterization of Holocene tidal inlet sequences: Marine Geology, v. 63, no. 1–4, p. 129–151, doi: http://dx.doi.org/10.1016/0025-3227(85)90081-7.

Mulhern, J.S., and Johnson, C.L., 2016, Time–space variability of paralic strata deposited in a high accommodation, high sediment supply setting: example from the Cretaceous of Utah, *in* Hampson, G.J., Reynolds, A.D., Kostic, B., and Wells, M.R. eds., Geological Society, London, Special Publications, Geological Society, London, Special Publication, 444.

Oertel, G.F., 1985, The barrier island system: Marine Geology, v. 63, no. 1, p. 1–18, doi: 10.1016/0025-3227(85)90077-5.

Olsen, T.R., Mellere, D., and Olsen, T., 1999, Facies architecture and geometry of landward-stepping shoreface tongues: the Upper Cretaceous Cliff House Sandstone (Mancos Canyon, south-west Colorado): Sedimentology, v. 46, no. 4, p. 603–625, doi: 10.1046/j.1365-3091.1999.00234.x.

Otvos, E.G., 2012, Coastal barriers - nomenclature, processes, and classification issues: Geomorphology, v. 139–140, no. 0, p. 39–52, doi: 10.1016/j.geomorph.2011.10.037.

Paola, C., and Foufoula-Georgiou, E., 2001, Statistical geometry and dynamics of braided rivers, *in* Mosley, M.P. ed., Gravel Bed Rivers V, New Zealand Hydrological Society, Wellington, p. 47–69.

Parker, G., 2006, 1D sediment transport morphodynamics with applications to rivers and turbidity currents: University of Illinois.

Penland, S., Boyd, R., and Suter, J.R., 1988, Transgressive depositional systems of the Mississippi Delta plain: Journal of Sedimentary Petrology, v. 58, no. 6, p. 932–949, doi: 10.1306/212F8EC2-2B24-11D7-8648000102C1865D.

Penland, S., and Suter, J.R., 1989, The geomorphology of the Mississippi River chenier plain: Marine Geology, v. 90, no. 4, p. 231–258, doi: http://dx.doi.org/10.1016/0025-3227(89)90127-8.

Phleger, F.B., 1969, Some general features of coastal lagoons, *in* Phleger, F.B. and Castañares, A.A. eds., Coastal Lagoons, A Symposium: Memoir of the International Symposium on Coastal Lagoons, Universidad nacional autónoma de México, p. 5–26.

Pirmez, C., and Imran, J., 2003, Reconstruction of turbidity currents in Amazon Channel: Marine and Petroleum Geology, v. 20, no. 6–8, p. 823–849, doi: 10.1016/j.marpetgeo.2003.03.005.

Posamentier, H.W., Jervey, M.T., and Vail, P.R., 1988, Eustatic controls on clastic deposition I - conceptual framework, *in* Wilgus, C.K., Hastings, B.S., Posamentier, H.W., Van Wagoner, J.C., Ross, C.A., and Kendall, C.G.S.C. eds., Sea-level changes: an integrated approach, SEPM Special Publication, 42, p. 109–124.

Rawn-Schatzinger, V., and Schatzinger, R.A., 1993, Annotated bibliography of selected references on shoreline barrier island deposits with emphasis on Patrick Draw Field, Sweetwater County, Wyoming: ITT Research Institute, U.S. Department of Energy, Technical Report, NIPER-622.

Reddering, J.S.V., 1983, An inlet sequence produced by migration of a small microtidal inlet against longshore drift: the Keurbooms Inlet, South Africa: Sedimentology, v. 30, no. 2, p. 201–218, doi: 10.1111/j.1365-3091.1983.tb00665.x.

Reinson, G.E., 1979, Barrier island systems, *in* Walker, R.G. ed., Facies Models, Geosciences Canada, Toronto, p. 57–74.

Reinson, G.E., 1992, Transgressive barrier island and estuarine systems, *in* Walker, R.G. and James, N.P. eds., Facies Models: Response to Sea-Level Changes, Geological Association of Canada, St. John's, Newfoundland, p. 179–194.

Reinson, G.E., Clark, J.E., and Foscolos, A.E., 1988, Reservoir geology of Crystal Viking Field, Lower Cretaceous estuarine tidal channel-bay complex, south-central Alberta: American Association of Petroleum Geologists Bulletin, v. 72, no. 10, p. 1270–1294.

Reynolds, A.D., 1999, Dimensions of paralic sandstone bodies: American Association of Petroleum Geologists Bulletin, v. 83, no. 2, p. 211–229, doi: 10.1306/00AA9A48-1730-11D7-8645000102C1865D.

Roehler, H.W., 1988, The Pintail coal bed and barrier bar G - a model for coal of barrier bar - lagoon origin, Upper Cretaceous Almond Formation, Rock Springs Coal Field, Wyoming: U.S. Geological Survey Professional Paper, v. 1398.

Roy, P.S., Cowell, P.J., Fernland, M.A., and Thom, B.G., 1994, Wave-dominated coasts, *in* Carter, R.W.G. and Woodroffe, C.D. eds., Coastal Evolution: Late Quaternary Shoreline Morphodynamics, Cambridge University Press, Cambridge, p. 121–186.

Sabins Jr, F.F., 1963, Anatomy of stratigraphic trap, Bisti field, New Mexico: American

Assocation of Petroleum Geologists Bulletin, v. 47, no. 2, p. 193–228, doi: 10.1126/science.58.1489.27.

Salzmann, L., Green, A., and Cooper, J.A.G., 2013, Submerged barrier shoreline sequences on a high energy, steep and narrow shelf: Marine Geology, v. 346, p. 366–374, doi: 10.1016/j.margeo.2013.10.003.

Sapozhnikov, V., and Foufoula-Georgiou, E., 1997, Experimental evidence of dynamic scaling and indications of self organized criticality in braided rivers: Water Resources Research, v. 33, no. 8, p. 1983–1991, doi: 10.1029/97WR01233.

Self, G.A., Breard, S.Q., Rael, H.P., Stein, J.A., Thayer, P.A., Traugott, M.O., and Easom, W.D., 1986, Lockhart Crossing Field: New Wilcox Trend in Southeastern Louisiana: American Association of Petroleum Geologists Bulletin, v. 70, no. 5, p. 501–515.

Shelton, J.W., 1967, Stratigraphic models and general criteria for recognition of alluvial, barrier-bar, and turbidity-current sand deposits: American Association of Petroleum Geologists Bulletin, v. 51, no. 12, p. 2441–2461, doi: 10.1306/5D25C27F-16C1-11D7-8645000102C1865D.

Short, A.D. (Ed.), 1999, Handbook of Beach and Shoreface Morphodynamics: John Wiley & Sons, Chichester.

Sixsmith, P.J., Hampson, G.J., Gupta, S., Johnson, H.D., and Fofana, J.F., 2008, Facies architecture of a net transgressive sandstone reservoir analog: the Cretaceous Hosta Tongue, New Mexico: American Association of Petroleum Geologists Bulletin, v. 92, no. 4, p. 513–547, doi: 10.1306/01020807017.

Sømme, T.O., Helland-hansen, W., Martinsen, O.J., Thurmond, J.B., Sømme, T.O., Helland-hansen, W., Martinsen, O.J., and Thurmond, J.B., 2009, Relationships between morphological and sedimentological parameters in source-to-sink systems: a basis for predicting semi-quantitative characteristics in subsurface systems: Basin Research, v. 21, no. 4, p. 361–387, doi: 10.1111/j.1365-2117.2009.00397.x.

van Straaten, L.M.J.U., 1965, Coastal barrier deposits in south- and north-Holland, in particular in the areas around Scheveningen and Ijmuiden: Neth., Geol. Sticht., Meded., N. Ser., v. 17, p. 41–75.

Stutz, M.L., and Pilkey, O.H., 2011, Open-ocean barrier islands: global influence of climatic, oceanographic, and depositional settings: Journal of Coastal Research, v. 27, no. 2, p. 207–222, doi: 10.2112/09-1190.1.

de Swart, H.E., and Zimmerman, J.T.F., 2009, Morphodynamics of tidal inlet systems: Annual Review of Fluid Mechanics, v. 41, no. 1, p. 203–229, doi: 10.1146/annurev.fluid.010908.165159.

Syvitski, J.P.M., and Milliman, J.D., 2007, Geology, geography, and humans battle for

dominance over the delivery of fluvial sediment to the coastal ocean: The Journal of Geology, v. 115, no. 1, p. 1–19, doi: 10.1086/509246.

Tizzard, P.G., and Lerbekmo, J.F., 1975, Depositional history of the Viking Formation, Suffield area, Alberta, Canada: Bulletin of Canadian Petroleum Geology, v. 22, no. 4, p. 715–752.

Vail, P.R., Mitchum Jr., R.M., and Thompson III, S., 1977, Seismic stratigraphy and global changes of sea level, part 3: relative changes of sea level from coastal onlap, *in* Payton, C.E. ed., Seismic Stratigraphy: Applications to Hydrocarbon Exploration, American Association of Petroleum Geologists Memior, 26, p. 63–81.

Van Wagoner, J.C., Posamentier, H.W., Mitchum, R.M., Vail, P.R., Sarg, J.F., Loutit, T.S., and Hardenbol, J., 1988, An overview of the fundamentals of sequence stratigraphy and key definitions, *in* Wilgus, C.K., Posamentier, H.W., Ross, C.K., and Kendall, C.G. eds., Sea-level Changes: An Integrated Approach, SEPM Special Publication, 42, Tulsa, p. 39–45.

Weidie, A.E., 1968, Bar and barrier island sands: Transactions - Gulf Coast Association of Geological Societies, v. 18, p. 405–415.

Weimer, R.J., 1966, Time-stratigraphic analysis and petroleum accumulations, Patrick Draw Field, Sweetwater County, Wyoming: American Association of Petroleum Geologist Bulletin, v. 50, p. 2150–2175, doi: 10.1306/5D25B713-16C1-11D7-8645000102C1865D.

Willis, A.J., and Moslow, T.F., 1994, Stratigraphic setting of transgressive barrier-island reservoirs with an example from the Triassic Halfway Formation, Wembley Field, Alberta, Canada: American Association of Petroleum Geologists Bulletin, v. 78, no. 5, p. 775–791, doi: 10.1306/A25FE3B5-171B-11D7-8645000102C1865D.

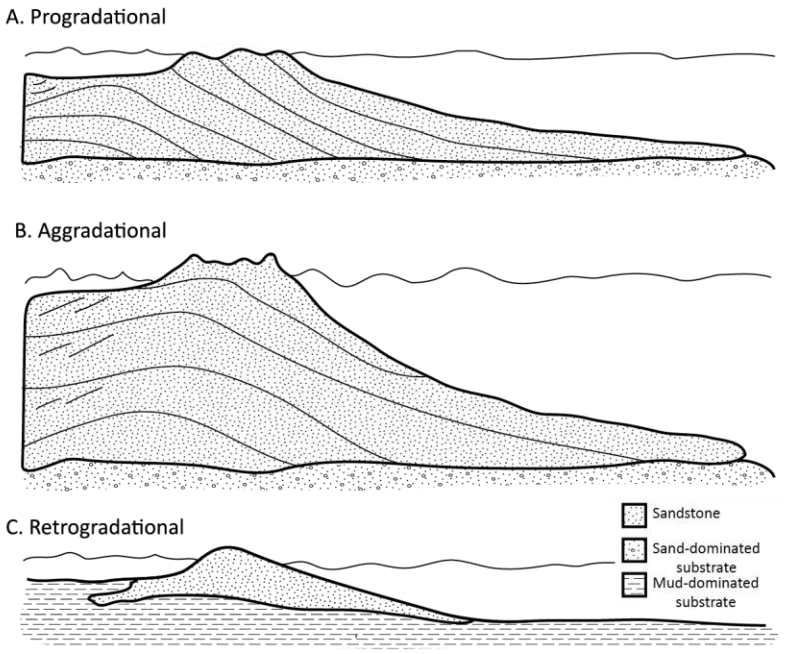

Figure 3.1. Schematic cross sections showing the three end-member types of barrier islands. (A) Progradational islands build seaward (Bernard et al., 1970). (B) Aggradational islands build vertically (Fisk, 1959; Morton, 1994). (C) Retrogradational islands move landward (Kraft and John, 1979). These sections are highly simplified, and are meant to show the overall difference in island geometry. Modified after Dickinson et al. (1972), Galloway and Hobday (1983), Moslow (1984), Galloway (1986), and Davis Jr. (1994).

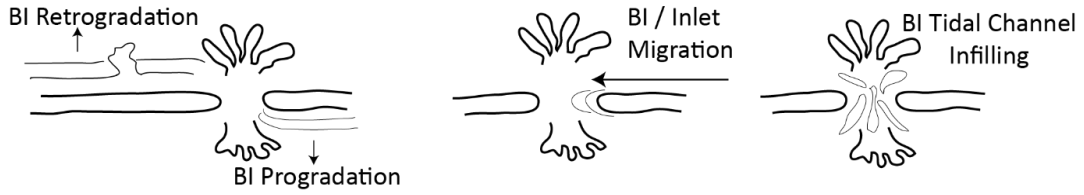

Figure 3.2. Modern barrier islands are highly ephemeral and display multiple directions of localized motion. Schematic plan-form maps show that (A) barrier islands move in the shore-perpendicular direction through basinward progradation or landward washover processes (Davis Jr., 1994). (B) Barrier islands move in the shore-parallel direction through tidal inlet migration and accretion driven by long-shore drift (Moslow and Tye, 1985; Hayes and FitzGerald, 2013). (C) Barrier islands build and accrete vertical with sufficient sediment supply and accommodation (Simms et al., 2006).

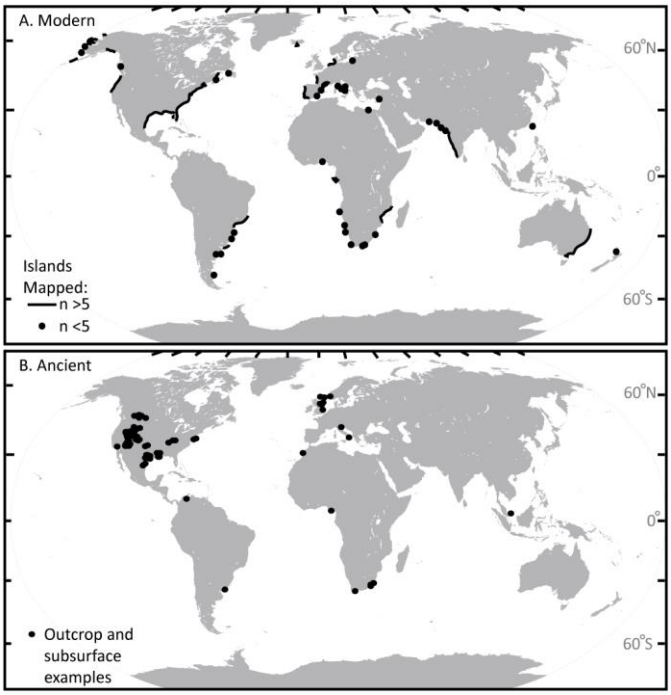

Figure 3.3. Distribution of modern (A) and ancient (B) barrier islands used in the databases.

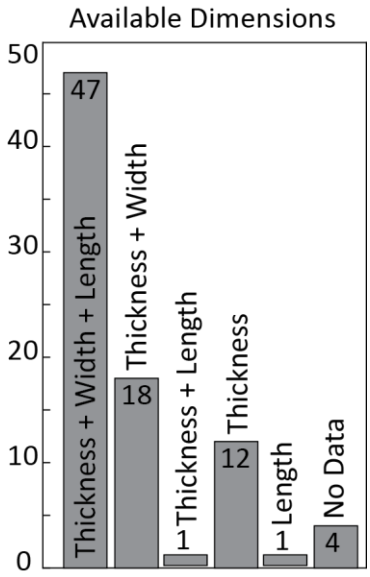

Figure 3.4. Histogram showing the dimension data available (length, width, and thickness) for the 83 ancient barrier island examples used in analysis.

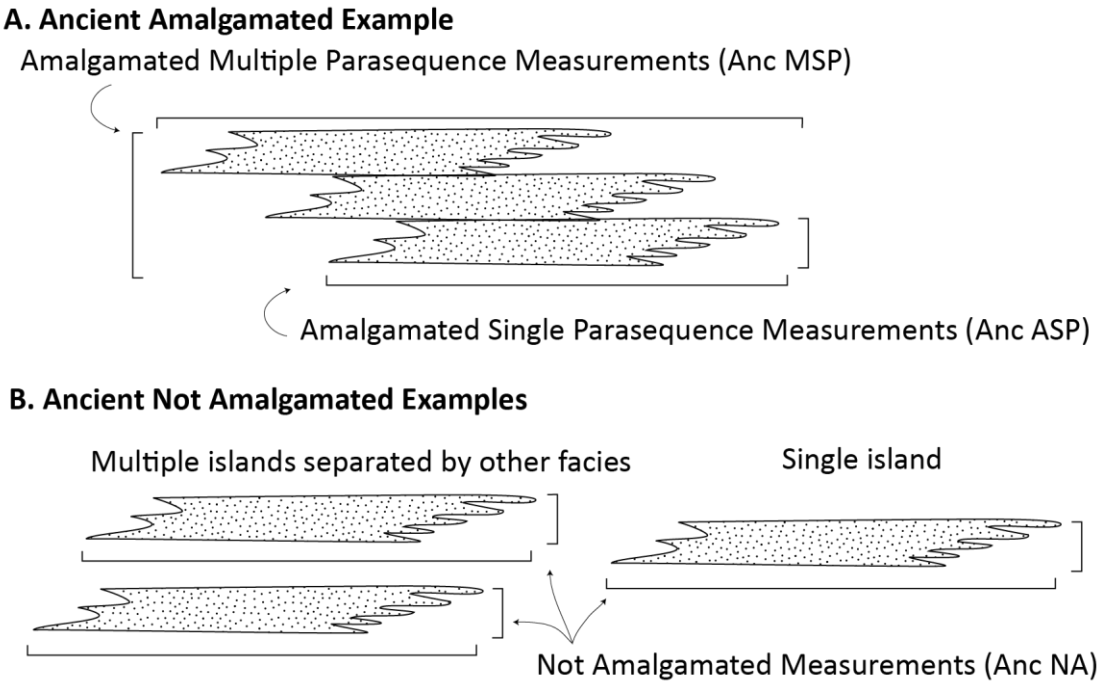

Figure 3.5. Diagram showing the ancient barrier island examples were separated by amalgamation.

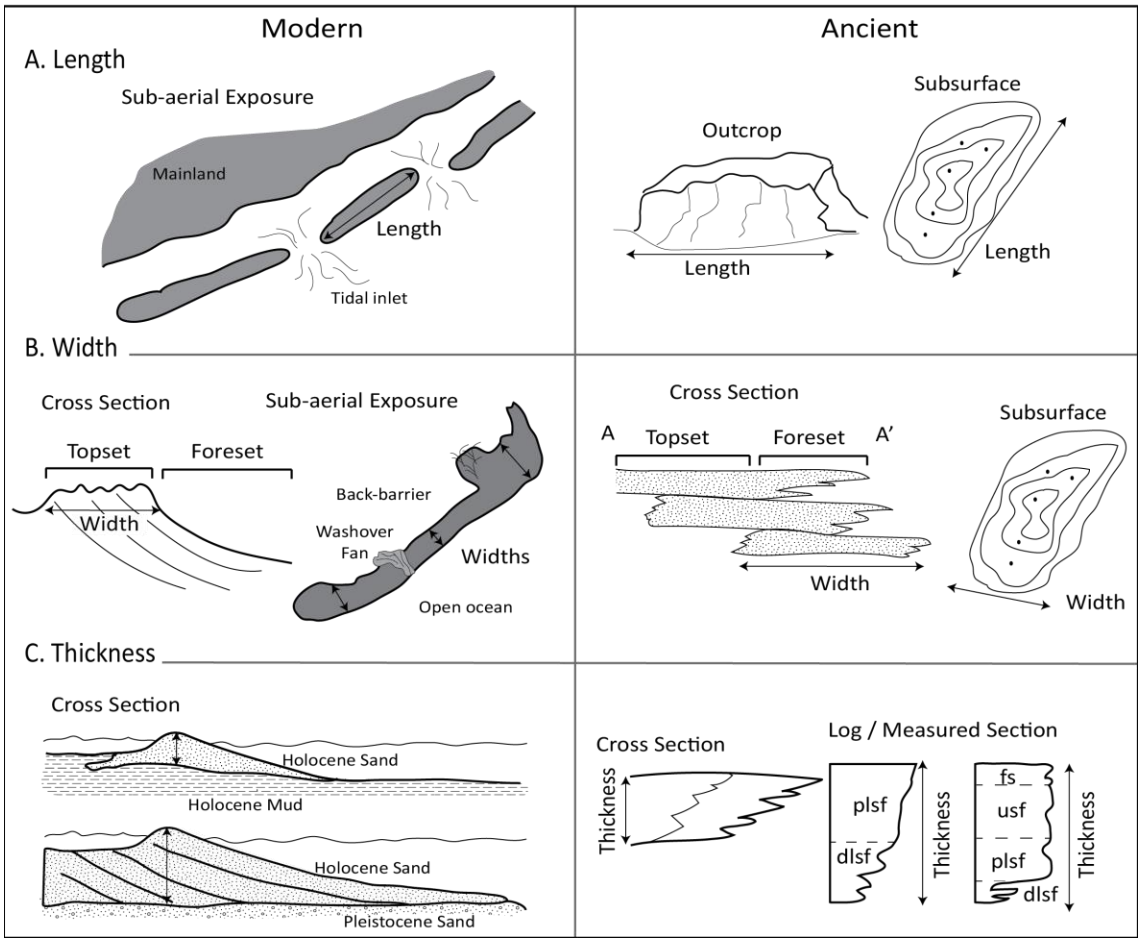

Figure 3.6. Modern and ancient barrier island measurement methods. Modern lengths (A) are measured along the island centerline parallel to the shoreline from inlet to inlet. Ancient lengths were measured in the strike direction while width are measured in the dip direction. Modern widths (B) are measured in across the island in the shore-perpendicular direction in three locations and averaged. Modern widths represent only the island topset. Ancient width measurements include both the topset and foreset width. Modern thickness (C) measurements were made to the underlying substrate. Ancient thicknesses are measured vertically through the preserved shoreface.

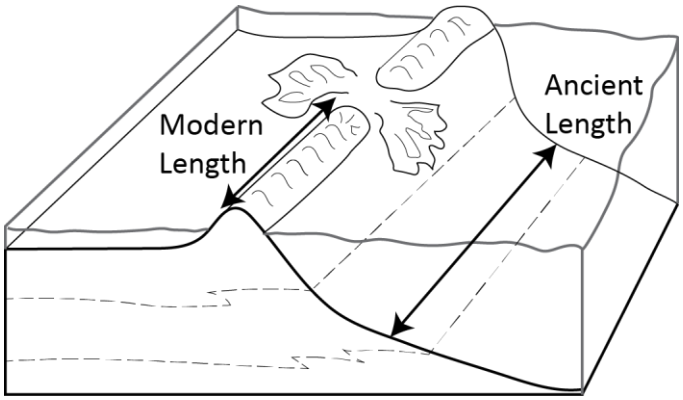

Figure 3.7. Block diagram showing the conceptual difference between modern and ancient length measurements. Modern lengths are limited by short-term inlet location while ancient lengths can span inlets, recording shore-perpendicular motion through time.

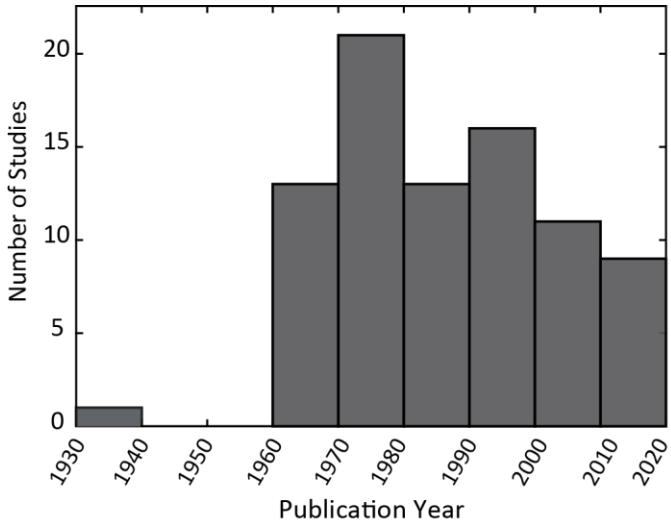

Figure 3.8. Plot of barrier island studies by publication year showing variable usage over time.

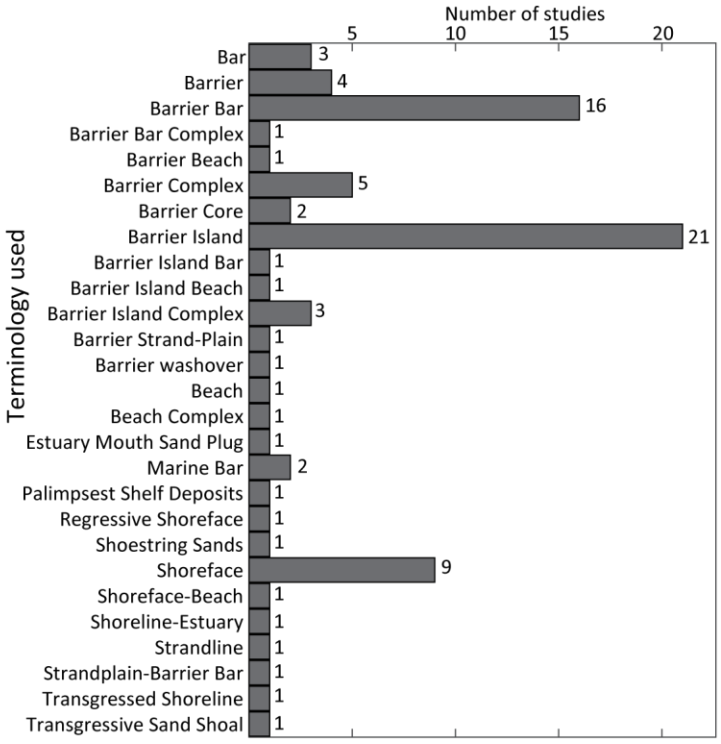

Figure 3.9. A variety of terminology is used to describe barrier islands. This bar graph shows the prevalence of each term within the database.

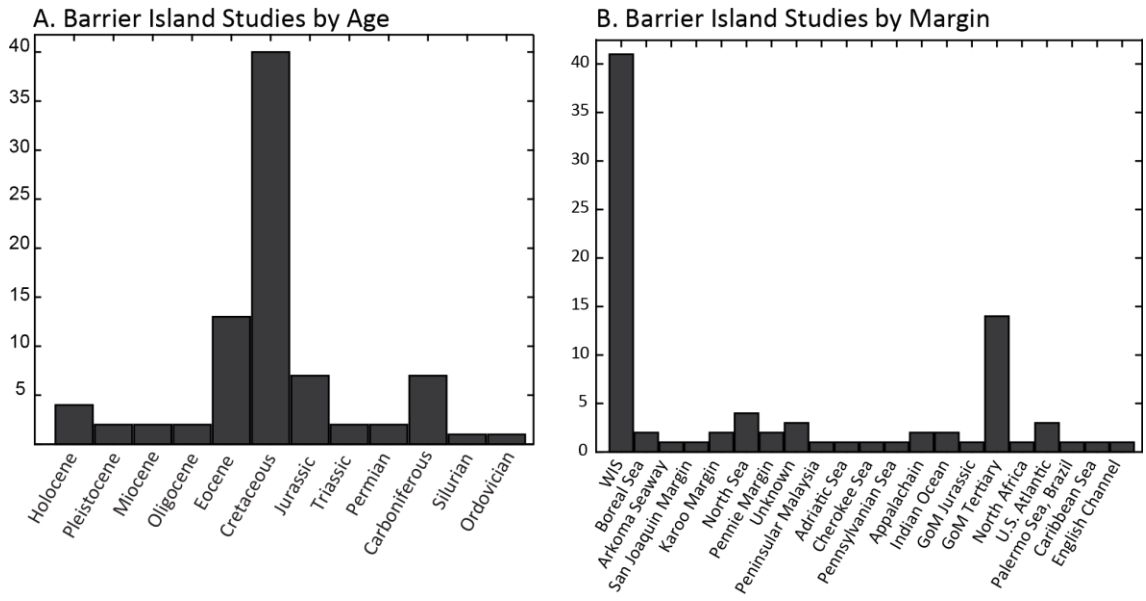

Figure 3.10 Age (A) and paleomargin (B) distribution of ancient barrier island studies.

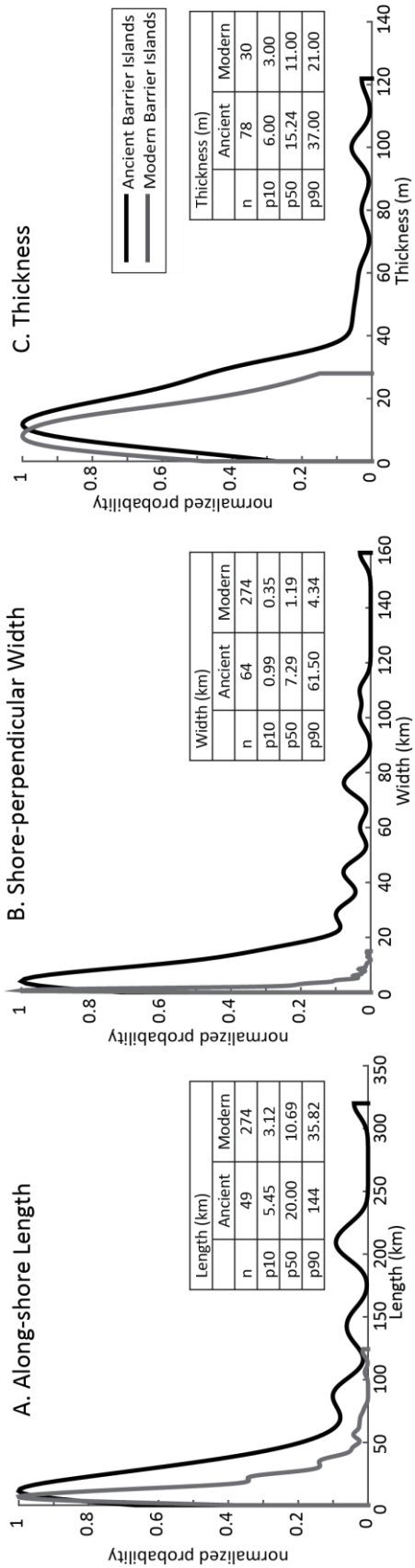

Figure 3.11. Normalized kernel distributions (nonparametric representations of the probability density function) showing the range of length (A), width (B), and thickness (C) values of modern barrier islands (gray) and ancient barrier islands (black). The lower ten percent (p10), median (p50), and upper ten percent (p90) values are listed for each dimension.

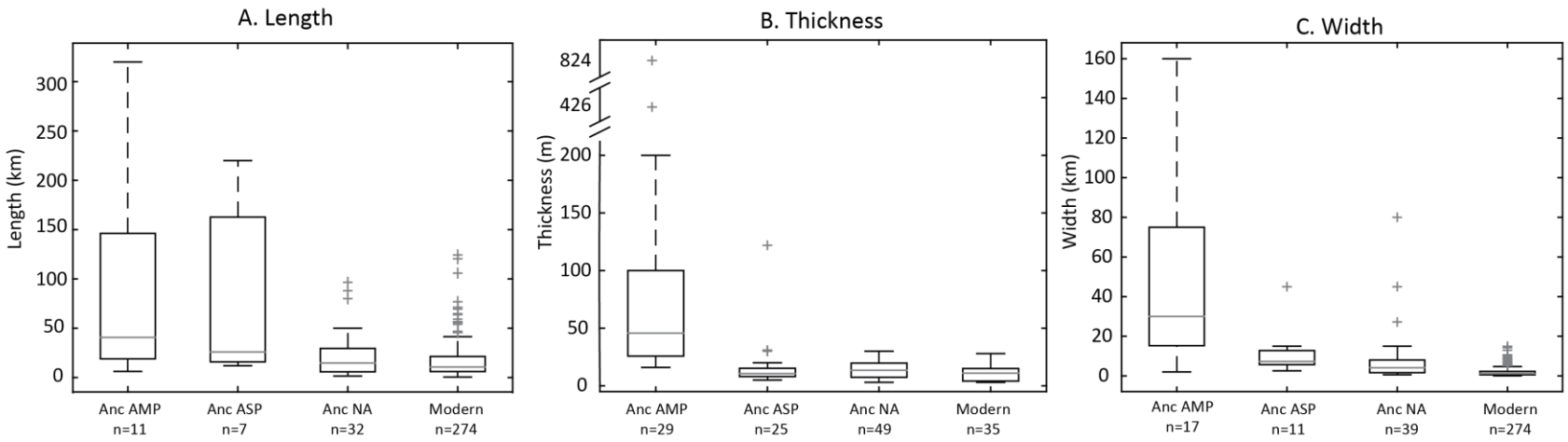

	Anc AMP	Anc ASP	Anc NA	Mod
n	11	7	32	274
p10	10.74	12.40	4.86	3.12
p50	40.70	26.00	14.7	10.69
Mean	93.00	77.53	22.28	16.18
p90	253.40	216.20	59.00	35.82

	Anc AMP	Anc ASP	Anc NA	Mod
n	29	25	49	35
p10	19.73	7.50	4.46	3.00
p50	45.72	10.50	13.50	11.00
Mean	102.90	17.29	14.04	10.96
p90	180.80	30.00	24.75	21.00

	Anc AMP	Anc ASP	Anc NA	Mod
n	17	11	39	274
p10	6.34	3.31	0.85	0.35
p50	30.00	7.24	4.08	1.19
Mean	46.36	11.15	8.01	1.90
p90	108.00	27.00	12.88	4.34

Figure 3.12. Box-and-whisker plots the ancient data separated as ancient amalgamated multiple parasequence (Anc AMP), ancient amalgamated single parasequence (Anc ASP), ancient not amalgamated (Anc NA) compared to the modern (Mod). While amalgamated ancient examples with multiple parasequences measured (Anc AMP) are larger than the other categories, comparisons between the single parasequence examples (Anc ASP and Anc NA) lend insight into barrier island preservation. Gray lines mark the median. Plus signs mark outliers. The lower ten percent (p10), median (p50), and upper ten percent (p90) values are listed for each dimension.

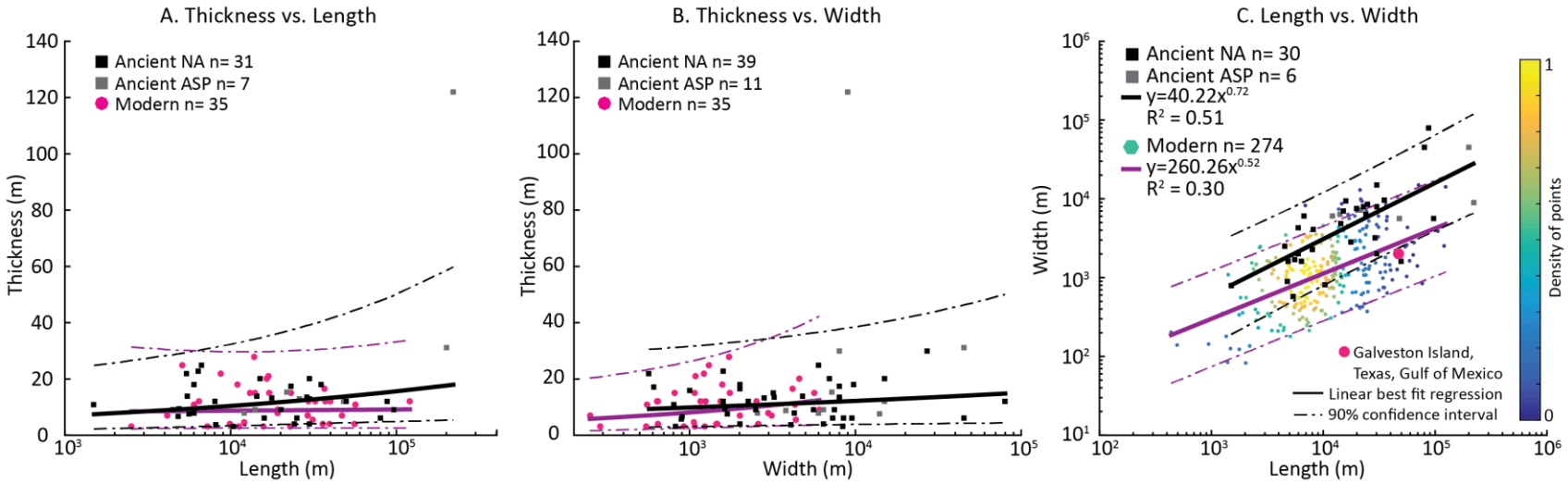

Figure 3.13. Cross plots of thickness versus length (A) and thickness versus width (B) for modern (pink), ancient not amalgamated (NA-black), and ancient amalgamated single parasequences (ASP-gray) barrier island dimensions. Length versus width (C) cross-plot showing ancient not amalgamated (NA - black), ancient amalgamated single parasequences (ASP-gray), and modern thickness data are colored by density (color bar on right), ranging from more dense data (yellow) to less dense (blue). On all three plots, the solid lines (modern: purple, ancient: black) show the best-fit trend through the data, while the dashed lines show the 10% and 90% confidence limits on the dataset. Galveston Island (pink circle) is large relative to the modern global dataset.

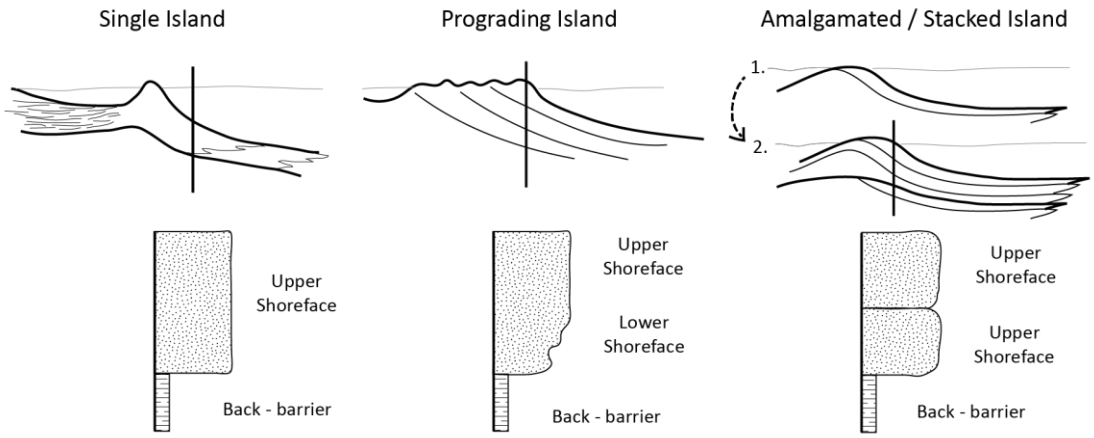

Figure 3.14. Schematic cross-sections and measured sections through barrier islands at three different stages of amalgamation. These sections illustrate that barrier island amalgamation and reworking likely increases as a function of time, therefore, most preserved barrier islands contain some degree of amalgamation. Additionally, the degree of amalgamation may be difficult to determine due to the similarity in the preserved facies.

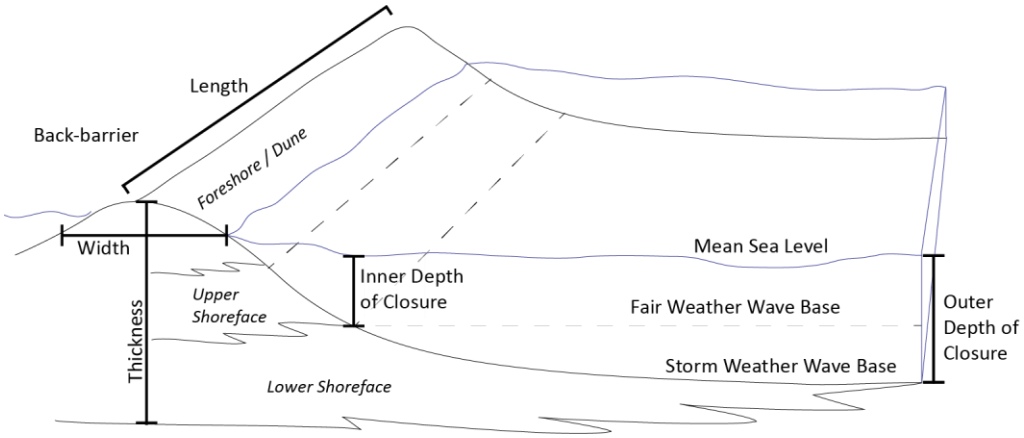

Figure 3.15. Schematic diagram of a barrier island showing the relationship between the inner and outer depth of closure and fair and storm weather wave base.

4. IS BARRIER ISLAND MORPHOLOGY A FUNCTION OF TIDAL AND WAVE REGIME?

Abstract

Classification of barrier island morphology stems from the seminal work of M. O. Hayes and others, which linked island shape to tidal range and wave height. Barrier island characterization is now assumed to be correlated to the coastal energy regime (i.e., wave-dominated, mixed energy, tide-dominated). If true, then this general relationship represents a process-based framework to link modern and ancient systems, and is key for determining paleomorphodynamic relationships. Here we present a new semiglobal database of barrier islands and spits (n=702). Shape parameters (aspect, circularity, and roundness) are used to quantify island boundary shape, and assess potential correlation with coastal energy regime using global wave and tide models. In adopting the energy classification as originally put forth (i.e., wave-dominated, wave-influenced mixed, tide-influenced mixed, tide-dominated), results show that wave-dominated islands have statistically different mean shape values from those in the mixed energy fields, but the two mixed energy designations are not distinct from each other. Furthermore, each energy regime field contains a wide range of island shapes, with no clear trends present. Linear regression modeling shows that tidal range and wave height account for less than 10% of the documented variance in island shape, a strong indication that other controls must be considered. Even when filtered by factors such as climate regime, tectonic

setting, and anthropogenic alteration, the dataset still shows similar means and ranges for barrier island shape across energy regimes, indicating complexity in the other 90% of controls. Therefore, while energy regime distinctions can be used descriptively, their utility in predicting and constraining island shape is limited: barrier island shape is not indicative of coastal energy regime, and vice versa. Our analysis also demonstrates empirical scaling relationships among modern barrier islands for the first time, with implications for subsurface prediction such as area prediction based on more easily measured length or width estimates.

Introduction

Barrier islands are dynamic and important geomorphic features, comprising 10% of the world's coastlines (Stutz and Pilkey, 2011) including large and growing population centers (Zhang and Leatherman, 2011). Barrier island characteristics and sedimentology are relatively well-documented (e.g., Leatherman, 1979; Davis Jr., 1994b; McBride et al., 2013), primarily through case studies of specific modern systems (Hayes, 1977; Heron Jr. et al., 1984; Davis Jr. and Kuhn, 1985; Moslow and Tye, 1985; Simms et al., 2006; Timmons et al., 2010) or particular coastline reaches (e.g., Hayes, 1994; Davis Jr et al., 2003; Short, 2006). The few available global perspectives mainly investigate the distribution of barrier islands (Glaeser, 1978; Henderson and Pilkey, 1989; Stutz and Pilkey, 2001, 2011; Pilkey et al., 2009), but not their morphology.

Coastal energy processes, particularly tidal range, are typically considered the primary controls on barrier island dynamics (e.g., Gierloff-Emden, 1961; Davies, 1964; Davies, 1973; Nummedal et al., 1977). Hayes (1979) made the influential observation

that barrier island shape relates to hydrodynamic regime, suggesting that tidal range and wave height dictate barrier island morphology. The hypothesis was developed through years of research (Hayes et al., 1973; Ray et al., 1973; Hayes, 1975; Hayes et al., 1976; Nummedal et al., 1977; Finley, 1978; Nummedal and Fischer, 1978; Hayden and Dolan, 1979) and summarized in a seminal figure (Hayes, 1979, Fig. 15), which plots tidal range versus wave height for 21 shorelines (Fig. 4.1). The analysis uses general island morphology (elongate or drumstick shaped) to define five different fields (Fig. 4.1): wave-dominated (WD), mixed energy, wave-dominated (MW), mixed energy, tide-dominated (MT), tide-dominated low (TDL), and tide-dominated high (TDH).

The link between barrier island shape and hydrodynamic regime stems from the hypothesis that tidal energy limits island length by inlet formation, and increases island width through welding at inlets, creating more rounded, drumstick-shaped islands on tide-dominated coasts (Hayes et al., 1973; Hayes and Kana, 1976). Conversely, barrier islands on wave-dominated coasts are primarily width-limited by washover processes (Hayes, 1979; Davis Jr., 1994a), resulting in elongate and cuspate morphologies (Ray et al., 1973). Hayes (1979) noted that climate modifies the effect of hydrodynamic regime on island morphology, and, therefore, restricted his hypothesis to temperate, mid-latitude regions.

Hayes' initial hypothesis has since been duplicated and adapted (Fig. 4.1; (Fitzgerald, 1982; Davis Jr. and Hayes, 1984; Boothroyd, 1985; Davis Jr., 1994a; FitzGerald et al., 1994; FitzGerald and Van Heteren, 1999; Stutz and Pilkey, 2011; McBride et al., 2013). Davis Jr. and Hayes (1984) recognized that tidal prism is a more direct hydrologic control than tidal range and emphasized the importance of the ratio

between tidal range and wave height, particularly along coastlines with moderate wave energy. However, the tidal range to wave height cross plot was only slightly modified in this publication (Fig. 4.1) and remains a seminal starting point for classifying coastlines.

Coastal geologists have long used tidal range and wave height to determine energy regime and infer island shape, citing the original work of Hayes (1979) and modifications of later authors (Davis Jr. and Hayes, 1984; see McBride et al., 2013 for review). Hayes' (1979) hypothesis was based on shoreline-scale observations, but it is commonly applied to individual islands. It is used to describe and classify barrier islands (e.g., Pilkey et al., 2009; Stutz and Pilkey, 2011; McBride et al., 2013; De Falco et al., 2015; Johnson et al., 2015; Taylor et al., 2015) and to infer processes. It has been applied to tidal inlets and deltas (e.g., Hubbard et al., 1979; Fitzgerald, 1982; FitzGerald, 1996; Carr-Betts et al., 2012; FitzGerald et al., 2012) and has become the basis of numerical models (e.g., Sennes et al., 2007; Olabarrieta et al., 2014; Guerin et al., 2016). Its ideas have also been used to interpret and make inferences about the rock record (e.g., Heward, 1981; Reinson, 1992; Cúneo et al., 2014).

The link between barrier island shape and hydrodynamic regime has not been revisited using modern global aerial imagery or global hydrodynamic data. This study presents a semiglobal database of morphometrics of modern barrier islands and spits and uses these data to test the assumed relationship between energy regime and island shape. Quantifying modern barrier islands and understanding controls on island morphology is a first step in developing paleomorphodynamic relationships to predict preserved barrier island geometry.

Database Development

The shape and dimensions of 702 modern barrier islands and spits were mapped from Google Earth imagery to create a spatially-referenced database (Table 4.1). Both barrier islands (visibly separated by water on all islands) and spits (partially attached; Oertel, 1985) were mapped from a variety of coastlines including those mentioned in Hayes (1979; U.S. Atlantic n=131, Alaska n=67, Iceland n=5, Gulf of Mexico n=69, German Bight n=26, Nova Scotia n=2) as well as several other coastal reaches (n_{total}=702; Fig. 4.2). The dataset is biased toward coastlines more conducive to mapping, such as those showing distinct separation between the barrier islands and the mainland. However, for the coastlines included, all visible islands and spits were mapped to limit selective sampling bias. Furthermore, the dataset encompasses a range of climate and tectonic settings (Fig. 4.2). The total length of coastlines with barrier islands included here is ~29,000 km. Both barrier islands and spits were included in analysis, but labeled separately, because they coexist in barrier island systems and are subject to the same processes (Oertel, 1985; Davis Jr., 1994a; Otvos, 2012).

Islands and spits were mapped at a scale of ~1:80,000. Each object was traced at the waterline to create a polygon, from which area and perimeter were calculated (Fig. 4.3). The attached edge of each spit was mapped with a straight line at the lateral limit of open back-barrier water (Fig. 4.3b). Length was measured in the shore-parallel direction, roughly tracing the centerline, and segmented to reflect the curvature of the island. Width was measured at three representative locations and averaged.

Barrier objects were mapped at the waterline displayed at the time of imaging and do not account for ocean elevation. This introduces some error in the above procedure

insofar as the barrier objects (islands and spits) were characterized at high, low, and middle tidal positions. The majority of the barrier objects are from low tidal range settings, however, minimizing the difference between high and low tide mappings. The back barrier segment of each object was identified as the first clear water boundary (Fig. 4.3). Marsh areas directly attached to an object were therefore included in an object's morphology. Free-standing vegetation within the lagoon clearly separated from the back-barrier edge was not included. Points were mapped densely along rugose stretches of coast and more widely spaced along straight segments. Points were then interpolated at a constant and sufficiently tight spacing to ensure no aliasing of feature geometry.

19 parameters were used to quantity object shape (Table 4.2). Aspect, circularity, and roundness are presented here, partly for simplicity, but also because they show the most differentiation, and therefore lend some insight into the range and variability of the data as a whole. Aspect compares the length and width of an object. Circularity uses area and perimeter measurements to compare island perimeter to the perimeter of a circle with the same area. Roundness compares the island area to the area of the minimum enclosing circle (Table 4.2). Combined, these three shape parameters provide a way to integrate the primary measurement types (i.e., length, width, area, and perimeter) and objectively compare barrier islands at multiple scales and locations.

Hydrodynamic data, climate, tectonic, anthropogenic alteration, and identifying information (name, state, country, continent, and margin) were assigned to each object using a variety of global databases (Table 4.1). Tidal range was determined using the TPXO 7.2 model for global ocean tides (Egbert et al., 1994; Egbert and Erofeeva, 2002; Egbert and Erofeeva, 2010). The TXPO inversion model fits the primary tidal constituent

equations to global ocean elevation data provided by the TOPEX/Poseidon satellite mission at ¼-degree resolution, providing a consistent way to determine tidal range globally. These data are similar to the values used by Hayes (Table 4.3) and to independent data (Elias and van der Spek, 2006; NOAA, 2013). In this work, tidal range was determined by summing the primary tidal constituents in the TPXO 7.2 model at the nearest grid position to each barrier object.

Mean significant wave height was determined from the NOAA WaveWatch III® version 4.18 model with hindcast reanalysis, from 2005 to 2015 (Tolman, 2014). Monthly significant wave height at the nearest grid position to each barrier object was collected over a 10-year period to produce a time-averaged quantity. As with the tidal model above, the WaveWatch III® database provides consistent global values compared to more limited buoy data.

Each object was assigned a climate designation following the Köppen-Geiger Climate Classification (Fig. 4.2a,b; Kottek et al., 2006). Tectonic classification is after Inman and Nordstrom (1971; Fig. 4.2c; Table 4.1). Anthropogenic alteration (0-3) was assigned based on visual assessment of shoreline modification and infrastructure on each island and spit (Table 4.1): 1 indicates some human infrastructure but not modification to the shoreline, 2 indicates some minor modifications to the shoreline, and 3 indicates significant modification to the shoreline (Fig. 4.2d).

The data used by Hayes (1979) were neither listed nor specifically cited, but instead attributed to a variety of studies for each coast. Therefore, the originally published measurement type and location of the tidal range and wave height values are unknown, making rigorous comparisons to the original study difficult. The tidal range

values from Hayes (1979), TPXO, and NOAA (2013) are similar for specific locations (e.g., Plum Island, MA and the Outer Banks, NC; Table 4.3) but differ for more broad reaches. Discrepancies likely result from averaging and differences in measurement location. For example, the highest tidal ranges in Bristol Bay, Alaska occur near the apex in Kvichak Bay and Nushagak Bay. However, islands mapped in this study were on the margins of the bay (200-600 km away) where the tidal range is lower (Table 4.3). Unsurprisingly, the values used by Hayes (1979), presumably to characterize the entire coastline, differ from the TPXO values. Tidal model data permit a consistent determination of tidal range by removing station location bias. Along a coastal reach tidal range varies by gauge location, with differing measurements at an open ocean buoy compared to a tidal inlet or lagoon station. Model data integrate measurements with predictive equations to create a more consistent method of comparison.

Analysis

We assessed the link between hydrodynamic regime and island morphology both qualitatively and statistically. The barrier islands and spits in each energy regime were extracted using the boundaries defined by Hayes (1979), and the range and distribution of their shape parameter values were compared (Fig. 4.4). The data were normalized using a log10 transform, and the distributions were then confirmed as normal using a Kolmogorov-Smirnov normality test (Massey Jr., 1951). ANOVA (analysis of variance (Hogg and Ledolter, 1987)) was used to statistically compare the means of the shape parameter values for the energy regimes (wave dominated (WD, n=410), mixed wave (MW, n=163), mixed tide (MT, n=113)). The number of islands in the tide-dominated

regimes (both tide-dominated low (TDL; n=12) and tide-dominated high (TDH; n=4)) are insufficient for analysis. The limited number of tide-dominated barrier objects is not a result any measurement bias in the database. It is worth re-emphasizing the point that there are simply fewer tide-dominated islands. This is the case largely because increased tidal energy limits barrier formation and stabilization, preventing shore-parallel island development (Davis Jr. and Hayes, 1984).

A statistical mean comparison tests (ANOVA, or analysis of variance) show that the normalized mean shape parameter values of the three energy regimes are not the same (Table 4.4). The multiple compares function, which reports 1:1 mean comparisons within the ANOVA, was used to assess the ANOVA output (Hochberg and Tamhane, 1987; Milliken and Johnson, 2009). Results show a statistically significant difference between the mean shape parameters for WD islands compared to both MW (p=0.00) and MT (p=0.00) islands. Barrier objects that fall within the MW and MT regimes, however, are not significantly different from each other (p=0.37-0.52). These results hold when only barrier islands are considered, versus barrier islands and spits (Table 4.4).

To determine whether variation in the sample size of barrier objects from different energy regimes influences the ANOVA results, the 1:1 mean comparison p-values for the entire dataset were compared to the results for equal sample sizes (Table 4.4). A random subset was selected from each sample set (i.e., WD, MW, MT) 500 times to test for sample size bias in the results. The minimum sample size was established in two ways. First, subselection size was determined by the minimum sample set in the database, which occurs in MT for both global barrier islands and spits (n=113) and global barrier islands (n=50). Second, a subselection size n=25 (roughly half the size of the minimum

number of samples in the MT regime) was also assessed. The mean p-values from those 500 selections are shown (Table 4.4). The mean p-value for the random subsets of the minimum sample size (n=113 and n=50) are similar to the results from the entire dataset. However, the mean p-value for random subsets with a set sample size (n=25) do not match the entire dataset. This demonstrates that variation in sample size present in the database does not fundamentally affect the results. A sample size of 25 is insufficient however, and indicates that a minimum number of barrier objects (~50 samples) are needed for statistical comparison. Thus omitting tide-dominated low (TDL, n=12) and tide-dominated high (TDH, n=4) from statistical analysis is justified. This also points to a likely under-representation of tide-dominated barrier islands (n=21) in the original classification (Hayes, 1979).

We used linear regression modeling to assess the dependence of island shape on tidal range and wave height for the entire dataset, without extracting the values by energy regime (Table 4.5). In the analysis, an ordinary least-squares approach was used to fit the response variables (shape parameters) to the data (tidal range and wave height). Although our model shows that island shape is dependent on tidal range (p=0.00) and wave height (p=0.00), these factors combined account for only 8.7 - 9.5% of the variance in island shape (Table 4.5).

Discussion

Analysis of a semiglobal database of barrier objects shows that the mean WD island shapes are statistically different from MW and MT islands, partly supporting Hayes' hypothesis. The decreased number of tide-dominated islands (n=16) relative to

wave-dominated (n=410) and mixed energy (n=279) supports the argument that tidal energy limits island formation and prevalence (Hayes, 1979; Davis Jr. and Hayes, 1984; Stutz and Pilkey, 2011). However, the variability and range of shape values within each energy regime limit the predictive power and utility of this approach (Fig. 4.4). The range of WD island shapes encompasses 87-100% of the range of the entire dataset (Table 4.6), reducing the utility of direct mean comparisons (ANOVA; Table 4.4). For example, if we consider only aspect values (Fig. 4.5), the most round islands (p10) and the most elongate (p90) plot across all three energy regimes. Conversely, islands along a single coastline with similar tidal range and wave heights can have drastically different shapes (Fig. 4.6). Combined, these plots (Figs. 4.5 and 4.6) show that tidal range and wave height do not effectively predict island shape and vice versa.

Davis Jr. and Hayes (1984) revised Hayes' initial hypothesis (Fig. 4.1), arguing, among other things, that the tidal range to wave height ratio is important for determining island shape. Cross-plots comparing tidal range to wave height ratio versus shape parameter values (Fig. 4.7) do not show any distinct trends even within the revised fields (Fig. 4.1). This suggest no correlation between tidal range to wave height ratio and island shape. Davis Jr. and Hayes (1984) recognized that elongate morphologies can develop on coasts with high tidal ranges (>3 m), and that drumstick morphologies can develop in areas with low wave energy (0.3 m). Islands of similar shape occur on each of the coastlines used by Hayes (Fig. 4.8), despite differing tidal range and wave height conditions.

Tidal range and wave height account for less than 10% of the variance in island shape (Table 4.5), negating much of the predictive utility of Hayes' hypothesis. The other

factors controlling >90% of island shape are complex and beyond the scope of this paper to fully investigate, but some key considerations are highlighted here. Hayes (1979) briefly discussed climate and tectonics in his original work, and suggested that the link between island shape and hydrodynamic regime is only valid along temperate, mid-latitude coasts. He hypothesized that ice cover, vegetation, and lithology would alter island morphology in polar and tropical climates. Hayes also only considered islands on coasts classified as trailing edge (i.e., passive margin) and marginal sea (partially enclosed passive margins) coasts by Inman and Nordstrom (1971). Filtering the database using climate and tectonics shows that the subgroups (e.g., islands in temperate climates) have shape value ranges similar to the global dataset (Fig. 4.9). Similarly, anthropogenic alteration clearly changes island shape, restricts island motion, or both in heavily developed areas (Stutz and Pilkey, 2005). Anthropogenically altered and unaltered islands span the same range of islands as the global dataset (Fig. 4.9). These filtered subsets indicate that limiting the dataset based on climate, tectonics, or alteration does not improve the broad viability of Hayes' hypothesis. We conclude that additional analysis is needed to determine how climate, tectonics, and alteration influence island morphology.

In addition to the global scale processes mentioned by Hayes, a variety of regional factors contribute to barrier island morphology. The underlying substrate (Mellett et al., 2012; Cooper et al., 2012) and pre-existing topography (Oost et al., 2012) can dictate island formation and motion. Shelf slope (Swift, 1975; Glaeser, 1978; Zecchin et al., 2011) and width (Curray, 1965) affect accommodation and, consequently, island development, shape, and motion (Roy et al., 1997). Relative sea level change also influences island motion, and consequently, island shape (Davis Jr., 1994b; Leatherman

et al., 2000; Zhang et al., 2002; Fruergaard et al., 2015). The lateral shoreline characteristics (headlands and embayment geometry (Roy et al., 1997)), proximal sub-environments (estuaries or deltas), and longshore currents (Simms et al., 2006; Aagaard, 2011), contribute to sediment availability and size (Nielsen et al., 1988; FitzGerald et al., 1994) and resulting island morphology. The magnitude and prevalence of storms (Kochel and Dolan, 1986; Morton, 2002; Houser et al., 2008; Shaw et al., 2014) can control the spatial distribution of sand within the barrier island system (Masselink and van Heteren, 2014).

Davis and Hayes (1984) also explored how the tidal prism may exert a more significant control on the motion of sediment than the tidal range (Gao and Collins, 1994). Tidal prism is the volume of water that flows through the tidal inlet between high and low tide; it is dependent on the tidal range, the surface area of the back barrier (O'Brien, 1969; Jarrett, 1976). The link between tidal prism and island morphology has long been recognized (Nummedal et al., 1977; Nummedal and Fischer, 1978) and plots comparing tidal range to tidal prism show two orders of magnitude variation in tidal prism along U.S. coastlines with consistent tidal ranges (Davis Jr. and Hayes, 1984). Despite these observations, energy regimes based on tidal range, rather than tidal prism, continue to be used describe and classify islands (Fig. 4.1 and references therein), perhaps because tidal prism is more complicated and less easily measured, and less commonly reported than tidal range.

The controls on sand movement with barrier island systems are inherently complex. Hayes (1979) argued that a high proportion of wave energy relative to tidal energy would increase the likelihood of washover, causing islands to remain narrow.

However, washover processes, and consequently island width, have also been linked to storm prevalence (Kochel and Dolan, 1986; Houser et al., 2008; Shaw et al., 2014), back barrier erosion (Timmons et al., 2010) and relative sea level change (Leatherman, 1983). Sand lobe accretion (or welding) at the margins of tidal inlets is described as a differentiating mechanism, creating 'drumstick' shaped islands attributed to meso-tidal and mixed energy coasts (Hayes et al., 1976; Hayes and Kana, 1976). Welding occurs on barrier islands traditionally considered to be both elongate (Moslow and Heron, 1994) and drumstick shaped (Hayes, 1994), and this could be contributing to the spectrum of island planforms observed globally. Similarly, inlet spacing and prevalence can be controlled by the location of storm scour channels and paleovalleys (Hayes and FitzGerald, 2013), in addition to tidal processes. Therefore, utilizing only tidal range and wave height overlooks other potential controls on sand motion at the shoreline. Though currently investigated at small scales (Masselink and Puleo, 2006; Herrling and Winter, 2014), bed-load shear stress could be a more accurate way to describe the combined effects of wave and currents on sand at the shoreface (Ward et al., 2015), eliminating the need for energy proxies (tidal range and wave height).

Ultimately, the above-mentioned processes contribute to the >90% of island shape variability not explained by tidal range and wave height, and we predict that the importance of each contributing factor varies by coastline. We argue that coastlines may need to be considered at a broader scales (100s of km) to understand the controls on island shape acting along individual margins (e.g., Hayes et al., 1976; Hayes, 1994; Morton, 1994). Island shape may be too nuanced and system-specific for global classification beyond Hayes' hypothesis. Further analysis is needed to determine whether

other processes can be used to define more predictive relationships between hydrodynamic regime and island morphology, and whether the energy regime boundaries need to be redefined or abandoned. In the meantime, Hayes' hypothesis should be used as it was initially designed, to describe the energy regime of broad coastlines, rather than to predict island shape.

Morphodynamic Implications

In addition to testing the link between tide and wave dominance on island shape, this new dataset permits quantitative inspection of barrier island size and geometry. Crossplots of barrier island and spit dimensions show the following scaling relationships: length:area, area:width, length:perimeter, length:width, and area:perimeter (Fig. 4.10). We argue that these results can be used predictively, and that they may help elucidate the underlying process controls. For example, if island length is known, then one can use the database to empirically constrain island area. These relationships are particularly useful in the ancient, where planform constraints are typically lacking.

The data also show the range of modern barrier island dimensions, which can help researchers select appropriate modern analogs. For example, barrier islands along the Texas Gulf of Mexico coast, particularly Galveston Island (Bernard et al., 1962), are commonly used as analogs for ancient barrier islands (Miller Jr., 1962; Shelton, 1967; Davies and Berg, 1969; Klein, 1974; Tizzard and Lerbekmo, 1975; Chiang, 1984). This dataset shows that the Texas barrier islands are large relative to global values (Fig. 4.10), suggesting they may not be appropriate analogs for all ancient systems. Ideas and understanding of modern barrier islands form the basis of ancient depositional models

and interpretations (Barwis and Hayes, 1979; Reinson, 1979; Galloway and Hobday, 1983; Galloway, 1986; Reinson, 1992). Quantitative understanding of modern controls and processes is fundamental to the development of paleomorphodynamic relationships and predicting barrier island reservoir geometries from subsurface data.

Conclusions

A semiglobal database of barrier island and spit plan-form geometry is constructed to test the long-standing relationships between coastal processes, expressed through wave height and tidal range, and island shape. Analysis of barrier island and spit morphology, quantified using aspect, circularity, and roundness parameters, shows that Hayes' hypothesis is statistically correct when comparing mean shape values of barrier objects in the wave-dominated (WD) regime to those in the mixed wave (MW) and mixed tide (MT) regimes. Mean shape values within the mixed-energy regimes are not statistically distinct. There is significant overlap and a wide range of shapes distributed across the WD, MW, and MT regimes, which makes the differentiation of island shape by energy regime impractical and nonrigorous. This result is supported by linear regression between coastal energy and morphology, which demonstrates that tidal range and wave height contribute less than 10% of island shape variance. Thus, a combination of other factors plays a large cumulative role in determining island planform. At this point, however, the mechanisms by which they contribute to barrier morphology remains unclear. For example, filtered subsets of the global database, such as climate or tectonic setting (cf. Hayes, 1979), show similar shape parameter ranges to the global dataset, as do anthropogenically altered and unaltered islands.

This analysis highlights the likelihood of a larger number of controlling variables in shaping barrier islands, such as sediment supply, substrate, relative sea level change, shelf morphology, and tidal prism. Moreover, the variability of individual barrier island morphology indicates that the controls and processes acting in one location may not be applicable at the global scale. Broadly, this analysis encourages a departure from directly linking barrier island planform to energy regime (at least as currently focused) and instead highlights the need to explore a wider array of possible relationships between island morphology and other controlling variables.

Lastly, morphometric data collected on barrier islands and spits show empirical scaling between length:area, area:width, length:perimeter, length:width, and area:perimeter, likely indicating underlying correlations surrounding the growth of depositional landscapes. The relationships are useful for subsurface scale estimation because planform data are typically sparse.

Acknowledgements

This research would not have been possible without the impressive and detailed work of M. O. Hayes and his contemporaries. We thank the sponsors of the Rocks2Models Consortium at the University of Utah, and C. Johnson's co-PI L. Stright. We appreciate access to GoogleEarth and acknowledge MatLab for academic software licenses. We thank our reviewers for their valuable contributions during the editing process.

References

Aagaard, T., 2011, Sediment transfer from beach to shoreface: the sediment budget of an accreting beach on the Danish North Sea Coast: Geomorphology, v. 135, no. 1-2, p. 143–157, doi: 10.1016/j.geomorph.2011.08.012.

Barwis, J.H., and Hayes, M.O., 1979, Regional patterns of modern barrier island and tidal inlet deposits as applied to paleoenvironmental studies, *in* Ferm, J.C., Horne, J.C., Weisenfluh, G.A., and Staub, J.R. eds., Carboniferous Depositional Environments in the Appalachian Region, University of South Carolina Geology Department, Columbia, S.C., p. 472–498.

Bernard, H.A., LeBlanc, R.J., and Major, C.F., 1962, Recent and Pleistocene geology of southeast Texas, Field excursion no. 3, *in* Rainwater, E.H. and Zingula, R.P. eds., Geology of the Gulf Coast and Central Texas and Guidebook of Excursions, Houston Geological Society, Houston, Texas, p. 175–224.

Boothroyd, J.C., 1985, Tidal inlets and tidal deltas, *in* Davis Jr., R.A. ed., Coastal Sedimentary Environments, Springer-Verlag, New York, p. 445–532.

Carr-Betts, E., Beck, T.M., and Kraus, N.C., 2012, Tidal inlet morphology classification and empirical determination of seaward and down-drift extents of tidal inlets: Journal of Coastal Research, v. 28, no. 3, p. 547–556, doi: 10.2112/JCOASTRES-D-11-00124.1.

Center for Operational Oceanographic Products and Services, 2013, Tides and Currents Maps: National Oceanic and Atmospheric Administration.

Chiang, K.K., 1984, The giant Hoadley gas field, south-central Alberta, *in* Masters, J.A. ed., Elmworth: Case Study of a Deep Basin Gas Field, American Association of Petroleum Geologists Memior, 38, p. 297–313.

Cúneo, N.R., Gandolfo, M.A., Zamaloa, M.C., and Hermsen, E., 2014, Late Cretaceous aquatic plant world in Patagonia, Argentina: PLoS ONE, v. 9, no. 8, p. 1–18.

Curray, J.R., 1965, Late Quaternary history, continental shelves of the United States, *in* Wright, H.E. and Frey, D.G. eds., The Quaternary of the United States, Princeton University Press, Princeton, New Jersey, p. 723–735.

Davies, J.L., 1964, A morphogenic approach to world shorelines: Zeitschrift für Geomorphologie, v. 8, p. 127–142.

Davies, J.L., 1973, Geographical Variation in Coastal Development: Oliver and Boyd, Edinburgh, 204 p.

Davies, D.K., and Berg, R.R., 1969, Sedimentary characteristics of Muddy barrier-bar reservoir and lagoonal trap at Bell Creek Field, *in* The Economic Geology of Eastern Montana and Adjacent Areas 20th Annual Conference 1969 Eastern Montana Symposium Oct 19-22, 1969, Montana Geological Society, Billings, p. 97–105.

Davis Jr, R.A., Yale, K.E., Pekala, J.M., and Hamilton, M. V., 2003, Barrier island stratigraphy and Holocene history of west-central Florida: Marine Geology, v. 200,

no. 1–4, p. 103–123, doi: http://dx.doi.org/10.1016/S0025-3227(03)00179-8.

Davis Jr., R.A., 1994a, Barrier island systems- a geologic overview, *in* Davis Jr., R.A. ed., Geology of Holocene Barrier Island Systems, Springer-Verlag, Berlin, p. 1–46.

Davis Jr., R.A. (Ed.), 1994b, Geology of Holocene Barrier Island Systems: Berlin, 464 p.

Davis Jr., R.A., and Hayes, M.O., 1984, What is a wave-dominated coast? Marine Geology, v. 60, no. 1–4, p. 313–329, doi: http://dx.doi.org/10.1016/0025-3227(84)90155-5.

Davis Jr., R.A., and Kuhn, B.J., 1985, Origin and development of Anclote Key, west-peninsular Florida: Marine Geology, v. 63, no. 1, p. 153–171, doi: http://dx.doi.org/10.1016/0025-3227(85)90082-9.

Egbert, G.D., Bennett, A.F., and Foreman, M.G.G., 1994, TOPEX/POSEIDON tides estimated using a global inverse model: Journal of Geophysical Research, v. 99, no. C12, p. 24821–24852, doi: 10.1029/94JC01894.

Egbert, G.D., and Erofeeva, S.Y., 2002, Efficient inverse modeling of barotropic ocean tides: Journal of Atmospheric and Oceanic Technology, v. 19, no. 2, p. 183–204, doi: 10.1175/1520-0426(2002)019<0183:EIMOBO>2.0.CO;2.

Egbert, G., and Erofeeva, L., 2010, The OSU TOPEX/Poseidon Global Inverse Solution TPXO: Oregon State University.

Elias, E.P.L., and van der Spek, A.J.F., 2006, Long-term morphodynamic evolution of Texel Inlet and its ebb-tidal delta (The Netherlands): Marine Geology, v. 225, no. 1–4, p. 5–21, doi: 10.1016/j.margeo.2005.09.008.

De Falco, G., Antonioli, F., Fontolan, G., Lo Presti, V., Simeone, S., and Tonielli, R., 2015, Early cementation and accommodation space dictate the evolution of an overstepping barrier system during the Holocene: Marine Geology, v. 369, p. 52–66, doi: 10.1016/j.margeo.2015.08.002.

Finley, R.J., 1978, Ebb-tidal delta morphology and sediment supply in relation to seasonal wave energy flux, North Inlet, South Carolina: Journal of Sedimentary Petrology, v. 48, no. 1, p. 227–238, doi: 10.1306/212F743C-2B24-11D7-8648000102C1865D.

FitzGerald, D.M., 1996, Geomorphic variability and morphologic and sedimentologic controls on tidal inlets: Journal of Coastal Research, v. SI, no. 23, p. 47–71.

Fitzgerald, D.M., 1982, Sediment bypassing at mixed energy tidal inlets, *in* Edge, B.L. ed., 18th International Conference on Coastal Engineering, p. 1094–1118.

FitzGerald, D.M., Buynevich, I., and Hein, C., 2012, Morphodynamics and facies architecture of tidal inlets and tidal deltas, *in* Davis Jr, R.A. and Dalrymple, R.W. eds., Principles of Tidal Sedimentology, Springer Netherlands, Dordrecht, p. 301–333.

FitzGerald, D.M., and Van Heteren, S., 1999, Classification of paraglacial barrier

systems: Coastal New England, USA: Sedimentology, v. 46, no. 6, p. 1083–1108, doi: 10.1046/j.1365-3091.1999.00266.x.

FitzGerald, D.M., Rosen, P.S., and van Heteren, S., 1994, New England barriers, *in* Davis Jr., R.A. ed., Geology of Holocene Barrier Island Systems, Springer-Verlag, Berlin, p. 305–394.

Fruergaard, M., Møller, I., Johannessen, P.N., Nielsen, L.H., Andersen, T.J., Nielsen, L., Sander, L., and Pejrup, M., 2015, Stratigraphy, evolution, and controls of a holocene transgressive – regressive barrier island under changing sea level: Danish North Sea coast: Journal of Sedimentary Research, v. 85, no. 7, p. 820–844.

Galloway, W.E., 1986, Reservoir facies architecture of microtidal barrier systems: American Association of Petroleum Geologists Bulletin, v. 70, no. 7, p. 787–808, doi: 10.1306/9488634E-1704-11D7-8645000102C1865D.

Galloway, W.E., and Hobday, D.K. (Eds.), 1983, Terrigenous Clastic Depositional Systems: Applications to Petroleum, Coal, and Uranium Exploration: Springer-Verlag, New York, 423 p.

Gao, S., and Collins, M., 1994, Tidal inlet equilibrium, in relation to cross-sectional area and sediment transport patterns: Estuarine, Coastal and Shelf Science, v. 38, no. 2, p. 157–172, doi: http://dx.doi.org/10.1006/ecss.1994.1010.

Gierloff-Emden, H.G., 1961, Nehrungen und Lagunen: Petermanns Geographische Mitteilungen, p. 81–92.

Glaeser, J.D., 1978, Global distribution of barrier islands in terms of tectonic setting: The Journal of Geology, v. 86, no. 3, p. 283–293.

Guerin, T., Bertin, X., and Dodet, G., 2016, A numerical scheme for coastal morphodynamic modelling on unstructured grids: Ocean Modelling, v. 104, p. 45–53, doi: 10.1016/j.ocemod.2016.04.009.

Hayden, B., and Dolan, R., 1979, Barrier islands, lagoons, and marshes: Journal of Sedimentary Research, v. 49, no. 4, p. 1061–1071, doi: 10.1306/212F78B0-2B24-11D7-8648000102C1865D.

Hayes, M.O., 1979, Barrier island morphology as a function of tidal and wave regime, *in* Leatherman, S.P. ed., Barrier Islands from the Gulf of Mexico to the Gulf of St. Lawrence, Academic Press, New York, p. 1–28.

Hayes, M.O., 1977, Development of Kiawah Island, South Carolina: Symposium of the Waterway, Port, Coastal and Ocean Division of ASCE, , no. 5, p. 828–847.

Hayes, M.O., 1975, Morphology of sand accumulation in estuaries: an introduction to the symposium, *in* Cronin, L.E. ed., Geology and Engineering, Academic Press, New York, N.Y., p. 3–22.

Hayes, M.O., 1994, The Georgia Bight barrier system, *in* Davis Jr., R.A. ed., Geology of Holocene Barrier Island Systems, Springer-Verlag, Berlin, p. 233–304.

Hayes, M.O., and FitzGerald, D.M., 2013, Origin, evolution, and classification of tidal inlets: Journal of Coastal Research, v. 69, p. 14–33, doi: 10.2112/SI_69_3.

Hayes, M.O., and Kana, T.W. (Eds.), 1976, Terrigenous clastic depositional environments: Technical Report - Coastal Research Division, Department of Geology, University of South Carolina, 184 p.

Hayes, M.O., Owens, E.H., Hubbard, D.K., and Abele, R.W., 1973, The investigation of form and processes in the coastal zone, *in* Coastal Geomorphology, Part 1, Coastal Processes, Publ. Geomorphol., State Univ. New York, Binghamton, New York, p. 11–41.

Hayes, M., Ruby, C.H., Stephen, M.F., and Wilson, S.J., 1976, Geomorphology of the southern coast of Alaska, *in* Coastal Engineering, p. 1992–2008.

Henderson, V., and Pilkey, O.H., 1989, Global controls on barrier island chain morphology: Gulf Coast Association of Geological Societies Transactions, v. 39, p. 385–385.

Heron Jr., S.D., Moslow, T.F., Berelson, W.M., Herbert, J.R., Steele III, G.A., and Susman, K.R., 1984, Holocene sedimentation of a wave-dominated barrier island shoreline: Cape Lookout, North Carolina: Marine Geology, v. 60, no. 1–4, p. 413–434, doi: http://dx.doi.org/10.1016/0025-3227(84)90160-9.

Herrling, G., and Winter, C., 2014, Morphological and sedimentological response of a mixed-energy barrier island tidal inlet to storm and fair-weather conditions: Earth Surface Dynamics, v. 2, no. 1, p. 363–382, doi: 10.5194/esurf-2-363-2014.

Heward, A.P., 1981, A review of wave-dominated clastic shoreline deposits: Earth-Science Reviews, v. 17, no. 3, p. 223–276, doi: http://dx.doi.org/10.1016/0012-8252(81)90022-2.

Hochberg, Y., and Tamhane, A.C., 1987, Multiple Comparison Procedures: John Wiley & Sons, New York, 450 p.

Hogg, R., and Ledolter, J., 1987, Engineering Statistics (MacMillan, Ed.): New York, 442 p.

Houser, C., Hapke, C., and Hamilton, S., 2008, Controls on coastal dune morphology, shoreline erosion and barrier island response to extreme storms: Geomorphology, v. 100, p. 223–240, doi: 10.1016/j.geomorph.2007.12.007.

Hubbard, D.K., Oertel, G., and Nummedal, D., 1979, The role of waves and tidal currents in the development of tidal-inlet sedimentary structures and sand body geometry: examples from North Carolina, South Carolina, and Georgia: Journal of Sedimentary Research, v. 49, no. 4, p. 1073–1091, doi: 10.1306/212f78b5-2b24-11d7-8648000102c1865d.

Inman, D.L., and Nordstrom, C.E., 1971, On the tectonic and morphologic classification of coasts: The Journal of Geology, v. 79, no. 1, p. 1–21, doi: 10.2307/30060828.

Jarrett, J.T., 1976, Tidal prism-inlet area relationships, *in* GITI Report 3: General

Investigations of Tidal Inlets, Coastal Engineering Research Center, Army Corps of Engineers, Ft. Belvoir, Virginia, p. 1–32.

Johnson, J.M., Moore, L.J., Ells, K., Murray, A.B., Adams, P.N., Mackenzie, R.A., and Jaeger, J.M., 2015, Recent shifts in coastline change and shoreline stabilization linked to storm climate change: Earth Surface Processes and Landforms, v. 40, no. 5, p. 569–585, doi: 10.1002/esp.3650.

Klein, G. deVries, 1974, Estimating water depths from analysis of barrier island and deltaic sedimentary sequences: Geology, v. 2, no. 8, p. 409–412, doi: 10.1130/0091-7613(1974)2<409:EWDFAO>2.0.CO;2.

Kochel, R.C., and Dolan, R., 1986, The role of overwash on a Mid-Atlantic Coast barrier island: The Journal of Geology, v. 94, no. 6, p. 902–906.

Kottek, M., Grieser, J., Beck, C., Rudolf, B., Rubel, F., Centre, P.C., and Wetterdienst, D., 2006, World map of the Köppen-Geiger climate classification updated: Meteorologische Zeitschrift, v. 15, no. 3, p. 259–263, doi: 10.1127/0941-2948/2006/0130.

Leatherman, S.P., 1983, Barrier island evolution in response to sea level rise: a discussion: Journal of Sedimentary Petrology, v. 53, no. 3, p. 1026–1033.

Leatherman, S.P. (Ed.), 1979, Barrier islands from the Gulf of St. Lawrence to the Gulf of Mexico: Academic Press, New York, 325 p.

Leatherman, S.P., Zhang, K., Douglas, B.C., Carolina, N., and Carolina, S., 2000, Sea level rise shown to drive coastal erosion: Eos, v. 81, no. 6, p. 55–57, doi: 10.1029/00EO00034.

Masselink, G., and van Heteren, S., 2014, Response of wave-dominated and mixed-energy barriers to storms: Marine Geology, v. 352, p. 321–347, doi: 10.1016/j.margeo.2013.11.004.

Masselink, G., and Puleo, J.A., 2006, Swash-zone morphodynamics: Continental Shelf Research, v. 26, no. 5, p. 661–680, doi: http://dx.doi.org/10.1016/j.csr.2006.01.015.

Massey Jr., F.J., 1951, The Kolmogorov-Smirnov test for goodness of fit: Journal of the American Statistical Association, v. 46, no. 253, p. 68–78.

McBride, R.A., Anderson, J.B., Buynevich, I. V, Cleary, W., Fenster, M.S., FitzGerald, D.M., Harris, M.S., Hein, C.J., Klein, A.H.F., Liu, B., de Menezes, J.T., Pejrup, M., Riggs, S.R., Short, A.D., et al., 2013, Morphodynamics of barrier systems: a synthesis, *in* Sherman, D.J. ed., Treatise on Geomorphology: Volume 10 Coastal Geomorphology, Academic Press, San Diego, p. 166–244.

Mellett, C.L., Hodgson, D.M., Lang, A., Mauz, B., Selby, I., and Plater, A.J., 2012, Preservation of a drowned gravel barrier complex: a landscape evolution study from the north-eastern English Channel: Marine Geology, v. 315-318, p. 115–131, doi: 10.1016/j.margeo.2012.04.008.

Miller Jr., D.N., 1962, Patterns of barrier bar sedimentation and its similarity to Lower

Cretaceous Fall River Stratigraphy, *in* Enyert, R.L. and Curry III, W.H. eds., Symposium of Early Cretaceous Rocks of Wyoming and Adjacent Areas 17th Annual Field Conference Guidebook, Wyoming Geological Association, p. 232–247.

Milliken, G.A., and Johnson, D.E., 2009, Analysis of Messy Data, Volume 1: Designed Experiments: Chapman & Hall / CRC Press, Boca Raton, FL, 674 p.

Morton, R.A., 2002, Factors controlling storm impacts on coastal barriers and beaches: a preliminary basis for near real-time forecasting: Journal of Coastal Research, v. 18, no. 3, p. 486–501.

Morton, R.A., 1994, Texas barriers, *in* Davis Jr., R.A. ed., Geology of Holocene Barrier Island Systems, Springer-Verlag, Berlin, p. 75–114.

Moslow, T.F., and Heron, S.D., 1994, The Outer Banks of North Carolina, *in* Davis Jr., R.A. ed., Geology of Holocene Barrier Island Systems, Springer-Verlag, Berlin, p. 47–76.

Moslow, T.F., and Tye, R.S., 1985, Recognition and characterization of Holocene tidal inlet sequences: Marine Geology, v. 63, no. 1–4, p. 129–151, doi: http://dx.doi.org/10.1016/0025-3227(85)90081-7.

Nielsen, L.H., Johannessen, P.N., and Surlyk, F., 1988, A Late Pleistocene coarse-grained spit-platform sequence in northern Jylland, Denmark: Sedimentology, v. 35, no. 6, p. 915–938, doi: 10.1111/j.1365-3091.1988.tb01738.x.

Nummedal, D., and Fischer, I.A., 1978, Process-response models for depositional shorelines: the German and the Georgia Bights, *in* Coastal Engineering Proceedings, American Society of Civil Engineers, New York, NY, p. 1215–1231.

Nummedal, D., Oertel, G.F., Hubbard, D.K., and Hine, A.C., 1977, Tidal inlet variability-Cape Hatteras to Cape Canaveral, *in* Coastal Sediments ’77, Proc. 5th Symp., WPCO Div. of ASCE, Charleston, South Carolina, p. 543–562.

O’Brien, M.P., 1969, Equilibrium flow areas of tidal inlets on sandy coasts: Journal of the Waterways and Harbors Division, v. WW1, p. 43–52.

Oertel, G.F., 1985, The barrier island system: Marine Geology, v. 63, no. 1, p. 1–18, doi: 10.1016/0025-3227(85)90077-5.

Olabarrieta, M., Geyer, W.R., and Kumar, N., 2014, The role of morphology and wave-current interaction at tidal inlets: an idealized modeling analysis: Journal of Geophysical Research, v. 119, no. 12, p. 8818–8837, doi: 10.1002/2014JC010191.

Oost, A.P., Hoekstra, P., Wiersma, A., Flemming, B., Lammerts, E.J., Pejrup, M., Hofstede, J., van der Valk, B., Kiden, P., Bartholdy, J., van der Berg, M.W., Vos, P.C., de Vries, S., and Wang, Z.B., 2012, Barrier island management: lessons from the past and directions for the future: Ocean & Coastal Management, v. 68, p. 18–38, doi: 10.1016/j.ocecoaman.2012.07.010.

Otvos, E.G., 2012, Coastal barriers - nomenclature, processes, and classification issues:

Geomorphology, v. 139-140, no. 0, p. 39–52, doi: 10.1016/j.geomorph.2011.10.037.

Pilkey, O.H., Cooper, J.A.G., and Lewis, D.A., 2009, Global distribution and geomorphology of fetch-limited barrier islands: Journal of Coastal Research, v. 254, no. 1971, p. 819–837, doi: 10.2112/08-1023.1.

Ray, P.K., Hayes, M.O., Stephen, M.F., and Ray, K.B., 1973, Multi-level cuspate features on microtidal barrier beaches, *in* Abstracts with Programs - Geological Society of America, Dallas, TX, p. 776–777.

Reinson, G.E., 1979, Barrier island systems, *in* Walker, R.G. ed., Facies Models, Geosciences Canada, Toronto, p. 57–74.

Reinson, G.E., 1992, Transgressive barrier island and estuarine systems, *in* Walker, R.G. and James, N.P. eds., Facies Models: Response to Sea-Level Changes, Geological Association of Canada, St. John's, Newfoundland, p. 179–194.

Roy, P.S., Cowell, P.J., Fernland, M.A., and Thom, B.G., 1997, Wave-dominated coasts, *in* Carter, R.W.G. and Woodroffe, C.D. eds., Coastal Evolution: Late Quaternary Shoreline Morphodynamics, Cambridge University Press, Cambridge, p. 121–153.

Sennes, G., Castelle, B., Bertin, X., Mirfenderesk, H., and Tomlinson, R.B., 2007, Modelling of the Gold Coast seaway tidal inlet, Australia: Journal of Coastal Research, v. SI 50, p. 1086–1091.

Shaw, J., You, Y., Mohrig, D., and Kocurek, G., 2014, Tracking hurricane-generated storm surge with washover fan stratigraphy: Geology, v. 43, no. 2, p. 127–130, doi: 10.1130/G36460.1.

Shelton, J.W., 1967, Stratigraphic models and general criteria for recognition of alluvial, barrier-bar, and turbidity-current sand deposits: American Assocation of Petroleum Geologists Bulletin, v. 51, no. 12, p. 2441–2461, doi: 10.1306/5D25C27F-16C1-11D7-8645000102C1865D.

Short, A.D., 2006, Australian beach systems—nature and distribution: Journal of Coastal Research, v. 22, no. 1, p. 11–27, doi: 10.2112/05A-0002.1.

Simms, A.R., Anderson, J.B., and Blum, M., 2006, Barrier-island aggradation via inlet migration: Mustang Island, Texas: Sedimentary Geology, v. 187, no. 1–2, p. 105–125, doi: 10.1016/j.sedgeo.2005.12.023.

Stutz, M.L., and Pilkey, O.H., 2001, A review of global barrier island distribution: Journal of Coastal Research, v. SI 34, p. 15–22, doi: 10.2307/25736270.

Stutz, M.L., and Pilkey, O.H., 2011, Open-ocean barrier islands: global influence of climatic, oceanographic, and depositional settings: Journal of Coastal Research, v. 27, no. 2, p. 207–222, doi: 10.2112/09-1190.1.

Stutz, M.L., and Pilkey, O.H., 2005, The relative influence of humans on barrier islands: humans versus geomorphology: Reviews in Engineering Geology, v. 16, no. 12, p. 137–147, doi: 10.1130/2005.4016(12).

Swift, D.J.P., 1975, Barrier-island genesis: evidence from the central Atlantic shelf, eastern U.S.A: Sedimentary Geology, v. 14, no. 1, p. 1–43.

Taylor, E.B., Gibeaut, J.C., Yoskowitz, D.W., and Starek, M.J., 2015, Assessment and monetary valuation of the storm protection function of beaches and foredunes on the Texas coast: Journal of Coastal Research, v. 31, no. 5, p. 1205–1216, doi: 10.2112/JCOASTRES-D-14-00133.1.

Timmons, E.A., Rodriguez, A.B., Mattheus, C.R., and DeWitt, R., 2010, Transition of a regressive to a transgressive barrier island due to back-barrier erosion, increased storminess, and low sediment supply: Bogue Banks, North Carolina, USA: Marine Geology, v. 278, no. 1-4, p. 100–114, doi: 10.1016/j.margeo.2010.09.006.

Tizzard, P.G.I., and Lerbekmo, J.F., 1975, Depositional history of the Viking Formation, Suffield area, Alberta, Canada: Bulletin of Canadian Petroleum Geology, v. 22, no. 4, p. 715–752.

Tolman, H.L., 2014, User manual and system documentation of WAVEWATCH III version 4.18: U. S. Department of Commerce, National Oceanic and Atmospheric Administration National Weather Service, National Centers for Environmental Prediction, College Park, MD, 282 p.

Ward, S.L., Neill, S.P., Van Landeghem, K.J.J., and Scourse, J.D., 2015, Classifying seabed sediment type using simulated tidal-induced bed shear stress: Marine Geology, v. 367, no. May, p. 94–104, doi: 10.1016/j.margeo.2015.05.010.

Zecchin, M., Ceramicola, S., Gordini, E., Deponte, M., and Critelli, S., 2011, Cliff overstep model and variability in the geometry of transgressive erosional surfaces in high-gradient shelves: the case of the Ionian Calabrian margin (southern Italy): Marine Geology, v. 281, p. 43–58, doi: http://dx.doi.org/10.1016/j.margeo.2011.02.003.

Zhang, K., Douglas, B., and Leatherman, S., 2002, Do storms cause long term beach erosion along the U.S. east barrier coast? The Journal of Geology, v. 110, no. 4, p. 493–502.

Zhang, K., and Leatherman, S., 2011, Barrier island population along the U.S. Atlantic and Gulf Coasts: Journal of Coastal Research, v. 272, no. 2, p. 356–363, doi: 10.2112/JCOASTRES-D-10-00126.1.

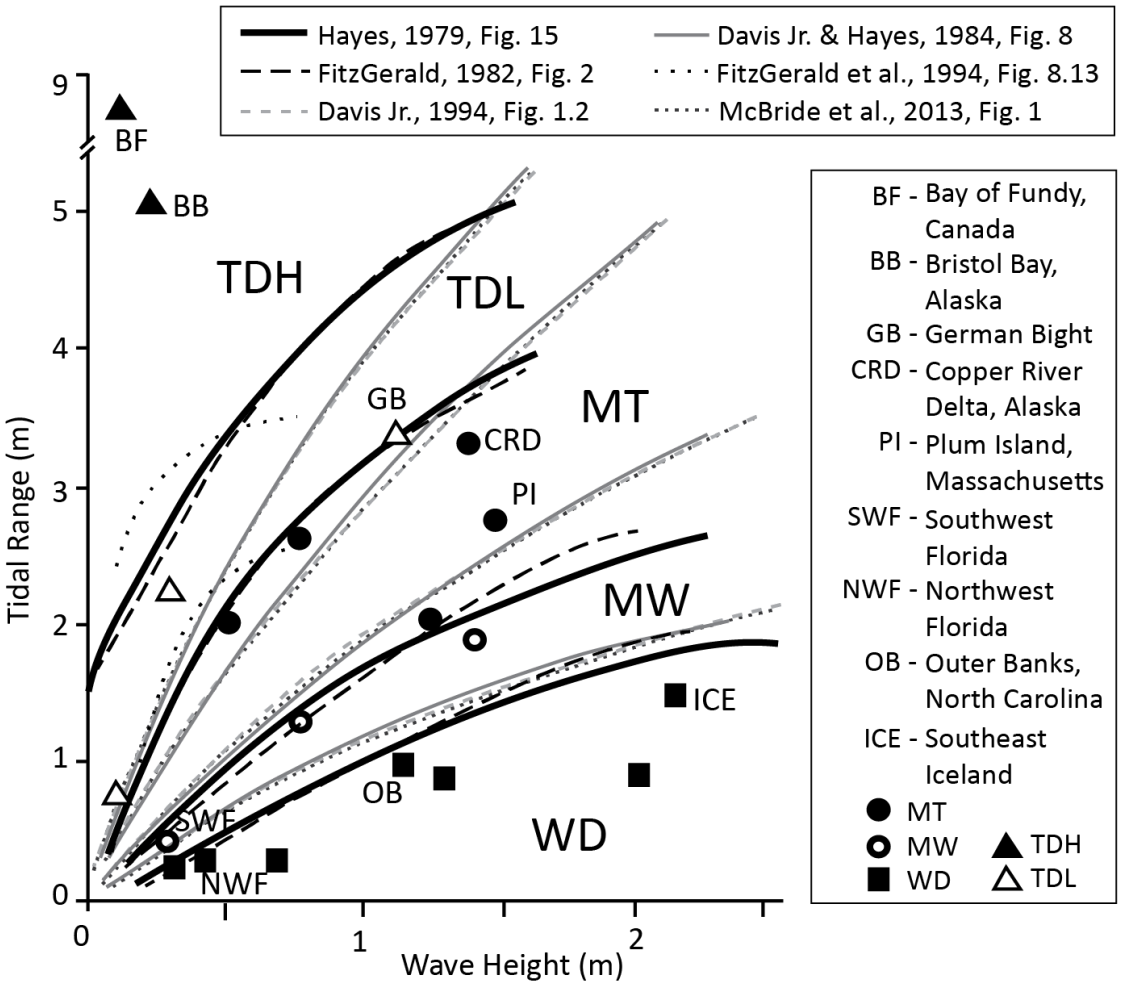

Figure 4.1. Tidal range versus wave height plot linking barrier island morphology to energy regimes after Hayes (1979) with identical data locations and boundaries labeled. Additional lines show subsequent duplication and modification of the energy regime fields. Abbreviations: WD-wave-dominated; MW - mixed energy, wave-dominated; MT - mixed energy, tide-dominated; TDL - tide-dominated low; TDH - tide-dominated high.

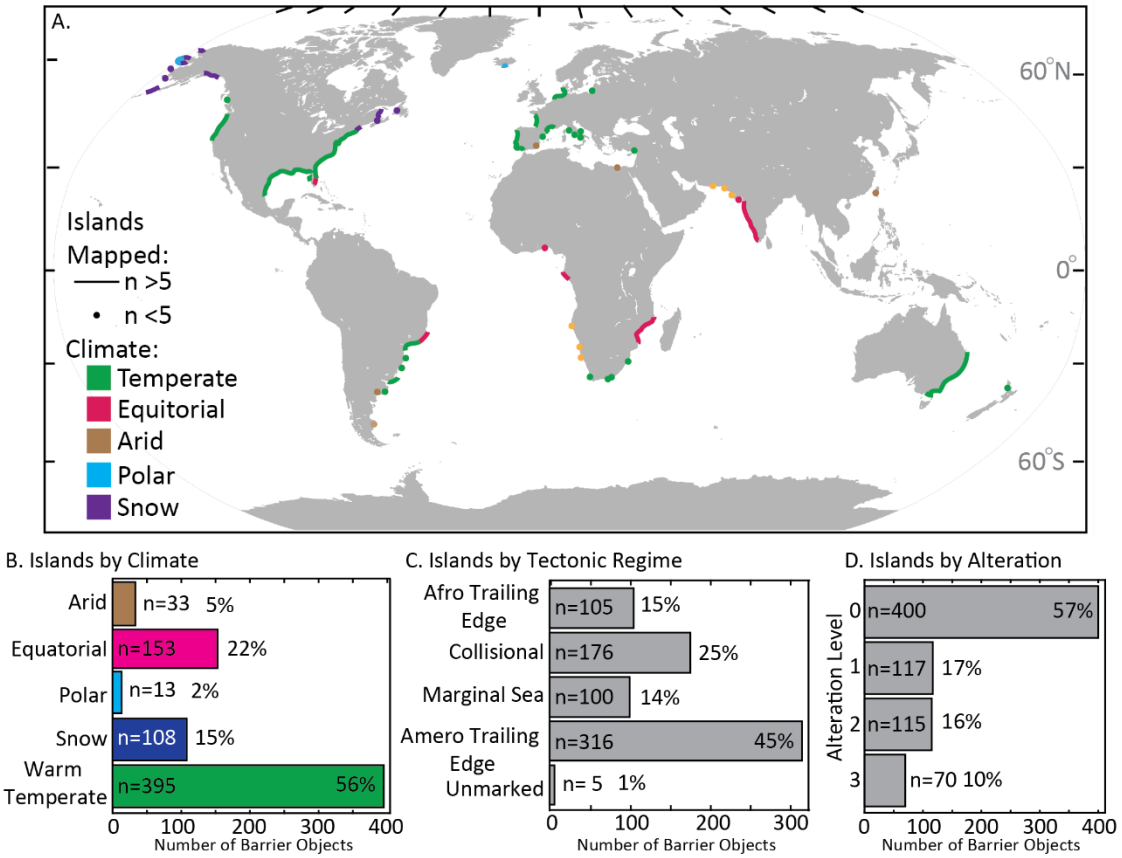

Figure 4.2. A) Map and histogram (B) of the global distribution of islands and spits mapped colored by climate. Climate designations from the Koppen-Gieger Classification (Kottek et al., 2006). C) Histogram showing the number of barrier islands and spits in each tectonic regime using the classification of Inman and Nordstrom (1971). D) Histogram showing the number of barrier islands and spits with each level of anthropogenic alteration.

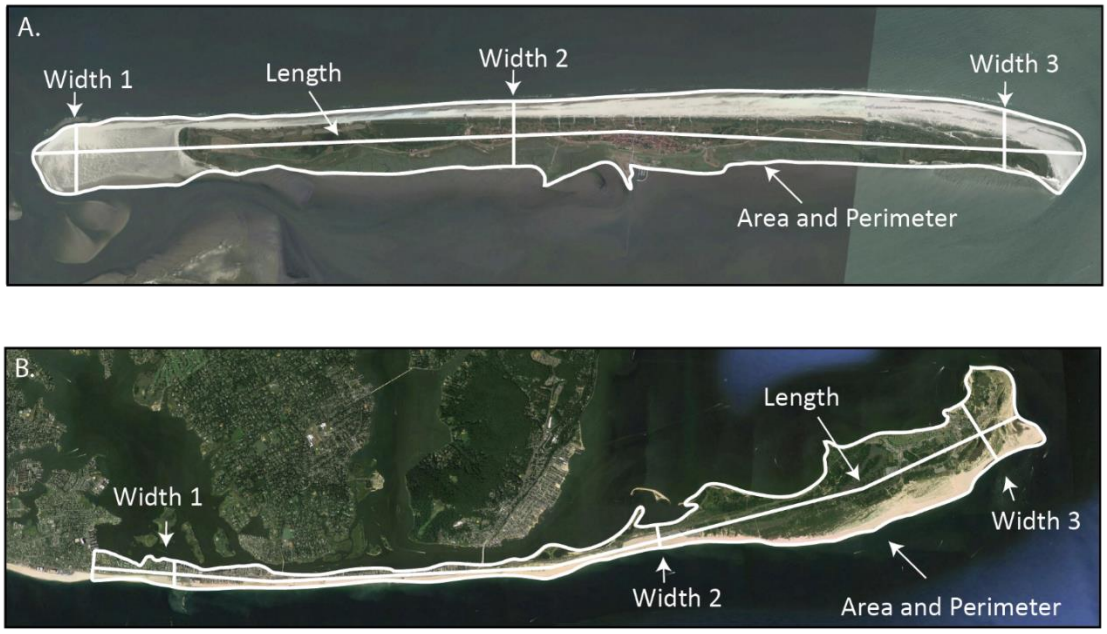

Figure 4.3. Example of A) barrier island and B) spit measurements mapped from a Google Earth images showing how area, perimeter, length, and width were mapped.

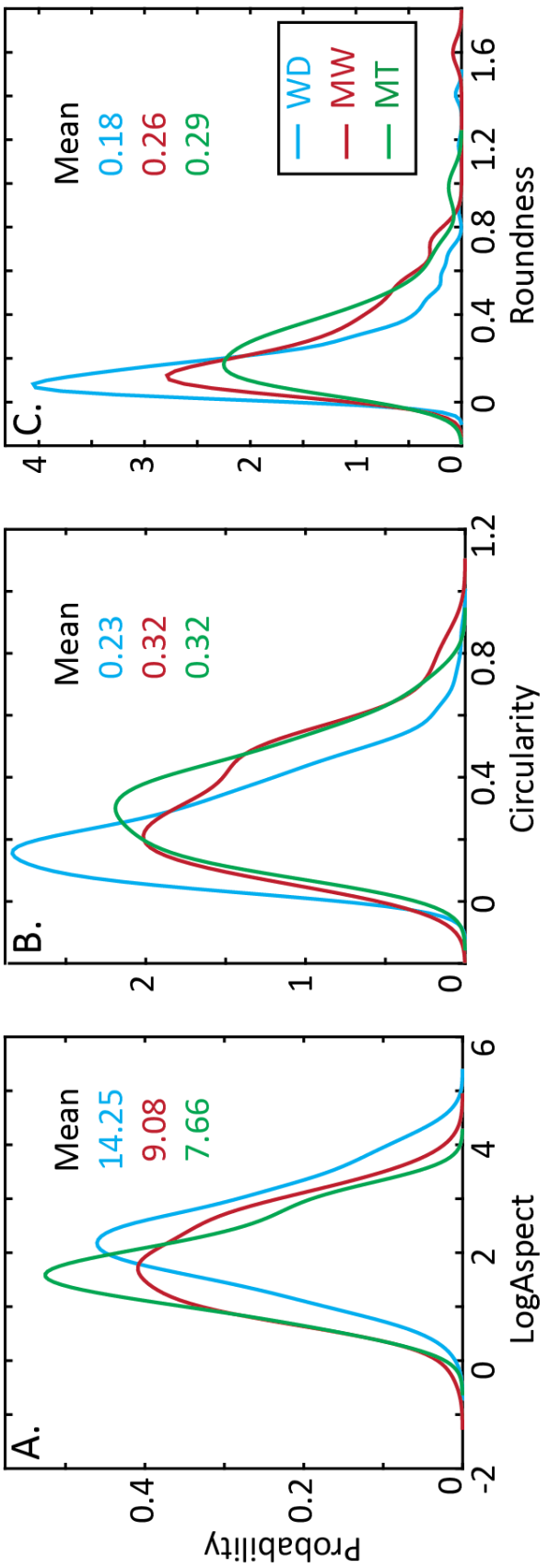

Figure 4.4. Kernel distributions (probability diagrams) show the range of aspect (A), circularity (B), and roundness (C) values for each energy regime. The peak of each curve indicates the most commonly occurring value. Abbreviations: WD-Wave-dominated; MW – mixed energy, wave-dominated; MT-mixed energy, tide-dominated.

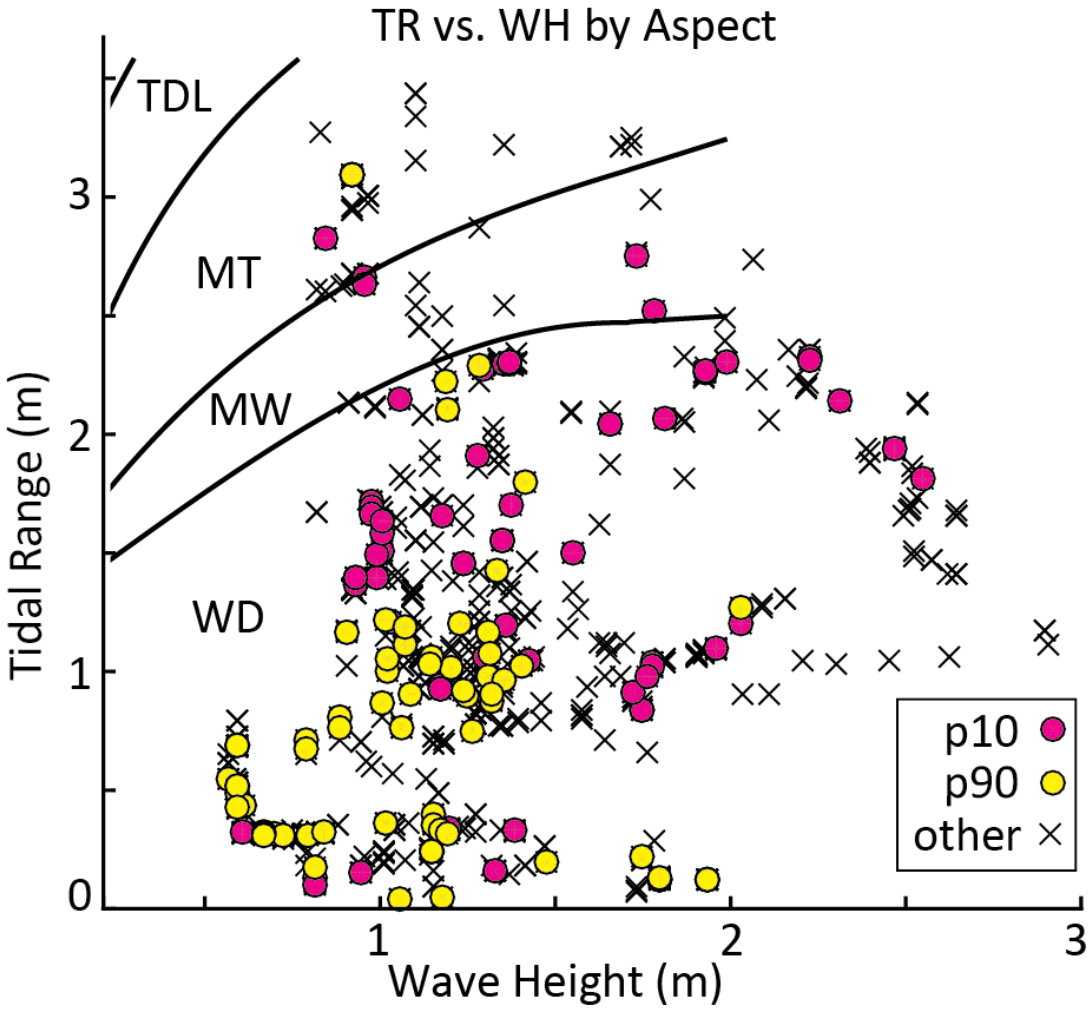

Figure 4.5. Tidal range versus wave height for barrier islands and spits colored by the most elongate 10% (p90) and the most round 10% (p10) of aspect values, both groups span the range of energy regimes (WD- Wave-dominated; MW – mixed energy, wave-dominated; MT-mixed energy, tide-dominated; TDL-tide-dominated low).

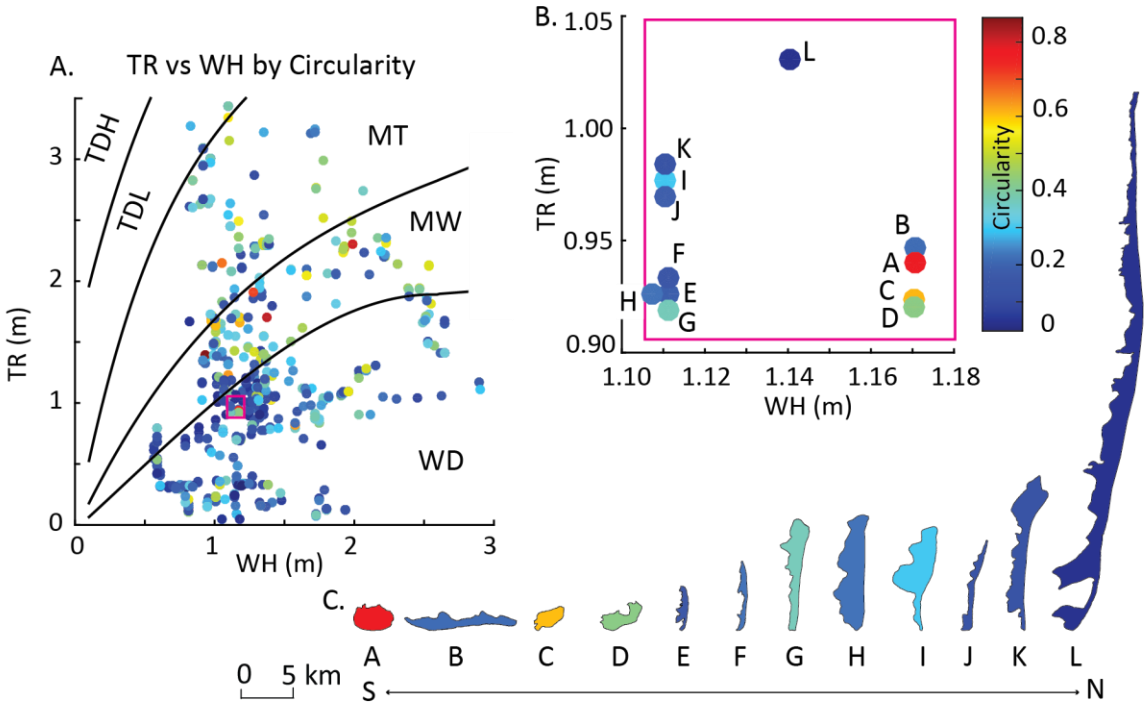

Figure 4.6. A. Tidal range (TR) versus wave height (WH) for barrier islands and spits colored by circularity. B. The inset plot (outlined in pink) and example islands show the range of (C) island shapes (A-L) along the U.S. Atlantic coast of Maryland and Virginia (~157 km mapped distance) which has consistent tidal range and wave height in the WD regime.

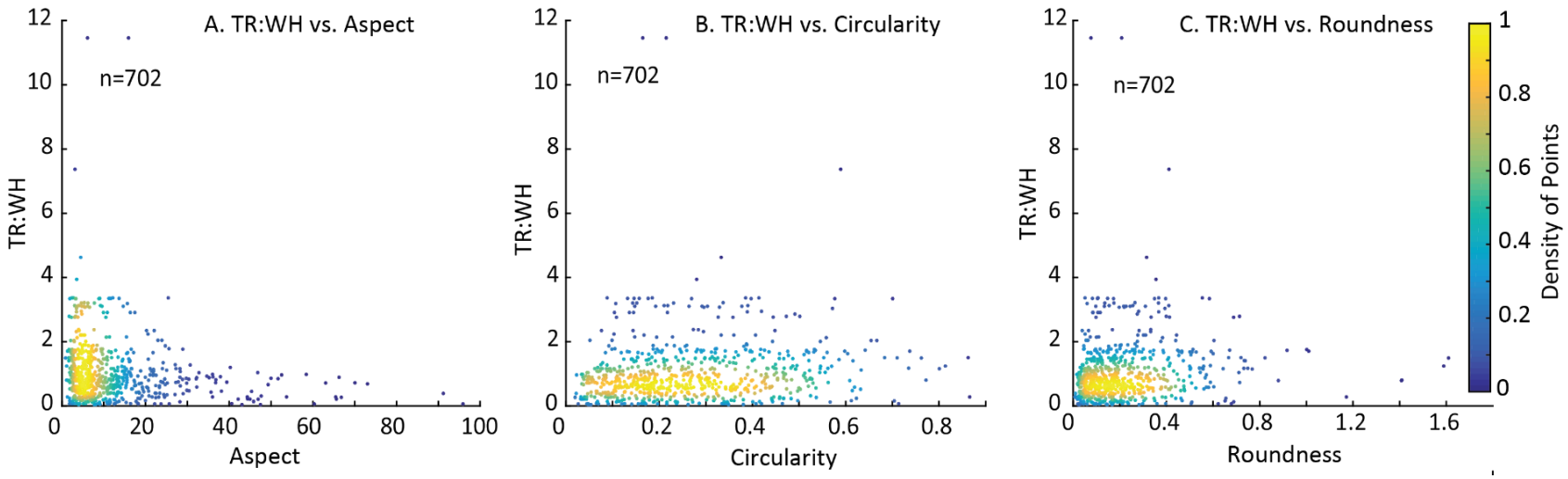

Figure 4.7. Cross plots of tidal range: wave height ratio (TR:WH) versus aspect, circularity, and roundness. Data are colored by the density of points on the plot, ranging from dense data (yellow) to sparse data (blue).

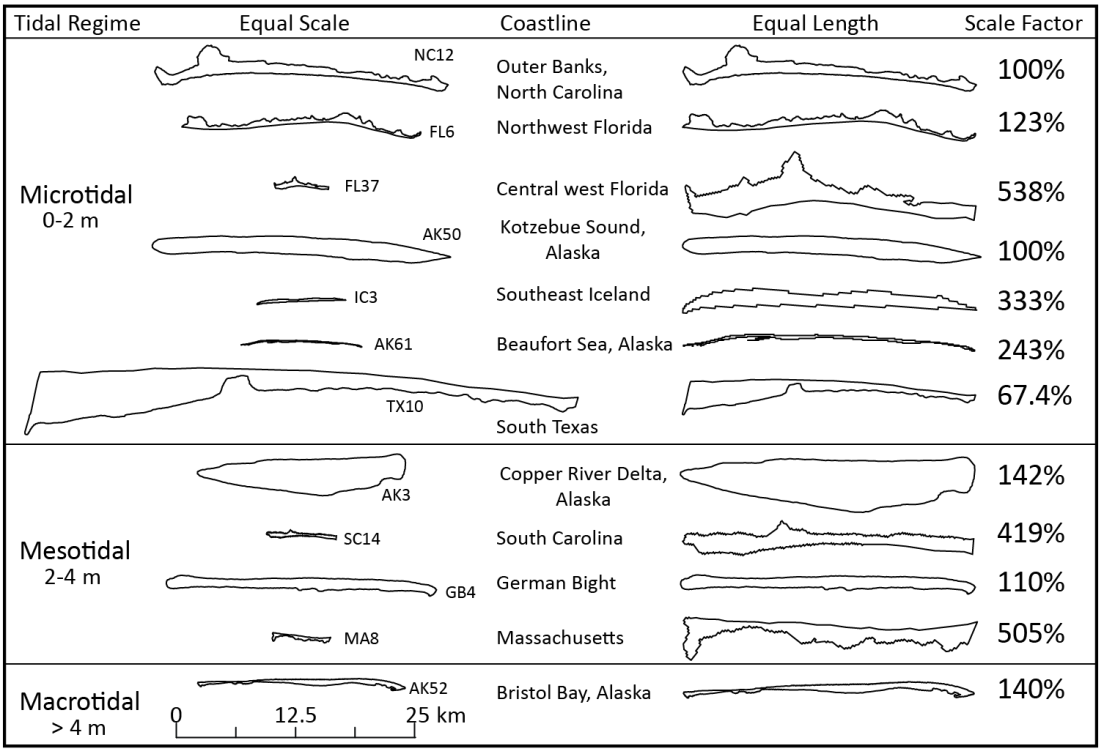

Figure 4.8. Select barrier islands from each of the 21 coasts used by Hayes (1979) are shown at their true size (left hand column) and set at the same length scale (right hand column) to show that islands of different sizes, from different tidal regimes, have similar morphologies.

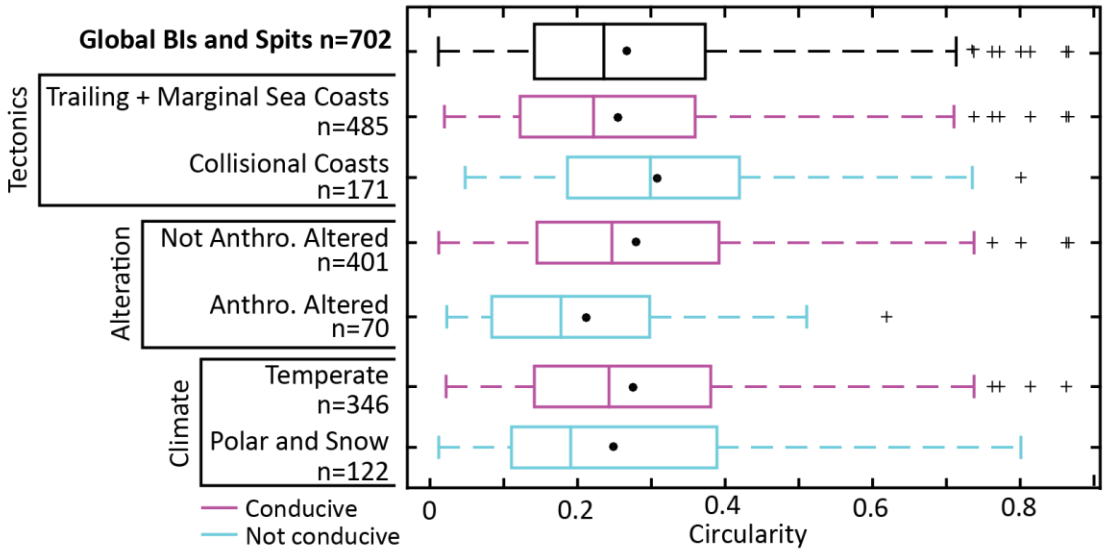

Figure 4.9. Box-and-whisker plots contrasting the global dataset (black) with the dataset filtered on the limiting criteria: climate, tectonics, and anthropogenic influence. Each criterion was split, comparing islands with characteristics conducive (pink) to linking barrier island (BI) shape to energy regime to those with conditions not conducive (blue). Vertical lines in each boxplot show the mean while the black dots show the mean. Anthro. – anthropogenically altered.

Figure 4.10. Cross plots showing the morphodynamic scaling relationships between island and spit dimensions (n=702). Lines of best fit are shown (black solid lines) as well as the 90% and 10% confidence intervals (dashed black lines) and R^2 regression coefficients. Data are colored by the density of points on the plot, ranging from dense data (yellow) to sparse data (blue). The barriers of the Texas Gulf of Mexico coast (black dots) are large relative to the global dataset (yellow-blue).

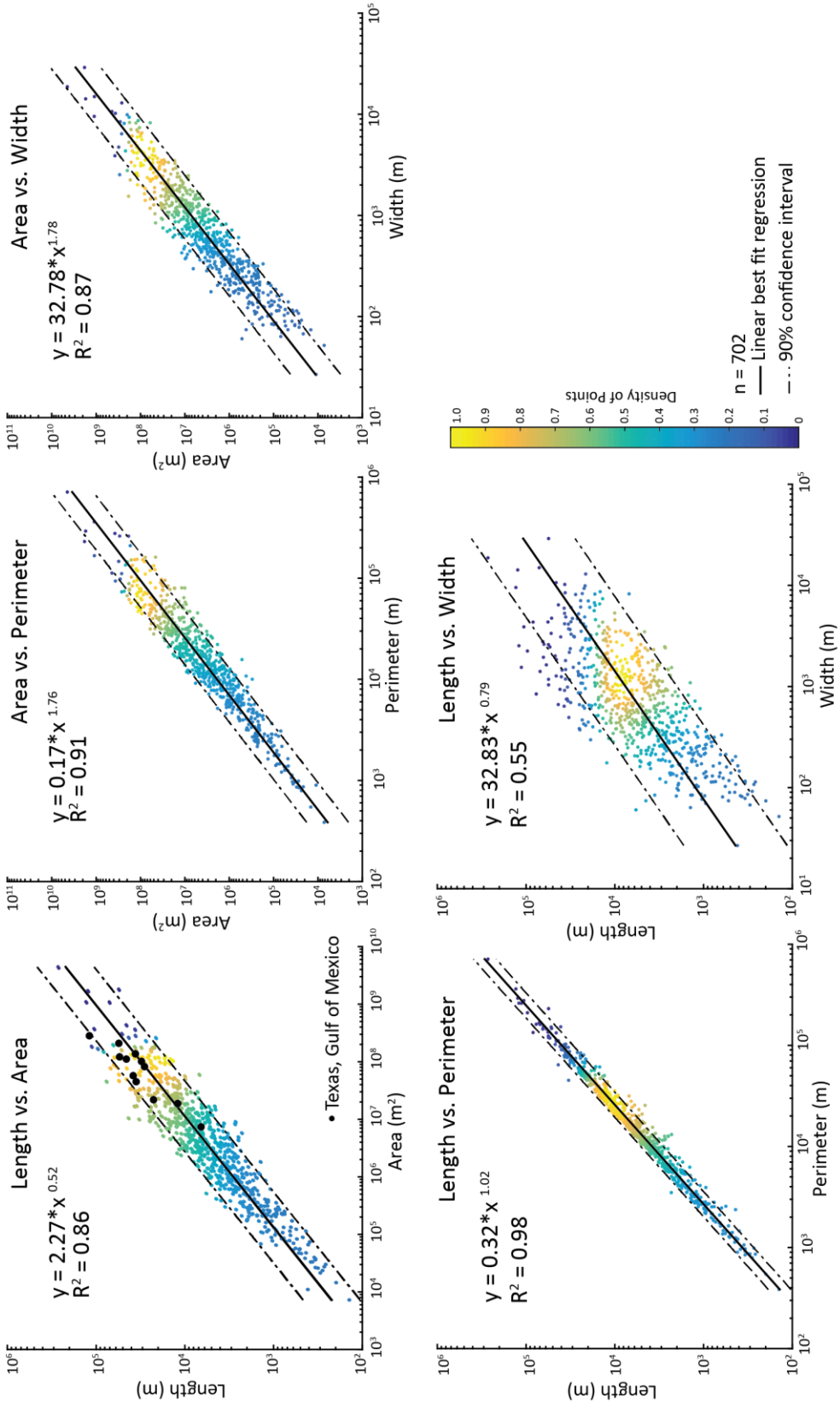
Length vs. Area
y = 2.27*x 0.52
R2 = 0.86
Length (m)
Area (m2)
• Texas, Gulf of Mexico
Area vs. Perimeter
y = 0.17*x 1.76
R2 = 0.91
Area (m2)
Perimeter (m)
Area vs. Width
y = 32.78*x1.78
R2 = 0.87
Area (m2)
Width (m)
Length vs. Perimeter
y = 0.32*x 1.02
R2 = 0.98
Length (m)
Perimeter (m)
Length vs. Width
y = 32.83*x 0.79
R2 = 0.55
Length (m)
Width (m)
Density of Points
n = 702
Linear best fit regression
90% confidence interval

Table 4.1. Description of Database Parameters and Sources

Parameter	**Method**	**Source**
Name	Common name of island.	From Google Earth labels or literature.
Type	Object type designation. Barrier islands are surrounded by water on all sides. Spits are attached on one side.	Roughly based on the accepted definitions of barrier islands and spits (Oertel, 1985; Otvos, 2012).
Area and Perimeter	Each island was traced at the waterline to create a polygon of the island shape, from which area and perimeter were calculated.	Polygon mapped in Google Earth.
Length	The length was mapped from one end of each island to the other roughly tracing the centerline. The line was segmented as needed to reflect the curvature of the island.	Line mapped in Google Earth.
Width	The width of each island was measured perpendicular to the shoreline in three representative locations spaced along the length of the island.	Line mapped in Google Earth.
Island Center	A representative point was visually approximated for the island center.	Point mapped in Google Earth.
Tidal Range	Sum of all tidal constituents for the location of the island center is used for the tidal range value for each island. All constituent values for each island were stored.	TPXO Tidal Model (Egbert and Erofeeva, 2010).
Wave Height	Mean annual wave height value for the location of the island center. Wave power and wave direction were also assigned to each island.	WaveWatch III® (Tolman, 2014).
Climate	Koppen-Gieger climate designation for the island center point location.	Koppen-Gieger Climate Map (Kottek et al., 2006).
Anthropogenic Alteration	Designated manually using a scale from 0-3:	Manually designated.
Coast Tectonic Type	Margin type designated based on the tectonic classification of coasts and shelves in Figure 4 of Inman and Nordstrom (1971). This scheme was chosen because it was used by both Hayes (1979) and more recently McBride et al. (2013).	Tectonic classification of coasts and shelves map (Inman and Nordstrom, 1971, Figure 4).

Table 4.2. Shape Parameter Equations

$Aspect = \frac{Length}{Width}$	$AP{:}SI = \frac{Area{:}Perimeter}{Shape\ Index}$
$Circularity = \frac{4\pi Area}{Perimeter^2}$	$AP{:}L = \frac{Area{:}Perimeter}{Length}$
$Roundness = \frac{4\sqrt{\frac{Area}{\pi}}}{Length^2}$	$AP{:}Aspect = \frac{Area{:}Perimeter}{Aspect}$
$Shape\ Index = \frac{.25\ Perimeter}{\sqrt{Area}}$	$Ellipse\ Area\ /\ Perimeter = \frac{\pi \frac{Length}{2}\ \frac{Width}{2}}{Area}$
$Ferret\ Diameter = 2\sqrt{\frac{Area}{\pi}}$	$*Shape\ 1 = \frac{Length\ Perimeter}{Area\ Width}$
$Elongation = \frac{\pi Length^2}{4Area}$	$*Shape\ 2 = \frac{Length\ Area}{Width}$
$Compactness = \frac{Perimeter^2}{4\pi Area}$	$*\ Shape\ 3 = \frac{Circularity}{Aspect}$
$Area{:}Perimeter = \frac{Area}{Perimeter}$	$*\ Shape\ 4 = \frac{Circularity}{Length}$
$Ellipticiy = \frac{\pi Length^2}{2Area}$	$*Shape\ 5 = \frac{Circularity}{Shape\ Index}$
$Ellipse\ Area\ /Area = \frac{\pi\ Length\ Width}{Area}$	

* indicates shape parameter developed for this study

Table 4.3. Comparison of Wave Height and Tidal Range and Values

		*Hayes WH (m)	**WaveWatch® WH (m)	*Hayes TR (m)	**TPXO TR (m)	Other TR (m)	Data Source
Bay of Fundy	BF	0.13	0.59	7	6.77		
Bristol Bay	BB	0.29	1.15	5	1.49	2.25 / 4.01	Port Moller, AK (NOAA 9463502) / Protection Point, Nushagak Bay, AK (NOAA 9465056)
Southwest Florida	SWF	0.28	0.57	0.4	0.58	0.46 /0.58	Egmont Key, Tampa Bay, FL (NOAA 8726347) / Clearwater Beach, FL (NOAA 8726724)
Northwest Florida	NWF	0.3	0.69	0.3	0.33	0.37	New Entrance Channel, St. Andrew Bay, FL (NOAA 8729136)
German Bight	GB	1.12	1.16	3.4	1.79	1.4-2.5	Elias and van der Spek (2006)
Copper River Delta, AK	CRD	1.42	1.95	3.3	2.31	3.1	Cordova, AK (NOAA 9454050)
Plum Island, MA	PI	1.5	0.95	2.8	2.64	2.44	Plum Island, Merrimack River Entrance, MA (NOAA 8440452)
Outer Banks, NC	OB	1.17	1.29	1	0.99	1.04	Cape Lookout, Atlantic Ocean, NC (NOAA 8656937)
Southeast Iceland	ICE	2.15	2.62	1.5	1.66		

* Values estimated from Figure 15 of Hayes (1979).
** Values for islands in each region averaged
TR – tidal range; WH – wave height

Table 4.4. ANOVA Multiple Compares p-values

		Global Barrier Islands and Spits			Global Barrier Islands		
	Sample size (n)	all	113	25	all	50	25
Aspect	WD vs MW	0	0.01	**0.32**	0	0	**0.06**
	MW vs MT	**0.52**	**0.57**	**0.71**	**0.55**	**0.57**	**0.66**
	WD vs MT	0	0	**0.17**	0	0	0.01
Circularity	WD vs MW	0	0	**0.27**	0	0	**0.05**
	MW vs MT	**0.74**	**0.74**	**0.72**	**0.71**	**0.69**	**0.74**
	WD vs MT	0	0	**0.17**	0	0	0.01
Roundness	WD vs MW	0	0.01	**0.29**	0	0	**0.08**
	MW vs MT	**0.37**	**0.43**	**0.67**	**0.47**	**0.52**	**0.67**
	WD vs MT	0	0	**0.14**	0	0	0.02

Bold – p-value >0.05 indicating the groups are not significantly different

Table 4.5. Linear Regression Model Results

	Aspect				Circularity				Roundness			
	R^2	β	SE	p	**R^2**	β	SE	p	**R^2**	β	SE	p
Global Barrier Islands and Spits (n=702)												
tr	8.66%	-0.22	0.03	0.00	9.45%	0.17	0.03	0.00	9.05%	0.24	0.04	0.00
wh		-0.36	0.09	0.00		0.36	0.07	0.00		0.38	0.09	0.00
Global Barrier Islands (n=308)												
tr	11.30%	-0.32	0.05	0.00	12.05%	0.27	0.05	0.00	11.37%	0.34	0.06	0.00
wh		-0.19	0.15	*0.21*		0.25	0.13	*0.06*		0.24	0.16	*0.13*

R^2 - r square value for the model; β - beta value, or slope of the linear model; SE - standard error of the model

Italics – p-value >0.05 are not significant, therefore variable (tr or wh) does not control island shape

tr-tidal range; wh-wave height

Table 4.6. Percent of the Total Range of Shape Parameter Values Encompassed by Each Energy Regime

		Global Barrier Islands and Spits	Global Barrier Islands
Aspect	WD	99.72%	99.72%
	MW	48.37%	33.59%
	MT	29.00%	25.52%
Circularity	WD	100.00%	100.00%
	MW	96.58%	96.58%
	MT	81.06%	75.18%
Roundness	WD	87.50%	87.48%
	MW	98.93%	98.88%
	MT	60.62%	60.23%

APPENDIX

$^{39}Ar/^{40}Ar$ AGE DATING METHODS

Supplementary Material

This is the supplementary material for Chapter 1: Time-space variability of paralic strata deposited in a high accommodation, high sediment supply setting: example from the Cretaceous of Utah. The supplementary material provided here includes the methodology for the $^{40}Ar/^{39}Ar$ analysis, which yielded a plateau age of 88.6 ± 0.79 Ma (1σ) for biotite from a bentonite bed within the lower John Henry Member (Figs. A1 & A2; Table A1).

Sample Location

One sample from a bentonite bed within the "A-B" interval of the lower John Henry Member was dated. The sample was gathered from a distinctly hardened white bed within a mudstone interval interpreted as offshore deposits of the "A-B" interval (GPS Location: 37.877627° latitude, -111.680229° longitude, elevation 2,204.315 m; Fig. 1.5). The sample was located about 20 m below the first continuously outcropping cliffband, interpreted as the deltaic "C" interval. This places the sample just below the correlative conformity that separates the "A-B" and "C" intervals in Buck Hollow. This correlative conformity becomes the Lower John Henry Member Sequence Boundary (LJHMSB) in Main Canyon (Fig. 1.12).

Dating Methods

The sample was dated using the $^{40}Ar/^{39}Ar$ method at the University of Vermont Noble Gas Lab for Argon Geochronology and Thermochronology. The sample was prepared by standard rock-crushing, mineral separation, and handpicking techniques.

After a final acetone wash, mineral separates were wrapped individually in aluminum foil and stacked with Fish Canyon sanidine (28.03 Ma; Renne *et al.* 1998), which was used to monitor the neutron dose. CaF_2 and K-glass were also included in the irradiation package and used to determine corrections for interfering nuclear reactions. Samples, flux monitors, CaF_2 and K-glass were irradiated together in a heat sealed, evacuated quartz tube for 2 hours in the CLICIT facility at the Oregon State University Radiation Center. The biotite sample was loaded directly into a well in a copper planchette and laser step heating for was conducted with a Santa Cruz Laser Microfurnace 75 W diode laser system. The released gas was purified with hot and cold SAES getters prior to analysis.

Argon isotopes were analyzed on a Nu Instruments Noblesse magnetic sector noble gas mass spectrometer via peak hopping on a single ion counter. Data from samples and flux monitors were corrected for blanks, mass discrimination, atmospheric argon, neutron-induced interfering isotopes, and the decay of ^{37}Ar and ^{39}Ar. Mass discrimination was calculated by analyzing known aliquots of atmospheric argon, for which $^{40}Ar/^{36}Ar$ measured in the range of 295.80 ± 1.18, and an assumed atmospheric value of 298.56 (Lee *et al.* 2006). Interfering nuclear reactions were corrected for by analyzing argon extracted from irradiated and fused optical grade CaF_2 and KSO_4. Correction factors used to account for interfering nuclear reactions for the irradiated samples are: $(^{40}Ar/^{39}Ar)_K = 9.78 \times 10^{-02} \pm 3.70 \times 10^{-2}$, $(^{36}Ar/^{37}Ar)_{Ca} = 1.10 \times 10^{-04} \pm 0.84 \times 10^{-4}$, $(^{39}Ar/^{37}Ar)_{Ca} = 6.92 \times 10^{-04} \pm 0.57 \times 10^{-4}$. A linear interpolation was used to calculate J factors for samples based on sample position between flux monitor packets in the irradiation tube. All ages were calculated using the isotope decay constants recommended by Steiger & Jäger (1977). The age calculations for inverse isochron and

apparent age data were achieved using both an in-house data reduction program and Isoplot 3.0 (Ludwig 2003). Errors on plateaus and weighted mean ages are quoted at the 1σ level and include precision associated with measurement of the irradiation parameter, J, for flux monitors. An aliquot of six biotite grains was extracted from the sample and analyzed (Figs. A1 & A2; Table A1). The aliquot data show a plateau age of 88.6 ± 0.79 Ma (1σ). Isochron age calculation is consistent, 88.5 ± 1.6 Ma (MSWD 1.08) and yield an initial (trapped) $^{40}Ar/^{36}Ar$ value within error of atmospheric value. See Table A1 for detailed data output. An initial single grain analysis was also performed with similar results but larger error.

Acknowledgements

We thank Daniel Jones, Laboratory Research Technician at the University of Vermont, for performing this analysis and Laura Webb, University of Vermont, for assistance in documenting the methods and results.

References

LEE, J.-Y., MARTI, K., SEVERINGHAUS, J.P., KAWAMURA, K., YOO, H.-S., LEE, J.B. & KIM, J.S. 2006. A redetermination of the isotopic abundances of atmospheric Ar. *Geochimica et Cosmochimica Acta*, **70**, 4507–4512, doi: http://dx.doi.org/10.1016/j.gca.2006.06.1563.

LUDWIG, K.L. 2003. User's manual for Isoplot/Ex rev. 3: a geochronological toolkit for Microsoft Excel. *Berkeley Geochronology Center Special Publication*, **4**, 71.

RENNE, P.R., SWISHER, C.C., DEINO, A.L., KARNER, D.B., OWENS, T.L. & DEPAOLO, D.J. 1998. Intercalibration of standards, absolute ages and uncertainties in $^{40}Ar/^{39}Ar$ dating. *Chemical Geology*, **145**, 117–152, doi: 10.1016/S0009-2541(97)00159-9.

STEIGER, R.H. & JÄGER, E. 1977. Subcommission on geochronology: convention on the use of decay constants in geo- and cosmochronology. *Earth and Planetary Science Letters*, **36**, 359–362, doi: http://dx.doi.org/10.1016/0012-821X(77)90060-7.

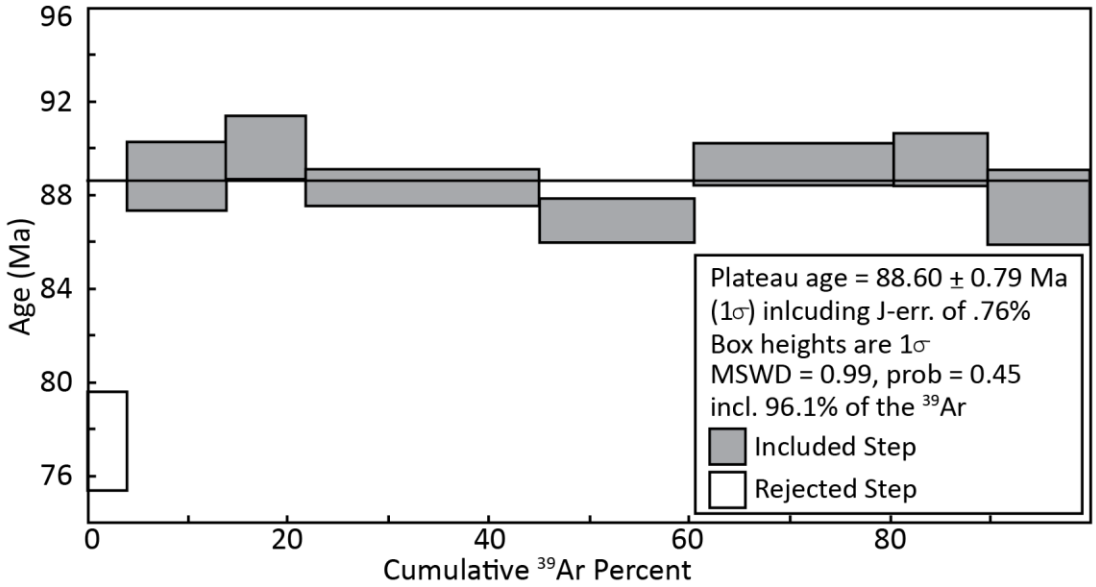

Figure A1: $^{40}Ar/^{39}Ar$ apparent age spectrum for bentonite sample from Buck Hollow. Apparent age box heights represent 1σ errors.

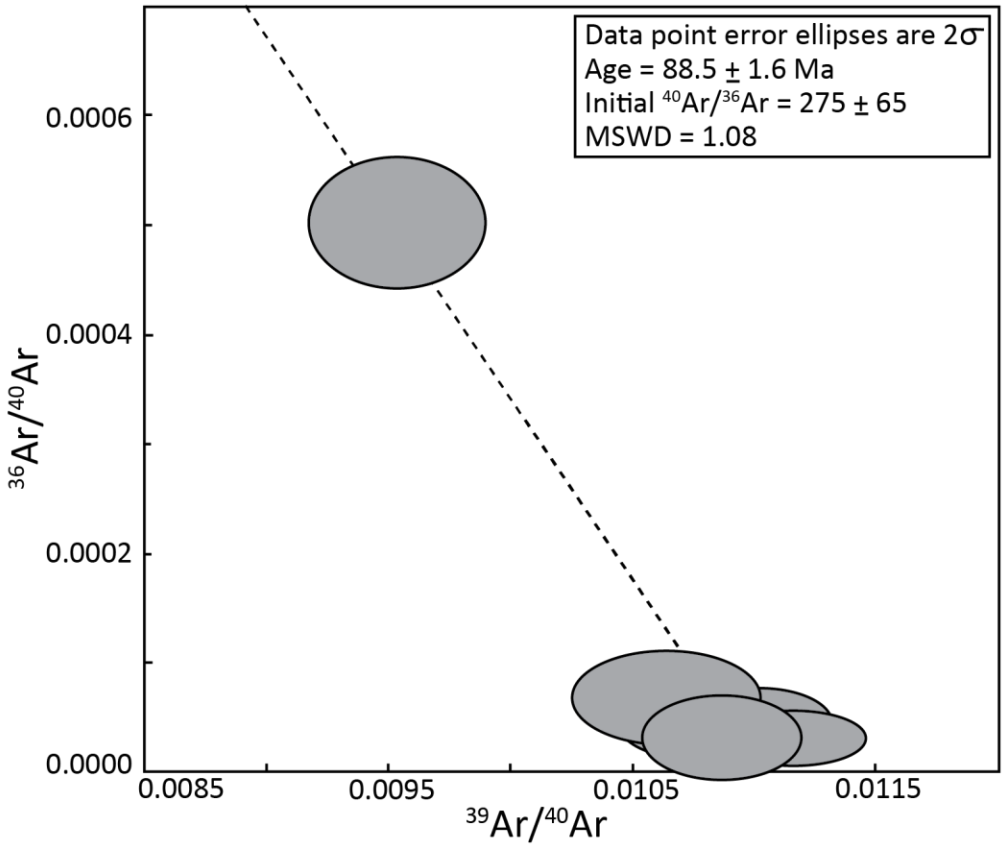

Figure A2: Isochron plot for biotite grains from bentonite sample. Ellipses represent 2σ confidence intervals.

Table A1: Detailed $^{40}Ar/^{39}Ar$ sample data table for bentonite sample from Buck Hollow. Results are plotted in Figs .A1 and A2.

Laser output (watts)	$^{40}Ar/^{39}Ar$	$^{40}Ar/^{39}Ar$ error	$^{38}Ar/^{39}Ar$	$^{38}Ar/^{39}Ar$ error	$^{37}Ar/^{39}Ar$	$^{37}Ar/^{39}Ar$ error	$^{36}Ar/^{39}Ar$	$^{36}Ar/^{39}Ar$ error	^{39}Ar (cps)	^{39}Ar error (cps)	Cumulative % ^{39}Ar	% ^{40}Ar*	Age (Myr)*	Age 1σ error (Myr)
3.8	85.285	2.114	0.01444	0.00162	5.4523	2.4029	0.02277	0.00357	304.7	7.3	3.89	92.0	77.52	2.12
4	91.763	1.494	0.01377	0.00122	2.7606	0.9457	0.00415	0.00139	774.0	12.4	13.78	98.7	88.84	1.58
4.2	93.991	1.383	0.01359	0.00085	0.5284	1.3459	0.00666	0.00170	619.0	8.9	21.68	97.9	90.05	1.48
4.5	91.181	0.809	0.01209	0.00033	0.2157	0.4400	0.00303	0.00056	1828.2	15.8	45.03	99.0	88.37	1.02
4.8	89.566	0.986	0.01227	0.00051	1.4242	0.7213	0.00296	0.00091	1198.3	13.0	60.34	99.0	86.96	1.15
5.1	92.127	0.929	0.01485	0.00068	0.7024	0.5541	0.00299	0.00069	1560.7	15.4	80.27	99.0	89.34	1.11
5.4	92.052	1.147	0.01202	0.00069	3.4569	1.0993	0.00296	0.00145	733.6	8.8	89.64	99.0	89.52	1.29
fuse	104.948	1.639	0.02429	0.00128	2.2814	0.9952	0.05293	0.00267	810.7	12.5	100.00	84.9	87.51	1.70

*J factor = 0.0005554 ± 0.0000042